THE UNIVERSITY *of* EDINBURGH

The role of microcephalin at mitosis

Carol-Anne Martin

Thesis submitted for the degree of Doctor of Philosophy
The University of Edinburgh
2011

This thesis is composed of original research undertaken by myself, and where the work of others is included their contributions have been duly acknowledged.

Carol-Anne Martin

July 2011

Acknowledgements

Firstly I would like to thank Andrew Jackson, who has been an excellent supervisor, and has supported me in every way throughout my PhD. Thanks for all the help and encouragement over the years. I have had a lovely time in the lab and could not have wished for a nicer supervisor.

Next I'd like to thanks all the members of the lab past and present for providing such a wonderful environment to work in. In particular I'd like to thank: Andrea for so much help and support over the past 4 years- making antibodies, FACs, cell culture (if I wrote everything down you've helped me with it'd take a whole page); Anna, my fellow microscope lover, for inspiring images, general PhD support and showing me the find and replace setting on word (you saved me hours); Bertrand, for getting me started on microscopes, photoshop and deconvolution; Bjorn for help with MCPH1 mouse; Ellie for fantastic supervision when I first started and for leaving a very well organised project for me to continue; Katy for being great fun to sit next to and not getting mad when my folders and lab books kept creeping over your mousepad! Louise for the mammoth effort of proof reading all the drafts of my thesis (epic! thank you so much), lots of PhD writing encouragement and help with all things PCR; Maggie for trying to organise me to deadlines, for proof reading, help with experiments and for very helpful discussions (and protocols) on caspases and phosphorylation; Martin (the cloning guru) for lots of experimental advice and for the horticultural oasis created in the office; Rachel for help with qPCR, lots of writing up PhD advice (formatting, endnote, illustrator, the list goes on..) and of course for all the fun late nights in the lab spent listening to Garrison FM.

The next big thank you goes to Paola Vagnarelli for generously providing me with lots of reagents, advice, and ideas over the last four years. Thanks for teaching me how to do LCL immunofluorescence, metaphase spreads, live imaging and for help with image analysis.

I would like to express my gratitude to Paul Perry and Matt Pearson for all the imaging support over the years and for patiently working through my MANY, often unique, imaging-related problems. Thanks to everyone in E2 for their help, advice and reagents, in particular Anne Seawright for her assistance with tissue culture, ordering and general lab stuff.

Thanks to Ian Adams for helpful discussions. Patricia Yeyati and Pleasantine Mill for sharing ideas, reagents and protocols. Sara Heras for help with sucrose gradients. Lizzie Freyer for help with FACs, NHS cytogenetics unit for preparing chromosome spreads and collecting metaphase spread images.

I would like to thank my friends and family for always being there and being interested in what I was doing (even when you received bewildering responses from me). Thanks also to my extended family (the Tindals) who have also been great help and support through these years.

The biggest thank you goes to my partner Chris who has shared all of the ups and downs of this thesis. Thank you for the midnight pickups from the lab, waiting until 9-10 pm before we can have dinner (which you have of course cooked) and accepting that weekends and holidays were just opportunities to cram in more experiments. Your unwavering support, encouragement and positivity managed to get me through this PhD with my sanity intact and for that I dedicate this thesis to you.

Abstract

A large brain is one of the most distinguishing features of humans compared to other members of the animal kingdom. During mammalian evolution there has been a disproportionate enlargement of the brain relative to body size and this expansion has been particularly prominent during the past 3 million years of human lineage. This must be the consequence of adaptive genetic alterations during mammalian evolution, but the genes and molecular processes altered are essentially unknown.

One approach for identifying candidate genes for brain size regulation is through characterisation of Mendelian disorders of brain development. In particular, primary microcephaly has received considerable interest as a model disease for studying brain size regulators because patients present with a profoundly reduced brain size but have no other malformations. Genetic studies have identified mutations in seven genes that can cause primary microcephaly. All the primary microcephaly proteins localise to the centrosome at some stage during the cell cycle and have roles in a diverse range of functions including centrosome maturation, centriole formation and microtubule organisation at the spindle pole. The precise mechanism leading to primary microcephaly is not known but a prevalent hypothesis is that centrosome dysfunction disrupts mitosis of neural progenitor cells. Despite there being strong evidence in support of this hypothesis for most primary microcephaly genes, MCPH1 (the first primary microcephaly gene to be identified) always appeared to be functionally distinct from other primary microcephaly proteins. Most work on MCPH1 has focussed on its role in the DNA damage response and cell cycle timing rather than on its mitotic role. As a result, the aim of this thesis is to perform a detailed analysis of MCPH1 function during mitosis.

In this thesis, three isoforms of MCPH1 were characterised and their localisation, expression and stability examined. It was established that MCPH1 is highly regulated during mitosis. MCPH1 transcript and protein levels vary significantly throughout the cell cycle and MCPH1 protein is targeted for degradation late in mitosis. In addition, MCPH1 is hyperphosphorylated during mitosis (in prometaphase-arrested cells) suggesting that phosphorylation could potentially regulate MCPH1 mitotic function. Twelve mitotic phosphorylation sites were identified by phosphopeptide

mapping, many of which were CDK1 and PLK1 consensus sites. Both PLK1 and CDK1 also contribute to MCPH1 phosphorylation *in vivo*. Although MCPH1 non-phosphorylatable mutants localise normally during mitosis, binding to interaction partners may be affected which may have functional consequences.

During mitosis MCPH1 localises to the centrosomes and kinetochores. Consistent with this localisation, RNAi-mediated knockdown of MCPH1 leads to metaphase arrest with multipolar spindles, major defects in chromosome alignment and loss of chromatid cohesion. In addition, MCPH1 deficient mouse embryonic fibroblast cells also demonstrate similar chromosome alignment defects, strengthening this finding in an independent system. Live-imaging of MCPH1 depleted cells demonstrate that a normal bipolar spindle and metaphase plate are initially formed, but subsequently chromosomes and chromatids drop off the metaphase plate and eventually the spindle collapses. This suggests that the primary function of MCPH1 is to allow timely progression through metaphase, possibly by mediating kinetochore-microtubule attachments to satisfy the spindle activated checkpoint.

Therefore my work describes several roles for MCPH1 in mitosis (centrosome stability, chromosome alignment and metaphase progression) suggesting that its role in mitosis could result in primary microcephaly in a number of different ways.

Table of Contents

List of Figures

List of Tables

Abbreviations

Amp^R	ampicillin resistance
APC/C	anaphase promoting complex or cyclosome
bp	base pair
BRCT	BRCA1 C-terminal
BSA	bovine serum albumin
cDNA	complementary DNA
Cm^R	chloramphenicol resistance
CMV	cytomegalovirus
CT	cycle threshold
CHX	cyclohexamide
CNN1	centrosomin motif 1
CNN2	centrosomin motif 2
DAPI	4',6-diamidino-2-phenylindole
DDR	DNA damage response
d.p.c	days post coitum
dH_2O	distilled water
DMEM	dulbecco's modified Eagle medium
DMSO	dimethyl sulfoxide
DNA	deoxyribonucleic acid
DNAase	deoxyribonuclease
dNTP	deoxyribonucleotide triphosphate
DSB	double strand break
DTT	dithiothreitol
E	embryonic day
ECACC	European cell culture collection
EDTA	ethylenediaminetetraacetic acid
EGTA	ethylene glycol tetraacetic acid
EtOH	ethanol
EUCOMM	European conditional mouse mutagenesis program

FCS	fetal calve serum
FL	full-length
kMT	kinetochore-microtubule
GFP	green fluorescent protein
HFB	human fetal brain
HR	homologous recombination
IR	irradiation
IRIF	irradiation induced foci
Kan^R	kanamycin resistance
kb	kilobases
kDa	kilodaltons
LB	luria-bertani
LBC	lymphoblastoid cells
M	molar
MEF	mouse embryonic fibroblast
mRNA	messenger ribonucleic acid
MOPD	microcephalic osteodysplastic primordial dwarfism
MOPS	3-(N-morpholino)propanesulfonic acid
MRI	magnetic resonance imaging
MTOC	microtubule organising centre
NHEJ	non-homologous end joining
NMD	nonsense mediated decay
Noc	nocodazole
PTC	premature termination codon
NMD	nonsense mediated decay
OD	optical density
ORF	open reading frame
PBS	phosphate buffered saline
PCC	premature chromosome condensation
PCM	pericentriolar material
PCR	polymerase chain reaction
PFA	paraformaldehyde

PIPES	*piperazine*-N,N′-bis(2-ethanesulfonic acid)
Purv A	purvalanol A
RNA	ribonucleic acid
RNase	ribonuclease
Rosc	roscovitine
RPMI	Roswell park memorial institute medium
RT	reverse transcriptase
qRT-PCR	quantitative real time PCR
S	short
SAC	spindle assembly checkpoint
s.d.	standard deviation
SDS	sodium dodecyl sulphate
s.e.m.	standard error of the mean
siRNA	small interfering RNA
ss	single stranded
SNP	single nucleotide polymorphisms
SVZ	sub-ventricular zone
TBE	tris/borate/EDTA
Tet	tetracycline
TMED	N,N,N',N'-tetramethylethylenediamine
Tm	melting temperature
Tris	tris(hydroxymethyl)aminomethane
TuRC	tubulin ring complex
UB	ubiquitin
UTR	untranslated region
UV	ultra-violet
V	volt
v:v	volume:volume
WCE	whole cell extract

1. Introduction

1.1. Brain development

1.1.1. Evolution of the mammalian brain

Most variation in brain size can be accounted for by differences in body weight (Jerison, 1973); as a general rule larger animals need larger brains to run their bodies. However, throughout mammalian and primate evolution there has been a disproportionate enlargement of the brain relative to body size (Northcutt and Kaas, 1995). For example, there is a 15-fold increase in relative brain size between mouse and man (Table 1.1). Although brain size has increased during primate evolution, expansion of the brain has been most prominent in the human lineage, with a tripling in brain size in the 3 million years after humans diverged from apes (Jerison, 1973). This expansion of the brain reflects an increase in the total cell number rather than cell size (Table 1.1) but does not result from a uniform increase in cell number in all areas of the brain; instead different areas of the brain have expanded at different rates.

Table 1.1. Relative brain size in selected animals

Species	Relative brain size (EQ)	Neurons in brain
Mouse	0.5	10^7
Monkey	2.09	10^9
Human	7.44	10^{11}

Relative brain size data is given as encephalization quotient (EQ) and taken from (MacPhail, 1982). Estimates of neuron number in the brain are taken from (Braitenberg, 2001). (Table reproduced from Fish *et al.*, 2008).

1.1.2. Evolution of the mammalian cerebral cortex

During mammalian evolution, it is the outer portion of the cerebrum, the cerebral cortex, which has expanded more in size than other areas of the brain (Finlay and Darlington, 1995; Northcutt and Kaas, 1995). This expansion has been through an increase in cortical surface area rather than cortical thickness (Rakic, 1995). For example, the 1000-fold increase in cortical surface area from mouse to man is only accompanied by a 2-fold increase in cortical thickness (Rakic, 1995). This huge increase in cortical surface area has not been accompanied by a proportional increase in skull size; instead the surface of the brain forms a series of folds and convolutions, called gyri and sulci, to accommodate it within the skull. This has led to the progression of the smooth brains (lissencephalic) of rodents to one of multiple folds and convolutions in humans (gyrencephalic) (Figure 1.1).

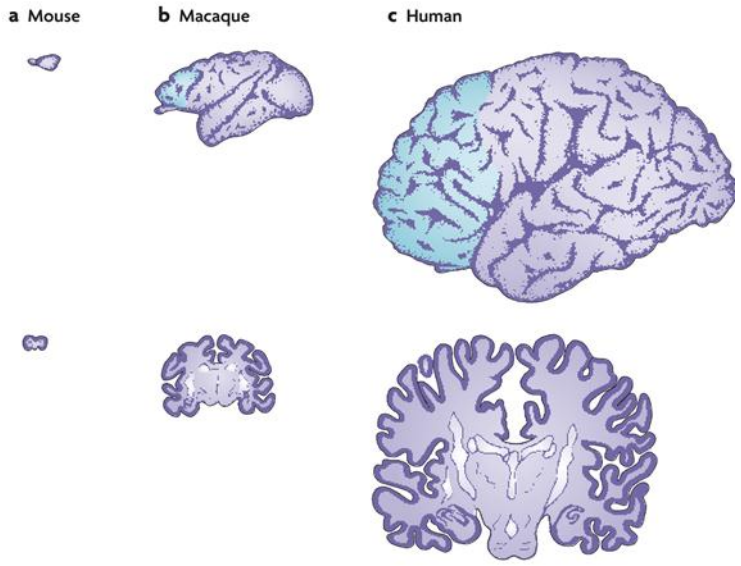

Figure 1.1 Comparison of the brain of a mouse, a macaque monkey and a human. The pictures are drawn to scale to demonstrate the actual difference in size. From mouse, macaque monkey to human brain there is a small increase in the thickness of the cortex (dark purple outline), a large expansion in surface area (1: 100: 1000 X respectively) and an increase in complexity of folding of the cortex. (Figure reproduced from Rakic, 2009).

1.1.3. Cell biology of cerebral cortex expansion

The cell-biological basis of the enormous expansion of the cerebral cortex surface area without a comparable increase in thickness has been addressed by the radial unit hypothesis (Rakic, 1988; Rakic, 1995). To understand the radial-unit hypothesis we need to understand how the cerebral cortex develops (reviewed by Bystron *et al.*, 2008; Nowakovski and Hayes, 2005). The cerebral cortex forms from the neural progenitors present in the ventricular and sub-ventricular zone that line the lateral ventricles of the brain. It is within this zone that neurons are generated and migrate outwards to form the six different layers of the cerebral cortex (The Bloulder Committee, 1970). The earliest neurons generated populate one of the inner-most layers whereas the neurons generated later pass the earlier neurons to form the outer-most layer of the developing cortex (Angevine and Sidman, 1961; Rakic, 1974). The radial unit hypothesis states that each neuron generated by a single founder neural progenitor cell follows the same migratory path and so these cells stack radially contributing to the thickness of the brain. Each neuron generated by a different founder neural progenitor cell will follow a different migratory path and will arrange tangentially across the cortical plate leading to lateral brain expansion (Figure 1.2) (Rakic, 1988; Rakic, 1995). Thus, during evolution only an increase in the number of the founder neural progenitor cells could lead to expansion of the cortical surface area.

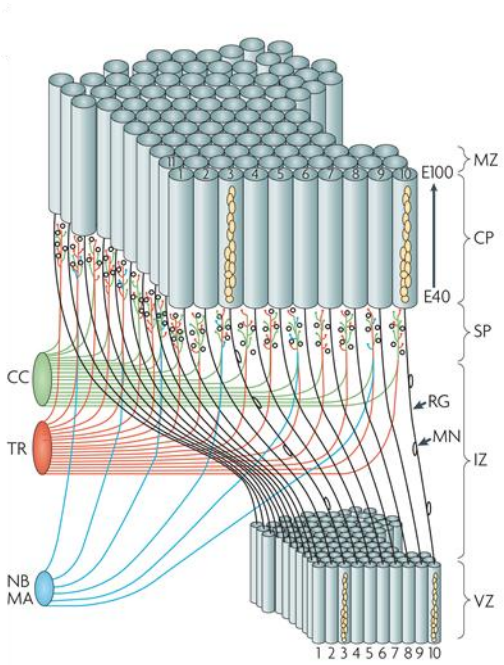

Figure 1.2. The model of radial neuronal migration.
The neurons (MN) generated at the ventricular zone (VZ) migrate through the intermediate zone (IZ) to the cortical plate (CP). The neurons generated from the same site of origin but at different times form a radial stack of cells (E40-E100). Neurons generated from a different site of origin (1-10) align laterally to one another. (Figure adapted from Rakic, 2009).

The principles of the radial unit hypothesis have been tested experimentally by expanding the neuronal progenitor population in the rodent brain through either decreasing the rate of apoptosis or increasing the rate of neuronal proliferation. The rate of apoptosis was decreased by inactivating the components of programmed cell death, caspase 3 and 9 (Kuida *et al.*, 1998; Kuida *et al.*, 1996). The rate of proliferation was increased by overexpression of an active form of β-catenin which can influence the decision of neuronal precursor cells to re-enter the cell cycle instead of differentiating (Chenn and Walsh, 2002). In all cases there was an increase in the number of precursor cells in the ventricular zone accompanied with lateral expansion of the cerebral cortex leading to the formation of an enlarged, folded cerebral cortex (Figure 1.3) (Chenn and Walsh, 2002; Kuida *et al.*, 1998; Kuida *et al.*, 1996).

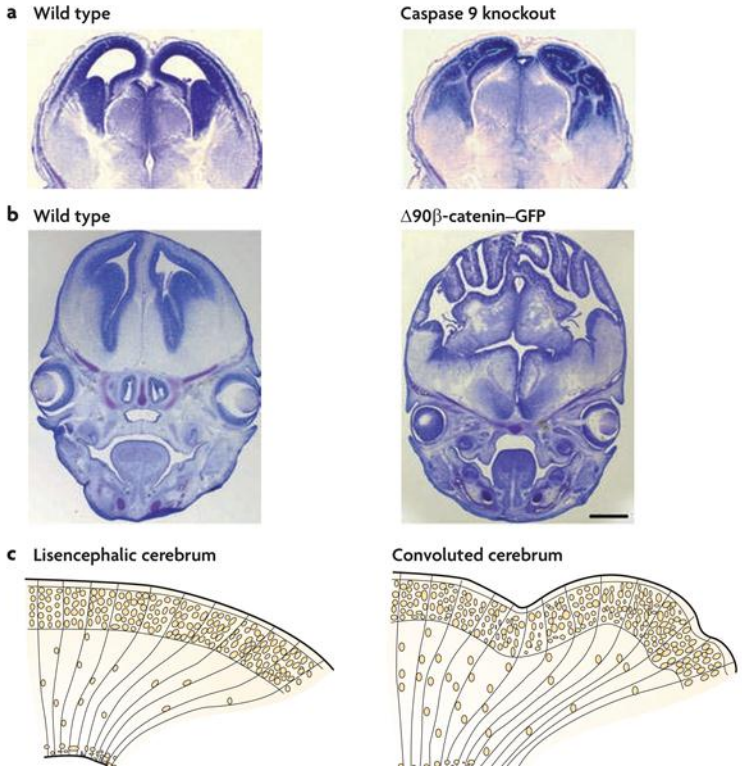

Figure 1.3. Enlargement of the cortex surface area by decrease in apoptosis or increase in proliferative divisions.
(A & B) Brain sections of a wild type mouse embryo (panel 1), an embryo deficient in caspase 9 (A, panel 2) or a transgenic mouse embryo expressing an activated form of β-catenin (B, panel 2). (C) Diagrams showing how the increased number of progenitor cells can equate to an increase in cortical surface area and folding rather than cortical thickness. (Original data from Chenn and Walsh, 2002; and Kuida *et al.*, 1996; Figure reproduced from Rakic, 2009).

1.1.4. Neural progenitor cells

The initial population of neuronal progenitor cells in the developing brain form the ventricular zone (The Bloulder Committee, 1970). These cells are initially thought to undergo rounds of symmetric cell divisions to produce two daughter cells also with neural progenitor cell fate thereby increasing the surface area and thickness of the ventricular zone (Caviness *et al.*, 1995). At a particular developmental stage, E33 in humans (Bystron *et al.*, 2006) and E10 in mice (Garcia-Moreno *et al.*, 2007), the

neural progenitor cells begin to switch to an asymmetric mode of division to produce one daughter cell that continues to proliferate and another which migrates out of the ventricular zone to become a neuronal cell or basal progenitor committed to neuronal cell fate (Chenn and McConnell, 1995; Iacopetti *et al.*, 1999; Takahashi *et al.*, 1995a; Takahashi *et al.*, 1996). This switch from symmetric to asymmetric divisions is gradual and as cells progress through the period of neurogenesis the number of asymmetric divisions to symmetric divisions increases (Figure 1.4) (Takahashi *et al.*, 1996). Changes in the proportions of these divisions, especially during the early rounds of symmetric divisions, are likely to have a significant impact on final neuronal output and cortical surface area (Caviness *et al.*, 1995). For example, seven extra symmetric divisions during this time could lead to a 1,000 fold increase in cortical surface area (Rakic, 2009).

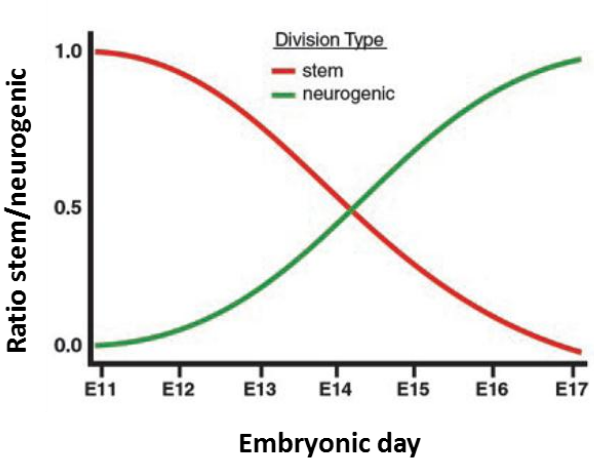

Figure 1.4. Symmetric versus asymmetric divisions during mouse neurogenesis.
The ratio of symmetric proliferative divisions (red) and asymmetric neurogenic divisions (green) is altered over the course of mouse neurogenesis (embryonic day 11-17). (Reproduced from Haydar *et al.*, 2003)

1.1.5. Regulation of the number of neural progenitor cells

The final number of neural progenitor cells is affected by changes to cell fate choice and cell survival. Each of these factors is described in detail below.

1.1.5.1. Cell fate determination

1.1.5.1.1. Apical and basal polarity

The neuroepithelial cells and radial glia that populate the ventricular zone are polarised at the apical and basal axis, maintaining contact with the ventricular surface and basal lamina throughout the cell cycle (Gal *et al.*, 2006; Hartfuss *et al.*, 2003; Noctor *et al.*, 2002). Neuroepithelial cells and radial glial can undergo symmetric or asymmetric divisions (reviewed by Huttner and Kosodo, 2005) and their apical and basal polarity is thought to impact on the mode of division of these cells (reviewed by Fietz and Huttner, 2010; Gotz and Huttner, 2005). The plasma membrane and associated cell cortex at the apical and basal poles are unique in composition (reviewed by Gotz and Huttner, 2005) and recently a number of associated proteins have been demonstrated to promote cell renewal and influence cell fate choice (reviewed by Fietz and Huttner, 2010). For example in mice, inheritance of the Par3 constituent of the apical cell cortex (Bultje *et al.*, 2009; Marthiens and ffrench-Constant, 2009) has been shown to influence daughter cell fate choice, with overexpression of Par3 promoting proliferation and Par3 depletion leading to neurogenesis (Bultje *et al.*, 2009; Costa *et al.*, 2008). In addition, some of the receptors important in mediating attachment to the basal lamina, such as integrin β1 and laminin α_2 and α_4 also promote progenitor cell fate (Radakovits *et al.*, 2009).

1.1.5.1.2. Spindle orientation and the segregation of cell fate determinants

The distribution of the apical and basal membranes to the daughter cells is ultimately determined by the alignment of the mitotic spindle in relation to the apical-basal axis. The final spindle orientation is established during metaphase (Haydar *et al.*, 2003); this specifies the position of the cytokinesis furrow (Rappaport, 1996) and the segregation of cell fate determinants to the daughter cells. Both the centrosome,

which nucleates microtubule asters, and some polarity determinants, that link the astral microtubules to the cell cortex, are required to correctly orientate the mitotic spindle (reviewed by Buchman and Tsai, 2007).

In *Drosophila* neuroblasts spindle pole orientation is important to actively control asymmetric cell divisions (reviewed by Gonczy, 2008; Knoblich, 2010). Early in the cell cycle one centrosome accumulates significant levels of pericentriolar material which enables it to nucleate a robust microtubule network and position the centrosome at the apical membrane (Figure 1.5). The second centrosome is devoid of PCM and moves through the cytoplasm until mitosis when it accumulates PCM and aligns at the basal membrane (Conduit and Raff, 2010; Januschke *et al.*, 2011; Rebollo *et al.*, 2007; Rusan and Peifer, 2007). In *Drosophila*, centrosome dysfunction (Basto *et al.*, 2006; Giansanti *et al.*, 2001; Lucas and Raff, 2007) or disruption of astral microtubules (Siller and Doe, 2008) leads to errors in the positioning of the spindle and often failed asymmetric neuroblast divisions.

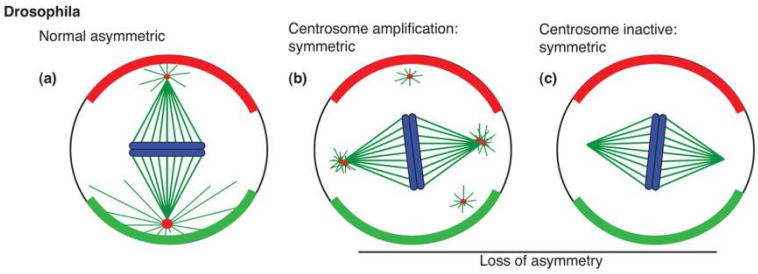

Figure 1.5. Asymmetric neuroblast divisions in *Drosophila*.
(a) Normal asymmetric neuroblast division. One centrosome, with a significantly expanded PCM, nucleates a robust array of microtubules to position the centrosome at the apical cortex (green). The other centrosome with less PCM moves through the cell, until prometaphase when it accumulates PCM and becomes positioned at the basal cortex (red). Correct spindle orientation in relation to apical and basal cortex can be lost by (b) centrosome amplification (Basto *et al.*, 2008), (c) loss of centrosomes (Basto *et al.*, 2006) or disruption of astral microtubules (Siller and Doe, 2008) which can often lead to a symmetric cell division. (Figure adapted from Megraw *et al.*, 2011).

In rodents, the centrosome and polarity determinants are thought to play a crucial role in the control of spindle pole orientation during symmetric divisions (Fietz and Huttner, 2010; Fish *et al.*, 2008; Gotz and Huttner, 2005). In many invertebrate systems such as *Drosophila* embryonic neuroblasts the mitotic spindle oscillates by 90° between symmetric and asymmetric divisions (Kaltschmidt *et al.*, 2000). However in the mammalian cerebral cortex, horizontal cleavages have not been widely reported (Estivill-Torrus *et al.*, 2002; Landrieu and Goffinet, 1979; Silva *et al.*, 2002; Smart, 1973). The mitotic spindle is usually vertical or nearly vertical and it is subtle changes in its orientation that is required to shift the plane of cell division from bisecting to bypassing the apical and basal membrane (Attardo *et al.*, 2008; Fish *et al.*, 2006; Kosodo *et al.*, 2004). The apical and basal membrane comprise of only 1-2% of the total cell membrane (Kosodo *et al.*, 2004) and so to ensure their equal segregation the positioning of the mitotic spindle has to be very precise. Loss of accuracy could lead to an increase in asymmetric divisions (Figure 1.6). Indeed in some cases disruption of the centrosome or microtubules did alter spindle orientation in neuronal progenitor cells correlating with a decrease in the progenitor cell population and increase in neuronal cell population thought to reflect an increase in asymmetric divisions (Feng and Walsh, 2004; Fish *et al.*, 2006; Lizarraga *et al.*, 2010). In addition, a reduction in brain size was often reported (Feng and Walsh, 2004; Lizarraga *et al.*, 2010). However in contrast to these results, spindle orientation and plane of cytokinesis was altered in mouse neuronal progenitor cells depleted of polarity determinant LGN without affecting the progenitor population. Cells were displaced from the ventricular zone but continued to proliferate maintaining a normal rate of neuronal production and unperturbed brain size (Konno *et al.*, 2008). Similar results were observed following depletion of LGN in neuroepithelium of chick embryo (Morin *et al.*, 2007). These findings suggest that cell fate choice is set regardless of spindle positioning and apical basal membrane inheritance. Thus, further work is required to examine the precise role spindle orientation and segregation of apical and basal domains plays in rodent cell fate choice.

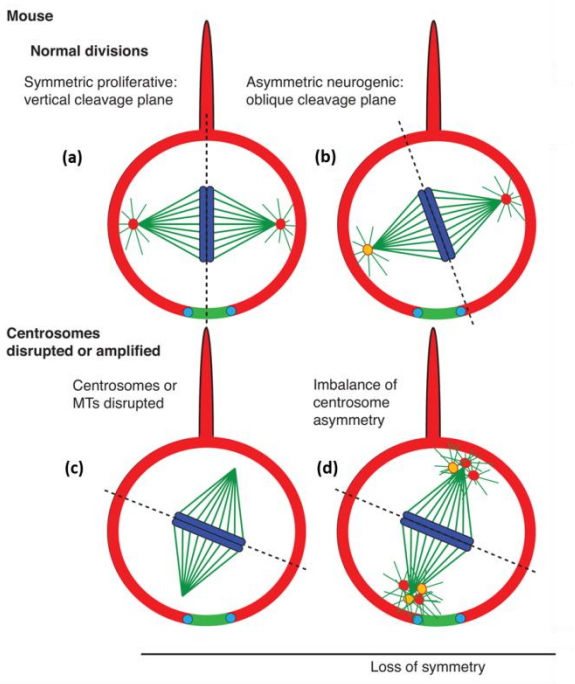

Figure 1.6. Symmetric and asymmetric cell divisions of mouse neuronal progenitors. (a) During normal symmetric divisions the cleavage plane bisects the apical domain and basal process. (b) During asymmetric divisions the plane of division bypasses the apical or basal process leading to asymmetric inheritance of cell fate determinants into daughter cells. (c & d) Spindle orientation is affected if the centrosomes or microtubules are disrupted, in some cases leading to asymmetric cell divisions. (Figure adapted from Megraw *et al.*, 2011)

1.1.5.1.3. Centrosome asymmetry

The centrosome pair that coordinate mitotic spindle pole orientation are not morphologically identical. Each centrosome consists of a pair of centrioles surrounded by PCM (reviewed by Azimzadeh and Bornens, 2007). One centrosome contains the mother centriole which is older than the other centrioles and contains unique structural appendages (Vorobjev and Chentsov Yu, 1982). Centrosome asymmetry is linked to cell fate choice in rodent radial glia. The centrosome, containing the oldest mother centriole is inherited by the radial progenitor cells whereas the centrosome containing the younger mother centriole is inherited by the differentiating cell (Wang *et al.*, 2009). Disrupting the unique appendages required for the mother centriole to mature, led to a reduction of the progenitor cell population linking centriole maturation to cell fate choice (Wang *et al.*, 2009).

Mechanistically it is unclear how centriole age could specify cell fate and a number of hypotheses have been proposed (Stearns, 2009). One possibility is that the appendages of the oldest mother centriole enable this centrosome to nucleate a more robust network of microtubules allowing accumulation of proteins that influence cell fate (Fuentealba *et al.*, 2008; Jakobsen *et al.*, 2011). Alternatively, the oldest mother centriole may be mediating an effect via the primary cilium; a microtubule based hair-like structure that emanates from most mammalian cell's surface. Primary cilia are also present in apical domains of neural progenitors and can act as a sensory organelle to transduce signals from the environment into the cell to regulate the proliferation and specification of these cells (reviewed by Lee and Gleeson, 2011; Louvi and Grove, 2011). The age of the mother centriole determines the timing of cilia formation in the two daughter cells following cell division (Anderson and Stearns, 2009). The cell that harbours the older mother centriole generates its primary cilium before its sister cell and as a result the two cells may differ in their response to extrinsic signals which may influence cell fate choice.

Centrosome asymmetry has also been reported in *Drosophila* stem cells. In the germline cells of male *Drosophila* the mother centrosome is always retained in the stem cell (Yamashita *et al.*, 2007). In *Drosophila* neuroblasts it is the younger daughter centrosome that is maintained in the stem cell and the mother centrosome is inherited into the neuroblast (Conduit and Raff, 2010; Januschke *et al.*, 2011). Thus, centrosome asymmetry may be a conserved feature of polarised stem cells.

1.1.5.1.4. Cell cycle length hypothesis

In the developing cerebral cortex the transition from proliferative to neurogenic cell divisions is accompanied by an increase in cell cycle length (Takahashi *et al.*, 1995b). Specifically, this is due to a lengthening of G_1 phase, all other cell cycle phases remain unchanged (Takahashi *et al.*, 1995b). Rather than a uniform change in cell cycle length of all cortical progenitor cells undergoing proliferative or neurogenic divisions (Cai *et al.*, 1997) it was established that it was the neurogenic subpopulation that had a significantly longer cell cycle than the proliferative population (Calegari *et al.*, 2005).

There are concerted mechanisms that control G_1 length and cell fate choice. Mitogenic factors such as bFGF can lead to a decrease in G_1 length whereas differentiation promoting factors such as NT3 can lead to an increase in G_1 length (Lukaszewicz *et al.*, 2002). Recent evidence has now convincingly demonstrated a causal relationship between cell cycle length and cell fate choice. Overexpression of CDK4/cyclin D1 or forced expression of cyclin D1 or E1 can shorten the length of G_1 phase, increasing the proportion of proliferative divisions during neurogenesis (Lange *et al.*, 2009; Pilaz *et al.*, 2009). In addition knockout of cyclin D2 in mouse could lengthen G1 phase leading to the opposite effect with a reduction in the progenitor population (Glickstein *et al.*, 2009)

How could an increase in the length of G_1 phase promote neurogenic divisions? One possible answer to this question has been addressed by the cell cycle length hypothesis (Calegari and Huttner, 2003). This hypothesis is based on the idea that cell fate is influenced by extrinsic and intrinsic factors, such as mitogenic and differentiating signals, that often exert their influence during G_1 phase of the cell cycle (Baek *et al.*, 2003). The length of the cell cycle corresponds to a window of increased sensitivity to these factors and they may only induce a certain cell fate if allowed to function for a sufficient length of time. In a short G_1 phase, cell fate determinants do not have sufficient time to induce differentiation and so both daughter cells maintain progenitor cell fate. If the G_1 phase is longer, cell fate determinants may be able to induce differentiation in one but not the other daughter cell. The unequal exposure to cell fate determinants may depend on cell intrinsic factors or depend on the location of the daughter cells within the developing cortex (Figure 1.7).

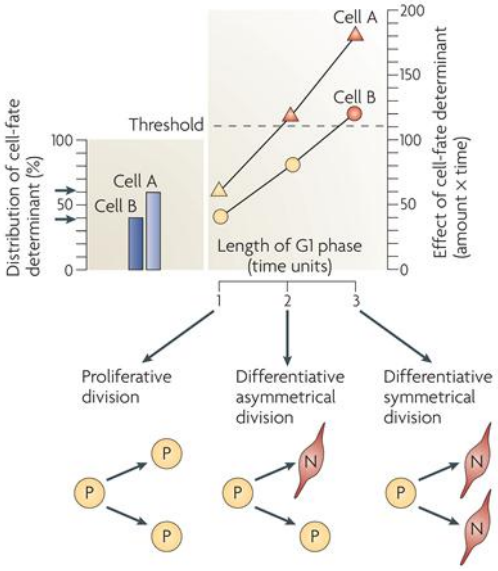

Figure 1.7. The cell-cycle length hypothesis.
A neurogenic cell-fate determinant is distributed unequally to daughter cells A and B (60% and 40% respectively). In a short G_1 phase length (time unit 1) both daughter cells will proliferate. An intermediate time in G_1 phase (time unit 2), daughter cell A will become a neuron and B will become a progenitor cell. At the longest G_1 length (time unit 3) both cell A and B will become neurons. (Figure reproduced from Gotz and Huttner, 2005)

1.1.5.1.5. Cilia and cell cycle length

Recently a link between cilia and the control of cell cycle length has been established. Cilia formation is cell cycle regulated process that occurs in quiescent (G_0) cells and is reabsorbed as cells re-enter the cell cycle (reviewed by Pan and Snell, 2007). Recently it has been demonstrated that the cilia can actually influence the timing of cell cycle entry. Two interacting proteins of the microtubule motor protein dynein, NDE1 and TCTEX-1, that control cilia length and reabsorption respectively also influence the timing of progression into S-phase of the cell cycle in a cilia dependent manner (Kim *et al.*, 2011; Li *et al.*, 2011). The cell cycle-length hypothesis (Section 1.5) predicts changes to the length of G_1 phase would affect cell fate choice during neuronal development. Indeed, *Tctex-1* knockdown in mouse (which led to increased time in G_1 phase) induced premature neuronal differentiation and overexpression of T94E variant TCTEX-1 (which led to an increase in S-phase) induced loss of neuronal differentiation (Li *et al.*, 2011).

1.1.5.2. Apoptosis

In addition to the mode and rate of cell divisions, the survival of the neuronal progenitor cells is also an important factor determining the size of the progenitor population. Widespread neuronal cell death does occur during fetal development (Haydar *et al.*, 1999; Thomaidou *et al.*, 1997) and perturbation of this process can greatly increase brain size. For example, inactivation of caspase 3 or caspase 9 (two of the effectors of apoptosis) decreases apoptosis of the progenitor cell population resulting in an enlarged cerebral cortex with an increased surface area (Kuida *et al.*, 1998; Kuida *et al.*, 1996). Conversely, activation of Notch and Ephrin A signalling leads to an increase in apoptosis, a reduction in the progenitor population and cortical size (Depaepe *et al.*, 2005; Yang *et al.*, 2004). The dramatic changes in cortical surface area observed by increasing or decreasing the rate of apoptosis is consistent with the principles of the radial-unit hypothesis (Figure 1.8) (Rakic, 1988) implicating apoptosis as a potential evolutionary regulator of cerebral cortex size.

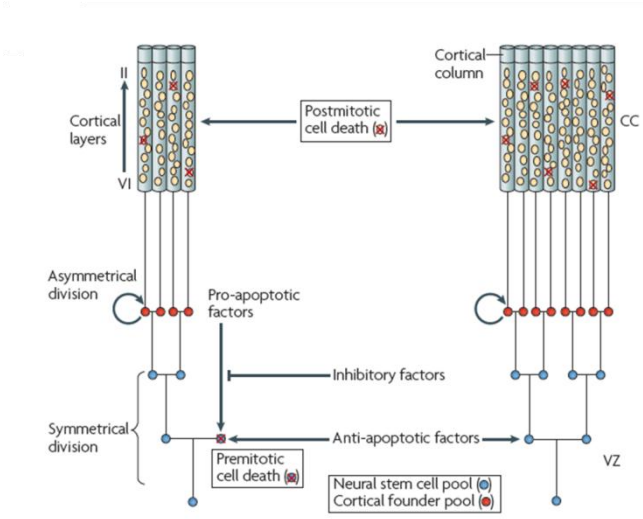

Figure 1.8. Effect of apoptosis on progenitor cell population and final brain size.
This model illustrates how changes to the rate of programmed cell death during the symmetric divisions of the neuronal progenitor cell population in the ventricular zone (VZ) can have a dramatic effect on the number of radial columns at the cerebral cortex (CC). This results in surface expansion of the cerebral cortex without changes in thickness (panel 2). In contrast, changes to the rate of programmed cell death during asymmetric divisions would affect the number of neurons within a radial column changing the thickness but not surface area of the cerebral cortex. (Figure reproduced from Rakic, 2009).

1.1.6. Conclusion

During human evolution there has been expansion of the cerebral cortex. This reflects lateral expansion of the cerebral cortex likely to be caused by an increase in the neuronal progenitor cell population. Expansion of the neuronal progenitor population could be accomplished by changes to cell survival or cell fate choice. Some of the proteins that play a role in these processes have been identified through mouse models or evolutionary studies but many of the proteins that play a role in brain size are unknown. Another way to identify candidate regulators of brain size is through the study of genetic neurodevelopmental disorders of brain size.

1.2. Autosomal recessive primary microcephaly

1.2.1. The clinical phenotype of primary microcephaly

Microcephaly is characterised by a reduced head circumference, at least 3 standard deviations below the age and sex-related mean (Ross and Frias 1977). Head circumference is used as a proxy measurement of brain size as the skull also enlarges concomitantly with brain growth. Thus the underlying cause of microcephaly is reduced growth of the brain.

Microcephaly can be caused by environmental and maternal factors such as maternal alcohol consumption during pregnancy or congenital toxoplasmosis (Cowie, 1960). In the absence of environmental and maternal factors genetic factors are considered (Bundey, 1992; Qazi and Reed, 1973). Primary microcephaly is a genetic disorder in which microcephaly occurs in isolation without any other malformations (Ross, 1977).

Primary microcephaly patients present with a significantly reduced head circumference at birth (Roberts *et al.,* 2002). Neuroimaging shows that there is a significant reduction in brain volume with size of the cerebral cortex most significantly affected (Figure 1.9)(Bond *et al.,* 2002). Consistent with the small size of the brain, some reduction in the volume of white matter and simplification of the gyral patterning is evident (McCreary *et al.,* 1996). In most cases, the architecture of

the brain is normal suggesting that defects in neuronal migration are unlikely (Bond *et al.*, 2002; Bond *et al.*, 2005; Guernsey *et al.*, 2010).

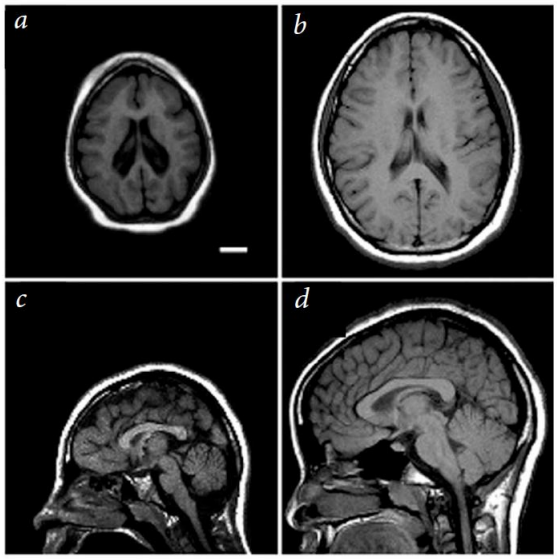

Figure 1.9. Neuroimaging of primary microcephaly patient.
Axial (A & B) and sagittal (C & D) magnetic resonance images (MRI) of primary microcephaly patient (A & C) and an unaffected individual of similar age and sex (B & D). The primary microcephaly patient shows significant reduction in the size of the cerebral cortex and simplification of the cerebral cortex gyral patterning. (Figure reproduced from Bond *et al.,* 2002).

All patients with primary microcephaly present with mental retardation (mild to severe) but do not show progressive decline in cognitive abilities or significant neurological deficits (Roberts *et al.*, 2002). Mild seizures have been reported in several cases (Darvish *et al.*, 2010; Passemard *et al.*, 2009; Shen *et al.*, 2005). Primary microcephaly is considered primarily a disorder of brain growth and usually normal height and weight are reported. However in some cases a reduction in height can occur but it is not as marked at the degree of microcephaly (Darvish *et al.*, 2010; Passemard *et al.*, 2009; Trimborn *et al.*, 2004).

1.2.2. Primary microcephaly, Seckel and MOPD-II

The extensive characterisation of primary microcephaly patients in recent years has broadened the phenotypic spectrum and it has become clear that there is overlap with primordial dwarfism disorders such as Seckel syndrome and microcephalic osteodysplastic primordial dwarfism-type II (MOPD-II) (Majewski and Goecke, 1982). Both Seckel syndrome and MOPD-II have microcephaly of similar severity to primary microcephaly but are accompanied with substantially, usually proportionate, short stature. Patients diagnosed with MOPD-II additionally present with distinct skeletal abnormalities which differentiate it from Seckel syndrome (Hall *et al.*, 2004). The molecular genetics of these disorders has highlighted the phenotypic relationship as Seckel syndrome and primary microcephaly share some disease causing genes (Section 1.2.5.2).

1.2.3. The primary microcephaly genes

Primary microcephaly is a rare autosomal recessive genetic disorder with incidence estimates ranging from 1/30,000 to 1/250,000 in different populations (Komai *et al.*, 1955; Van Den Bosch, 1959). It is genetically heterogeneous and currently seven causative genes have been identified: encoding MCPH1 (Jackson *et al.*, 2002), WDR62 (Bilguvar *et al.*, 2010; Nicholas *et al.*, 2010; Yu *et al.*, 2010), CDK5RAP2 (Bond *et al.*, 2005), CEP152 (Guernsey *et al.*, 2010), ASPM (Bond *et al.*, 2002), CPAP (Bond *et al.*, 2005) and STIL (Kumar *et al.*, 2009). Further genetic heterogeneity is likely to exist since at least 30% of primary microcephaly families of Pakistan, Indian and Iranian ethnicity do not show linkage to any of the seven loci identified (Darvish *et al.*, 2010; Gul *et al.*, 2006; Kumar *et al.*, 2004; Roberts *et al.*, 2002) .

1.2.4. Paralogues and orthologues of primary microcephaly proteins

Orthologues and paralogues of the primary microcephaly genes have been identified (Table 1.2). One potential explanation to account for brain specific phenotype in primary microcephaly patients is the existence of paralogues in humans that can supply functional redundancy in all tissues except the brain (first proposed in (Bond

and Woods, 2006). Indeed characterised paralogues exist for CDK5RAP2, WDR62 and CPAP, namely myomegalin, MAPKBP1 and TCP10 respectively (Hung *et al.*, 2000; Nicholas *et al.*, 2010; Verde *et al.*, 2001). In addition potential paralogues for CEP152, ASPM and CPAP have also recently been identified (Megraw *et al.*, 2011). Further work to determine if there are differences in tissue expression and functional redundancy between primary microcephaly proteins will substantiate this hypothesis.

Table 1.2. Primary microcephaly genes paralogues and orthologues

Gene	Other names	Paralogues	Orthologues	
			D. melanogaster	***C. elegans***
MCPH1	BRIT1	None	Mcph1	W04A8.1?
WDR62	-	MAPKBP1	CG7337	H24G06.1
CDK5RAP2	CEP215	Myomegalin	Centrosomin (Cnn)	SPD-5?
CEP152	-	C10orf118	Asterless (Asl)	None
ASPM	-	hSif1	Abnormal spindle (Asp)	ASPM-1
CPAP	CENPJ	TCP10	dSas4	SAS-4
STIL	SIL	None	Ana2	SAS-5

1.2.5. The mutations in primary microcephaly genes

In this section I describe the mutation spectrum for each primary microcephaly gene and make predictions on the potential effect these mutations have on the proteins they encode (Section 1.2.5). I then address the evolution of these genes (Section 1.2.6) and describe the function of each of the primary microcephaly proteins (Section 1.3).

1.2.5.1. MCPH1

Microcephalin (MCPH1) is the focus of this thesis and so the MCPH1 mutations causative of primary microcephaly is described in detail. *MCPH1* is a 14 exon gene that encodes an 835 amino acid protein with 3 BRCA1 C-terminal domains (BRCT) (Jackson *et al.*, 1998). The 13 reported *MCPH1* mutations comprise of nonsense mutations, large deletions and missense mutations (Summarised in Figure 1.10 and Table 1.3) (Alderton *et al.*, 2006; Darvish *et al.*, 2010; Jackson *et al.*, 2002; Leung *et al.*, 2011; Trimborn *et al.*, 2005).

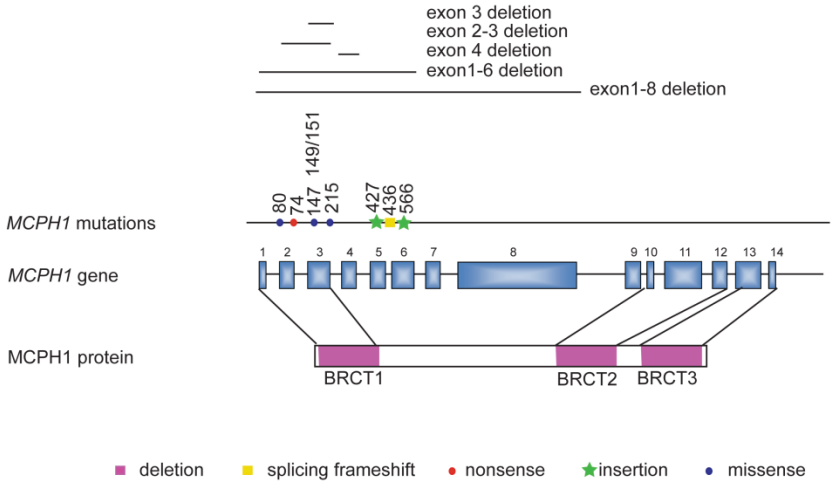

Figure 1.10. Primary microcephaly mutations in *MCPH1*.
The type and location of MCPH1 mutations are represented on a schematic of the *MCPH1* gene and protein. Exons are depicted as blue boxes and BRCT protein domains are represented by the purple boxes. (Original data from Alderton *et al.*, 2006; Darvish *et al.*, 2010; Jackson *et al.*, 2002; Kaindl *et al.*, 2010; Leung *et al.*, 2011; Trimborn *et al.*, 2005)

Table 1.3. Summary of *MCPH1* mutations

Gene mutation	Predicted protein effect	Reference
c. 74C>G	S25X	(Jackson *et al.*, 2002)
c. 80C>G	T27R	(Trimborn *et al.*, 2005)
c. 147C>G	H49E	(Darvish *et al.*, 2010)
c. 149T>G/151A>G	V50G/ I51V	(Leung *et al.*, 2011)
c. 215C>T	S72L	(Darvish *et al.*, 2010)
c. 427InsA	143fs	(Alderton *et al.*, 2006)
c. 436+1G>T	splicing	(Darvish *et al.*, 2010)
c. 566InsA	N189fs	(Darvish *et al.*, 2010)
c. del exon 3	Truncated protein	(Darvish *et al.*, 2010)
c. del exon 2-3	Truncated protein	(Darvish *et al.*, 2010)
c. del exon 4	Truncated protein	(Darvish *et al.*, 2010)
c. del exon 1-6	No protein product	(Darvish *et al.*, 2010)
c. del exon 1-8	No protein product	(Leung *et al.*, 2011)

The presence of large homozygous genomic deletions in conjunction with multiple frameshift mutations suggest that complete loss of function of MCPH1 can cause primary microcephaly. Indeed, lymphoblastoid cell lines (LBC) derived from patients with *MCPH1*$^{\Delta ex1\text{-}8}$, *MCPH1*^{C74G} and *MCPH1*^{427InsA} mutations lacked detectable MCPH1 protein (Alderton *et al.*, 2006; Leung *et al.*, 2011; Tibelius *et al.*, 2009).

The highly conserved BRCT1 domain may be a functionally critical domain since all four missense mutations are clustered here and a truncated MCPH1 protein missing some of this domain has been reported in a primary microcephaly patient (Figure 1.10) (Darvish *et al.*, 2010; Leung *et al.*, 2011; Trimborn *et al.*, 2005). Further investigation into the consequences of these missense mutations on the protein they encode will help establish the potential contribution of this domain to disease pathogenesis.

1.2.5.2. Other primary microcephaly genes

The mutations identified in the other primary microcephaly genes are summarised in Figure 1.11.

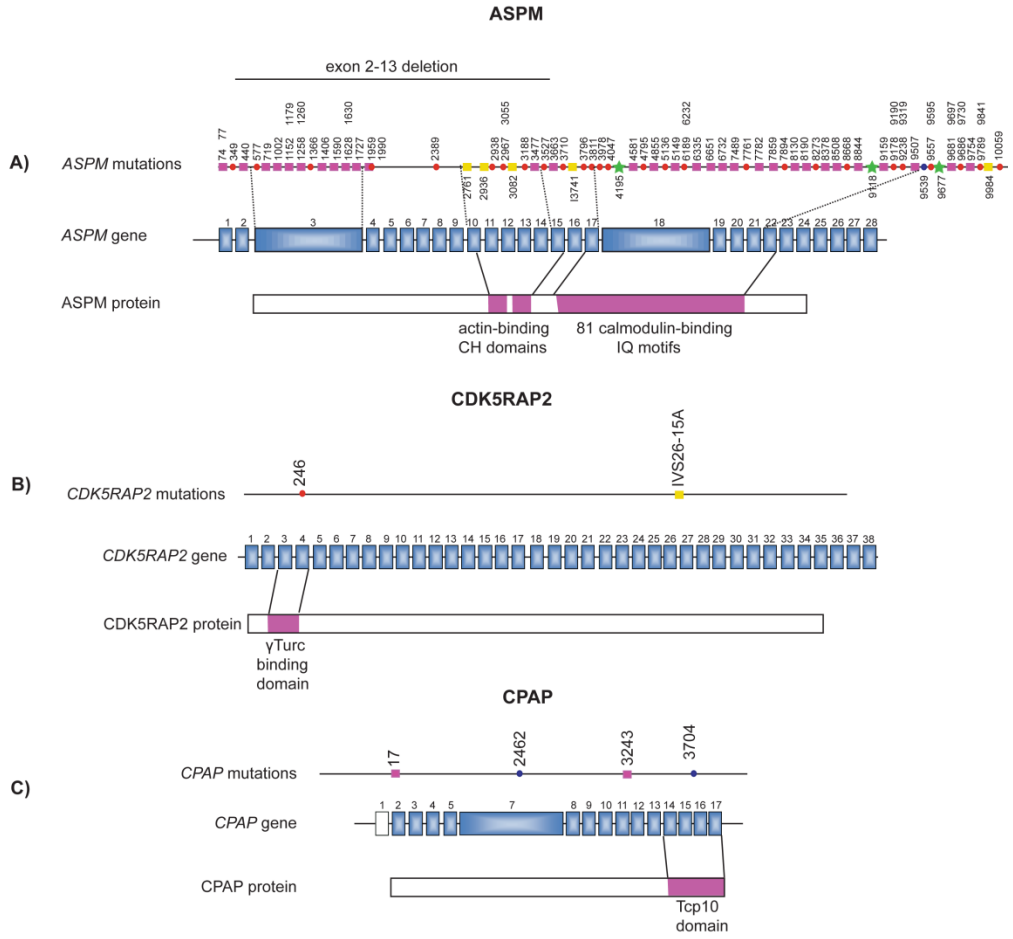

Figure 1.11. Primary microcephaly mutations within *ASPM*, *CDK5RAP2*, *CPAP*, *STIL*, *WDR62* and *CEP152*.
Schematic representation of primary microcephaly genes (A) *ASPM* (B) *CDK5RAP2* (C) *CPAP* (D) *STIL* (E) *WDR62* (F) *CEP152*. The exons are depicted by blue boxes with substantially larger exons expanded. Protein domains are represented by the purple boxes. The position and type of mutation causative of primary microcephaly are shown next to the gene and protein. Mutations leading to severe cortical malformations (E) and Seckel syndrome (F) are also represented. (Original data from Bhat *et al.*, 2011; Bilguvar *et al.*, 2010; Bond *et al.*, 2002; Bond *et al.*, 2005; Bond *et al.*, 2003; Darvish *et al.*, 2010; Guernsey *et al.*, 2010; Gul *et al.*, 2006; Kaindl *et al.*, 2010; Kalay *et al.*, 2010; Kumar *et al.*, 2004; Kumar *et al.*, 2009; Muhammad *et al.*, 2009; Nicholas *et al.*, 2010; Nicholas *et al.*, 2009; Saadi *et al.*, 2009; Shen *et al.*, 2005; Yu *et al.*, 2010).

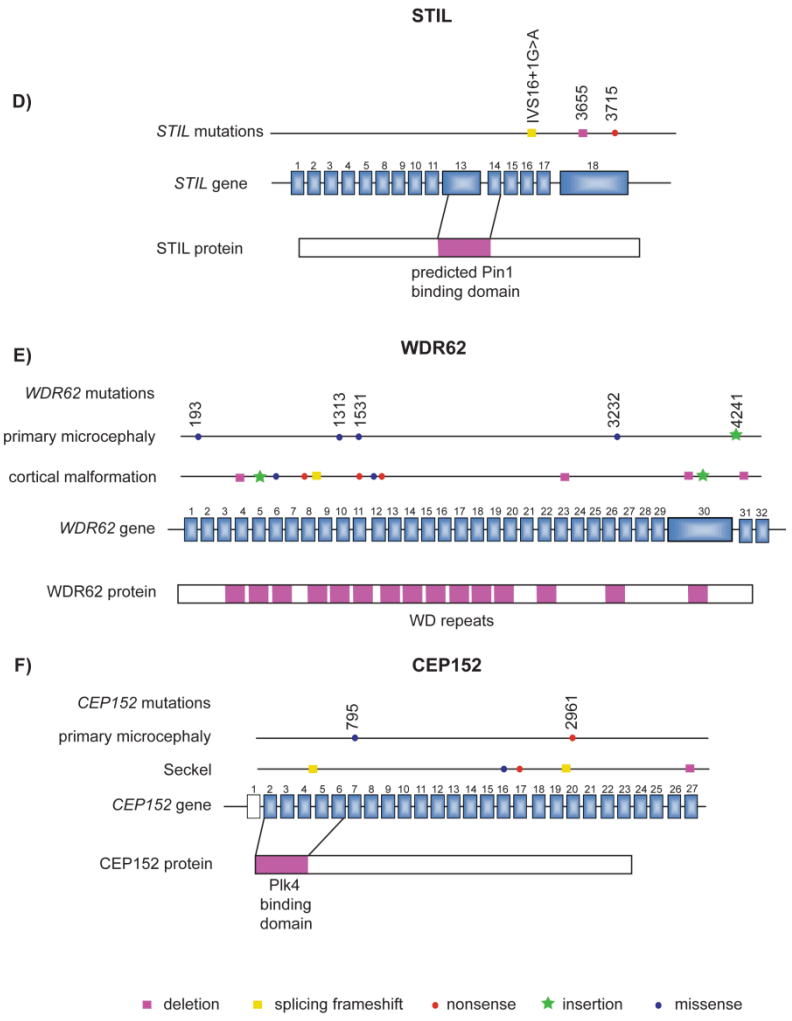

Figure 1.11. Primary microcephaly mutations within *ASPM*, *CDK5RAP2*, *CPAP*, *STIL*, *WDR62* and *CEP152*.
Schematic representation of primary microcephaly genes (A) *ASPM* (B) *CDK5RAP2* (C) *CPAP* (D) *STIL* (E) *WDR62* (F) *CEP152*. The exons are depicted by blue boxes with substantially larger exons expanded. Protein domains are represented by the purple boxes. The position and type of mutation causative of primary microcephaly are shown next to the gene and protein. Mutations leading to severe cortical malformations (E) and Seckel syndrome (F) are also represented. (Original data from Bhat *et al.*, 2011; Bilguvar *et al.*, 2010; Bond *et al.*, 2002; Bond *et al.*, 2005; Bond *et al.*, 2003; Darvish *et al.*, 2010; Guernsey *et al.*, 2010; Gul *et al.*, 2006; Kaindl *et al.*, 2010; Kalay *et al.*, 2010; Kumar *et al.*, 2004; Kumar *et al.*, 2009; Muhammad *et al.*, 2009; Nicholas *et al.*, 2010; Nicholas *et al.*, 2009; Saadi *et al.*, 2009; Shen *et al.*, 2005; Yu *et al.*, 2010).

From investigating the primary microcephaly mutation spectrum (Figure 1.11) and that of allelic disorders a number of interesting observations can be made.

1) The presence of a large number of homozygous frameshift mutations dispersed throughout the *ASPM* gene and a homozygous genomic deletion of exon 2-13 (Nicholas *et al.*, 2009) suggests primary microcephaly can be caused by complete loss of ASPM protein (Figure 1.11A)(Bond *et al.*, 2002; Bond *et al.*, 2003; Darvish *et al.*, 2010; Gul *et al.*, 2006; Kumar *et al.*, 2004; Muhammad *et al.*, 2009; Nicholas *et al.*, 2009; Saadi *et al.*, 2009; Shen *et al.*, 2005).

2) The frameshift mutations identified in *CDK5RAP2* and *CPAP* are also likely to lead to be null alleles; however only a few mutations have been reported per gene and identification of more mutations would substantiate this hypothesis (Bond *et al.*, 2005) (Figures 1.11B & C).

3) The frameshift mutations identified in *STIL* may encode a truncated protein as STIL mutant transcripts would contain a premature terminating codon (PTC) in the last exon of the gene which may not be targeted for nonsense mediated decay (NMD) (Figure 1.11D)(Kumar *et al.*, 2009). In addition the splicing mutation reported for STIL may also be hypomorphic through a combination of exon skipping which is common for this type of mutation (Al-Dosari *et al.*, 2010).

4) The mutation spectrum of *WDR62* reveals a general correlation between missense mutations, possibly causing partial loss of protein function, resulting in primary microcephaly and frameshift mutations, leading to complete loss of protein function, resulting in a more severe phenotype with cortical malformations (Figure 1.11E) (Bhat *et al.*, 2011; Bilguvar *et al.*, 2010; Nicholas *et al.*, 2010; Yu *et al.*, 2010). Similarly there may be some association between hypomorphic CEP152 missense mutations and primary microcephaly (Guernsey *et al.*, 2010) and more severe frameshift mutations with Seckel syndrome (Figure 1.11F)(Kalay *et al.*, 2010).

5) Homozygous missense mutations have been identified in *ASPM* and *CPAP* which may pinpoint functionally critical domains (Figure 1.11A and C) (Bond *et al.*, 2005; Darvish *et al.*, 2010).

1.2.6. Adaptive evolution of the primary microcephaly genes

Primary microcephaly leads to a brain volume comparable in size to early hominids (Wood and Collard, 1999). Thus, through the primary microcephaly phenotype, loss of function of any of the primary microcephaly proteins has been implicated in the determination of brain size. It is tempting to speculate that gain of function evolutionary changes to the primary microcephaly genes may partly underlie changes in brain size during evolution.

Significantly, evolutionary studies of *MCPH1, ASPM, CDK5RAP2* and *CPAP* genes have demonstrated that they have undergone a period of positive selection during primate evolution (Evans a *et al.*, 2004; Evans b *et al.*, 2004; Evans *et al.*, 2006; Wang and Su, 2004). *MCPH1* and *ASPM* genes have been suggested to have continually responded to positive selection during the evolution of modern humans (Evans *et al.*, 2005; Mekel-Bobrov *et al.*, 2005). However these findings have been widely disputed (Currat *et al.*, 2006; Timpson *et al.*, 2007; Yu *et al.*, 2007) and it was argued that demographic effects of population growth could also explain these observations (Currat *et al.*, 2006). In addition numerous studies had not found a meaningful association between the human MCPH1 and ASPM haplotypes, reportedly associated with evolutionary selection, brain size or IQ (Dobson-Stone *et al.*, 2007; Mekel-Bobrov *et al.*, 2007; Rushton *et al.*, 2007; Timpson *et al.*, 2007; Woods *et al.*, 2006).

However, recently it has been demonstrated that some of the MCPH loci can contribute to variation in brain size and structure adding weight to these evolutionary findings. Two studies found an association between single nucleotide polymorphisms (SNPs) in MCPH1, ASPM or CDK5RAP2 loci and variation in brain size (Rimol *et al.*, 2010; Wang *et al.*, 2008). The studies of Rimol *et al*. (2010) and Wang *et al*. (2008) considered a larger number of SNPs, many of which were located outwith the coding sequence and contributed to sex-specific changes.

1.3. Function of primary microcephaly proteins

The primary microcephaly proteins play a role in a diverse range of functions. Here we focus on describing the functions of the primary microcephaly proteins in processes such as mitosis, cell cycle progression and checkpoint control that could impact neurogenesis. The focus of this thesis, MCPH1, is described in Section 1.5.

1.3.1. STIL, CPAP and CEP152- regulators of centriole duplication

1.3.1.1. Centriole duplication

The centrosome is composed of two cylindrical structures called centrioles surrounded by pericentriolar material (PCM) (reviewed by Azimzadeh and Bornens, 2007). The walls of centrioles are constructed of nine sets of microtubules arranged in a radially symmetric manner highly conserved among all species (reviewed by Azimzadeh and Marshall, 2010; Marshall, 2009). The centrioles are essential for the duplication of the centrosome, which occurs mainly during S phase of the cell cycle. At this stage, the two centrioles separate and a daughter centriole assembles at the proximal ends of each centriole (Chretien *et al.*, 1997; Kuriyama and Borisy, 1981; Vorobjev and Chentsov Yu, 1982). The initial structure used to build the daughter centriole can vary between species. In *C. elegans*, the earliest detectable structure is a central tube; microtubules assemble around its circumference to form the mature centriole (Figure 1.12A) (Pelletier *et al.*, 2006). In higher organisms, such as *Drosophila* and vertebrates, a cartwheel structure comprised of nine radial spokes projecting from a central hub is initially formed and microtubules assemble around this (Figure 1.12B) (Anderson and Brenner, 1971; Cavalier-Smith, 1974; Guichard *et al.*, 2010).

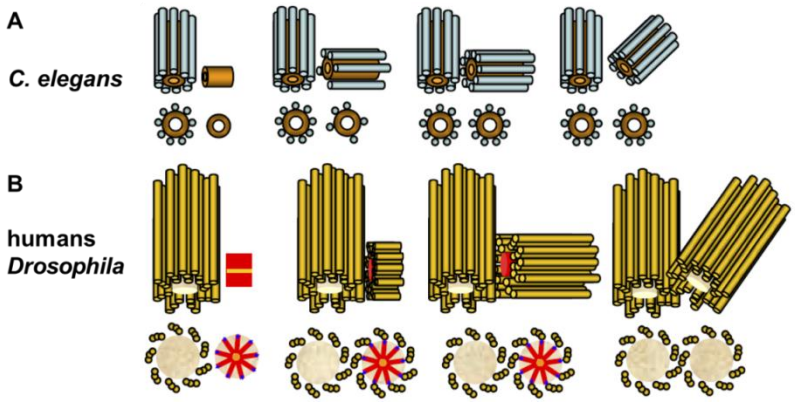

Figure 1.12 Centriole duplication in *C. elegans* and higher organisms.
(A) Schematic of procentriole formation in *C. elegans*. A central tube is formed perpendicular to the wall of the mother centriole. Nine microtubules assemble around the central tube as it increases in length. The central tube remains part of the daughter centriole. (B) Schematic of procentriole formation in higher organisms. A cartwheel structure is formed consisting of nine radial spokes emanating from a central hub. Microtubules assemble around the cartwheel and it increases in length. The cartwheel structure can be lost or remain in the daughter centriole depending on the species. (Figure reproduced from Loncarek and Khodjakov, 2009).

The process of centriole duplication is a highly ordered and well conserved sequence of events. The core components were initially identified in *C. elegans* by siRNA and mutation screens, this includes SPD-2 (Kemp *et al.*, 2004; Pelletier *et al.*, 2004), ZYG1 (O'Connell *et al.*, 2001), SAS-5 (Delattre *et al.*, 2004), SAS-6 (Leidel *et al.*, 2005) and SAS-4 (Leidel and Gonczy, 2003). These proteins are recruited in a specific order to assemble a procentriole (Figure 1.13A). SPD-2 and ZYG-1 are recruited prior to central tube formation and play a regulatory role in procentriole formation (Pelletier *et al.*, 2006). SPD-2 and ZYG-1 recruit SAS-5 and SAS-6 which are required for central tube formation. Finally SAS-4 is recruited and is required for the addition of microtubules to the perimeter of the central tube (Pelletier *et al.*, 2006).

Counterparts of all these proteins have been identified in other species such as *Drosophila* and humans and in most cases there is some functional conservation between species (Figure 1.13B). The only exception is SPD-2, although human and *Drosophila* orthologues exist they do not play an essential role in centriole duplication (Dix and Raff, 2007; Giansanti *et al.*, 2008; Gomez-Ferreria *et al.*, 2007; Zhu *et al.*, 2008). In *Drosophila* and humans there are also a few additional proteins

that play a role in procentriole formation that have not been identified in *C. elegans* (Dobbelaere *et al.*, 2008; Goshima *et al.*, 2007; Kleylein-Sohn *et al.*, 2007). Very significantly, three primary microcephaly proteins are orthologues of these *C. elegans* proteins with conserved roles in centriole duplication.

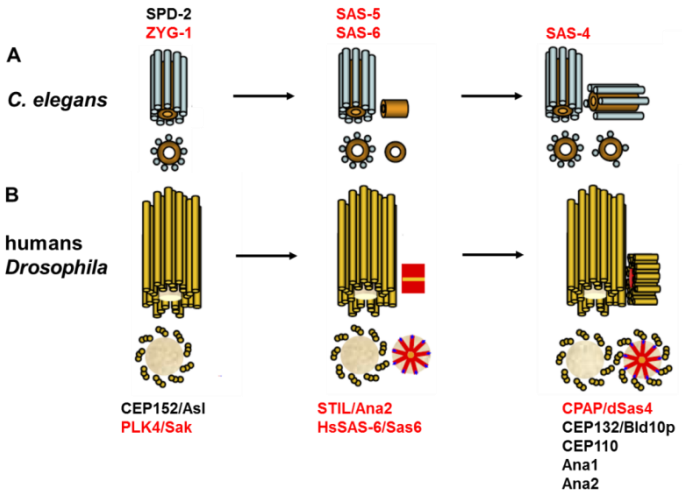

Figure 1.13. Functional conservation of proteins essential for procentriole formation. Proteins required for centriole duplication in *C. elegans* (A), *Drosophila* and humans (B). The proteins highlighted in red have functional orthologues in *C. elegans*, *Drosophila* and humans.(Figure adapted from Loncarek and Khodjakov, 2009).

1.3.1.2. STIL

It has recently been demonstrated that the primary microcephaly protein STIL is orthologous to the *C. elegans* SAS-5 protein and *Drosophila* Ana2 protein (Stevens *et al.*, 2010a). In *C. elegans* embryos SAS-5 is essential for centriole duplication (Delattre *et al.*, 2004) and with SAS-6 is required to form the central tube, the first step in *C. elegans* procentriole formation (Pelletier *et al.*, 2006). In *Drosophila*, Ana2 plays a similar role in the early steps of centriole formation required with dSas6 to form the building blocks of the procentriole cartwheel structure (Stevens *et al.*, 2010b). In fact, overexpression of Ana2, Sak and dSas-6 in *Drosophila* spermatocytes is sufficient to drive formation of highly ordered structures resembling the inner cartwheel (Stevens *et al.*, 2010b). The role of Ana2 in centriole duplication has been established from RNAi screens of S2 cells (Dobbelaere *et al.*, 2008;

Goshima *et al.*, 2007). *Drosophila ana2* mutant flies have not been reported and so the role of Ana2 in fly development has not been established.

It has not been definitively confirmed that STIL plays a role in centriole duplication in vertebrates but it appears likely that it is required for this process. In zebrafish loss of function of Stil is embryonic lethal. Embryos show evidence of a mitotic defect with disorganised mitotic spindles often lacking one or both centrosomes (Pfaff *et al.*, 2007). It was also reported that *Stil*$^{-/-}$ mouse embryonic fibroblast (MEF) cells often lacked detectable centrioles (Castiel *et al.*, 2010). In addition, *Stil* mutant mice showed defects characteristic of aberrant cilia function, such as randomized left–right asymmetry and neural tube abnormalities which may be caused by a centriolar defect (Izraeli *et al.*, 1999). In contrast, primary microcephaly patients with *STIL* mutations do not present with phenotypes characteristic of cilia defects (reviewed by Cardenas-Rodriguez and Badano, 2009) consistent with our hypothesis that *STIL* mutations lead to a C-terminal truncation in humans rather than loss of function (Section 1.2.5).

1.3.1.3. CPAP

The primary microcephaly protein CPAP and its orthologues in *Drosophila* and *C. elegans* are required for centriole duplication (Basto *et al.*, 2006; Kohlmaier *et al.*, 2009; Leidel and Gonczy, 2003). In humans, overexpression of CPAP leads to excessive lengthening of the parental and daughter centrioles (Kohlmaier *et al.*, 2009; Schmidt *et al.*, 2009; Tang *et al.*, 2009). Despite the extended centriolar structure, immunofluorescence and electron microscopy analysis demonstrated a morphology similar to genuine centrioles (Schmidt *et al.*, 2009; Tang *et al.*, 2009). Thus it was proposed that CPAP may be required to promote centriole elongation.

In *C. elegans* SAS-4 plays a role in the later stage of procentriole formation required for the addition of microtubules around the periphery of the central tube (Pelletier *et al.*, 2006). During human procentriole formation, the cartwheel structure is formed, microtubules are assembled and elongate (Figure 1.10). The first microtubule of the triplet is thought be nucleated from the γ-tubulin ring complex (γTuRC) assembled at the prximal end of the centriole (Guichard *et al.*, 2010). Echoing the findings in

worm, CPAP may play a role in procentriole elongation by promoting recruitment and/or attachment of microtubules to the centriole. Indeed CPAP can interact with α and β tubulin dimers and possesses microtubule depolymerisation activity (Hung *et al.*, 2004) which are essential for its role in centriole elongation (Tang *et al.*, 2009).

1.3.1.4. CEP152

CEP152 has been identified as an additional centriole duplication factor in humans and *Drosophila* which has not been identified in worms. It is required early in the procentriole formation pathway and may play a similar regulatory role to SDP2 in *C. elegans*.

In *Drosophila* the CEP152 orthologue, asterless (Asl), is required for centriolar duplication. Loss of Asl in *Drosophila* caused failure of centriole duplication with a reduction in the number of centrioles and centrosomes observed in mutant flies (Blachon *et al.*, 2008; Dobbelaere *et al.*, 2008). Asl functions early in the centriole duplication pathway where it appears to be acting as a molecular scaffold for Sak (ZYG-1 in *C. elegans*), necessary for its recruitment to the centriole and function in centriole duplication (Dzhindzhev *et al.*, 2010). Similar to dSas4 flies, *asl* knockout flies do survive into adulthood but they exhibit characteristics of a cilia defect including uncoordinated movement (due to loss of mechanosensory function in neurons) and immotile sperm (Basto *et al.*, 2006; Blachon *et al.*, 2008).

In vertebrates CEP152 also appears to be a critical component of the centriole assembly pathway. CEP152 morphilino depletion in zebrafish led to reduced cilia formation (Blachon *et al.*, 2008). In humans, depletion of CEP152 by RNAi prevents normal centriole duplication and PLK4 (ZYG-1 in *C. elegans* and Sak in *Drosophila*) overexpression mediated centrosome amplification (Cizmecioglu *et al.*, 2010; Dzhindzhev *et al.*, 2010; Hatch *et al.*, 2010). CEP152 functions early in the centriole assembly pathway, acting with PLK4 to initiate centriole formation and is required for CPAP and hSAS6 localisation to the centriole (Cizmecioglu *et al.*, 2010; Dzhindzhev *et al.*, 2010; Hatch *et al.*, 2010).

1.3.1.5. Centrioles and PCM recruitment

The centrioles act as a scaffold for the recruitment of PCM (Basto *et al.*, 2006; Bobinnec *et al.*, 1998; Conduit *et al.*, 2010; Kirkham *et al.*, 2003; Salisbury, 2003). Thus, the centriolar proteins such as CPAP, CEP152 and STIL may also play a role in establishing the size of PCM. Indeed a correlation between SAS-4 levels, centriole length and PCM size has been established in *C. elegans* (Kirkham *et al.*, 2003) and a relationship between Asl (CEP152) and PCM incorporation into centrosomes has also been established in *Drosophila* (Conduit *et al.*, 2010).

1.3.1.6. STIL, CPAP and CEP152 in primary microcephaly

STIL, CPAP and CEP152 or their orthologues play a key role in centriole biogenesis and it is likely that in their absence, centrioles and cilia would not be formed. Indeed, this is the case in *dsas4* and *asl Drosophila* models (Basto *et al.*, 2006; Dzhindzhev *et al.*, 2010). It seems to be very unlikely that humans lacking centrioles and cilia would only present with a small brain and be otherwise phenotypically normal, especially considering the key role cilia plays in human development (Goetz and Anderson, 2010). Thus, it could be hypothesised that primary microcephaly patient mutations in STIL, CPAP and CEP152 only lead to partial loss of protein function. This possibility is consistent with the mutation spectrum of STIL and CEP152 (Section 1.2.5.2.) and although complete loss of CPAP protein function was suggested due to CPAP mutation spectrum hypomorphic mutations could not be excluded.

1.3.2. CDK5RAP2 maintains centrosome structure

CDK5RAP2 appears to play a different role at the centrosome to CPAP, CEP152 and STIL. Whereas CPAP and CEP152 localise to the centrioles (Hatch *et al.*, 2010; Kleylein-Sohn *et al.*, 2007), CDK5RAP2 localises to the PCM surrounding the centrioles (Barrera *et al.*, 2010; Fong *et al.*, 2008) where it plays a key role in maintaining centrosome structure with a plethora of cellular phenotypes arising with its loss.

1.3.2.1. CDK5RAP2 as a microtubule organiser

CD5RAP2 belongs to the centrosomin family of proteins which are conserved from yeast to humans (Megraw *et al.*, 2011). Centrosomin proteins are composed of two highly conserved domains, called centrosomin motifs 1 and 2 (CNN1 and CNN2) (Barr *et al.*, 2010; Sawin *et al.*, 2004; Zhang and Megraw, 2007). The CNN1 domain is required for γ-tubulin recruitment and/or tethering in *S. pombe*, *Drosophila* and humans (Fong *et al.*, 2008; Sawin *et al.*, 2004; Venkatram *et al.*, 2004; Zhang and Megraw, 2007) which is important to confer microtubule nucleation capacity and organisation (reviewed by Luders and Stearns, 2007). In humans, the CNN1 region of CDK5RAP2 is sufficient to interact with members of the γ-TuRC playing a direct role in its recruitment to the PCM (Fong *et al.*, 2008). Independent of a role in γ-TuRC tethering, the CNN1 domain of CDK5RAP2 can also act as a regulator of microtubule nucleation, required to stimulate microtubule nucleation of purified γ-TURC (Choi *et al.*, 2010).

In *Drosophila*, Cnn plays a key role in assembling the PCM and is required for the recruitment of most PCM proteins tested during mitosis (Lucas and Raff, 2007; Megraw *et al.*, 1999; Vaizel-Ohayon and Schejter, 1999). In fact, only the depletion of Plk1 could equally perturb PCM protein recruitment and it is thought these two proteins could function together to initiate PCM maturation (Dobbelaere *et al.*, 2008).

CDK5RAP2 does not appear to play such a key role in assembling the PCM. Modest decreases in levels of PCM proteins, such as pericentrin, CEP192 and NEDD1 were reported following CDK5RAP2 RNAi in HeLa cells (Haren *et al.*, 2009) and a

reduction in AKAP450 was reported in chicken DT40 cells with loss of CNN1 or CNN2 domain (Barr *et al.*, 2010). This difference in phenotype between *Drosophila* and mammals may be due to the CDK5RAP2 mammalian paralogue myomegalin which also localises to the centrosome (Shimada *et al.*, 2007; Verde *et al.*, 2001) and may function redundantly with CDK5RAP2 partially compensating for its loss (Bond and Woods, 2006). It would be interesting to establish if depletion of CDK5RAP2 and myomegalin would lead to a similar phenotype as loss of Cnn.

1.3.2.2. CDK5RAP2 in centrosome structure

During the cell cycle, the centrosomes and centrioles undergo a number of conformational changes (reviewed by Azimzadeh and Bornens, 2007); CDK5RAP2 appears to play an important role in maintaining appropriate structure in accordance with cell cycle stage. In vertebrates, CDK5RAP2 plays a conserved role in maintaining cohesion between the two centrosomes until G_2 phase of cell cycle. This finding was established in an RNAi screen of HeLa cells, *Cdk5rap2*$^{-/-}$ MEFs and chicken DT40 cells, where loss of the CNN1 motif was sufficient to cause this phenotype (Barr *et al.*, 2010; Barrera *et al.*, 2010; Graser *et al.*, 2007b). The primary cause of loss of cohesion is unclear. A fibrous protein linker, consisting of proteins such as rootletin and C-NAP1 (Bahe *et al.*, 2005; Yang *et al.*, 2006), is thought to link two parent centrioles to maintain centrosome cohesion (Figure 1.14) and may be disrupted due to loss of CDK5RAP2 since parental centrioles were separated and displacement of rootletin was reported (Barrera *et al.*, 2010).

In addition to playing a role in centrosome cohesion, the CDK5RAP2 orthologue in mouse is also required to maintain centriole engagement between parent and daughter centriole (Barrera *et al.*, 2010) (Figure 1.14). This premature centriole disengagement appears to licence further centriole duplication which leads to formation of excess centrioles and multipolar mitosis in *Cdk5rap2*$^{-/-}$ MEFs (Barrera *et al.*, 2010). Centriole engagement usually persists until anaphase of mitosis, a process regulated by the separase protein and PLK1 (Tsou and Stearns, 2006; Tsou *et al.*, 2009), Cdk5rap2 may play a role in this regulatory process.

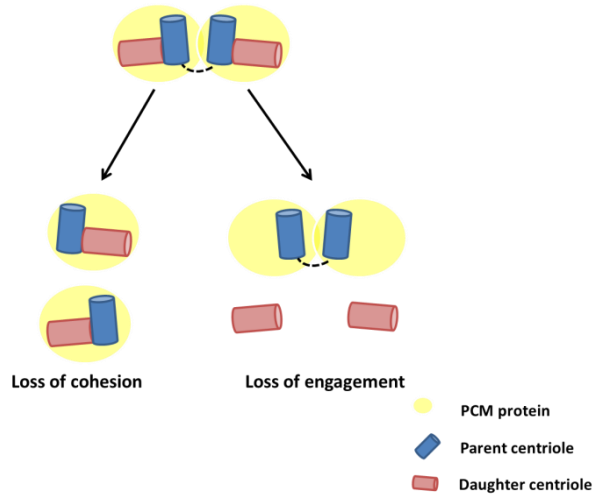

Figure 1.14. CDK5RAP2 in centriole linkage.
The centriole parent (blue) and daughter (pink) are tightly bound in an engaged state. Each centriole pair is connected by protein linker (dotted line) which runs between the parental centrioles and maintains centrosome cohesion. Loss of cohesion and engagement occurs at G_2 phase and anaphase respectively but can occur prematurely when CDK5RAP2 is depleted.

CDK5RAP2 and Cnn also play a conserved role in tethering the centrosomes to the spindle pole during mitosis in chicken DT40 cells and *Drosophila* embryos (Barr *et al.*, 2010; Lucas and Raff, 2007). In chicken, both the CNN1 and CNN2 are required for this function (Barr *et al.*, 2010). It has been proposed that CDK5RAP2 may function in this process through its role in recruitment of AKAP450 (Barr *et al.*, 2010). AKAP450 interacts with $p150^{glued}$ (Kim *et al.*, 2007): part of the NuMA-dynein-dynactin complex required to link the centrosome to spindle pole (Merdes *et al.*, 1996; Silk *et al.*, 2009).

1.3.3. ASPM in mitotic microtubule nucleation and organisation

ASPM plays a similar role to CDK5RAP2 in nucleation and organisation of the spindle microtubules. ASPM localises to the centrosome and minus end of microtubules during mitosis in *Drosophila*, *C. elegans*, rodents and humans (do Carmo Avides and Glover, 1999; Fish *et al.*, 2006; van der Voet *et al.*, 2009; Zhong *et al.*, 2005). *Drosophila asp* mutants (ASPM orthologue) have unfocused mitotic spindle morphology causing metaphase arrest in larval neuroblasts and maternal

effect lethal phenotype in syncytial embryo (Casal *et al.*, 1990; Gonzalez *et al.*, 1990). Asp appears to be required for the organisation and aggregation of microtubules into spindle poles which it can achieve even in the absence of the centrosome (Morales-Mulia and Scholey, 2005; Wakefield *et al.*, 2001). In addition, Asp is required with γ-TuRC to restore microtubule nucleation capacity of salt stripped centrosomes *in vitro*, a function that requires Plk1 dependent phosphorylation (do Carmo Avides and Glover, 1999; do Carmo Avides *et al.*, 2001). It is likely that Asp performs this function by organizing the γ-TURC within the PCM to form a nucleating centre for microtubules but it is possible it could play a regulatory role in nucleation similar to CDK5RAP2 (Choi *et al.*, 2010).

In mice neuroepithelial cells, Aspm is required to promote symmetric cell divisions by maintaining spindle orientation in the correct position relative to the apical-basal axis (Fish *et al.*, 2008; Fish *et al.*, 2006). Interestingly Aspm is not required for the initial alignment of the spindle established during metaphase but it is required to maintain the orientation during anaphase and telophase (Fish *et al.*, 2008; Fish *et al.*, 2006). A function in spindle positioning has also been reported for the ASPM orthologue in *C. elegans*, ASPM-1. ASPM-1 forms a complex with LIN-5 and CMD-1 at the spindle pole which is required with the motor protein dynein to maintain the correct spindle rotation and positioning during *C. elegans* meiotic divisions (van der Voet *et al.*, 2009).

1.3.4. Summary

The primary microcephaly proteins are required for a diverse range of functions at the centrosome. CPAP, CEP152 and STIL and orthologues belong to a conserved pathway of proteins required to initiate centriole duplication during G_1 to S phase of the cell cycle. CDK5RAP2 plays an important structural role at the centrosome throughout the cell cycle and ASPM is required during mitosis to focus and nucleate microtubules at the centrosome (Figure 1.15).

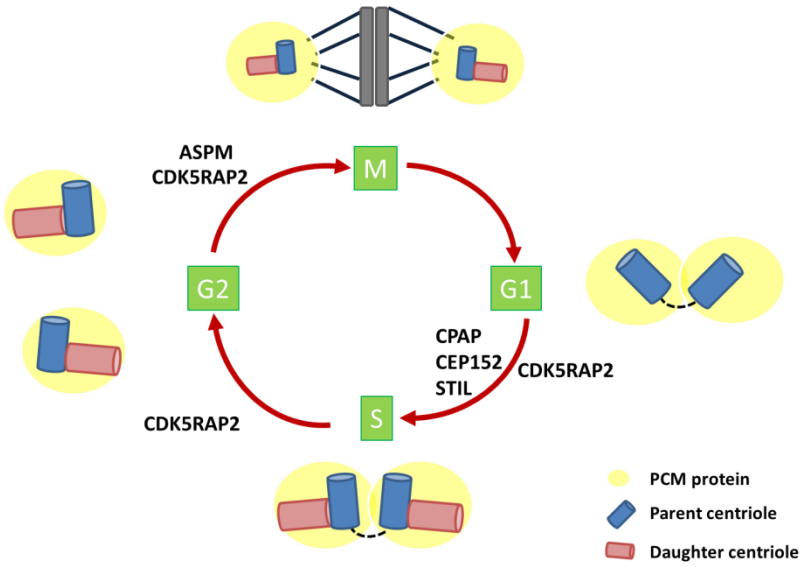

Figure 1.15. Primary microcephaly proteins at the centrosome.
Schematic of the centrosome cycle and stages each of the primary microcephaly proteins or orthologues play a functional role.

1.3.5. Primary microcephaly proteins in cell cycle progression

Some of primary microcephaly proteins also function in cell cycle progression. For example, ASPM and STIL appear to function as tumour promoters in certain cellular contexts. Proliferation of glioblastoma cells was associated with increased expression of ASPM (Hagemann *et al.*, 2008). Increased expression of STIL was found in multiple cancers correlating with an increase in proliferation and metastatic potential (Erez *et al.*, 2004; Ramaswamy *et al.*, 2003). Consistent with this finding MEF cells lacking Stil are characterised by decreased proliferation showing slow growth and a low mitotic index (Castiel *et al.*, 2010). Stil may be required for G_2/M phase progression as it negatively regulates Chfr, an E3 ligase (Castiel *et al.*, 2010), which can delay mitotic entry in response to stress (Matsusaka and Pines, 2004).

1.3.6. WDR62

WDR62 is the most recently identified primary microcephaly protein and so far little is known about its function. *Wdr62* mRNA is expressed in the ventricular and subventricular zone of mouse neuroepithelium consistent with a role in proliferation (Bilguvar *et al.*, 2010; Nicholas *et al.*, 2010). Expression is high in the mouse

neuroepithelium during the period of neurogenesis then subsequently decreases as neurogenesis recedes. Consistent with *wdr62* transcript levels WDR62 protein in mouse fetal brain showed similar expression patterns (Bilguvar *et al.*, 2010).

Similar to the other primary microcephaly proteins, WDR62 localises to the centrosome and spindle poles during mitosis. Indeed, WDR62 was identified as an interactant of the centrosomal protein CEP170 (Hutchins *et al.*, 2010). At interphase WDR62 is cytoplasmic localising to the golgi apparatus (Nicholas *et al.*, 2010; Yu *et al.*, 2010). The spindle pole localisation of green fluorescent protein (GFP) tagged WDR62 was abrogated by recapitulating a patient missense mutation suggesting the pathogenicity of these mutations could be due to the absence of WDR62 from the spindle poles (Nicholas *et al.*, 2010). Further studies of WDR62 will hopefully provide further insight into its function.

1.4. The role of the primary microcephaly proteins in brain size determination

1.4.1. Spindle orientation and cell fate choice

The orientation of the mitotic spindle during neuronal progenitor cell divisions can affect the distribution of cell fate determinants to daughter cells and possibly their cell fate choice (Sections 1.1.5.1-2). Most of the primary microcephaly proteins function at the centrosome which has a conserved role in setting up spindle orientation relative to polarity cues (reviewed by Buchman and Tsai, 2007). Thus, through disruption of various centrosomal functions it is very possible that all of the primary microcephaly proteins could disrupt spindle orientation in neuronal progenitor cells. For instance, *Drosophila*, *dsas-4* (CPAP), *asl* (CEP152) or *cnn* (CDK5RAP2) mutant flies show an increase in spindle misalignment with respect to cortical cues during asymmetric neuroblast divisions (Basto *et al.*, 2006; Blachon *et al.*, 2008; Giansanti *et al.*, 2001). This caused increase in abnormal asymmetric larval neuroblast divisions resulting in failed cytokinesis or a symmetric division but did not affect final brain size (Basto *et al.*, 2006; Giansanti *et al.*, 2001; Lucas and Raff, 2007).

Likewise, in mouse neuronal progenitor cells acute depletion of Aspm or expression of a truncated form of CDK5RAP2 (*Cdk5rap2*^{an}), lacking most of CNN1 domain, leads to an improperly aligned spindle with respect to the apical-basal axis (Fish *et al.*, 2008; Fish *et al.*, 2006; Lizarraga *et al.*, 2010). This phenotype correlated with an expanded neuronal layer and decrease in progenitor pool which may be due to loss of symmetric divisions (Fish *et al.*, 2006; Lizarraga *et al.*, 2010).

In addition the *Cdk5rap2*^{an} mouse has microcephaly of equivalent severity to primary microcephaly patients in certain genetic backgrounds (Lizarraga *et al.*, 2010). A reduced brain size was not observed in a subsequent *Cdk5rap2*$^{-/-}$ mouse published by Barrera *et al*. which led to the production of a truncated CDK5RAP2 protein most equivalent to that predicted for primary microcephaly patients (Barrera *et al.*, 2010), a microcephaly phenotype could be strain dependent. *Aspm* mutant mice expressing truncated forms of Aspm also displayed mild microcephaly (Pulvers *et al.*, 2010). However, in contrast to acute Aspm knockdown, this phenotype does not appear to be caused by changes to cell fate choice (Pulvers *et al.*, 2010) and may have alternative basis.

1.4.2. Cilia and cell cycle length

The primary microcephaly proteins localise to the centrosome and it is possible that they are required for the formation/ proper functioning of cilia. Depletion of many centrosomal proteins is sufficient to disrupt cilia and indeed *asl*, and *dsas4* *Drosophila* mutants or *Sil* knockout mice exhibited characteristics of a cilia defect (Basto *et al.*, 2006; Blachon *et al.*, 2008; Izraeli *et al.*, 1999). Disruption of cilia may affect the cells response to environmental signals or change cell cycle length, both of which could lead to cell fate choice changes (Han and Alvarez-Buylla, 2010; Kim *et al.*, 2011; Lee and Gleeson, 2011; Li *et al.*, 2011; Louvi and Grove, 2011).

1.4.3. Apoptosis

In addition to cell fate choice, changes to cell survival could also affect final brain size (Section 1.1.5.2). One possibility is that the primary microcephaly proteins might be required to ensure proper chromosome segregation (first proposed by (Kouprina *et al.*, 2004)). In rodents and humans, a surprising number of cerebral

cortical neurons are aneuploid arising due to defects in chromosome segregation (Kaushal *et al.*, 2003; McConnell *et al.*, 2004; Rehen *et al.*, 2001; Rehen *et al.*, 2005; Yang *et al.*, 2003). Absence of any of the primary microcephaly proteins may reduce the fidelity of chromosome segregation causing a higher incidence of chromosome aneuploidy (Thompson and Compton, 2008) and possibly a decrease in cell fitness (Torres *et al.*, 2008; Weaver *et al.*, 2007). Consistent with this some of the primary microcephaly proteins or their orthologues, such as ASPM, CPAP and CDK5RAP2, are required for normal chromosome segregation and often cell survival (Cho *et al.*, 2006; Eppig and Barker, 1984; Higgins *et al.*, 2010; Lizarraga *et al.*, 2010; van der Voet *et al.*, 2009). In addition, neuroblasts of *asl Drosophila* mutants also show increase in aneuploidy (Giansanti *et al.*, 2001). The reduction in neuronal progenitor population reported in *Cdk5rap2*^{an} mouse embryos is also associated with an increase in chromosome missegregation and cell death which may also be a contributing factor to the microcephaly observed in these mice (Lizarraga *et al.*, 2010).

1.5. MCPH1

MCPH1 was the first primary microcephaly protein to be identified in 2002 (Jackson *et al.*, 2002). Of the seven primary microcephaly proteins now identified, MCPH1 appears to play the most distinct role. Whereas functional studies of other primary microcephaly proteins have focused on characterising a centrosomal role, MCPH1 functional studies have concentrated on other areas. Given this protein is the subject of this thesis, a comprehensive overview of all the functions of MCPH1 is provided.

1.5.1 *MCPH1* transcript expression

MCPH1 transcript expression is consistent with a function in brain development. *In situ* hybridisation of *Mcph1* in the fetal mouse brain demonstrated that *Mcph1* is expressed during neurogenesis with high levels in the lateral ventricles (Jackson *et al.*, 2002). In humans, RT-PCR detected *MCPH1* expression in the fetal brain as well as other tissues such as liver and kidneys (Jackson *et al.*, 2002).

Although *MCPH1* expression is associated with cell proliferation during development, it is down-regulated in several types of human cancer such as ovarian and breast cancer (Rai *et al.*, 2006; Rai *et al.*, 2008) and it has been therefore suggested that *MCPH1* could function as a tumour suppressor.

1.5.2 MCPH1 protein and BRCT domains

Microcephalin (MCPH1) is predicted to contain 3 BRCT domains one at the N-terminus and two at the C-terminus (Figure 1.10) (Jackson *et al.*, 2002). BRCT domains are common to many of the proteins involved in transducing DNA damage and cell cycle signals (Huyton *et al.*, 2000). Members of this family include proteins that are required for DNA damage signal transduction such as BRCA1, 53BP1 and MDC1 and those directly involved DNA repair, such as XRCC1 and DNA ligase IV. Several studies have shown that the BRCT domains mediate protein–protein interactions, between BRCT domains in different proteins or more often between BRCT domain and proteins with a different structure (Glover *et al.*, 2004). In particular, tandem BRCT domains contain a phospho-protein recognition domain (Manke *et al.*, 2003; Yu *et al.*, 2003) that may specifically result in the protein binding phosphorylation targets of the cell cycle and DNA damage pathway kinases. Roles for MCPH1 in cell cycle regulation and DNA repair have now been established by functional studies.

1.5.3 MCPH1 in chromosome condensation

Microcephalin plays a role in cell cycle timing by regulating the onset of chromosome condensation during mitosis. This function was initially identified when it was demonstrated that MCPH1 primary microcephaly is allelic to premature chromosome condensation (PCC) syndrome (Trimborn *et al.*, 2004). Patients with PCC syndrome have the same clinical phenotype as primary microcephaly but also presented with abnormally condensed chromosomes (Neitzel *et al.*, 2002). Cytogenetic analysis of primary microcephaly patients with *MCPH1* mutations demonstrates similarly high numbers (7-17%) of prophase-like cells (Figure 1.16).

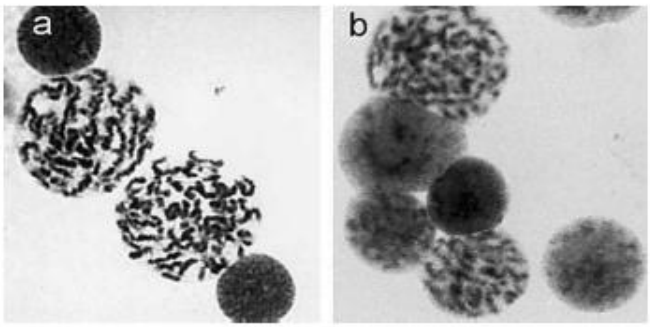

Figure 1.16. PCC in blood cells of MCPH1 primary microcephaly patients.
Prophase like cells in peripheral blood lymphocytes of MCPH1 primary microcephaly patients (a) and patients with PCC syndrome (b) that also have mutations in *MCPH1*. (Figure reproduced from Trimborn *et al.,* 2004).

These prophase-like cells result from the early onset of chromosome condensation in G_2 and late decondensation post mitosis (Neitzel *et al.*, 2002; Trimborn *et al.*, 2004). This PCC phenotype can also be recapitulated by RNAi mediated depletion of MCPH1 (Trimborn *et al.*, 2004; Trimborn *et al.*, 2006). The role of MCPH1 in chromosome condensation appears to be mediated through the condensin II complex which is required for mitotic chromosome assembly (reviewed by Nasmyth and Haering, 2005). RNAi-mediated depletion of condensin II subunits rescues the PCC phenotype in MCPH1 patient LBC or MCPH1 RNAi cells (Trimborn *et al.*, 2006). MCPH1 interacts with condensin II subunit CAPG2 via residues 376–485 suggesting it may play a direct role in condensin II regulation. However, this interacting region is not required for the rescue of the PCC phenotype in *Mcph1*$^{-/-}$ MEFs (Wood *et al.*, 2008). Instead the N-terminal BRCT1 domain is required to prevent PCC (Wood *et al.*, 2008) and following the identification of the X-ray crystal structure of the N-terminus of MCPH1 a hydrophobic pocket on the surface of the BRCT1 domain was identified as essential to this function (Richards *et al.*, 2010). The MCPH1 BRCT domain does interact with the SET nuclear oncogene which has also been recently implicated in regulation of condensin II mediated chromosome condensation (Leung *et al.*, 2011) and it is possible that MCPH1 negatively regulates condensin II through this interaction.

MCPH1 could also regulate condensin II function indirectly. The action of condensin II in prophase chromosome condensation is regulated during the cell cycle by CDK1 mediated phosphorylation (Abe *et al.*, 2011). CDK1 kinase activity is regulated during the cell cycle by post-translational modifications, for example interphase CDK1 is phosphorylated on T14 and Y15 resulting in inhibition of kinase activity (Mueller *et al.*, 1995; Parker and Piwnica-Worms, 1992). *MCPH1* LBC and *Mcph1* mutant *Drosophila* have reduced inhibitory tyrosine phosphorylation of CDK1 (Alderton *et al.*, 2006; Brunk *et al.*, 2007) which could lead to aberrant activation. Indeed in MCPH1 LBC the level of pY15-CDK1 is nearly normal in G_1 phase but drops in S and G_2 phase temporally correlating with an increase in cells with PCC (Alderton *et al.*, 2006). Thus it appears that through perturbing cell cycle timing MCPH1 can also affect condensin II-mediated chromosome condensation.

It has been hypothesised that the role of MCPH1 in chromosome condensation may contribute to MCPH1 disease pathogenesis (Leung *et al.*, 2011) since missense mutations affecting the BRCT1 domain (which is required for chromosome condensation) can lead to primary microcephaly (Darvish *et al.*, 2010; Leung *et al.*, 2011; Trimborn *et al.*, 2005). However, there have been no reports of abnormal chromosome condensation due to mutations of other primary microcephaly genes and so this is unlikely to be a shared pathway contributing to pathogenesis.

1.5.4. MCPH1 in the DNA damage response

1.5.4.1. ATM and ATR DNA damage response

The ATM pathway primarily responds to double strand breaks in DNA caused by ionising radiation (Canman *et al.*, 1998). Following DNA damage, the MRN complex, consisting of MRE11, RAD50 and NBS1, and ATM are rapidly recruited to sites of damage (reviewed by Lavin, 2007).The ATM protein then becomes fully activated and can phosphorylate downstream targets such as H2AX, BRCA1, 53BP1 and CHK2 to coordinate cell cycle arrest and DNA repair (reviewed by Derheimer and Kastan, 2010; Li and Zou, 2005).

Upon exposure to irradiation (IR), MCPH1 co-localizes with numerous proteins associated with the ATM damage response pathway such as NBS1, p-ATM, γH2AX,

MDC1 and 53BP1 (Jeffers *et al.*, 2008; Lin *et al.*, 2005; Rai *et al.*, 2006; Xu *et al.*, 2004). MCPH1 is recruited to irradiation induced foci (IRIF) early in the ATM DNA damage response (DDR) depending only on H2AX for foci formation and independent of NBS1, ATM, MDC1, BRCA1 and 53BP1 (Jeffers *et al.*, 2008; Wood *et al.*, 2007). H2AX may be directly required for MCPH1 recruitment to IRIF since both proteins can interact *in vitro* (Wood *et al.*, 2007) possibly via the C-terminal tandem BRCT domains which are required for MCPH1 recruitment to sites of DNA damage (Jeffers *et al.*, 2008; Wood *et al.*, 2007). Depletion of MCPH1 in U20S cells impairs the recruitment of NBS1, ATM, MDC1 and 53BP1 to sites of irradiation (IR) induced DNA damage (Lin *et al.*, 2005; Rai *et al.*, 2006). However, contradictory results were published in MCPH1 patient LBC which do not show defective recruitment of NBS1 and 53BP1 in response to IR (Gavvovidis *et al.*, 2010).

MCPH1 is also implicated early in the ATR response after UV. Three complexes, RPA, ATR-ATRIP and 9-1-1 (RAD9, RAD1 and HUS1) are among the earliest response elements in this pathway (reviewed by Cimprich and Cortez, 2008; Flynn and Zou, 2011). UV results in an increase in single stranded DNA which is coated by replication protein A (RPA). The RPA coated ssDNA then recruits the ATR-ATRIP (Zou and Elledge, 2003) and plays an important role in localising the 9-1-1 complex (Ellison and Stillman, 2003; Majka *et al.*, 2006; Zou *et al.*, 2003). ATR can then phosphorylate downstream targets such as TOPBP1 and CHK1 to coordinate DNA repair and cell cycle arrest (reviewed by Li and Zou, 2005). Upon exposure to UV, MCPH1 localises to UV-induced foci and is required for the recruitment of ATR and RPA suggesting that MCPH1 may regulate the binding of RPA to damaged ssDNA (Rai *et al.*, 2006).

1.5.4.2 MCPH1 in cell cycle checkpoints

Following DNA damage it is important to stall cell cycle progression until the damage is repaired. Checkpoints exist to delay cell cycle progression at the G_1/S, S and G_2/M phases of the cell cycle and these can be activated by the ATR and ATM pathway. The primary effector kinases of the ATR and ATM pathways are CHK1 and CHK2 respectively which inactivate the CDC25 family of phosphatases

(CDC25A, B and C in humans) to prevent the removal of inhibitory CDK phosphorylations until the DNA damage is repaired (reviewed by Boutros *et al.*, 2006).

The role of MCPH1 in the downstream integrity of the cell cycle checkpoints in response to ATM pathway activation is controversial. Knockdown of MCPH1 by siRNA in U2OS cells leads to a significant increase in cells showing failed S-phase and G_2/M checkpoint arrest following IR (Lin *et al.*, 2005; Xu *et al.*, 2004). However LBC with truncating MCPH1 mutations (Gavvovidis *et al.*, 2010), *Mcph1*$^{-/-}$ chicken DT40 cells (Brown *et al.*, 2010) and *mcph1* mutant *Drosophila* larvae (Rickmyre *et al.*, 2007) do not show deficient G_2/M phase arrest following IR.

These differences may be attributable to *CHK1* and *BRCA1* transcript and protein levels in the cell, which are decreased following MCPH1 RNAi (Lin *et al.*, 2005; Xu *et al.*, 2004; Yang *et al.*, 2008) but unperturbed in MCPH1 LBC (Alderton *et al.*, 2006; Gavvovidis *et al.*, 2010). CHK1 and BRCA1 are important regulators of S and G_2/M checkpoint arrest (Liu *et al.*, 2000; Sorensen *et al.*, 2003; Xu *et al.*, 2001) and so differences in protein levels may account for the discrepancies between RNAi and patient cells. It is possible that a decrease in CHK1 and BRCA1 levels only occur as an immediate response to acute MCPH1 depletion whereas cells adapt to genetic ablation of MCPH1 by upregulating redundant pathways to compensate for reduction in CHK1 and BRCA1 levels.

Although the G_2/M checkpoint was intact, the MCPH1 LBC and *Mcph1*$^{-/-}$ DT40 cells did exhibit a delay in resolving H2AX foci and re-entering mitosis following IR (Brown *et al.*, 2010; Gavvovidis *et al.*, 2010). However rather than defective DDR, chromosome hypercondensation was proposed to account for both of these observations.

MCPH1 does appear to be required for G_2/M phase arrest in response to activation of ATR DDR by UV and replication interference. In LBC MCPH1 function was placed downstream of CHK1 regulating CDC25A stability (Alderton *et al.*, 2006). DNA damage leads to CHK1 mediated phosphorylation of CDC25A targeting it for ubiquitination and subsequent degradation (Busino *et al.*, 2003; Jin *et al.*, 2003; Xiao

et al., 2003). CDC25A levels can trigger the G_2/M phase checkpoints through regulation of CDK1-cyclin B activity (Boutros *et al.*, 2006). In MCPH1 LBC CDC25A was aberrantly stabilised leading to a reduction of inhibitory phosphorylation of CDK1 and defective G_2/M phase arrest (Alderton *et al.*, 2006).

1.5.4.3. DNA damage repair

In addition to sensing DNA damage, MCPH1 is also involved in the repair process of double strand breaks (DSB). DSB can be repaired by two conserved pathways, homologous recombination (HR) and non-homologous end joining (NHEJ) (reviewed by Pardo *et al.*, 2009). MCPH1 appears to play a role in both of these pathways. Using an HR repair analysis system, a defect in homologous recombination efficiency was demonstrated in *Mcph1*$^{-/-}$ MEFS (Wood *et al.*, 2008). Defective HR and NHEJ are also evident on RNAi depletion of MCPH1 (Peng *et al.*, 2009). The function of MCPH1 is also physiologically important playing a role in meiotic homologous recombination DNA repair in mice spermatocytes (Liang *et al.*, 2010).

How does MCPH1 function in both these repair processes? It appears that MCPH1 has a direct and indirect role in DSB repair. MCPH1 directly interacts with BRCA2 and RAD51, two central components of HR. This binding is required for recruitment and/or retention of BRCA2/RAD51 complex at sites of DNA damage (Liang *et al.*, 2010; Wu *et al.*, 2009). MCPH1 also plays an indirect role in the DSB repair processes via the regulation of chromatin structure, which is important to allow DDR proteins access to sites of DNA damage (Morrison *et al.*, 2004; Tsukuda *et al.*, 2005; van Attikum *et al.*, 2004). MCPH1 can modulate HR repair through Condensin II. MCPH1 interacts with condensin II and it is the condensin II binding region that can is required for MCPH1 HR function (Wood *et al.*, 2008). It also plays a role as a regulator of the SWI/SNF chromatin remodelling complex. Following DNA damage, MCPH1 interaction with the SWI/SNF component BAF170 is increased due to ATR/ATM dependent phosphorylation of BAF170. This interaction appears to be required for relaxation of chromatin structure in MCPH1 deficient cells and access of repair proteins such as RAD51, phospho-RPA and KU70 to sites of DNA damage (Peng *et al.*, 2009). Additional studies are required to establish if the role of MCPH1

in chromatin remodelling affects the recruitment of other DDR proteins such as ATM, ATR and NBS.

1.5.4.4. Genomic stability

MCPH1 is also required for genomic stability as expected from its functions in DDR and repair. *Mcph1*$^{-/-}$ mice are hypersensitive to irradiation with a significantly reduced survival rate compared to wild-type animals. In addition MEFs and T lymphocytes isolated from *Mcph1*$^{-/-}$ mice also showed an increase in chromosomal breaks in response to irradiation (Liang *et al.*, 2010). Moderate radiosensitivity was also reported for *Mcph1* null DT40 (Brown *et al.*, 2010) and MCPH1-RNAi cells (Lin *et al.*, 2005).

1.5.4.5. Summary: MCPH1 in the DNA damage response

In summary, multiple roles have been suggested for MCPH1 in the ATM and ATR DDR including sensing DNA damage, controlling cell cycle checkpoints and HR and NHEJ repair. Unfortunately, there is no unifying model of MCPH1 function in the DDR pathway and some conflicting data exists. In particular the role of MCPH1 in ATM response is unclear and results differ between chronic versus acute MCPH1 depletion and type of mutation. The role of MCPH1 in chromatin remodelling does appear to account for some of the functions of MCPH1 in DDR detection and repair.

It is also worth noting that the role of MCPH1 in the ATR response is consistent with the clinical phenotype of primary microcephaly patients which shows some phenotypic overlap with Seckel syndrome, a disorder associated with defective ATR signalling (Alderton *et al.*, 2004; O'Driscoll *et al.*, 2003). Defects in the ATM DDR, such as mutations in NBS1 and ATM result in Nijmegen breakage syndrome and ataxia teleangiectasia respectively (Savitsky *et al.*, 1995; Varon *et al.*, 1998). These disorders are characterised by defective response to IR, unusual sensitivity to X-rays and predisposition for malignancies (reviewed by Shiloh, 1997) which have not been reported in MCPH1 primary microcephaly patients.

1.5.5 Transcriptional regulation

As discussed in section 1.5.4.2, there is evidence to suggest that MCPH1 regulates the transcription of DDR genes, CHK1 and BRCA1, when acutely depleted (Lin *et al.*, 2005; Xu *et al.*, 2004; Yang *et al.*, 2008). MCPH1 positive regulation of CHK1 and BRCA1 is mediated through an interaction with the transcription factor E2F1 (Yang *et al.*, 2008). MCPH1 interacts with E2F1 via the BRCT2/3 domain; overexpression of this domain alone prevents MCPH1-E2F1 interaction and inhibits the role of MCPH1 in transcriptional induction in some E2F1 promoters. MCPH1 also regulated the expression of a subset of other E2F target genes such as DDR genes RAD51, TOPBP1 and DDB2 as well as pro-apoptotic genes such as p73, caspase 3 and 7 (Yang *et al.*, 2008). It is unclear if the role of MCPH1 in the transcriptional regulation of these genes is also only an acute response to MCPH1 depletion similar to BRCA1 and CHK1.

1.5.6. Centrosomal role for microcephalin

Since centrosomal function is shared between all of the MCPH proteins, a role for MCPH1 at the centrosome has been investigated. MCPH1 localises to the centrosome at various stages of the cell cycle depending on the organism. In human cell lines a centrosomal localisation has been demonstrated at interphase and mitosis (Rai *et al.*, 2008; Tibelius *et al.*, 2009). In chicken DT40 cells GFP-tagged MCPH1 localises to the centrosome throughout the cell cycle, the N-terminus BRCT1 domain is implicated in recognition of a centrosome component for this localisation (Jeffers *et al.*, 2008). In *Drosophila* embryos, MCPH1 has a nuclear localisation during interphase and it is a short isoform comprising of only one N-terminal BRCT domain that localises to the centrosome during mitosis (Brunk *et al.*, 2007).

A study of MCPH1 LBC showed MCPH1 together with PCNT is required for the recruitment of CHK1 to interphase centrosomes (Tibelius *et al.*, 2009). CHK1 is required during an unperturbed cell cycle to maintain inhibitory phosphorylation of CDK1 and CDC25B at the centrosome thereby controlling entry into mitosis (Kramer *et al.*, 2004). MCPH1 LBC also presented with reduced inhibitory phosphorylation of centrosomal CDK1 and CDC25B (Tibelius *et al.*, 2009). This

correlated with the reduction in CHK1 centrosome levels and premature entry into mitosis demonstrated by premature chromosome condensation (Neitzel *et al.*, 2002; Tibelius *et al.*, 2009; Trimborn *et al.*, 2004). Thus, MCPH1 function was placed upstream of CHK1, and PCNT, in preventing initial activation of CDK1 at the centrosome. However recently the localisation of CHK1 to the centrosome has been disputed and it has been proposed that it is nuclear CHK1 preventing premature activation of nuclear CDK1 that affects entry into mitosis (Enomoto *et al.*, 2009; Matsuyama *et al.*, 2011). Thus, MCPH1 may play a role in CDK1 activation at the centrosome by a CHK1 independent mechanism. MCPH1 localises to the nucleus during interphase (Lin *et al.*, 2005) and could also play a role in preventing premature activation of CDK1 through a nuclear pathway.

During mitosis centrosome defects were also reported in MCPH1-deficient cells. RNAi mediated depletion of MCPH1 in U2OS cells induced loss of spindle integrity, spindle disorganisation, chromosome congression defects and cytokinesis failure (Rai *et al.*, 2008). It is unclear from this study the underlying mechanism of these phenotypes. The authors proposed that elevated Aurora A and PLK1 protein levels may in part play a role in these phenotypes (Rai *et al.*, 2008).

1.5.7 *Drosophila* melanogaster model of microcephalin

Recently the developmental role of microcephalin in cell cycle regulation has been studied in a *Drosophila* model. The *Drosophila* orthologue of *MCPH1*, *mcph1*, is expressed in *Drosophila* larval brains (Brunk *et al.*, 2007; Rickmyre *et al.*, 2007) and homozygous mutations in *mcph1* males leads to low penetrance defects in adult brain structure (Rickmyre, Dasgupta et al. 2007).

Mcph1 is cyclically localised during the embryonic cell cycle and is essential for early embryonic cell cycles (Brunk *et al.*, 2007; Rickmyre *et al.*, 2007). Similarly to *ASPM* and *CDK5RAP2* orthologues, *asp* and *cnn*, homozygous null mutations in *mcph1* leads to a maternal effect lethal phenotype due to mitotic arrest occurring in the early syncytial cell cycles, when *mcph1* expression is highest (Brunk *et al.*, 2007; Rickmyre *et al.*, 2007). Nuclei in such embryos rapidly arrest in a metaphase-like

state with fragmented, misaligned DNA, broad mitotic spindles and detachment of centrosomes from spindle poles.

Further analysis of the early cell cycles demonstrated that from the first mitotic division the centrosome and nuclear cycles were uncoordinated (Brunk *et al.*, 2007). This phenotype is either a consequence of Chk2-mediated mitotic arrest or triggers such an arrest as mutation of *chk2* supresses the defects in *mcph1* embryos allowing syncytial divisions to continue until cellularisation (Rickmyre *et al.*, 2007).

1.5.8. Summary of MCPH1 depletion phenotypes

Table 1.4. MCPH1 deletion phenotypes

Mutation	System	Knockdown or mutant phenotype	reference
mutation	human LBC	Defective G_2/M arrest, impaired CDC25A degradation and low levels of Tyr 15-CDK1. Also failure to inhibit CDC45 loading onto chromatin after DNA damage induced replication arrest.	(Alderton *et al.*, 2006)
mutation/ RNAi	human LBC HeLa	Premature chromosome condensation in early G_2 phase and delayed decondensation post mitosis.	(Trimborn *et al.*, 2004)
mutation	human	Failure to recruitment CHK1 and PCNT to interphase centrosomes. Deregulated activation of centrosomal CDK1-cyclin B.	(Tibelius *et al.*, 2009)
mutation	human	Proficient G_2/M checkpoint in response to IR. Delay in resolving H2AX foci and re-entering mitosis following IR.	(Gavvovidis *et al.*, 2010)
mutation	Chicken (DT40)	Proficient G_2/M checkpoint following IR. Moderate radiosensitivity. IR induced centrosome amplification. Sustained CHK1 phosphorylation after IR.	(Brown *et al.*, 2010)
Mutation	Mouse	Mice severely radiosensitive and infertile due to defective meiotic homologous recombination. MEFs and lymphocytes showed increased chromosomal breakage following IR.	(Liang *et al.*, 2010)
Mutation	Mouse	Gene-trap in intron 12 of Mcph1 deleting BRCT3 domain. Normal brain and body size but reduced survival rate. Misregulated chromosome condensation. Normal DDR to IR.	(Trimborn *et al.*, 2010)
Mutation	Mouse	Defective HR repair and misregulated chromosome condensation.	(Wood *et al.*, 2008)
mutation	*Drosophila*	Uncoordinated centrosome and nuclear cycles followed by mitotic arrest during early syncytial divisions.	(Brunk *et al.*, 2007)
mutation	*Drosophila*	Homozygous adult males have defective mushroom body structure. Mitotic arrest during syncytial divisions which can be supressed by Chk2 mutation. Genomic instability and chromatin bridging observed during anaphase.	(Rickmyre *et al.*, 2007)
RNAi	U2OS	Decrease in CHK1 and BRCA1 expression levels. Failure of S phase and G_2/M checkpoint in response to IR. Increased sensitivity to DNA damage.	(Lin *et al.*, 2005)
RNAi/ Stable RNAi	HEK293/ U2OS	Decrease in transcript levels of some E2F1 target genes such as BRCA1, CHK1, p107, APAF1, p73, caspase 3 & 7 and other E2F target genes such as TOPBP1, RAD51 and DDB2.	(Yang *et al.*, 2008)
RNAi	U2OS	Increased chromosomal aberrations. Failure to recruit NBS1, 53BP1, MDC1, p-ATM to IRIF and ATR, RPA to UV-induced foci.	(Rai *et al.*, 2006)
RNAi	U2OS	Impaired S phase and G_2/M checkpoint. Decreased expression of CHK1 and BRCA1	(Xu *et al.*, 2004)
RNAi	HTC75	Inhibition of foci formation in response to DNA damage at telomeres.	(Kim *et al.*, 2009)

Table 1.4. MCPH1 deletion phenotypes

Mutation	System	Knockdown or mutant phenotype	reference
RNAi	U2OS	Defective HR and NHEJ repair. Decreased association of SWI SNF with chromatin and decreased chromatin relaxation.	(Peng *et al.*, 2009)
RNAi	U2OS	Loss of spindle integrity, spindle disorganisation, chromosome congression defects and cytokinesis failure	(Rai *et al.*, 2008)

1.5.9. Conclusion: the role of MCPH1

MCPH1 plays an important role in a number of signal transduction pathways including the DDR and cell cycle timing. To achieve these functions MCPH1 BRCT domains may be particularly important possibly enabling it to act as a scaffold for a range of phosphorylated proteins during signal transduction.

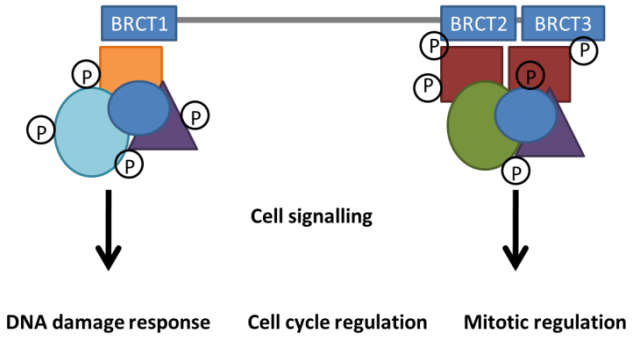

Figure 1.17. Model of MCPH1 function
MCPH1 may play a role in multiple signal transduction pathways by acting as a scaffold for multiple proteins

1.6. Thesis aims and objectives

1.6.1. Hypothesis: Primary microcephaly proteins function in a common pathway that regulates brain growth

Seven genes have been identified as being mutated in primary microcephaly patients (Section 1.2.4). A variety of types of mutations have been reported that are likely to lead to loss of protein, a single amino acid change or a truncated protein product (Section 1.2.5). All mutations lead to a significant decrease in prenatal brain size

which is likely to be attributed to a decrease in neuronal progenitor population (Section 1.1.3). The reduced population of progenitor cells could be due to an increase in cell death, changes to cell fate choice or alterations in the timing of the cell cycle (Section 1.1.5).

It is possible that mutation of primary microcephaly genes leads to the same phenotype through one common pathway (Cox *et al.*, 2006). Given that all of these proteins localise to the centrosome such a common pathway may well act at the centrosome.

The centrosomal function of all the proteins have not yet been characterised but those that have, play a role in centriole duplication (CEP152, CPAP and STIL), centrosome stability (CDK5RAP2) or spindle pole focusing (ASPM and CDK5RAP2) (Section 1.3). These are diverse centrosomal functions but could all affect centrosomal function at mitosis and impact neurogenic proliferations. One possibility is that the primary microcephaly proteins impair microtubule nucleation/organisation which could consequently affect spindle pole positioning, the orientation of cleavage plane and segregation of cell fate determinants (Section 1.1.5.1.2). Impaired centrosome function can also cause defects in chromosome segregation leading to aneuploidy (Ganem *et al.*, 2009) and possibly decreased cell fitness (Thompson and Compton, 2008; Torres *et al.*, 2008; Weaver *et al.*, 2007). Alternatively it may be that the primary microcephaly proteins perturb cilia function which could lead to changes in cell fate choice (Section 1.1.5.1.5).

Currently it is unclear what pathways are shared by the primary microcephaly proteins. To provide further insights the function of MCPH1 was explored in this thesis. This protein has always appeared to be functionally distinct from other primary microcephaly proteins and so any shared function could be highly informative. Since a potential mechanism leading to primary microcephaly is likely to perturb cell divisions (Sections 1.1.3 & 1.1.4) MCPH1 role in mitosis in a vertebrate system was investigated.

1.6.2. Thesis aims

A greater understanding of the role of MCPH1 in mitosis could provide important clues to identifying a single pathway that explains how primary microcephaly proteins regulate brain growth. Thus, the main aim of this thesis is to characterise MCPH1 function in mitosis. To address this, my main aims are to:

1) Characterise MCPH1 isoforms and cell cycle regulation of expression.

2) Establish localisation of human MCPH1 during the cell cycle.

3) Define mitotic functions of MCPH1.

4) Investigate post-translation regulation of MCPH1 during mitosis.

In addition mechanistic characterisation of MCPH1 function in mitosis may offer additional insight in to the coordination of mitotic events.

Chapter 2. Materials and Methods

2.1. General Reagents

2.1.1. Sources of reagents

Chemicals were purchased from Sigma Aldrich, BDH Laboratory Supplies (AnalaR, VWR), Fisher Chemicals, and Amersham Biosciences (GE Healthcare). Enzymes were obtained from New England Biolabs, Promega and Roche. Cell culture material was purchased from Gibco (Invitrogen) or Sigma-Aldrich unless otherwise stated.

2.1.2. Preparation of buffer solutions

All commonly used buffers were made using dH_2O. Solutions were sterilised by autoclaving at 121°C for 15 min. Solutions that could not be autoclaved were passed through a 0.22 μm filter (Millipore).

Table 2.1. Commonly used buffers

Drug	Final Concentration
10 X TBE	0.89 M Tris base, 0.89 M boric acid, 20 mM EDTA
10 X TBS	0.5 M Tris base, 1.5 M NaCl, (pH adjusted to 7.5 with HCl)
10 X Tris-glycine running buffer	250 mM Tris base, 1.92 M glycine, 1% (w/v) SDS
1 X Western transfer buffer	25 mM Tris base, 192 mM glycine, 0.1% (w/v) SDS, 20% (v/v) methanol
NETN	20 mM Tris-HCl pH 8, 100 mM NaCl, 1 mM EDTA, 0.5% NP40
WCE buffer	50 mM Tris-HCl pH 8, 280 mM NaCl, 0.5% NP40, 0.2 mM EDTA, 0.2 mM EGTA, 10% Glycerol
PHEM	25 mM Hepes-NaOH pH 6.8, 100 mM EGTA, 60 mM PIPES, 2 mM $MgCl_2$
4 X protein sample loading buffer	0. 5 M Tris-HCl pH 6.8, 50% (v/v) Glycerol, 2% (w/v) SDS, 0.1% (w/v) Bromophenol blue
PreScission cleavage buffer	50 mM Tris-HCl pH 7.5, 150 mM NaCl, 1 mM EDTA, 1 mM DTT
Kinase reaction buffer	50 mM Tris-HCl pH 7.5, 10 mM $MgCl_2$, 2 mM EGTA
TE	10 mM Tris-HCl pH 8, 1 mM EDTA

2.1.3. Preparation of cell culture drug stock solutions

Drugs were added to tissue culture media immediately prior to use and used at the working concentrations indicated in Table 2.1.3. Stock solutions were made in tissue culture hoods in dimethyl sulfoxide (DMSO) or autoclaved dH_2O before aliquoting and storing them at -20˚C.

Table 2.2. Drug stock solutions

Drug	Solvent	Stock concentration	Working concentration
MG132	DMSO	20 mM	10 µM
Purvalanol A	DMSO	10 mM	20 µM
Roscovitine	DMSO	12.5 mM	50 µM
B12536	DMSO	10 mM	100 nM
Z-VAD-FMK	DMSO	10 mM	10 µM
Nocodazole	DMSO	200 µg/ml	200 ng/ml
Taxol	DMSO	10 mM	10 nM-10µM
Thymidine	H_2O	200 mM	2 µM
Colcemid	DMSO	1 mg/ml	0.1 µg/ml
Doxycycline	H_2O	50 mg/ml	10-1000 ng/ml
G418	H_2O	100 mg/ml	2 mg/ml

2.1.4. Plasmids

Plasmids used throughout this study are listed in Tables 2.3-2.5. Those that were created for this work were constructed using standard cloning techniques and oligonucleotides described in Appendix 1 b.

Table 2.3. Plasmids used in this thesis

Plasmid	Description	Source
pTRE_tight	Amp^R mammalian expression vector controlled by a tetracycline inducible promoter	Clontech
pDEST_EGFP	Kan^R and Cm^R mammalian expression vector with a gateway cassette and a N-terminal EGFP tag controlled by CMV promoter	LMBP
pDONR221	Kan^R *E. coli* expression vector with a Gateway entry cassette and T7 promoter	Invitrogen
pCDNA3.1_DEST_MYCHIS	Amp^R and Cm^R mammalian expression vector with a gateway cassette and a C-terminal MYCHis tag controlled by CMV promoter	A. Jackson lab created by A .Jackson
pMT107	Amp^R mammalian expression vector with Ubiquitin cloned in frame with N-terminal $(His6)_8$ controlled by CMV promoter	Kind gift from P. Clarke lab
pTRE_EGFP_DEST	Tetracycline inducible mammalian expression vector engineered with an N-terminal EGFP tag and gateway cassette	A. Jackson lab created by CA. Martin
pGEX4T3_GST_DEST_STREP	Amp^R and Cm^R mammalian expression vector with a gateway cassette and a C-terminal MYCHis tag controlled by CMV promoter	A. Jackson lab created by M. Reijns

Table 2.4. Gateway entry vectors created for this thesis

Plasmid	Description
pDEST221_FL	attB-FL without stop codon recombined in frame with pDEST221 expression vector
pDEST221_FLX	attB-FL recombined in frame with pDEST221 expression vector
pDEST221_S	attB-S without stop codon recombined in frame with pDEST221 expression vector
pDEST221_SX	attB-S recombined in frame with pDEST221 expression vector
pDEST221_Δ8	attB-Δ8 without stop codon recombined in frame with pDEST221 expression vector
pDEST221_Δ8X	attB-Δ8 recombined in frame with pDEST221 expression vector
pDEST221_1-223X	attB-MCPH1 nt. 1-669 with stop codon recombined in frame with pDEST221 expression vector
pDEST221_BRCT1	attB-MCPH1 nt. 1-267 recombined in frame with pDEST221 expression vector
pDEST221_BRCT1X	attB-MCPH1 nt. 1-267 with stop codon recombined in frame with pDEST221 expression vector
pDEST221_NBX	attB-MCPH1 nt. 246-1923 with stop codon recombined in frame with pDEST221 expression vector
pDEST221_BRCT2/3X	attB-MCPH1 nt 1902-2508 recombined in frame with pDEST221 expression vector

FL = full-length isoform of MCPH1, S = short isoform of MCPH1, ∆8 = MCPH1 isoform lacking exon 8.

Table 2.5 a. Gateway destination vectors created for this thesis

Plasmid	Description
pTRE_EGFP_FL	MCPH1(FL) recombined in frame with N-terminal EGFP-tag of pTRE_EGFP_DEST expression vector
pTRE_EGFP_FL^{T1877G}	T1877G mutation in FL in pTRE_EGFP
pTRE_EGFP_FL $^{T267G\_C268A\_A269T}$	T267G, C268A and A269T mutations in FL in pTRE_EGFP,
pTRE_EGFP_FL^{A360G}	A360G mutation in FL in pTRE_EGFP,
pTRE_EGFP_FL^{A360G_C361A_A362T}	A360G, C361A and A362T mutations in FL in pTRE_EGFP
pTRE_EGFP_FL ^{T573G}	T573G mutation in FL in pTRE_EGFP.
pTRE_EGFP_FL^{T573G_C574A}	T573G and C574A mutations in FL in pTRE_EGFP
pTRE_EGFP_FL^{T762G}	T762G mutation in FL in pTRE_EGFP
pTRE_EGFP_FL^{T762G_C763A}	T762G and C763A mutations in FL in pTRE_EGFP
pTRE_EGFP_FL^{T831G}	T831G mutation in FL in pTRE_EGFP
pTRE_EGFP_FL^{T831G_C832A_A833T}	T831G, C832A and A833T mutations in FL in pTRE_EGFP
pTRE_EGFP_FL^{A861G_G862C}	A861G and G862C mutations in FL in pTRE_EGFP
pTRE_EGFP_FL^{A861G_G862A}	A861G and G862A mutations in FL in pTRE_EGFP
pTRE_EGFP_FL^{T999G}	T999G mutation in FL in pTRE_EGFP
pTRE_EGFP_FL^{T999G_C1000A}	T999G and C1000A mutations in FL in pTRE_EGFP
pTRE_EGFP_FL^{T1095G}	T1095G mutation in FL in pTRE_EGFP
pTRE_EGFP_FL^{T1095G_C1096A_A1097T}	T1095G, C1096A and A1097T mutations in FL in pTRE_EGFP
pTRE_EGFP_FL^{T1251G}	T1251G mutation in FL in pTRE_EGFP
pTRE_EGFP_FL^{T1251G_C1252A_A1253T}	T1251G, C1252A and A1253T mutations in FL in pTRE_EGFP
pTRE_EGFP_FL^{A1449G_G1450C}	A1449G and G1450C mutations in FL in pTRE_EGFP
pTRE_EGFP_FL^{A1449G_G1450A}	A1449G and G1450A mutations in FL in pTRE_EGFP
pTRE_EGFP_FL^{A1752G_G1753C}	A1752G and G1753C mutations in FL in pTRE_EGFP

Table 2.5 b. Gateway destination vectors created for this thesis

Plasmid	Description
pTRE_EGFP_FL^{A1644G_G1645A}	A1644G and G1645A mutations in FL in pTRE_EGFP
pTRE_EGFP_FL^{A2307G_G2308C}	A2307G and G2308C mutations in FL in pTRE_EGFP
pTRE_EGFP_FL^{A2307G_G2308A}	A2307G and G2308A mutations in FL in pTRE_EGFP
pTRE_EGFP_FL^{S89A,S254A,S548A}	S89A,S254A, S548 in FL in pTRE_EGFP
pTRE_EGFP_FL^{S277A,S287A,S417A,S769A}	S277A, S287A, S417A, S483A, S769A in FL in pTRE_EGFP
pTRE_EGFP_S	Short isoform of MCPH1 recombined in frame with N-terminal EGFP-tag of pTRE_EGFP
pTRE_EGFP_Δ8	Δ8 isoform ofMCPH1 recombined in frame with N-terminal EGFP-tag of pTRE_EGFP
pTRE_EGFP_Δ8^{D621E}	D621E in Δ8 in pTRE_EGFP
pTRE_EGFP_Δ8^{D625E}	D625E in Δ8 in pTRE_EGFP
pTRE_EGFP_BRCT1	BRCT1 domain of MCPH1(aa 1-89) recombined in frame with N-terminal EGFP-tag of pTRE_EGFP
pTRE_EGFP_NTERM	N-terminal of MCPH1 (aa 1-223) recombined in frame with N-terminal EGFP-tag of pTRE_EGFP
pCDNA3.1_FL_MYCHIS	Full-length MCPH1 recombined in frame with C-terminal MYCHIS-tag of pCDNA3.1_MYCHIS
pCDNA3.1_S_MYCHIS	Short isoform of MCPH1 recombined in frame with C-terminal MYCHIS-tag of pCDNA3.1_MYCHIS
pCDNA3.1_Δ8_MYCHIS	Δ8 isoform of MCPH1 recombined in frame with C-terminal MYCHIS-tag of pCDNA3.1_MYCHIS
pGEX_GST_BRCT1_STREP	BRCT1domain of MCPH1 (aa 1-89) recombined in frame with N-terminal GST-tag and C-terminal STREP-tag of pGEX_GST_STREP
pGEX_GST_NB_STREP	NB domain of MCPH1 (aa 83-835) recombined in frame with N-terminal GST-tag and C-terminal STREP-tag of pGEX_GST_STREP
pGEX_GST_BRCT2/3_STREP	BRCT2_BRCT3 domains of MCPH1 (aa 644-835) recombined in frame with N-terminal EGFP-tag of pTRE_EGFP_DEST expression vector

2.2. Microbial methods

2.2.1. Growth of bacteria

E. coli strains were grown at 37˚C in/on Luria-Bertani (LB) broth medium. To maintain selection for plasmid DNA in transformed cells the relevant antibiotic(s) (Table 2.3) were added to LB at the required concentration.

2.2.2. Preservation of bacteria

For storage of *E. coli*, 500 µl of stationary phase cell culture was mixed with 500 µl of 50% glycerol and stored in 2 ml Cryo-screw capped tubes (Greiner) at -80°C.

2.2.3. Transformation of *E. coli*

2.2.3.1. Preparation of chemically-competent cells for cloning

Preparation of chemically-competent *E. coli* was performed in-house by Martin Reijns. "*E. coli* DH5α or DB3.1 cells were grown overnight on LB-agar. The next day, a single colony was taken and 5 ml of rich LB with 20 mM $MgSO_4$ was inoculated and grown overnight to stationary phase. Following this, 250 ml of LB with 20 mM $MgSO_4$ was inoculated with 2 ml of the stationary-phase culture and incubated at 23˚C in a shaking incubator at a minimum of 200 rpm until OD_{600} reached 0.4-0.6 (usually 8-10 h). The culture was then cooled on ice for about 15 min and cells were kept on ice for all subsequent steps. Cells were sedimented (10 min, 3,000 rpm, 4˚C) and gently resuspended in 80 ml of ice-cold sterilised TB buffer (10 mM Pipes-HCl pH 6.7, 15 mM $CaCl_2$, 0.25 M KCl, 55 mM $MnCl_2$). Cells were left on ice for 10 minutes, centrifuged for 10 minutes at 3,000 rpm at 4˚C, and gently resuspended in 20 ml of ice-cold TB buffer. After adding 1.5 ml of DMSO followed by a final 10 min incubation on ice, cells were dispensed into 200 µl aliquots in cold, sterile tubes and snap-frozen in liquid nitrogen. Aliquots were stored at –80˚C until required for transformation" (Martin Reijns, 'An analysis of Lsm protein complexes' University of Edinburgh).

2.2.3.2. Transformation of chemically-competent cells

For transformation of chemically-competent *E. coli*, approximately 1 ng of plasmid DNA, or 4 μl of a ligation reaction was added to 50 μl of competent cells. Cells and DNA were incubated on ice for 30 min before 45 sec heat-shock at 42˚C. Following 2 min recovery on ice, the cells were resuspended in 1 ml of LB and incubated at 37˚C for 60 min with shaking. 300 μl of cells were spread on to LB-agar plates containing the appropriate antibiotic(s). The plates were incubated overnight at 37˚C to achieve discrete colonies.

2.3. Cell culture methods

2.3.1. Preparation and growth of cell lines

2.3.1.1. Mammalian cell lines

HeLa, U20S, Cos7and HEK293 cell lines were obtained from the European collection of cell cultures (ECACC). U2OS cells stably expressing GFP tagged α-tubulin and RFP tagged histone 2B is an unpublished reagent kindly provided by W.E Earnshaw lab, University of Edinburgh.

Cells were cultured in Dulbecco's Modified Eagle Medium (DMEM) (Gibco) and maintained in a 37 °C incubator with 5 % CO_2. Cells were trypsinised in trypsin:versene (1:1, v:v) at 37°C for 5 min and passaged at 1:6-1:9.

Lymphoblastoid cells (LBCs) were obtained from human primary microcephaly patients and were transformed with Epstein Barr virus in house by Sean O'Neil. The LBCs were cultured in Roswell park memorial institute medium (RPMI) 1640 (Gibco) and maintained at 2-5x10^5cells/ml.

All media was supplemented with 10 % fetal calve serum (FCS, HyClone, Thermo Fischer Scientific), 200 mM $_L$-Glutamine, 100 U/ml penicillin and 100 μg/ml streptomycin.

2.3.1.2. Chicken cell lines

Chicken DT40 cells stably expressing GFP tagged MCPH1 Short (created by Paola Vagnarelli) were cultured in RPMI-1640 supplemented with 10% FCS, 1 % Chicken Serum (Gibco), 200 mM $_L$-Glutamine, 100 U/ml penicillin, 100 μg/ml streptomycin and 2 mg/ml G418. Cells were maintained between 5-10x10^5cells/ml in a 37°C incubator with 5% CO_2. Large volumes up to 250 ml were maintained in 850 cm^2 roller bottles (BD) rotating at 20 rpm on a miniPERM Universal Turning Device (Greiner Bio One).

2.3.1.3. Preparation of primary mouse embryonic fibroblasts cell lines

Mouse embryonic fibroblasts were prepared from embryos collected at 13.5 days post coitum (E13.5). Each embryo was isolated from the decidua and placed in DMEM culture media. The tails were collected for genotyping and the heads and abdominal cavities removed. Each embryo was minced using a clean scalpel, transferred into a T25cm^2 tissue culture flask and maintained in DMEM, 10% FCS, 0.1 mM βME, 100 U/ml penicillin and 100 μg/ml streptomycin. Fibroblast colonies were visible following culture for 48 hours at 37° C in 5% CO_2 and 10% O_2. Cells were trypsinised in trypsin:versene (1:1, v:v) at 37°C for 5 min and passaged at 1:3. MEFs were maintained up to passage 6, after which cells become senescent and begin to display centrosome abnormalities (Borel *et al.*, 2002).

2.3.2. Preservation of mammalian and avian cells

For storage of tissue culture cells, 2-7 x10^6 adherent cells or 1-3 x10^6 of non-adherent cells were harvested and resuspended in 1 ml of FCS, 10 % DMSO. The cells were stored in 2 ml cryostat tubes in liquid nitrogen.

2.3.3. Synchronization of mammalian cultured cells

2.3.3.1. G_1/S cell arrest using thymidine block

HeLa cells were synchronised at the G_1/S border by a double thymidine block. Thymidine was added to the media of HeLa cells that were 30-40% confluent to give 2 mM final concentration. The cells were incubated at 37 °C for 19 hr, then washed 3

times in PBS and incubated in fresh media for 9 hr at 37 °C. The second thymidine treatment was then performed for 15 hr. The cells were released from G_1/S arrest by removal of thymidine and allowed to progress through the cell cycle during which cells were harvested at various time points. To synchronise transfected cells usually a single thymidine block of 2 mM for 19 hr was performed immediately following transfection.

2.3.3.2. Prometaphase arrest using nocodazole block

Mammalian cultured cells were synchronised at prometaphase by a nocodazole block. When cells were 80-90% confluent, nocodazole was added to the media at a final concentration of 200 ng/ml and cells were incubated at 37°C for 16 hr. Mitotic cells were then collected by mitotic shake off and either used immediately for cell extracts or washed in PBS and released into fresh media. Cells were collected at various time points following release from nocodazole block.

2.3.4. Transfection of cultured mammalian cells

2.3.4.1. Short interfering RNA transfections

Short interfering RNA (siRNA) oligonucleotides were transfected into monolayer cells using Oligofectamine™ (Invitrogen). HeLa or U2OS cells were 30-50% confluent at time of transfection. For each transfection of a 6-well plate, two complexes were prepared. The first contained 200 pmol of siRNA in 175µl of Opti-MEM I Medium (Invitrogen) and the second contained 3µl Oligofectamine in 12µl Opti-MEM. After 5-10 min incubation the solutions were combined for 15-20 min and then added to the cells. The cells were incubated in 800 µl Opti-MEM with the transfection mixture for 4-6 hr after which the complexes were replaced with media. To efficiently deplete some target mRNAs, two consecutive transfections were performed 24 hr apart.

2.3.4.1.1. siRNA oligonucleotide design

siRNA oligos for RNA interference in cultured mammalian cells were designed using a siRNA design tool from the Whitehead Institute (available online at http://jura.wi.mit.edu/bioc/siRNA). The Whitehead siRNA design algorithm (Yuan *et al.*, 2004) was used to identify potential target sequences that satisfied the following

criteria. First, the siRNA targeted sequence is 19 nucleotides in length. Second, the target sequence had a GC content of 30-50%. Third, target sequences had less than 15-16 contiguous base pairs of homology to other coding sequences.

2.3.4.2. DNA Transfections

DNA was transfected into monolayer cells using Lipofectamine™ 2000 (Invitrogen). HeLa, U2OS, Cos-7 or HEK293 cells were 90% confluent at time of transfection. For each transfection of a well of a 6-well plate two complexes were prepared. The first contained 1-2 μg of DNA in 250 μl of Opti-MEM I Medium (Invitrogen) and the second contained 2 μl Lipofectamine in 250 μl Opti-MEM. After 5 min incubation the solutions were mixed for 20 min and then added to the cells. The cells were incubated in 1.5 ml Opti-MEM with the transfection mixture for 4-6 hr after which the complexes were replaced with media.

2.3.4.3. siRNA and DNA co-transfections

siRNA oligonucleotides and DNA was co-transfected in to monolayer cells using Lipofectamine™ 2000 (Invitrogen) . HeLa or U2OS cells were 60% confluent at time of transfection. For each transfection of a well of a 6-well plate two complexes were prepared. The first contained 1 μg of DNA and 200 pmol of siRNA oligo in 250 μl of Opti-MEM I Medium (Invitrogen) and the second contained 2 μl Lipofectamine in 250 μl Opti-MEM. After 5 min incubation the solutions were combined for 20 min and then added to the cells. The cells were incubated in 1.5 ml Opti-MEM with the transfection mixture for 4-6 hr after which the complexes were replaced with media.

2.3.4.4. Relative surface area of culture vessels

The volumes of reagent stated for mammalian cell transfections describe 6-well plate formats. Often 12-well format or 100-mm dishes were used. The equivalent volumes can be calculated from Table 2.6 below.

Table 2.6. Relative surface area of culture vessels									
Culture Vessel	**24-well**	**12-well**	**6-well**	**35-mm**	**60-mm**	**100-mm**	**150-mm**	**T25**	**T75**
Surface Area (cm^2)	2	4	10	10	20	60	140	25	75
Ratio to 24-well plate	1	2	5	5	10	30	70	12.5	37.5

2.4. Nucleic Acid methods

2.4.1. General Methods

2.4.1.1. Spectrophotometric quantification of nucleic acids

The concentration of nucleic acids was determined by measuring the optical density at 260 nM using a NanoDrop 1000 UV-Vis Spectrophotometer (Thermo FisherScientific). 1 µl of each sample was used for each measurement. The purity of the nucleic acid sample was determined by measuring the absorbance at 230 nM, 260 nM and 280 nM. The 260/280 ratio of a sample free of protein contamination should be 1.8-2.2 and a 230/260 ratio ≥1.7 indicates a sample free of carbohydrates and lipids.

2.4.1.2. Agarose gel electrophoresis

Nucleic acid samples were analysed in agarose gels ranging from 0.8% to 2% agarose/TBE (w:v). Gels were prepared by dissolving agarose (Hi-Pure Low EEO agarose, Biogene) in 60 ml of 1x TBE buffer by boiling and adding ethidium bromide to a final concentration of 0.5 µg/ml. The samples were mixed with 6 X DNA loading buffer (6 X DNA loading buffer: 30% (v/v) glycerol, 0.4% (w/v) Orange G), loaded on to the gel and 80-150 volts applied to resolve the nucleic acid fragments by size. The nucleic acids were visualised using a UV transilluminator (BioDoc-It System,UVP). For reference, markers containing DNA fragments of known sizes were included (1kb DNA Ladder (Invitrogen) or 100bp DNA Ladder (Promega).

2.4.2. DNA methods

2.4.2.1. Purification of DNA from *E.coli* cells

2.4.2.1.1. Small scale preparation of plasmid DNA

Plasmid DNA was prepared using the QIAprep Spin Miniprep Kit (Qiagen), following the manufacturers' instructions. DNA was extracted from 5 ml of stationary phase *E. coli* culture and eluted in 50 μl of elution buffer (10mM Tris-HCl pH 8.5).

2.4.2.1.2. Large scale preparation of plasmid DNA

Depending on required yield and quality, plasmid DNA was isolated using the Endofree Plasmid Maxi Kit, QIAGEN Plasmid Maxi Kit or the QIAGEN Plasmid Midi Kit (Qiagen). DNA was extracted from 150-250 ml of stationary phase *E. coli* following the manufacturers' instructions and eluted in 500 μl of TE.

2.4.2.2. Purification of DNA from human cells

DNA was isolated from human cells using the Qiamp DNA extraction kit (Qiagen) following the manufacturers' instructions. DNA was extracted from approximately 1 $x10^6$ LBCs and eluted in 50 μl elution buffer.

2.4.2.3. DNA sequencing

Dye terminator sequencing reactions (ABI) were performed and processed by the Institute of Genetics and Molecular Medicine (IGMM) sequencing service on a 3130/3730 genetic analyser (Applied Biosystems). The DNA sequencing data was analysed using Sequencher 4.10.1 (Gene Codes Corp.).

2.4.2.4. Restriction digests

Plasmid DNA was digested with the appropriate restriction endonuclease in the buffer supplied by the manufacturer (NEB or Roche). To ensure complete restriction digestion before subsequent cloning steps the digest was performed in 20 μl with 2 – 5 μg of DNA and 20 U of the appropriate enzyme(s) and incubated overnight at

37°C. For double digests the optimal buffer conditions were selected for both enzymes using the manufacturers' guidelines.

2.4.2.5. Purification of restriction digested DNA

DNA fragments produced by restriction digestion were resolved by agarose gel electrophoresis. The desired DNA fragment was excised from the gel using a scalpel and purified using the QiaQuick Gel Extraction kit (Qiagen) according to the manufacturers' instructions. DNA was eluted in 30 µl elution buffer and stored indefinitely at -20˚C.

2.4.2.6. Amplification of DNA by polymerase chain reaction

2.4.2.6.1. Primer Design to amplify DNA for cloning

Primers to amplify DNA were designed using the primer design program Primer3 (available online at http://frodo.wi.mit.edu/primer3/ eye). The primers selected usually had a melting temperature (T_m) of around 55˚C (45-65˚C) which did not differ by more than 4°C between the forward and reverse primers in a pair. The nearest neighbour formula was used to predict the T_m (˚C) of primers (SantaLucia, 1998).

2.4.2.6.2. Polymerase chain reaction

Specific regions of DNA were amplified using the polymerase chain reaction (PCR). Specifically designed oligonucleotide primers (Appendix 1 d) were annealed to denatured template DNA and extended by a thermostable DNA polymerase. Different taq polymerases were utilised: FastStartTaq (Roche) for standard PCR, ExpandTaq (Roche) and PhusionFlashTaq (Finnzymes) for when a high level of polymerase accuracy is required.

A typical PCR mixture contained: 1-100 ng template DNA (plasmid or genomic), 1 X PCR buffer (provided by manufacturer), 0.2 mM dNTP (Roche), 0.1-0.5 µM forward primer, 0.1-0.5 µM reverse primer, 0.5 U taq polymerase and H_2O up to a total reaction volume of 25 µl.

PCRs were performed on a DNA Engine Tetrad 2 thermal cycler (MJ Research). A typical PCR program is as follows:

	Denaturation	94˚C	2 min	
25-35 x	Denaturation		94˚C	15 sec
	Annealing		45-65˚C	30 sec
	Extension		72˚C	45 sec per kb
	Extension	72˚C	7 min	

*Annealing temperature is based on the melting temperature of primer set used in each PCR.

2.4.2.7. Purification of PCR products

To purify PCR products the QiaQuick PCR Purification kit (Qiagen) was used according to the manufacturers' instructions. DNA was eluted in 30 µl of elution buffer and stored indefinitely at -20˚C.

2.4.2.8. Genotyping of mouse embryos

To genotype mice for the insertion of the *Mcph1* gene trap cassette a PCR was performed using DNA isolated from mouse embryonic tail. Each embyo tail was lysed in 50 µl of 25 mM NaOH and 0.2 mM EDTA by boiling at 95°C for 30 min. After boiling, the mixture was cooled at room temperature for 5 min and then 50 µl of 40 mM Tris-HCl pH 4 was added to neutralise the base. The PCR consisted of 1 µl of template, 1 X ReddyMix PCR master mix (Thermo Scientific) and 1 µM of each oligonucleotide (Appendix 1 d) in a 25 µl final volume. Thermal cycling conditions were as follows:

	Denaturation	94˚C	2 min	
30x	Denaturation		95˚C	45 sec
	Annealing		58˚C	45 sec
	Extension		72˚C	45 sec
	Extension	72˚C	5 min	

2.4.2.9. Site directed mutagenesis

2.4.2.9.1. Primers for site-directed mutagenesis

Mutagenic primers for use in site-directed mutagenesis were designed using the Quickchange Primer Design Program (available online at http://www.genomics.agilent.com). The design algorithm adhered to a number of rules. The primers were between 25 and 55 bases in length, with a melting temperature (T_m) of ≥78˚C (see below) and the desired mutation was located near the middle of the primer with a minimum of ~10–15 bases of correct sequence on either side. The T_m of primers was calculated using the following formula:

$$T_m = 81.5 + 0.41(\%GC) – 675/N - \%\ mismatch$$

in which N is the primer length in bases and the values for %GC and % mismatch are whole numbers.

2.4.2.9.2. Site directed mutagenesis

Point mutations were introduced into plasmid vectors using the PCR based QuikChange method (Stratagene). In brief, primers containing the desired mutation(s) (Appendix 1a) were designed to anneal to the same sequence on opposite strands of the plasmid. The primers are extended by PCR generating a mutated plasmid. The PCR product is treated with *DpnI* to digest the methylated parental DNA template and thereby select for the mutation-containing synthesized DNA.

The PCR was composed as follows: 50 ng plasmid, 0.25 mM dNTPs, 0.2 µM mutagenic primers (forward and reverse), 1 X DNA polymerase buffer with $MgCl_2$ (provided by Stratagene) and 1.25U of *Pfu*Turbo DNA polymerase (Stratagene). Cycling parameters for site directed mutagenesis were as follows:

Denaturation		95˚C	1 min
18x	Denaturation	95˚C	30 sec
	Annealing	55˚C	1 min
	Extension	68˚C	1 min per kb
Extension		68˚C	10 min

The PCR product was incubated with 10 U of *DpnI* (NEB) at 37˚C overnight to digest parental vector DNA. Following incubation, 0.5-1 µl of the *DpnI* treated DNA was used for transformation into DH5α *E. coli* (Section 2.2.3.2). Resulting colonies were miniprepped and screened by sequencing (Section 2.4.2.3).

2.4.2.10. Ligation of DNA molecules

Ligations were performed using T4 DNA ligase (Roche). Briefly, 100-200 ng of vector DNA, 2 to 3 times this molar amount of insert DNA, 1 U T4 DNA Ligase and 1x Ligation Buffer (provided by Roche) were incubated for 4 hr at room temperature. Following incubation, 1 µl ligation mixture was used to transform *E. coli*

2.4.2.11. Site-specific recombination of DNA molecules

Recombination cloning was performed using Gateway Technology (Invitrogen) following the manufacturers' protocol. Gateway technology is based on the properties of bacteriophage lambda which can mediate recombination at specific sites known as *att* sites (reviewed by Nash, 1981). Recombination occurs between *att*B and *att*P sites to give *att*L and *att*R sites or vice versa depending on the reaction components. This system is used to facilitate transfer of DNA sequences (flanked by modified *att* sites) between vectors. Two recombination reactions are required to clone a PCR product into the desired vector.

Initially, an *att*B PCR product (generated by primers containing *att*B sites) is recombined with an *att*P containing donor vector to create an *att*L containing entry clone. This reaction is catalysed by the BP clonase enzyme mix. Specifically, 75 ng of pDONR221 vector, 75 ng of *att*B-PCR product, 1x BP Clonase II Enzyme mix (containing λ integrase and *E. coli* Integration Host Factor) was incubated for 1-16 hr at room temperature. To terminate the BP reaction 1 µl of the supplied Proteinase K solution was added followed by 10 min incubation at 37°C. Following reaction termination 1 µl of the recombination mixture was used for transformation into DH5α *E. coli* (Section 2.2.3.2) and the resulting colonies were screened by sequencing (Section 2.4.2.3).

The final destination vector is created by recombination of an *att*L entry clone with an *att*R destination vector to create an *att*B containing clone catalysed by LR Clonase enzyme mix. Specifically, 75 ng of entry clone, 75 ng of destination vector, 1 x LR Clonase II Enzyme mix (containing λ integrase, *E.coli* Integration Host Factor and Excisionase proteins) were incubated for 1-16 hr at room temperature. The LR reaction was terminated, transformed and screened as stated above.

2.4.3. RNA Methods

2.4.3.1. Purification of RNA from human cells

RNA was prepared from cells using the RNeasy Mini Kit (Qiagen). RNA was isolated from approximately $2x10^5$ HeLa cells following the manufacturers' instructions. Cells were homogenised using a Qiashredder column (Qiagen) by centrifugation at 16,000 g for 2 min. To eliminate genomic DNA contamination an on-column treatment with 30 U RNase-free DNase I (Qiagen) for 15 min was also included. RNA was eluted into 50 µl RNase-free water and stored indefinitely at -80°C.

2.4.3.2. Reverse transcription of RNA

DNA complementary to first strand RNA was generated using reverse transcriptase and random oligomer primers. A typical reaction mixture contained 1 µg of each RNA sample, 40 U Protector RNase Inhibitor (Roche), 100 pmol random primers (Promega), 5 mM DTT made up to 14 µl with RNase-free H_2O. To melt RNA secondary structures the reaction was incubated at 70°C for 5 min immediately followed by 5 min on ice. The reverse transcription mix was then added (1 µM dNTPs, 20 U AMV Reverse Transcriptase (Roche), 1 X AMV Reverse Transcriptase buffer (Roche), made up to 6 µl with RNase-free H_2O). The reaction was incubated at 42°C for 60 min then the enzyme was deactivated at 75°C for 8 min. cDNA was stored at -20°C until required.

2.4.3.3. Quantitative real-time PCR (qRT-PCR)

Quantitative measurements of gene expression were obtained using real-time PCR on reverse transcribed (RT) RNA. In brief, PCR was used to amplify specific cDNA

sequences and the amount of PCR product at each stage of PCR cycle was measured using the double stranded DNA (dsDNA) binding dye SYBR Green as a reporter. When possible, primers were designed to be intron spanning to distinguish amplification of genomic DNA and to generate a PCR product of similar size (~200 bp).

A typical reaction consisted of 50 ng template cDNA, 1 X Brilliant II Sybr Green qPCR Master Mix(Stratagene), 0.3 µM passive reference dye (ROX) and 0.2 µM of each oligonucleotide primer (Table 1d) in a 10 µl volume. The themo-cycling reactions were performed in 384 well PCR plates (ABgene) with optically clear plate seals (ABgene) using an ABI Prism HT7900 Sequence Detection System (Applied Biosciences). A typical PCR program was as follows:

	Denaturation	95˚C	10 min
40x	Denaturation	95˚C	15 sec
	Annealing & Extension	60˚C	1 min

The 7900HT continuously detected the fluorescence of each well in the plate in real time, producing a cycle threshold (C_T) value for each well. This indicates the cycle number at which the amount of fluorescence detected reaches a fixed threshold. The C_T values for each target gene were normalised to the housekeeping gene. It was assumed for this calculation that the amplification efficiencies of the target and housekeeping gene were approximately equal. The relative expression of target genes to a calibrator (siLUC treated or asynchronous control) was calculated using the comparative C_T method ($2^{-\Delta\Delta CT}$) method (Livak and Schmittgen, 2001) and were represented as fold mRNA induction .

2.5. Protein methods

2.5.1. Protein preparation from cultured mammalian cells

2.5.1.1. Whole cell protein preparations

Protein was extracted from cultured mammalian cells by detergent mediated cell lysis. Cells were harvested and lysed by resuspending in whole cell extract (WCE) buffer (supplemented with phosphatase inhibitors; 5 mM NaF, 0.8 mM Na_3VO_4, 1 mM β-glycerophosphate and EDTA free protease inhibitor tablet (Roche)) for 30 minutes on ice. The WCE buffer volume was adjusted according to the type and number of cells harvested. For example, 2 $x10^5$ HeLa cells were resuspended in 50-80 µl of WCE buffer. The extract was clarified by centrifugation at 17,000 g for 10 min on a Heraeus Fresco 17 Centrifuge (Thermo Electron Corporation). The supernatant was removed and stored at -80 °C until required.

2.5.1.2. Nuclear and Cytoplasmic protein preparations

Nuclear and cytoplasmic proteins were extracted from cells using the NE-PER Nuclear and Cytoplasmic Extraction Reagents (Thermo Scientific) following the manufacturers' protocol. $2x10^6$ HeLa cells were harvested and reagent volumes adjusted accordingly. All reagents were supplemented with 1µg/ml of pepstatin, leupeptin and aprotinin to inhibit proteases.

2.5.2. Recombinant protein isolation from *E. coli*

For recombinant protein expression in *E. coli* the Overnight Express Autoinduction System 1 from Novagen was used according to the manufacturers' instructions. In brief, 2-3 fresh colonies were used to inoculate 50 ml of LB, with antibiotics and ONEX solutions 1, 2 and 3 (0.01, 0.05 and 0.001 times the culture volume respectively). Cultures were grown at 25°C for 32 hrs and then the cells harvested.

Harvested cell pellets were resuspended in NETN (Table 2.1) buffer; 10 ml for 50 ml ONEX expression culture. Cells were lysed by sonication in a Soniprep 150 sonicator set to 3 X 10 sec bursts of maximum amplitude and 10 sec pauses in

between. The lysed cell mixture was clarified by centrifugation at 16,000 g for 15 min at 4°C in a Heraeus Megafuge 1.0R centrifuge. The supernatant was used for purification immediately.

Cell lysate was incubated with Glutathione agarose beads (GS4B, Amersham) for 4 h at 4˚C with rotation. Approximately 150 µl of GS4B beads (bed volume) were used for 50 ml of ONEX expression culture. The agarose beads were sedimented by centrifugation at 300 g for 2 min and washed three times in 5 ml and two times in 1ml of NETN buffer. For GST pulldown experiments the beads were resuspended in NETN buffer and stored at 4°C until required. For Streptactin pulldown assays the beads resuspended in 0.5 ml of PreScission cleavage buffer (Table 2.1) with 10 U of precision protease (GE healthcare) and incubated at 4°C for 16 hr with agitation. The recombinant protein was collected from the eluate; the beads were subsequently washed in 250 µl of PreScission cleavage buffer and supernatant collected. The eluate and wash solutions were aliquoted and stored at -80˚C.

2.5.3. Protein quantification

To determine the concentration of proteins in cell extracts or purified recombinant protein the Bradford assay was performed with the Bio-Rad Protein Assay kit. Initially, a standard curve was drawn using a BSA concentration range of 0.2, 0.4, 0.6, 0.8 and 1.0 mg/ml, provided by manufacturer. 20 µl of each solution was mixed with 1 ml of 1 X Bradfords dye reagent and the A_{595} was measured after 5 min. Absorbance readings were plotted against protein concentration and a line of best fit was plotted. To measure unknown protein concentrations, 1-20 µl of protein sample was mixed with 1 ml of 1 X Bradfords dye reagent and A_{595} was measured after 5 min. The absorbance reading was compared to the BSA standard curve to calculate protein concentration.

2.5.4. In-vitro protein phosphorylation assay

Protein phosphorylation assays were performed with cyclin B-CDK1 (Cell Signaling). To perform the kinase assays, 4 µg of Strep-tagged protein fragments (Section 2.5.2) and 100 ng cyclin B-CDK1were added to kinase reaction buffer

(Table 2.1) (supplemented with 1 mM DTT, 200 µM ATP and 0.5 µM NaF). For further purification of Strep-tagged fragments, 15 µl (bed volume) of Streptactin agarose (IBA) was added and the kinase reaction was incubated for 30 min at room temperature. The beads were sedimented by centrifugation at 500 g for 2 min in a Heraeus Fresco 17 Centrifuge, washed twice in 500 µl PBS and resuspended in 15 µl 4 X SLB. Samples were analysed by SDS-PAGE (Section 2.5.5), followed by silver staining (Section 2.5.6) or western blotting (Section 2.5.7).

2.5.5. SDS-PAGE

Protein samples were separated according to their molecular weight by SDS-PAGE using either the Mini-PROTEAN®3 (Biorad) or NuPage®Novex (Invitrogen) gel systems.

Tris-Glycine gels were used at resolving concentrations ranging from 6%-15%. The resolving gel mixture was composed of 375 mM Tris pH 8.8, 0.1% (w/v) SDS, 0.1% (w/v) ammonium persulphate. For different resolving concentrations the amount of 30% acrylamide/bis-acrylamide (Sigma-Aldrich) and N'N'N'N'-tetramethylethylenediamine (TEMED) was adjusted accordingly (0.08 µl/ml TEMED in 6% acrylamide, 0.06 µl/ml TEMED in 8% acrylamide or 0.04 µl/ml TEMED in 10-15% acrylamide) . The stacking gel contained 125 mM Tris pH 6.8, 0.1% SDS, 0.1% ammonium persulphate, 4.2% acrylamide/bisacrylamide and 1 µl/ml TEMED. Alternatively, 4-12% Bis-Tris gels (Invitrogen) were used when greater separation of a wide range of molecular weight proteins was required on the same gel. Protein samples were electrophoresed alongside precision plus protein standards (BioRad) or SeeBlue® Plus2 Pre-Stained Standard (Invitrogen). High molecular weight proteins (> 250kDa) proteins were resolved on a 3-8% Tris-Acetate gel (Invitrogen) alongside HiMark™ Pre-Stained High Molecular Weight Protein Standard (Invitrogen).

Protein samples were denatured by heating at 70°C for 20 min in 1 X protein sample loading buffer (Table 2.1) and loaded onto the gel. The gels were electrophoresed in different types of running buffer depending on the gel composition: 1 X Tris-Glycine running buffer (Table 2.1), 1 X Tris-Acetate running buffer (Invitrogen) or 1 X

MOPs running buffer for Bis-Tris gels (Invitrogen). A constant voltage of 150-200 volts was applied until the desired separation was achieved.

2.5.6. Staining of protein gels

2.5.6.1. Coomassie Blue staining

To allow visualisation of abundant protein bands following SDS-PAGE, SimplyBlue™ SafeStain (Invitrogen) was used. After electrophoresis the gel was washed three times for five min in 100 ml of dH_2O and then mixed in 20 ml of the staining solution for 1 h, followed by destaining for 1-3 hr in dH_2O.When protein bands were isolated for mass spectrometry care was taken to minimise keratin contamination by using clean equipment and fresh solutions.

2.5.6.2. Silver Staining of protein gels

Recombinant protein bands after SDS-PAGE were detected by silver staining using the SilverSNAP® stain for Mass Spectrometry (Thermo Scientific) and by following the manufacturers' instructions.

2.5.7. Western blotting

Proteins were transferred from the SDS-polyacrylamide gel to nitrocellulose membrane (Amersham) using a Mini-Trans-Blot Cell system (Bio-Rad Laboratories). Electrophoretic blotting was performed in 1 X western transfer buffer (Table 2.1) at 100 V for 1-2 hr.

After electrophoretic transfer, the nitrocellulose membrane was blocked to prevent non-specific protein binding. To block, the membrane was incubated with either 5% Marvel (Premier Foods) or 5% BSA (Roche) in TBST (Table 2.1) for 1 hr at room temperature with constant agitation. Primary antibodies were added to the blocking solution at the appropriate dilution (Appendix A2 a) and incubated overnight at 4°C. The membrane was washed 3 times for 5 min in TBST and then the appropriate HRP labelled secondary antibody (Appendix A2 b), diluted in appropriate blocking solution, was added to the membrane for 1 hr.

To detect horse radish peroxidase (HRP) immobilised onto membrane, ECL detection kit (Amersham Biosciences) was used according to the manufacturers' instructions. For a 20 cm^2 nitrocellulose membrane, 2 ml of ECL solution (1:1 mixture of solutions A and B) was added to the protein side of the nitrocellulose membrane and incubated for 1 min at room temperature. The membrane was blotted to remove any excess liquid, placed between two acetate sheets and exposed to photographic film (Kodak Biomax XAR Film). Film was developed using a Konika SRX-101A Developer. For enhanced sensitivity, ECL Plus (Amersham Biosciences) was used according to the manufacturers' instructions.

2.5.8. Western blot image analysis

A rough quantification of the relative band intensities of Western blots was performed using Adobe Photoshop 7.0. An area encompassing one protein band was defined and the same area was used for each measurement. The mean pixel intensity was calculated for each area. Intensity values for the background of a matched area were also obtained and subtracted from the band signal. Intensities were expressed as a ratio relative to uncleaved protein band.

2.5.9. Phosphorylation site mapping of proteins by mass spectrometry

Band samples containing the protein of interest were analysed by the FingerPrints Proteomics Facility of Dundee University. The samples were digested by trypsinisation and subject to a three stage analysis using the nanoLC-MS mass spectrometer (Liquid Chromatography, Mass Spectrometry, Dionex/LC Packings) coupled to a 4000 QTRAP (Applied Biosystems/Sciex). Initially proteins are identified by LC- MS-MS spectrometer (Dionex/LC Packings). Then phosphorylated peptides were identified by parent ion scanning followed by tandem MS to determine the site of phosphorylation. A mascot report was then generated from a comparison of the tandem MS data and the known protein sequence, including phosphorylation sites.

2.6. Microscopy methods

2.6.1. Fixation of cells

Suspension cells were adhered to poly-L-lysine slides (VWR) and adherent cells on to untreated (VWR) or to poly-L-lysine coated coverslips (Becton Dickinson). Depending on the antibody the cells were either fixed in -20ºC methanol for 7 min or 4% PFA (TAAB) in PHEM (Table 2.1) for 5-15 min. Usually, methanol fixation was used for visualisation of proteins located at the centrosomes or microtubules and PFA for kinetochore staining and visualisation of DNA morphology. Following PFA fixation, cells were permeabilised by treatment in 0.2% triton-X-100 in PHEM for 2 min. Cells were then washed in PBS 3 times for 5 min and stored at 4°C until required.

2.6.2. Immunostaining

Fixed cells were blocked in PBS/1% bovine serum albumin (Sigma-Alrich) for at least 30 min. Primary antibodies were diluted in blocking solution (see Appendix 2 a for dilutions used) and incubations were performed for 30 min at 37ºC in a humidity chamber. The cells were then washed three times in PBS for 5 min before incubation with appropriate secondary antibodies (Appendix 2 b) and 4'6-diamidino-2-phenylindole (DAPI) (1 μg/ml) for 30 min. Samples were washed and mounted in Vectashield (Vector Laboratories) and analysed immediately by microscopy (Section 2.6.3).

2.6.3. Microscopy

2.6.3.1. Microscopy of fixed cell preparations

Imaging was performed using an Axioplan 2 widefield fluorescence microscope (Ziess) fitted with an objective mounted PIFOC for accurate sectioning of cell thickness. Single-images or Z-series were collected using either a 63 X or 100 X Plan-APOCHROMAT (1.4 NA) objective. The microscope contained a three colour single-emission filter wheel (FITC; 489 nm excitation, 508 nm emission, TRITC; 550 nm excitation, 570 nm emission, DAPI; 359 nm excitation, 461 nm emission).

Images were captured with a CoolSnap camera (Roper Scientific) using Ivision image capture software.

2.6.3.2. Microscopy of live cells

For live-cell imaging, U2OS cells stably expressing RFP-H2B and EGFP-ATUB were seeded on to 60 mm glass coverslips (VWR).The coverslips were sealed in to a closed chamber system with Leibovitz L-15 medium (Gibco). TRITC and FITC 3D image data sets were collected with a DeltaVision system microscope (Applied Precision, Issaquah, WA) heated to 37°C equipped with a dry 40 X APROCHROMAT objective. Images with Z-optical spacing of 1-2 µm were recorded every 10 min for a 3 hr period.

2.6.3.3. Processing of 3D datasets

Images were deconvolved using constrained iterative restoration as implemented in Volocity software 5.4.2 (PerkinElmer). Three-dimensional data sets were converted to maximum intensity projections in Volocity and then converted into TIFF files. The TIFF files were imported into Adobe Photoshop 7.0 for final presentation. In Photoshop, levels were adjusted across each entire image to lower nonspecific background and haze. When comparing fluorescent signals between images, levels were adjusted proportionately.

2.6.3.4. Quantification of fluorescent signals in 3D datasets

Fluorescence intensity analysis of 3D datasets was performed using Volocity software 5.4.2. A region covering each centrosome was defined in a deconvolved 3D dataset and the signal through all the sections was summed. Intensity values for the cytoplasmic background of matched volume were obtained and subtracted from the centrosome signal. Intensities were expressed as a ratio relative to wild type.

2.6.4. Fluorescence activated flow cytometry

Cells were harvested by trypinisation, and transferred to a 15ml falcon tube. Before each washing step the cells were pelleted by centrifugation for 2 min at 800 g. The cells were washed once in DMEM, once in PBS/0.1 mM EDTA and then resuspended in 100 µl of PBS/0.1 mM EDTA. Cells were then fixed in 900 µl 70%

EtoH/H_2O added drop-wise and stored at -20°C. The cells were washed twice in PBS and finally resuspended in PBS containing 100 μg/ml RNase A and 50 μg/ml propidium iodide for 40- 60 min. Cell sorting was performed on a FACScalibur (BD Biosciences) by Elizabeth Freyer, MRC HGU. Data was analysed using FlowJo software (v7.6.1, Tree Star).

Chapter 3. Characterisation of *MCPH1* isoforms in the cell cycle

Recent studies on the *Drosophila melanogaster* orthologue of *MCPH1* revealed the existence of several alternatively spliced variants of *mcph1* (Brunk *et al.*, 2007; Rickmyre *et al.*, 2007). Two of the isoforms exhibit different mitotic localisation patterns and appear to play distinct roles in the cell cycle (Brunk *et al.*, 2007).

During my MSc maxi-project ('Defining the functional role of a short isoform of microcephalin in humans and *Drosophila melanogaster'*, University of Edinburgh, 2007) I experimentally confirmed the presence of alternative splicing of *MCPH1* in humans, similar to in *Drosophila*.

In Chapter 3, *MCPH1* alternative splicing in humans is characterised. *MCPH1* isoform expression in the developing human brain and the effect of primary microcephaly *MCPH1* mutations on isoform protein expression was characterised to assess the potential contribution of the isoforms to the pathogenesis of primary microcephaly. To establish if alternative MCPH1 isoforms could perform different functions, tissue specific isoform expression and differential regulation during the cell cycle was also examined.

3.1. *MCPH1* is alternatively spliced

MCPH1 is a fourteen exon gene located on chromosome 8 at cytogenetic band p23 (Figure 3.1A). The full-length (FL) transcript containing all fourteen exons is annotated in Ensembl (ENST00000344683) and has been the subject of all MCPH1 functional studies published to date. Two sites of alternative splicing at intron 8 and exon 8 were identified from bioinformatics and experimentally (Figure 3.1B). One transcript, called *MCPH1*(*S*), contains unspliced intron 8 resulting in a premature stop codon and corresponds to the annotated transcript ENST00000519480 in Ensembl. A second transcript, called *MCPH1*(*Δ8*), contains spliced exon 8 and was identified by RT-PCR and sequencing of HeLa mRNA (Figure 3.1C). The splicing of exon 8 is not predicted to alter the frame of the coding sequence.

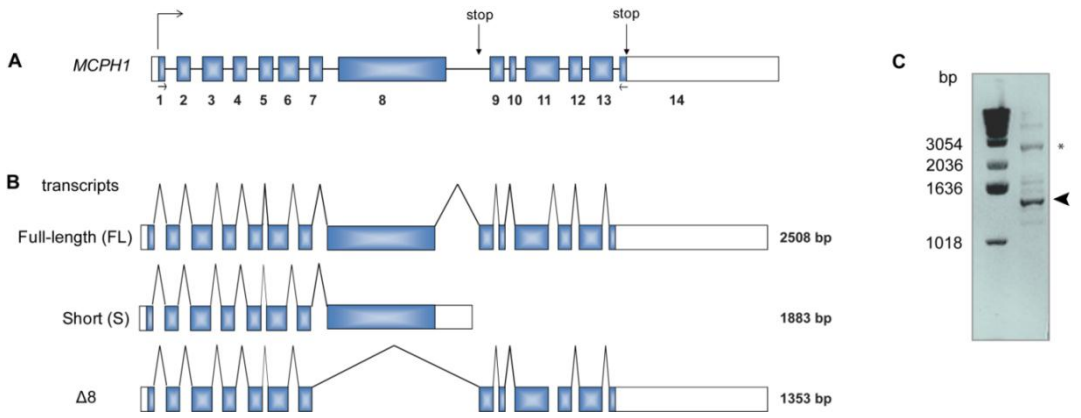

Figure 3.1. Human microcephalin.
(A) Genomic organisation of *MCPH1*. Schematic drawing illustrating the exons (boxed) and coding sequence (blue) of *MCPH1*. The positions of the translational start site, the two alternative stop sites and primers used for RT-PCR are also indicated. (B) Potential alternative splice variants of *MCPH1*. Schematic drawing showing transcripts resulting from alternative splicing of intron 8 (short) and exon 8 (Δ8). The predicted sizes of transcripts are indicated. (C) RT-PCR of the *MCPH1*(*Δ8*) transcript from HeLa RNA. The approximately 1,400 bp PCR product (denoted by arrowhead) was sequenced confirming the *MCPH1*(*Δ8)* transcript sequence. The approximately 2,800 bp PCR product (denoted by asterisk) is the expected size of *MCPH1*(*FL*).

3.2. *MCPH1* is alternatively spliced in human fetal brain

During my MRes maxi-project ('Defining the functional role of a short isoform of microcephalin in humans and *Drosophila melanogaster*', University of Edinburgh, 2007) alternative splicing of MCPH1 intron 8 (generating the S isoform) was confirmed in the developing human brain.

As our main interest is to study the potential role of MCPH1 during neurogenesis, alternative splicing of exon 8 (resulting in the Δ8 isoform) was also examined by RT-PCR of human fetal brain. The primers were designed to amplify sequence unique to each of the transcripts (Figure 3.2A). The S transcript contains intron 8 and although FL or Δ8 transcripts share the same exons there are unique exon junctions (exon8/9 junction (FL) and exon7/9 junction (Δ8)). RT-PCR products representing FL, S and Δ8 transcripts were generated (Figure 3.2B) confirming that alternative splicing occurs during neurogenesis.

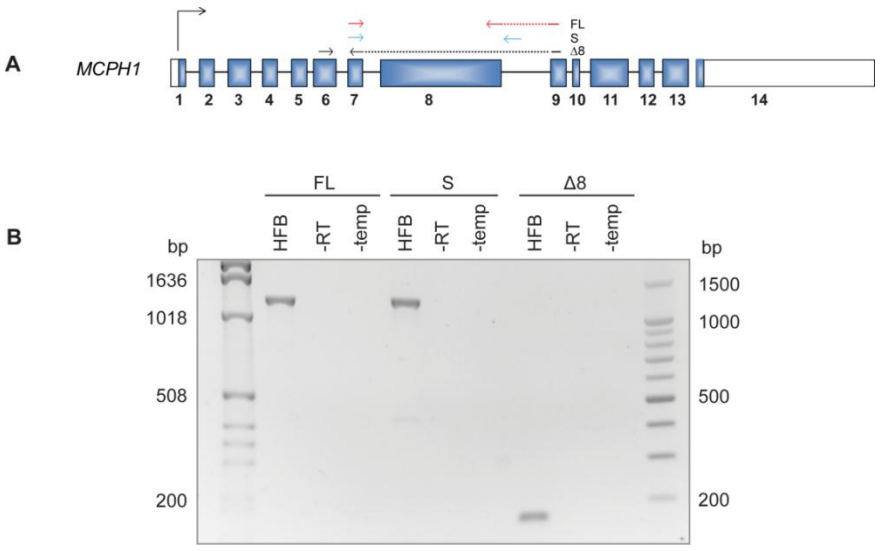

Figure 3.2. Expression of human MCPH1 FL, S and Δ8 transcripts.
(A) RT-PCR primer locations in *MCPH1*. The location of the primer pairs designed to amplify FL (red arrows), S (blue arrows) or Δ8 (black arrows) transcript sequence. (B) RT-PCR demonstrates the synthesis of processed mRNAs representing human MCPH1 FL, S and Δ8 isoforms. RNA extracted from human fetal brain (HFB) was reverse transcribed to make cDNA for PCR analysis (lanes 1, 4, 7). HFB RNA without reverse transcriptase (-RT) and H_2O (-temp) were included as controls. Primers were designed that would specifically amplify products from mRNA encoding FL (lanes 1-3), S (lanes 4-6) or Δ8 (lanes 7-9). The forward and reverse primers used were intron spanning allowing products generated from genomic or unspliced primary transcripts to be distinguished from processed transcripts.

3.3. MCPH1 isoform protein expression

The alternative splicing described (Figure 3.1 & 3.2) would encode three protein isoforms. The FL transcript encodes the longest protein isoform containing all three BRCT domains, the S transcript contains only one functional, N-terminal BRCT domain and the Δ8 transcript encodes all three BRCT domains but is lacking most of the inter-BRCT spacer region (Figure 3.3A).

To determine if MCPH1 FL, S and Δ8 are expressed as proteins in cultured human cells, the proteins recognised by a MCPH1 antibody was examined. Anti-MCPH1 antibody raised in rabbits against GST-tagged MCPH1 (Lin *et al.*, 2005) was used to probe immunoblots of lymphoblastoid cell (LBC) extracts derived from a control and primary microcephaly patient ($MCPH1^{322\text{-}1G>C}$). $MCPH1^{322\text{-}1G>C}$ is a splicing mutation in intron 4 that results in a frameshift and substantial premature protein truncation ($MCPH1^{107fs}$). It is likely the $MCPH1^{322\text{-}1G>C}$ transcript is targeted for nonsense mediated decay (NMD) (reviewed by Nicholson and Muhlemann, 2010). The anti-MCPH1 antibody detected two protein bands migrating at approximately 90 and 65 kDa that were absent in $MCPH1^{107fs}$ LBC extracts (Figure 3.3B) and corresponded to the predicted molecular weight of the MCPH1 FL (93 kDa) and S isoform (68 kDa).

To further confirm that the two protein bands correspond to FL and S isoforms their open reading frames (ORF) were cloned into pCDNA3.1_DEST_MYC_His using gateway technology. These transgenes were then expressed in HEK293 cells and the protein mobility compared with endogenous protein (Figure 3.3C). The transgenic FL and S protein, recognised by the increase in abundance and additional molecular mass of the epitope tag, exhibited similar mobility to the endogenous proteins.

A strong protein band corresponding to MCPH1(Δ8) was not reproducibly detectable in LBC or HEK293, although the MCPH1 antibody used could detect transgenic $MYC(His)_6$-tagged Δ8 protein (Figure 3.3C).

.

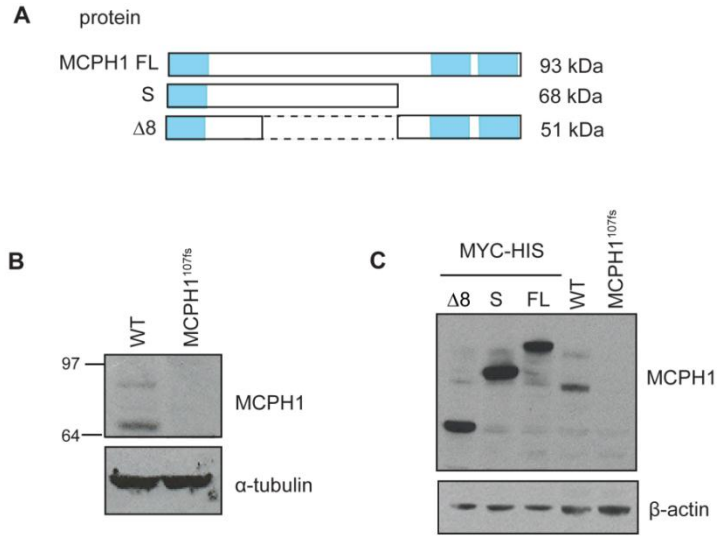

Figure 3.3. Immunoblot detection of MCPH1 FL and S isoforms.
(A) Schematic of potential MCPH1 isoforms. BRCT domains are represented in blue and predicted molecular weight of each isoform indicated. (B) Whole cell extracts of control and MCPH1^{107fs} LBC were analysed by Western blotting with antibodies to MCPH1 and α-tubulin (loading control). (C) Protein extracts from HEK 293 cells transiently expressing MYC(His)$_6$-tagged MCPH1(FL), MCPH1 (S) and MCPH1 (Δ8) isoforms were compared to extracts from control and MCPH1^{107fs} LBC. Extracts were Western blotted with MCPH1 and β-actin antibodies (loading control).

3.4 siRNA can be used to specifically deplete MCPH1 isoforms

To further confirm that the alternatively spliced transcripts detected by RT-PCR corresponded to the protein bands detected by immunoblotting with MCPH1 antibody, RNAi oligonucleotides were designed to target specific isoforms. The location of the oligonucleotide target sequence is represented in the schematic of the MCPH1 gene (Figure 3.4A). FL oligonucleotide targets sequence in the FL transcript, S targets sequence in the S transcript whereas #2 and #3 target FL, S and Δ8 transcripts. To measure the efficiency of the RNAi mediated knockdown, transcript levels and protein abundance were analysed.

The MCPH1 FL, S and Δ8 transcript levels were examined by quantitative RT-PCR. The forward and reverse primers used were based on those designed in Figure 3.2A & B. FL and Δ8 primer sets were intron spanning and gave rise to single products of the expected sizes. It was not possible to design S primer set that was intron spanning

so MCPH1 intronic primers were also included as an extra control to detect genomic DNA or unspliced primary transcripts. The RNAi oligonucleotides resulted in depletion of specific transcripts as expected from their target sequence (Figure 3.4B). Expression of Δ8 increased when FL or S transcripts were knocked down, this may be a compensatory mechanism for the loss of other isoforms.

The changes in transcript levels corresponded to the isoform protein abundance providing confirmation that these transcripts are expressed as proteins (Figure 3.4 C). Three additional bands were detected with the MCPH1 antibody in HeLa cells (Figure 3.4 C, denoted by asterisks) but their abundance was not affected by RNAi suggesting that they are non-specific.

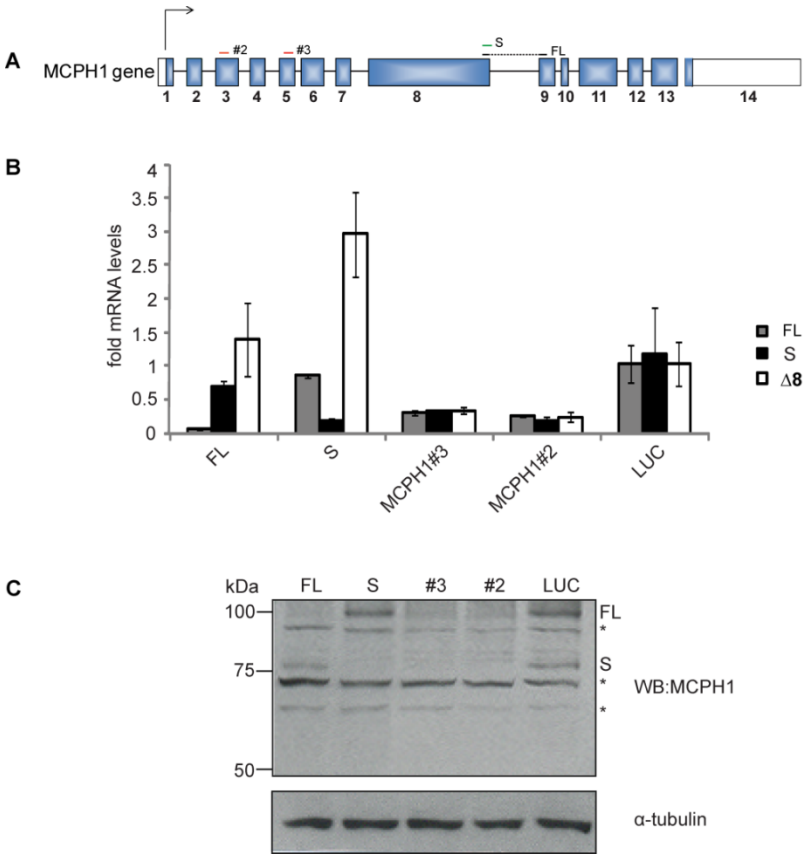

Figure 3.4. Targeted knockdown of MCPH1 isoforms by siRNA.
(A) siRNA oligonucleotide target sequence locations in *MCPH1*. The location of the siRNA oligonucleotides designed to target FL (black line); S (green line) or all three isoforms (red lines) are depicted on the schematic. (B) qRT-PCR analysis of siRNA mediated MCPH1 transcript depletion. HeLa cells were transfected with 100 nM of control siRNA (siLUC) or MCPH1 siRNA (described in A) at 0, 24 and 48 hr. After 72 hr RNA was extracted from cells and reverse transcribed into cDNA for qPCR analysis of FL (black), S (white) or ∆8 (grey) expression levels. Data is shown as fold induction from siLUC controls and represented as the mean ± s.d. of triplicate qPCR wells. (C) Immunoblot detection of siRNA mediated MCPH1 protein depletion. HeLa cells from (B) were also used to make protein extracts and analysed by Western blotting with antibodies to MCPH1 and α-tubulin (loading control). Asterisks denote the positions of non-specific protein bands.

3.5. MCPH1 FL and S are absent in MCPH1 patient cells

To determine whether the loss of MCPH1 FL and/or S isoform may be relevant to the pathogenesis of primary microcephaly, protein expression was examined in MCPH1 patient-derived cell lines. LBC with *MCPH1* truncating mutations (*MCPH1*$^{322\text{-}1G>C}$, *MCPH1*$^{74C>G}$ and *MCPH1*^{427InsA}), a large scale deletion (*MCPH1*$^{\Delta 1\text{-}8}$) and a missense mutation (*MCPH1*$^{262G>C}$) were analysed. The mutations of primary microcephaly patients were originally identified in the lab by Andrew Jackson (*MCPH1*$^{IVS322G>C}$, *MCPH1*$^{74C>G}$, *MCPH1*^{427InsA}, *MCPH1*$^{262G>C}$) and Louise Bicknell (*MCPH1*$^{\Delta 1\text{-}8}$).

The primary microcephaly patient-derived LBC were genotyped to confirm the presence of the expected *MCPH1* mutations. Genomic DNA was extracted from LBC pellets, relevant *MCPH1* coding exons amplified by PCR and sequenced. The expected mutations were confirmed using Mutation Surveyor (Figure 3.5A) (the genotype of *MCPH1*$^{\Delta 1\text{-}8}$ LBC had recently been confirmed by Louise Bicknell so is not shown). The locations of the causative mutations in MCPH1 are illustrated (Figure 3.5Bi) and the predicted protein effect of each mutation represented in the table (Figure 3.5Bii). All the mutations are located within coding sequence for FL, S and Δ8 isoforms of *MCPH1* but their effect on isoform protein production has not been characterised.

To address what the cellular consequences of these mutations were, extracts were prepared from a control and the *MCPH1* patient-derived LBC lines described. In addition, extracts from HEK293 cells overexpressing MYC$(His)_6$-tagged FL and S were included. Western blotting revealed that both isoforms, which co-migrated with epitope-tagged FL and S, were not present in any of the *MCPH1* LBCs (Figure 3.5C). Thus, both missense and frameshift mutations result in loss of MCPH1 FL and S isoform protein.

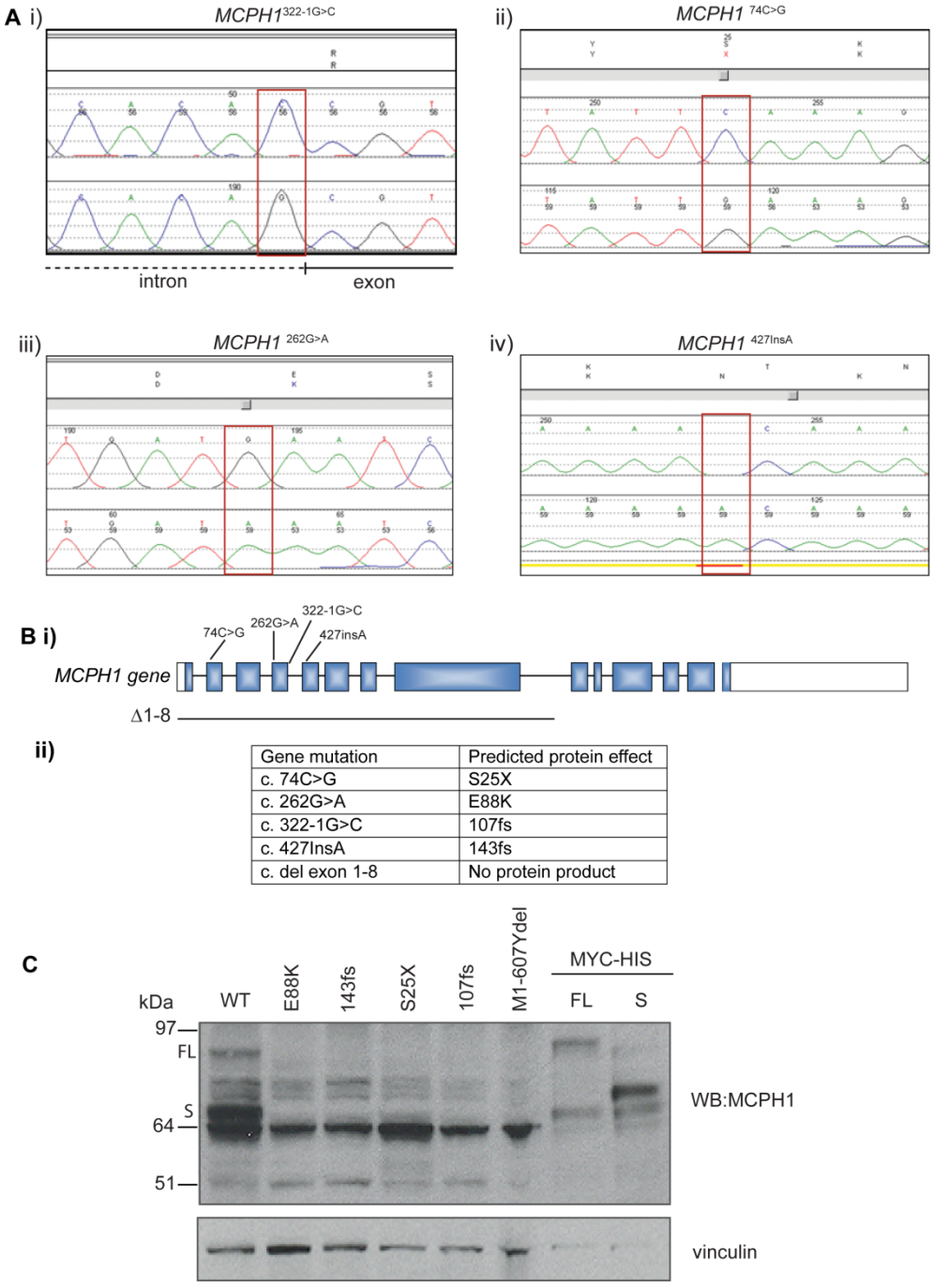

Gene mutation	Predicted protein effect
c. 74C>G	S25X
c. 262G>A	E88K
c. 322-1G>C	107fs
c. 427InsA	143fs
c. del exon 1-8	No protein product

Figure 3.5. Immunoblot detection of MCPH1 isoforms in MCPH1 patient-derived LBC. (A) Genotyping of MCPH1 patient LBC. Genomic DNA was isolated from MCPH1 patient-derived LBC, MCPH1 exons were amplified by PCR, sequenced and analysed by Mutation Surveyor. (B) (i) Schematic of *MCPH1* and location of causative mutations identified in primary microcephaly patients. (ii) Table representing the MCPH1 genetic mutations and their predicted effect on MCPH1 protein. (C) Cell extracts from control (WT) and five MCPH1 patient-derived LBC lines were compared to extracts from HEK293 cells transiently over-expressing MYC(His)$_6$-tagged FL and S. Extracts were Western blotted with MCPH1 and vinculin antibodies (loading control).

3.6. Tissue-specific differences in *MCPH1* isoform expression

Previously, using RT-PCR, expression of human *MCPH1* was detected in a variety of fetal and adult tissues (Jackson *et al.*, 2002). The primers used for PCR detected exon 1-6 of *MCPH1* and therefore all isoforms would be detected. To characterise the expression pattern for each isoform, transcript levels were measured in a range of human adult tissue using qRT-PCR.

The isoforms could be detected in all tissues tested (brain, heart, kidney, skeletal muscle, liver, spleen, thymus, adipose, colon, esophagus, lung, ovary, small intestine, testes, thyroid) indicating ubiquitous expression (Figure 3.6A-C). Relatively high levels of all isoforms were detected in the fetal brain, substantially higher than adult brain, consistent with *MCPH1* alternative splice isoforms playing a role in neurogenesis (Figure 3.6A-C). There are some tissue-specific differences in expression, for example higher levels of the S isoform are observed in testes (Figure 3.6B) and higher levels of Δ8 in heart and liver (Figure 3.6C). This suggests that MCPH1isoforms may play distinct roles in addition to brain-related functions.

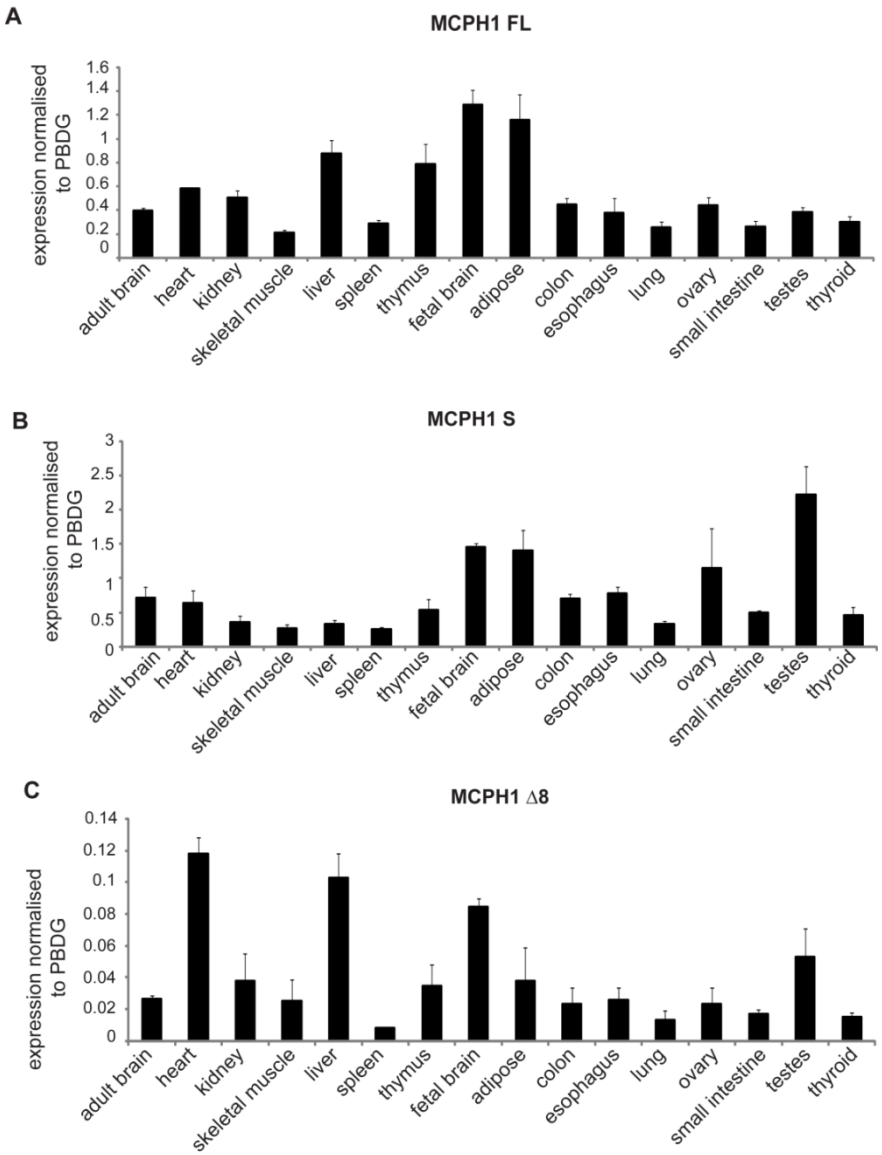

Figure 3.6. Expression patterns of *MCPH1* isoforms in human tissue.
qRT-PCR demonstrates tissue specific differences in *MCPH1* isoform expression. RNA isolated from human tissue panel was reverse transcribed to make cDNA for qPCR analysis of FL (A), S (B) or Δ8(C) expression levels. Values were normalised to the housekeeping gene porphobilinogen deaminase (PBDG). PBDG expression was established as having good inter-tissue reproducibility with C_T values between 21-24 cycles. Data are shown as mean ± s.d. of triplicate qPCR wells.

3.7. Cell-cycle differences in MCPH1 isoform expression

Although all transcripts are expressed in human fetal brain suggesting a role in neurogenic proliferation, each isoform may be required for distinct functions during cell proliferation. To determine if the isoforms are regulated differently during the cell cycle, transcript and protein levels were analysed.

HeLa cells were synchronised by a double thymidine block, released and collected at various time points. Isoform transcript levels were measured as the cells progressed through the cell cycle by using quantitative RT-PCR (Figure 3.7A). Whereas the expression levels of FL remained constant throughout the cell-cycle (black line), S (red) and Δ8 (green) levels varied. There was an incremental increase in Δ8 levels as the cells progressed from G_2/M phase into G_1 and S transcript levels peaked at S phase with lower levels in G_1 and G_2/M.

Western blot analysis of extracts with the MCPH1 antibody also showed relative differences in isoform protein abundance through the cell cycle (Figure 3.7B). FL protein levels were high in G_1 to S phase whereas S protein levels were low. During G_2/M phase FL protein levels were reduced whereas S levels increased. The decrease in abundance of FL protein in G_2/M is not due to changes in FL transcript levels suggesting there may be a post translational mechanism that targets the protein for degradation. Cell cycle progression was followed by immunodetection of cell cycle markers polokinase1, cyclin A, cyclin B1 and phospho-histone H3 (Figure 3.7B) and by FACs analysis of DNA content in propidium iodide stained cells (Figure 3.7C).

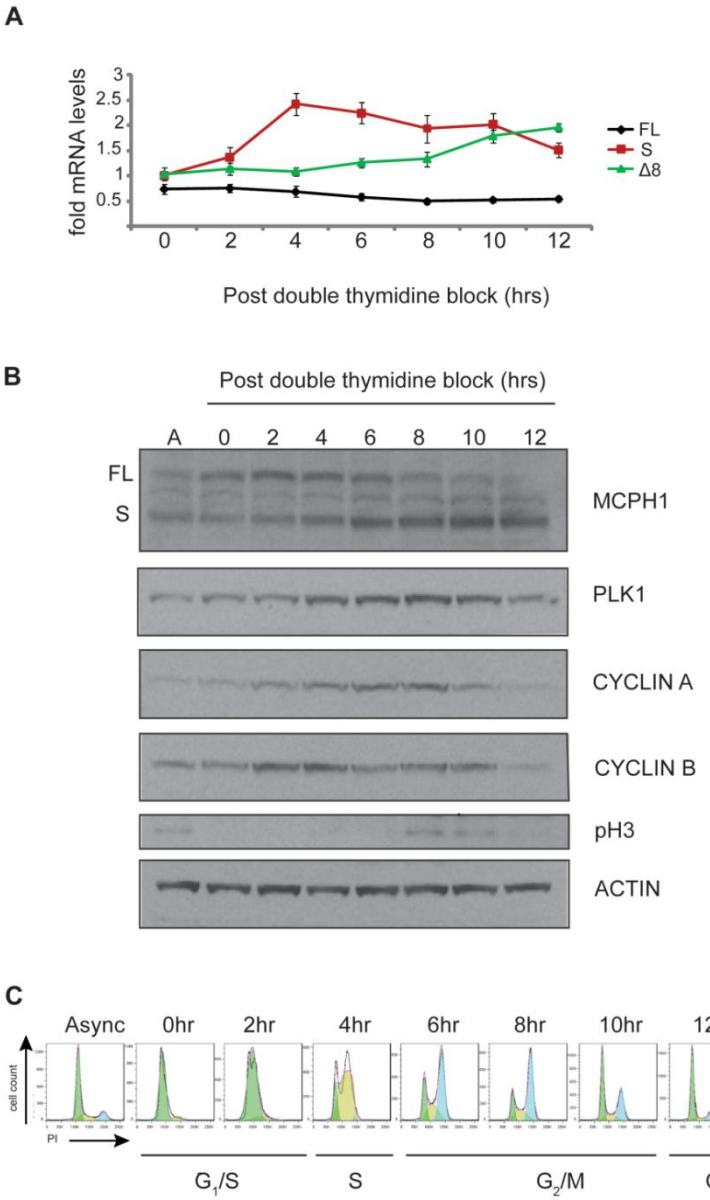

Figure 3.7. MCPH1 isoform levels during the cell cycle.
(A) qRT-PCR demonstrates cell cycle specific differences in *MCPH1* isoform expression. HeLa cells were synchronised during a double thymidine block, released to progress through the cell-cycle and RNA extracted from cells at indicated time points. RNA was reverse transcribed to make cDNA for qPCR analysis of FL (black), S (red) or Δ8 (green) expression levels. Values were normalised to the housekeeping gene PDGB which showed constant levels of expression throughout the cell cycle. Data is presented as mean ± s.e.m. of triplicate qPCR wells from three independent experiments. (B) Immunodetection of MCPH1 demonstrates cell cycle specific differences in isoform protein levels. Protein extracts from HeLa cells, synchronised as described in (A), were analysed by Western blotting with antibodies to MCPH1, β-actin (loading control), polokinase1, cyclin A, cyclin B1 and phospho-histone H3 (pH3 blotting performed by Rachel Rigby). (C) Cells were treated with propidium iodide (PI) and DNA content sorted by FACs. Analysis was performed in FlowJo using the Dean-Jett-Fox model (FlowJo analysis performed by Rachel Rigby). G_1 is shown in green, S phase in yellow and G_2/M in blue.

3.8. Discussion

Recent studies on the *Drosophila* orthologue of *MCPH1* revealed the existence of alternatively spliced variants of *mcph1* (Brunk *et al.*, 2007; Rickmyre *et al.*, 2007). Two of these isoforms exhibited distinct localisation patterns during mitosis and appeared to play distinct roles in the cell cycle in *Drosophila* syncytial embryos (Brunk *et al.*, 2007).

In Chapter 3, alternative splicing of human MCPH1 was characterised. The contribution of the isoforms to the pathogenesis of primary microcephaly was investigated and the potential separation of isoform function was also examined.

3.8.1. Alternative splice isoforms of MCPH1

In this chapter, RT-PCR of human fetal brain RNA established alternative splicing of MCPH1 intron 8 and exon 8 (Figure 3.2). These transcripts encode three proteins, one that contains all three BRCT domains (FL), one lacking the C-terminal tandem BRCT domains (S) and one lacking the majority of the inter-BRCT space (Δ8). An MCPH1 antibody detected both the FL and S isoform. These isoforms were absent in MCPH1 patient LBC and co-migrated with epitope-tagged versions of FL and S (Figure 3.3 & 3.5). In addition, RNAi oligonucleotides designed to specifically target individual isoforms led to a concomitant decrease in transcript and protein (Figure 3.4).

In contrast to MCPH1 FL and S, MCPH1(Δ8) protein could not be detected by Western blot. The MCPH1 antibody could detect MYC$(His)_6$-tagged Δ8 protein (Figure 3.3 C) but could not detect a protein band of the correct molecular weight that was either absent in MCPH1 patient-derived cells (Figure 3.3 & 3.5) or cells with siRNA mediated depletion of Δ8 (Figure 3.4). It is likely that this isoform is translated and not subject to NMD as it shares a transcriptional start site and termination codon with FL (Figure 3.1). It is possible that endogenous Δ8 protein is present at much lower abundance than FL and S and may be difficult to detect by Western blotting (similar difficulty reported in detecting PLK4 by Western blot (Cunha-Ferreira *et al.*, 2009)). Lower abundance of MCPH1(Δ8) may be due to lower transcript levels or reduced protein stability (for example, MCPH1(Δ8) may be

subject to rapid degradation or post-translational regulation). MCPH1(Δ8) may be detectable by Western blot from extracts of tissues, such as heart or liver, where transcript levels were highest (Figure 3.6).

3.8.2. Contribution of MCPH1 isoforms to primary microcephaly pathogenesis

It has been proposed that the brain specific phenotype of primary microcephaly could arise due to the existence of paralogues that can supply functional redundancy in all tissues except the brain (Bond and Woods, 2006; Megraw *et al.*, 2011). Indeed, potential paralogues have been identified for all primary microcephaly genes except *STIL* and *MCPH1* (Table 1.2). It is possible that the brain specific phenotype of MCPH1-linked primary microcephaly arises due to loss of only one MCPH1 isoform to which the neuronal progenitor cells are uniquely sensitive. However, the preliminary studies of this thesis are inconsistent with this hypothesis. First, all the MCPH1 isoform transcripts are expressed in fetal brain so all the protein isoforms may play a role in neurogenic proliferation (Figure 3.6). Second, all the reported MCPH1 mutations are within the coding region for FL, S and Δ8 (Figure 1.8 & 3.5) and all 5 MCPH1 patient mutations tested led to loss of MCPH1 FL and S protein (Figure 3.5). Primary microcephaly FL and S protein with the E88K substitution were also not detectable (Figure 3.5) suggesting that this substitution may lead to loss of MCPH1 protein stability. This was consistent with work from my Masters project ('Defining the functional role of a short isoform of microcephalin in humans and *Drosophila melanogaster*', University of Edinburgh, 2007) that demonstrated that the introduction of E88K substitution into recombinant BRCT1 domain had a huge impact on this domains solubility. There are three other MCPH1 missense mutations that have been identified (Darvish *et al.*, 2010; Trimborn *et al.*, 2005) and it would be interesting to determine the effect these have on the MCPH1 protein.

Thus, primary microcephaly cannot be assigned to loss of one particular MCPH1 isoform that is specifically expressed in the human fetal brain. However it is still possible there are uncharacterised MCPH1 isoforms with a different expression

pattern in the brain or that the already characterised isoforms have different functions in the neuronal progenitor cells.

3.8.3. Potential roles of MCPH1 isoforms

What is the biological purpose of generating alternative isoforms? In *Drosophila*, it serves as a mechanism by which to separate localisation and function during the cell cycle (Brunk *et al.*, 2007). *Mcph1* mutant embryos arrest during the syncytial divisions due to uncoordinated centrosome and nuclear cycles. Only Mcph1(S) can rescue this phenotype possibly due to its unique centrosomal localisation.

From the published MCPH1 biology it is likely that the MCPH1 isoforms identified will behave differently. The BRCT domains are phospho-protein binding modules (Manke *et al.*, 2003; Yu *et al.*, 2003) and their absence is likely to have functional consequences for the protein. For example the BRCT2/3 domain, which is absent in MCPH1(S), has been implicated in a number of important processes. Firstly, it is required for recruitment of MCPH1 to sites of DNA damage (Jeffers *et al.*, 2008; Wood *et al.*, 2007; Wu *et al.*, 2009). Secondly, it is required for MCPH1 oligomerisation and to function in E2F1 mediated transcriptional regulation (Yang *et al.*, 2008). The inter-BRCT space, most of which is missing in MCPH1(Δ8), has also been implicated in a number of important processes. MCPH1(Δ8) lacks the condensin II interaction site which is required for MCPH1 to function in homologous recombination (Wood *et al.*, 2008) and also lacks a strong bipartite nuclear localisation signal (PSORT II predictions) which may affect its subcellular localisation. It is interesting that the MCPH1 orthologue identified in chicken (cMcph1) also lacks most of the inter-BRCT space and has a very similar sequence alignment to MCPH1(Δ8) (Jeffers *et al.*, 2008). Further work will determine if there are multiple cMcph1 isoforms in chicken or if the cMcph1 orthologue identified performs all cMcph1 functions in chicken.

Indeed there were considerable differences in isoform transcript and protein levels during the cell cycle (Figure 3.7) consistent with the idea that different isoforms may be required at different stages of the cell cycle. The high levels of FL protein present during S-phase could reflect the requirement for this isoform to function in

homologous recombination (Liang *et al.*, 2010; Peng *et al.*, 2009; Wood *et al.*, 2008) which predominantly occurs during this time in the cell cycle. The higher levels of MCPH1(S) protein during G_2 to M phase may be important in mitosis as suggested from work in *Drosophila* syncytial embryos that show Mcph1(S) is required to coordinate nuclear and centrosomal divisions (Brunk *et al.*, 2007). The variation in MCPH1 levels during the cell cycle is also the first piece of evidence to demonstrate that MCPH1 is a cell cycle regulated protein. It is interesting that FL levels are decreased during G_2/M, by a mechanism independent of transcription. FL may be subject to post-translational regulation possibly targeting it for degradation. This finding is further elaborated in chapter 6 where post-translational regulation of MCPH1 is the main focus.

In addition to a role in neurogenesis MCPH1 isoforms may play other functionally important physiological roles *in vivo*. Although expression was ubiquitous in adult tissue tested, expression levels of isoforms varied between tissues. For example, higher levels of Δ8 transcript expression were observed in heart and liver (Figure 3.6 A). The S transcript was highly expressed in adult testes (Figure 3.6 B) which may correlate with the high levels of cell proliferation in this organ. Consistent with this, it has been demonstrated that Mcph1 is required for the development of mice spermatocytes (Liang *et al.*, 2010). However, this developmental defect is linked to a perturbation of meiotic homologous recombination which is likely to be the function of Mcph1(FL) rather than Mcph1(S) (see above). Nevertheless Mcph1(S) may be playing additional uncharacterised roles in the testes.

Chapter 4. Localisation studies of MCPH1 isoforms

In *Drosophila melanogaster*, the Mcph1 isoforms localised to distinct subcellular compartments during mitosis which may underlie their different functions during the cell cycle. The Long isoform localised as discrete foci on the mitotic DNA whereas the Short isoform appears to localise to the centrosomes and mitotic spindle in syncytial embryos (Brunk *et al.*, 2007).

In Chapter 3, the human MCPH1 isoforms FL, S and Δ8 were characterised. MCPH1 FL and S are orthologous to Mcph1 Long and Short in *Drosophila* and may also show distinct localisations. Chapter 4 describes the localisation of each of the MCPH1 isoforms with particular focus on mitotic distribution. In addition, individual MCPH1 domains were investigated to establish their roles in directing MCPH1 localisation.

4.1. MCPH1 isoforms exhibit distinct localisations during interphase

To determine the intracellular distribution of each of the MCPH1 isoforms, transcripts were cloned into the pEGFP_DEST vector and transiently expressed in Cos-7 cells under a cytomegalovirus (CMV) promoter. Expression of each of the N-terminally GFP-tagged isoforms was confirmed by immunoblot analysis with an anti-GFP antibody (Figure 4.1 A). Immunofluorescence demonstrated that during interphase all the isoforms were present in the nucleus but only GFP-MCPH1(Δ8) was found in the cytoplasm (Figure 4.1 B). Often the GFP-tagged MCPH1 isoforms formed nuclear aggregates (Figure 4.1 B). Nuclear aggregates were usually found in the cells with the greatest levels of GFP-tagged protein and so it is likely to be an artefact of protein overexpression.

Consistent with the immunofluorescence, biochemical fractionation of HeLa cells into nucleus and cytoplasm-enriched fractions demonstrated that endogenous MCPH1 FL and S were only found in the nuclear fraction (Figure 4.1 C). Psort II sequence based localisation predictions also predicted a nuclear distribution for MCPH1 FL, S and Δ8 and a cytoplasmic localisation for MCPH1(Δ8) only (Figure

4.1 D). Thus, the MCPH1 isoforms have a distinct intracellular localisation, they all localise to the nucleus, but only MCPH1(Δ8) can localise to the cytoplasm which may enable it to play a distinct function from MCPH1 FL and S during interphase.

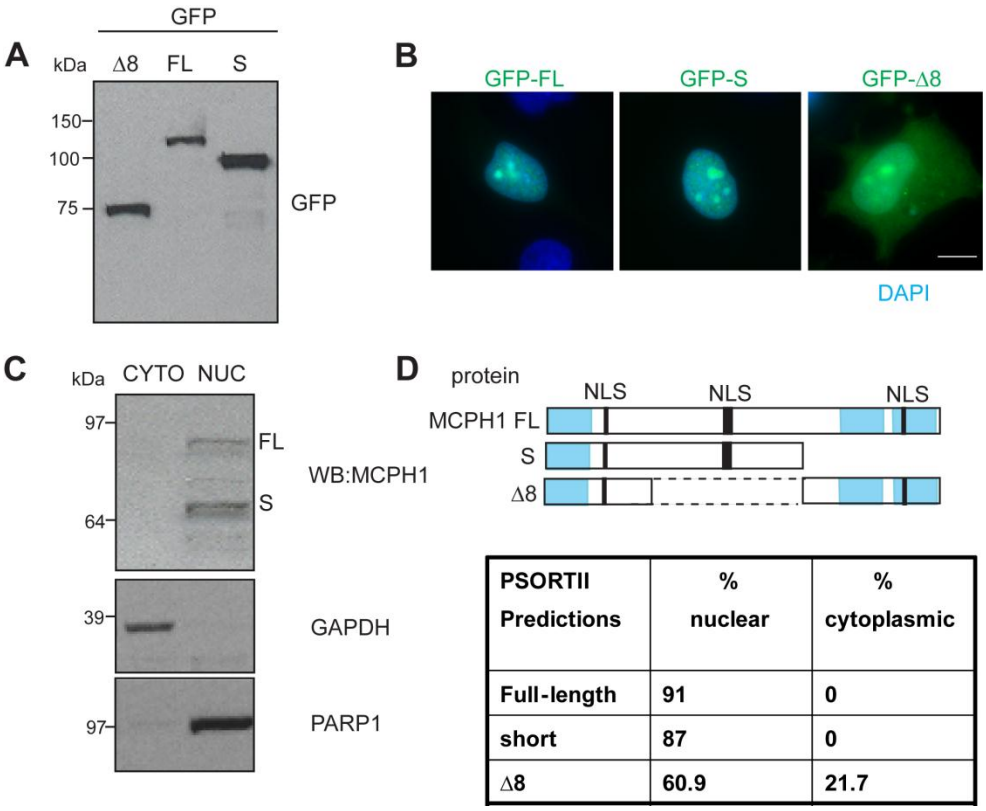

PSORTII Predictions	% nuclear	% cytoplasmic
Full-length	91	0
short	87	0
Δ8	60.9	21.7

Figure 4.1. Localisation of MCPH1 isoforms during interphase.
(A) GFP-tagged MCPH1 isoform protein expression. Cell lysate from Cos-7 cells transfected with pEGFP_MCPH1_FL, S or Δ8 vectors was electrophoresed on a 10% polyacrylamide gel and Western blotted with anti-GFP antibodies. (B) Localisation of GFP-tagged MCPH1 isoforms during interphase. Cos-7 transfectants treated as in (A) were fixed in methanol and stained with DAPI to visualise DNA (blue). Images were of single planes captured on a fluorescence widefield microscope. Scale bar represents 10 µm. (C) Endogenous MCPH1 FL and S protein are enriched in nuclear preparations. Fractions enriched for nuclear or cytoplasmic components were obtained by hypotonic lysis of HeLa cells. Proteins were separated on a 4-12% Bis-Tris polyacrylamide gel and Western blotted with MCPH1 antibody. Appropriate fractionation was verified by immunoblotting for the nuclear protein PARP1 and cytoplasmic marker GAPDH. (D) Bioinformatic predictions of endogenous MCPH1 isoform localisation. Schematic of location of PSORT II predicted nuclear localisation signals (NLS) and table of PSORT II cytoplasmic and nuclear localisation scores.

4.2. MCPH1(Δ8) localises to the centrosome during interphase

It has been established by indirect immunofluorescence and biochemical purification that MCPH1 localises to the centrosome during interphase (Tibelius *et al.*, 2009; Zhong *et al.*, 2006). To determine what isoforms localise to the centrosome, co-immunofluorescence of GFP-tagged MCPH1 isoforms and a centrosome marker (γ-tubulin) was undertaken. During interphase, GFP-Δ8 did co-localise with γ-tubulin whereas FL and S were absent from the centrosomes (Figure 4.2). Thus only MCPH1Δ8 can localise to the centrosome during interphase and it is likely that it is this isoform that is detected at the centrosome by indirect immunofluorescence.

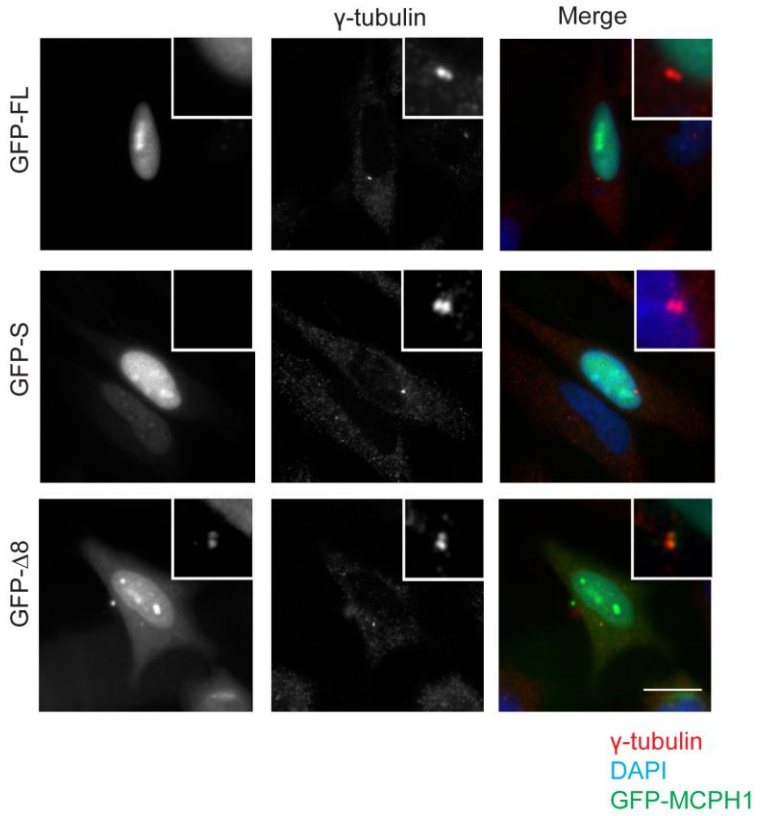

Figure 4.2. Centrosomal localisation of MCPH1 Δ8 during interphase.
(A) Co-localisation of GFP-tagged MCPH1 isoforms with the centrosome. HeLa cells transiently expressing GFP-tagged MCPH1 FL, S or Δ8 isoforms were fixed in methanol and stained with ϒ-tubulin (red) antibodies to visualise the centrosome. Images were of single planes captured on a fluorescence widefield microscope. The insets show 4 x magnified images of the centrosomes. Scale bar represents 10 μm.

4.3. MCPH1 isoforms exhibit distinct subcellular localisation during mitosis

4.3.1. Inducible regulation of MCPH1 expression

After establishing MCPH1 isoform localisation during interphase, the mitotic distribution was investigated. It had been previously established in the lab (Kathy Surinya & Andrew Jackson, unpublished) that over-expression of MCPH1(FL) with a CMV-driven promoter led to a G_2 phase arrest making visualisation of GFP-MCPH1 localisation during mitosis very difficult with the current vector system. To circumvent this problem a tetracycline inducible vector with a GFP N-terminal tag was generated (Figure 4.3A). In this system MCPH1 expression is under the control of an inducible promoter enabling regulation of expression to levels permissive for cell cycle progression.

To characterise the regulation of MCPH1 levels by the tetracycline inducible promoter, dose-response and the kinetics of induction were examined. HeLa tetracycline-on cells were transfected with the pTRE_GFP_MCPH1(FL) vector and treated with varying levels of doxycycline (0, 0.1, 1, 10, 100, 1000 ng/ml). Expression levels, measured by immunoblotting of cell extracts with anti-GFP antibody, were detectable at doxycycline concentrations above 10 ng/ml and maximal activation was achieved at 100 ng/ml (Figure 4.3B). To measure the kinetics of induction, GFP-MCPH1(FL) expression levels were measured after treatment with 1 μg/ml of doxycycline for 0, 2, 4, 6 and 8 hr. Following 2 hr of induction, GFP-MCPH1(FL) was detectable by Western blot showing a rapid response to doxycycline treatment (Figure 4.3C). These experiments demonstrated that the inducible promoter exhibited a sensitive and rapid response to doxycycline and would therefore allow fine-tuning of MCPH1 expression levels.

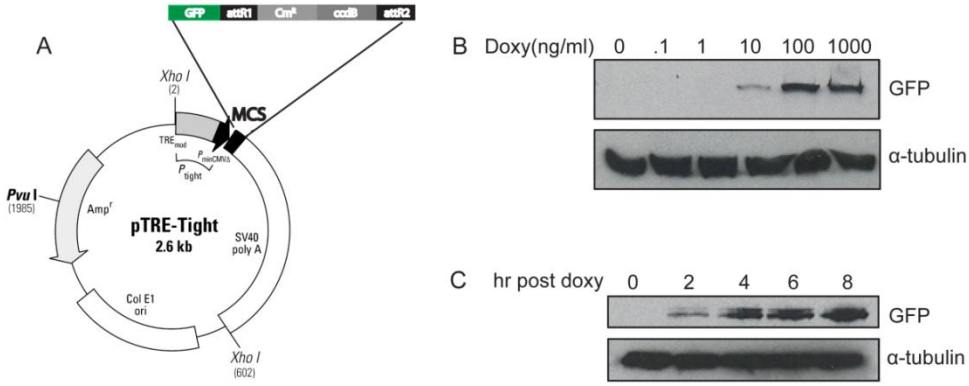

Figure 4.3. Tetracycline-inducible gene expression system.
(A) Schematic of pTRE_tight_EGFP_DEST. Tetracycline-inducible expression vector pTRE_tight was engineered with EGFP ORF and Gateway destination cassette by conventional cloning methods (see Table 2.3 for cloning details). (B) Dose-response of MCPH1(FL) induction after doxycycline treatment. HeLa Tet-On cells were transfected with pTRE_tight_EGFP plasmid expressing GFP-MCPH(FL) and grown in the presence of the indicated amounts of doxycycline for 16 hr. The cells were harvested, 40 µg of protein from cell extracts was separated on a 8 % polyacrylamide gel and Western blotted with GFP and α-tubulin antibodies (loading control). (C) Kinetics of MCPH1(FL) induction after doxycycline treatment. HeLa Tet-On cells were transfected with pTRE_tight_EGFP plasmid expressing GFP-MCPH1(FL) and grown in the presence of 1 µg/ml doxycycline for up to 8 hr. The cells were harvested at the indicated time points, and 55 µg of protein from extracts was Western blotted.

4.3.2. MCPH1 isoform localisation during mitosis

The tetracycline responsive promoter allowed expression levels that permitted a small fraction of cells to progress into mitosis whilst over-expressing MCPH1. This was observed by immunofluorescence as an increase in GFP-MCPH1 mitotic cells. To increase this proportion further, following transfection, cells were synchronised by a single thymidine block, released and fixed when the mitotic cell population is enriched (Figure 4.4A). This protocol was followed for the majority analysis of mitotic cells over-expressing MCPH1.

Following this protocol the localisation of GFP-MCPH1(FL) was analysed. Immunofluorescence of mitotic cells expressing GFP-tagged MCPH1(FL) and co-stained for α-tubulin, a microtubule marker, showed that MCPH1(FL) was present as discrete foci at the plus and minus ends of the microtubules of the mitotic spindle (Figure 4.4B). This localisation was maintained from prometaphase through to late anaphase. However by late anaphase MCPH1(FL) only weakly associates to the plus end of microtubules (see also Figure 4.6 and 6.10A). At telophase the nuclear envelope reforms and MCPH1(FL) diffusely localises to the nucleus. This distinct distribution is likely to represent MCPH1(FL) localisation to the centromeres on DNA and centrosomes at the spindle poles but requires confirmation by co-immunofluorescence with the appropriate markers. These findings were reproducible in unsynchronised cells over-expressing GFP-tagged MCPH1(FL), confirming this localisation is independent of synchronisation treatment. Thus, it appears that during mitosis MCPH1(FL) localises to the centromeres and centrosomes.

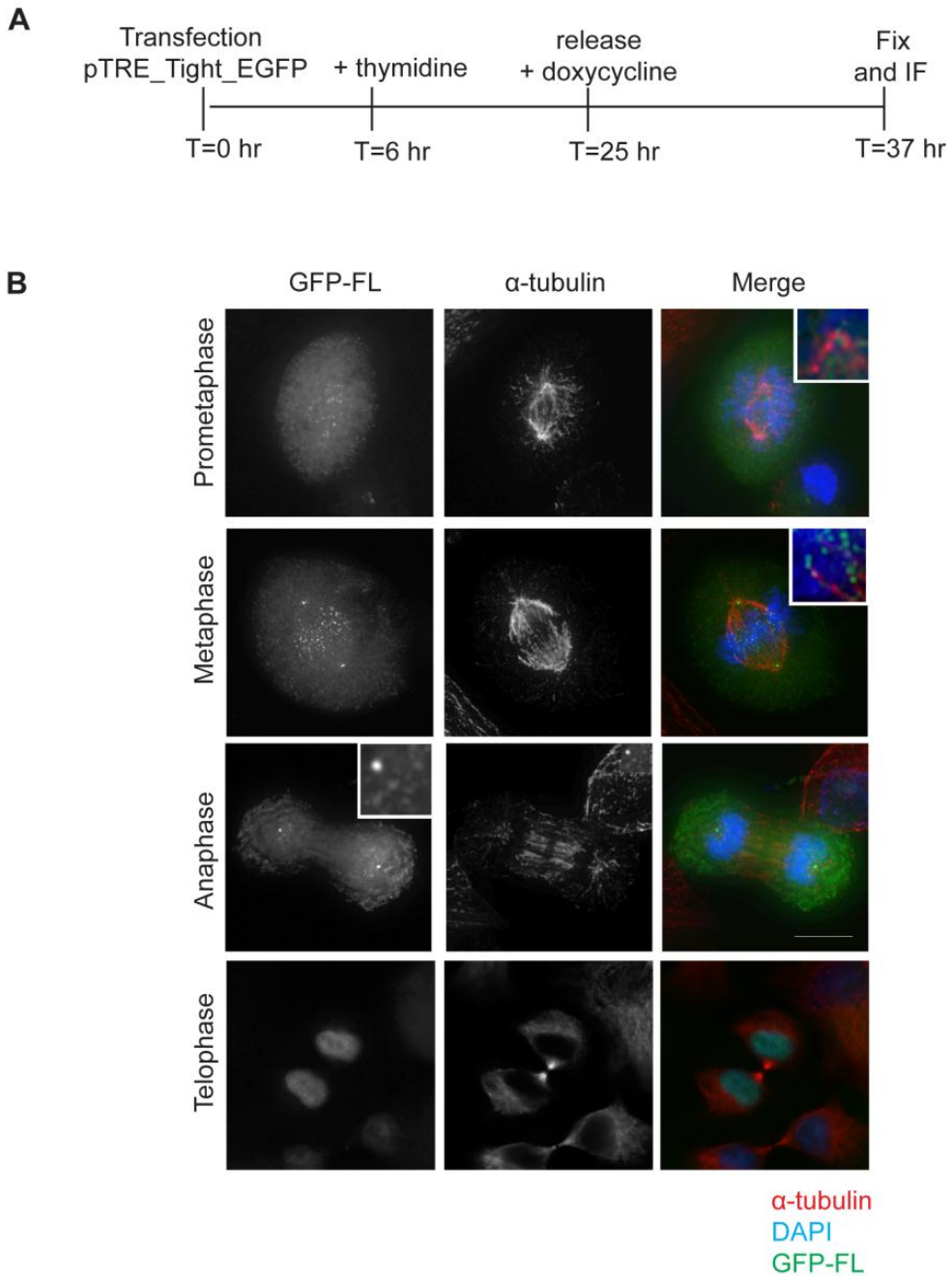

Figure 4.4. Localisation of GFP-tagged MCPH1 FL during mitosis.
(A) Diagrammatic representation of pTRE_tight_EGFP transfection, thymidine block and doxycycline treatment protocol. HeLa Tet-On cells were transfected with pTRE-Tight_EGFP_MCPH1 vector. After 6 hr cells were treated with thymidine for 19 hr, followed by a 12 hr release with doxycycline treatment to induce GFP- tagged protein expression. (B) HeLa Tet-On cells treated according to the protocol in (A) were fixed in methanol and stained with α-tubulin (red) antibody to visualise the mitotic spindle. DNA was stained with DAPI (blue). Images are projections of deconvolved z-stacks captured on a widefield microscope. Insets represent 4 X magnification images showing the localisation of GFP-MCPH1(FL) at the centrosome in prometaphase, centromeres in metaphase and anaphase. Scale bar represents 10 µm.

The metaphase localisation was compared between GFP-tagged MCPH1 FL, S, Δ8 and MYC(His)$_6$ as a control. Expression of each of the GFP-tagged isoforms at mitosis was confirmed by immunoblot analysis of extracts from cells arrested in prometaphase with nocodazole treatment (Figure 4.5A). Immunofluorescence with α-tubulin demonstrated that similarly to GFP-MCPH1(FL), the Δ8 isoform also localised to discrete foci at the spindle pole and DNA (Figure 4.5B). In addition to punctate staining on the DNA, GFP-MCPH1(Δ8) also diffusely localises to the DNA, suggesting it can associate with the chromosomes. Surprisingly, MCPH1(S) showed a diffuse cellular localisation with no association to any subcellular compartments, similar to the MYC(His)$_6$ control (Figure 4.5B). Thus, there are similarities between MCPH1 FL and Δ8 localisation during mitosis but MCPH1(S) is distinct from both.

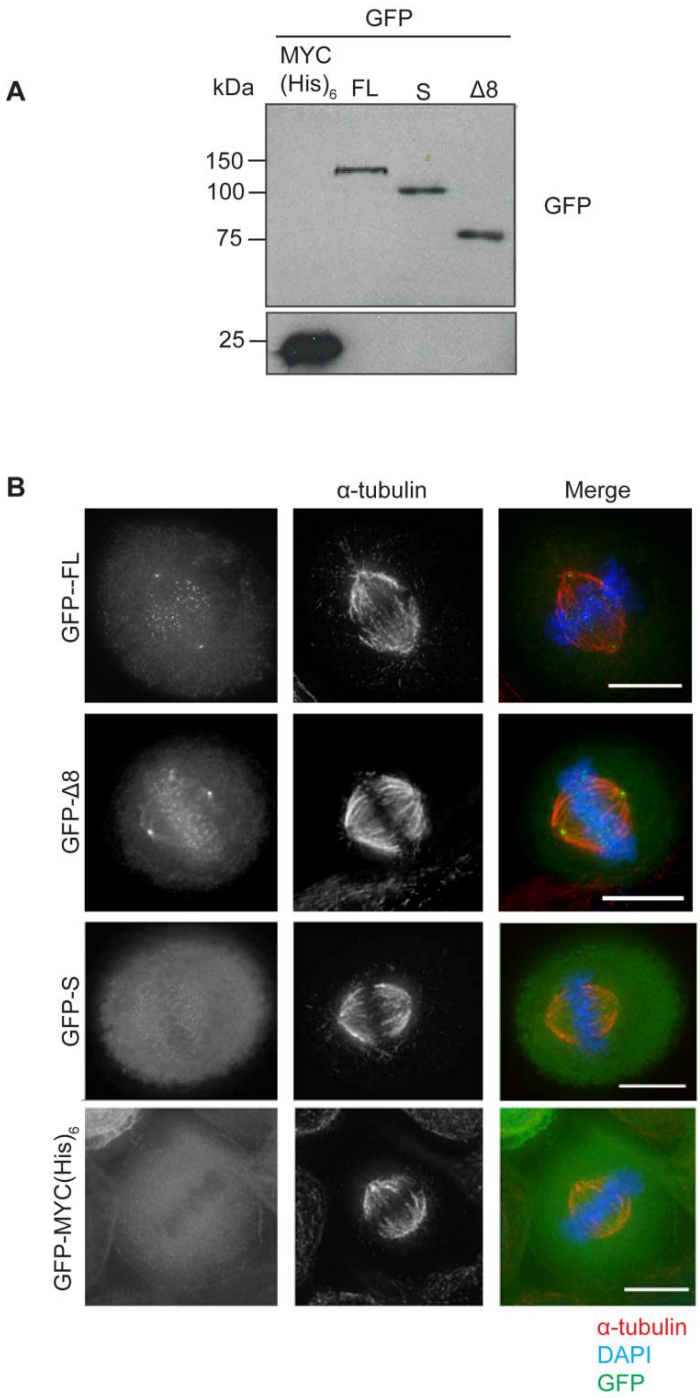

Figure 4.5. Localisation of GFP-tagged MCPH1 isoforms during metaphase.
GFP-tagged MCPH1 isoform protein expression during mitosis. (A) HeLa Tet-On cells were transfected with pTRE_Tight_EGFP_MCPH1 FL, S or Δ8 vectors, treated with doxycycline and nocodazole for 16 hr. Cell lysates were fractionated on a 10% polyacrylamide gel and Western blotted with anti-GFP antibodies. Both panels represent immunoblots of the same exposure. (B) HeLa Tet-On cells transiently expressing GFP-tagged MCPH1 isoforms were fixed in methanol, immunostained with α-tubulin (red) antibodies to reveal the microtubules and DAPI to visualise the DNA. GFP-MCPH1(FL) metaphase cell from Figure 4.4 was included for comparison. Scale bar represents 10 µm.

4.4. MCPH1(FL) and Δ8 localise to the kinetochores

During mitosis, GFP-tagged MCPH1(FL) localised to discrete foci at the plus-end of microtubules (Figure 4.5). This localisation appeared to be centromeric or kinetochore associated and to confirm this GFP-MCPH1(FL) expressing cells were stained with anti-centromere antibodies (ACA). ACA antibody serum is isolated from patients with scleroderma CREST that produce autoantibodies against a variety of characterised centromeric and kinetochore proteins including CENP-A, CENP-B and CENP-C (Earnshaw and Rothfield, 1985). MCPH1(FL) co-localised with ACA from prometaphase through to anaphase (Figure 4.6A). At anaphase MCPH1(FL) begins to redistribute to the chromatin (Figure 4.6A). This dynamic cell-cycle dependent co-localisation is most consistent with MCPH1(FL) being a component of the kinetochore.

Many of the components of the kinetochore are transiently associated and often their concentration levels at the kinetochore are influenced by the kinetochore-microtubule (kMT) attachment state. To determine whether MCPH1(FL) kinetochore localisation is affected by microtubule attachment state, GFP-MCPH1(FL) localisation was examined following treatment with the microtubule destabilising agent, nocodazole, or microtubule stabiliser, taxol. Under these conditions, both MCPH1(FL) and ACA immunostaining was maintained at the kinetochores (Figure 4.6B). This indicates that distribution of MCPH1(FL) to the kinetochores was independent of the microtubules suggesting it is a core component of the kinetochores.

Both MCPH1 FL and Δ8 can localise to the kinetochores suggesting that a shared domain is responsible for this localisation. FL and Δ8 isoforms share amino acid residues 1-223 and 608-836 which contain all three BRCT domains (Figure 4.6C). To further narrow-down the region of MCPH1 required for directing MCPH1 kinetochore localisation, various fragments of MCPH1 (residues 1-89, 1-223 and 634-836) were cloned into the pTRE_EGFP_DEST vector, expressed in HeLa cells and kinetochore localisation investigated by immunofluorescence (Figure 4.6D). None of these fragments are sufficient for kinetochore localisation, suggesting all BRCT domains may be required for this localisation.

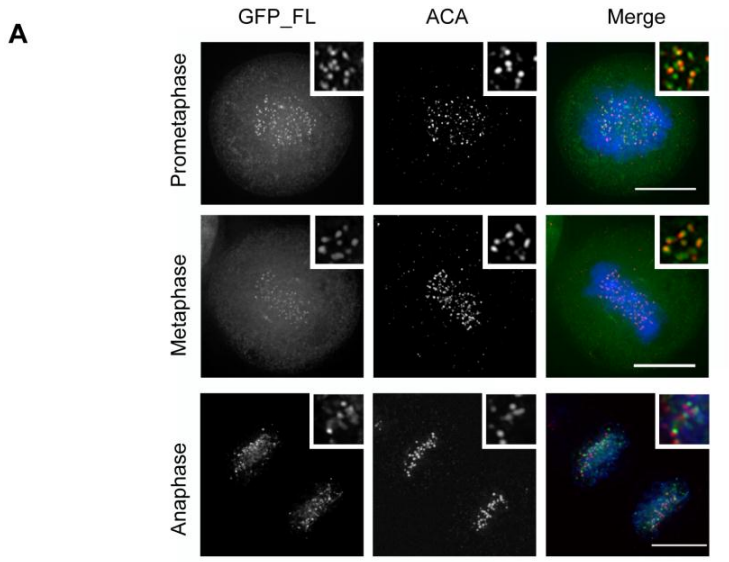

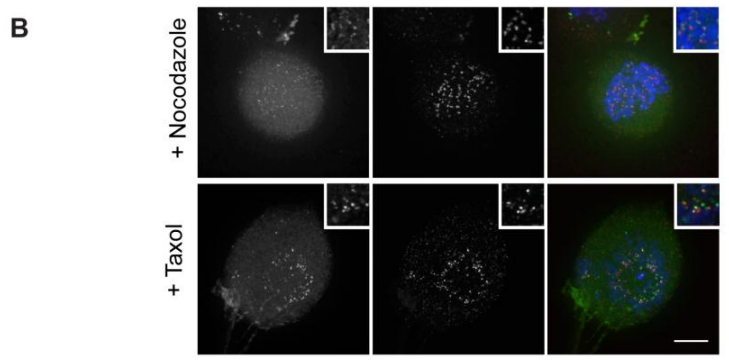

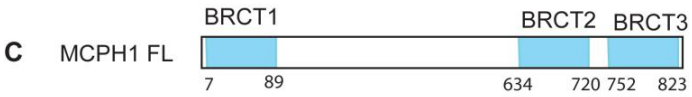

D

Protein fragment	Amino Acids	Kinetochore localisation
GFP-MCPH1FL	1-836	+
GFP_MCPH1S	1-608	-
GFP-MCPH1Δ8	1-223 & 608-836	+
GFP-MCPH1Nterm	1-223	-
GFP-MCPH1BRCT1	1-89	-
GFP-MCPH1BRCT2,3	634-836	-
GFP-MYC(His)$_6$		-

Figure 4.6. Analysis of kinetochore localisation of MCPH1.
(A) Co-localisation of GFP-tagged MCPH1 FL with the kinetochore. Cells expressing GFP-MCPH1(FL) were fixed in 4 % PFA , stained with DAPI to visualise DNA and with anti-centromeric antibodies (ACA) (red). (B) GFP-tagged MCPH1 FL localisation to the kinetochore is independent of kMT attachment status. Synchronised cells expressing GFP-MCPH1(FL) were treated with nocodazole or taxol for 4 hr. The cells were then fixed in methanol and stained with ACA antibodies and DNA was visualised by DAPI. The insets are 3 x magnified images. Scale bars are 10 µm. (C) Schematic representation of MCPH1 protein showing location of BRCT domains. (D) Table summarising the GFP-MCPH1 fragments expressed and their localisation to the kinetochores.

4.5. MCPH1(FL) localises to the centrosomes in a microtubule-dependent manner

GFP-tagged MCPH1 FL and Δ8 appeared to localise to the centrosome during mitosis (Figure 4.5). MCPH1(Δ8) localisation to the centrosomes during interphase has already been established (Figure 4.2). To confirm that GFP-MCPH1(FL) localised to the centrosome at mitosis co-immunofluorescence with pericentrin, a marker for the centrosome, was performed (Figure 4.7A). GFP-MCPH1(FL) staining is often distinct from pericentrin (a marker for the pericentriolar material (PCM)) as often two distinct foci per centrosome could be visualised. This suggests that MCPH1 may localise to the centrioles rather than PCM. However this has not been formally validated by co-localisation with centriolar markers.

To examine the dependence of MCPH1(FL) mitotic centrosome localisation upon microtubules, HeLa cells expressing GFP-MCPH1(FL) were treated with nocodazole for 4 hr. Under these conditions, pericentrin immunostaining was maintained at the centrosomes, much of GFP-MCPH1(FL) staining was lost but there is still some weak association with the centrosomes, possibly co-localising with the centrioles (Figure 4.7B). This indicates that although there is a microtubule-dependent pool of MCPH1(FL) there also appears to be microtubule independent pool of MCPH1(FL) suggesting MCPH1 is a bonafide constituent of the centrosome.

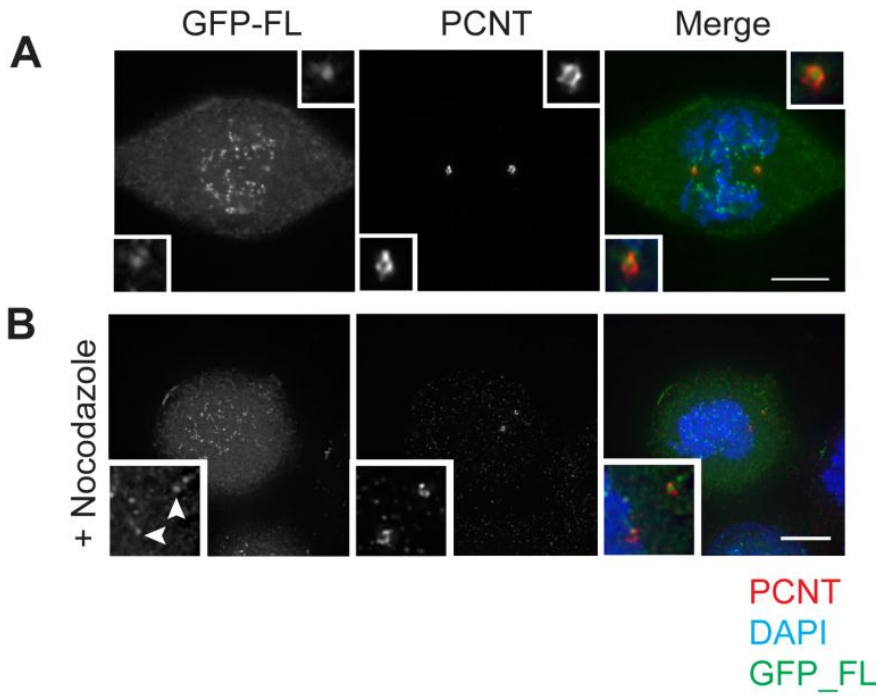

Figure 4.7. Localisation of GFP-MCPH1 FL to the centrosome during mitosis.
(A) Co-localisation of GFP-tagged MCPH1(FL) with centrosome marker pericentrin. HeLa Tet-On cells transiently expressing GFP-tagged MCPH1(FL) were fixed in methanol, immunostained for the centrosome with pericentrin antibodies (PCNT) (red). (B) GFP-tagged MCPH1(FL) localises to centrosome in a microtubule dependent and independent manner. Synchronised cells expressing GFP-MCPH1(FL) were treated with nocodazole for 4 hr. The cells were then fixed in methanol and stained with pericentrin antibodies. The insets show 3 x magnified images. The arrowheads in B show GFP-MCPH1(FL) associated with pericentrin. DNA was visualised by DAPI. Scale bars are 10 μm.

4.6. MCPH1 N-terminus is sufficient for centrosomal localisation

This thesis has established that MCPH1 FL and Δ8 can localise to the centrosomes suggesting that a shared domain is responsible for MCPH1 centrosomal localisation. FL and Δ8 share amino acid residues 1-223 and 608-836 which contain all three BRCT domains (Figure 4.8A). To further narrow-down the region of MCPH1 required for directing MCPH1 centrosomal localisation, various fragments of MCPH1 (residues 1-89, 1-223 and 634-836) were cloned into the pTRE_EGFP_DEST vector and expressed in HeLa cells. The centrosomal localisation is investigated by co-immunofluorescence with γ-tubulin (Figure 4.8B).

As shown in Figure 4.8C, the N-terminus (aa residues 1-223) is sufficient for centrosomal localisation at interphase and mitosis. This region contains the BRCT1 domain (aa residues 1-89), a protein-protein interaction module, which alone is not sufficient for a strong centrosomal localisation (Figure 4.8B) but may be necessary for its recruitment.

A

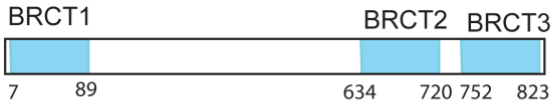

B

Protein fragment	Amino Acids	Centrosome localisation
GFP-MCPH1FL	1-836	+
GFP_MCPH1S	1-608	-
GFP-MCPH1Δ8	1-223 & 608-836	+
GFP-MCPH1Nterm	1-223	+
GFP-MCPH1BRCT1	1-89	-
GFP-MCPH1BRCT2,3	634-836	-
GFP-MYC(His)$_6$		-

C

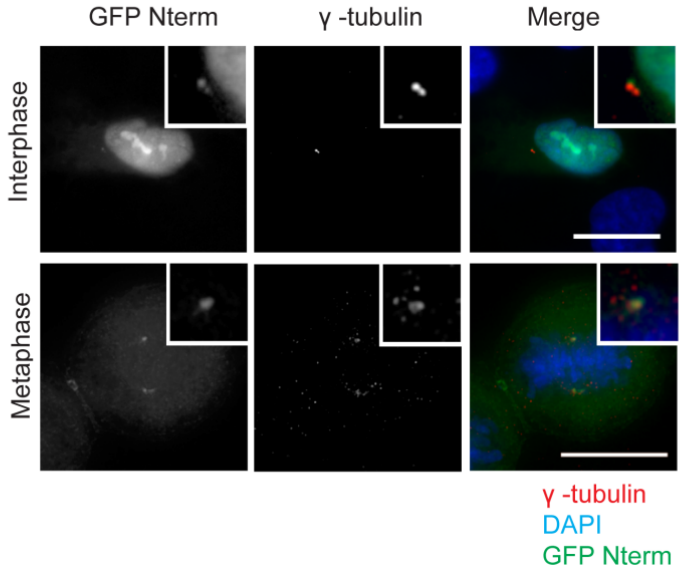

Figure 4.8. Analysis of centrosomal localisation of MCPH1 fragments.
(A) Schematic representation of MCPH1 protein showing location of BRCT domains. (B) Table summarising the GFP-MCPH1 fragments analysed and their centrosomal localisation. (C) MCPH1 Nterm localises to the centrosome. Images showing the localisation of GFP-MCPH1 Nterm (green), ϒ-tubulin (red) and DNA (blue) in HeLa cells. The insets are 3 x magnified images. Scale bar represents 10 µm.

4.7. The BRCT1 domain of MCPH1 interacts with centrosomal component PCNT

The BRCT1 domain is required for an interaction with centrosomal protein γ-tubulin by GST pull-down assays (Elen Griffiths HGU, personal communication). This suggests that although this domain alone is not sufficient for centrosome localisation it may still be important for mediating some centrosomal interactions and for centrosomal recruitment; indeed in DT40 cells, the BRCT1 domain is required for cMcph1 centrosomal localisation in irradiated cells (Jeffers *et al.*, 2008).

Therefore, the interaction of BRCT1 with other centrosomal proteins was investigated using recombinant GST or GST-BRCT1 in pull-down assays from HeLa cell lysates. In this experiment, the interaction between BRCT1 and γ-tubulin was confirmed (Figure 4.9A). Additionally, a novel interaction with pericentrin was identified (Figure 4.9B). Interestingly, BRCT1 only interacts with the 350 kDa isoform of pericentrin (PCNT B) and not the C-terminally truncated isoform (PCNT A) (Figure 4.9B) (Flory and Davis, 2003; Li *et al.*, 2001; Miyoshi *et al.*, 2006). Only PCNT B contains the PACT domain, which is important for centrosomal targeting (Gillingham and Munro, 2000), suggesting that this interaction may be relevant to the centrosomal function/localisation of MCPH1. Indeed an interaction between MCPH1 and PCNT has been subsequently confirmed by endogenous immunoprecipitation (Tibelius *et al.*, 2009). Thus, BRCT1 is sufficient for an interaction with two key centrosome components pericentrin and γ-tubulin which may play a role in recruitment of MCPH1 to the centrosome.

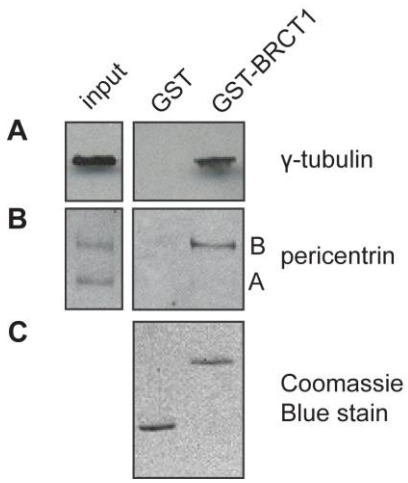

Figure 4.9. MCPH1-BRCT1 interacts with pericentrin and ϒ-tubulin.
Two experiments were performed in which HeLa lysates were incubated with glutathione-S-sepharose beads coated with GST (control) or GST tagged MCPH1 BRCT1. After washing, the binding of ϒ-tubulin (A) and pericentrin (B) was assessed by immunoblotting. The lane marked input was 5% of the volume used for pull-down. (C) Prior to pull-down analysis equivalent amounts of the GST proteins was determined by Coomassie blue staining.

4.8. Discussion

In this chapter, MCPH1 isoform localisation during mitosis was investigated and it was established that specific MCPH1 isoforms (characterised in Chapter 3) localise to the kinetochore and centrosome. This is the first conclusive evidence that MCPH1 can localise to the kinetochores during mitosis. This possibility was first raised by the localisation of *Drosophila* GFP-Mcph1(L) to discrete foci on the DNA during mitosis (Brunk *et al.*, 2007). Similar to in *Drosophila*, MCPH1(FL) (orthologue of Mcph1(L)) can localise to kinetochores.

4.8.1. Validation of epitope-tagged localisation studies

Attempts have been made to validate the epitope-tagged localisation studies by indirect immunofluorescence using commercially available MCPH1 antibodies (Bethyl laboratories #A300-368A, Abcam #ac2612 and Abnova #6265,), published antibodies (Lin *et al.*, 2005; Tibelius *et al.*, 2009) and some developed in the A. Jackson lab. Unfortunately none of these antibodies could unequivocally detect MCPH1 localisation at the kinetochores or centrosomes by immunofluorescence, despite three of these antibodies being reported to detect MCPH1 at the centrosome (Rai *et al.*, 2008; Tibelius *et al.*, 2009; Zhong *et al.*, 2006). Many of the antibodies simply do not detect MCPH1 cytologically, as there was no co-localisation when GFP-MCPH1(FL) was expressed. Other antibodies, particularly mouse monoclonals developed with Carl Smythe (University of Sheffield), did detect over-expressed GFP-MCPH1(FL) but did not reproducibly detect MCPH1 at the centrosome and kinetochore. It is likely that in this case the MCPH1 epitopes may be masked at the centrosome/kinetochore or that the antibody cannot gain access to the epitope in this location (Martinez-Campos *et al.*, 2004). Indeed detection of GFP-MCPH1(FL) at the centrosomes and kinetochores with an anti-GFP antibody has also been difficult to show. Alternatively endogenous levels of MCPH1 may be so low that it is difficult to detect with traditional immunofluorescence (Cunha-Ferreira *et al.*, 2009). Some of these limitations may be overcome by using enzyme-amplification techniques, such as the tyramide amplification kit (Perkin-Elmer Life Sciences), which can significantly increase immunofluorescence sensitivity (Bobrow *et al.*, 1992; van Gijlswijk *et al.*, 1997).

4.8.2. MCPH1 kinetochore localisation

MCPH1(FL) localisation to the kinetochores was demonstrated by the co-localisation with anti-centromeric antibodies (ACA) during mitosis (Figure 4.6A). The inner kinetochore consists of a large network of proteins called the constitutive centromere associated network (CCAN) that assembles on centromeric chromatin throughout the cell-cycle (reviewed by Amor *et al.*, 2004). ACA is reactive against CENP-A, CENP-B and CENP-C, all components of the CCAN (Earnshaw and Rothfield, 1985). MCPH1 appears to localise to the kinetochores during mitosis; this temporal localisation is more consistent with MCPH1 being a component of the outer kinetochore. The outer kinetochore assembles on the CCAN prior to mitosis and their role is to ensure correct segregation of the chromosomes through functionally mediating microtubule attachments during mitosis (reviewed by Cheeseman and Desai, 2008; Przewloka and Glover, 2009). The MCPH1 kinetochore localisation therefore suggests that it too may function in this process.

In immunofluorescence experiments, the MCPH1(FL) signal often appeared immediately adjacent to the ACA signal rather than completely overlapping it. Technically, the experiments performed in this thesis have not been designed to address MCPH1(FL) localisation on such a fine scale. Future experiments using temperature control and capturing every channel of a single z-section will ensure greater accuracy during acquisition. This combined with specific markers to define the centromere and outer kinetochore will enable the exact location of MCPH1 to be determined.

Some proteins are more transiently associated with the kinetochores, for example some microtubule motors or plus-end binding proteins (reviewed by Maiato *et al.*, 2004). The localisations of these transient components of the kinetochore are often influenced by the microtubule attachment state. Some plus-end binding proteins require microtubules to localise to the kinetochores, for example EB1 (Tirnauer *et al.*, 2002) whereas some microtubule motor proteins, such as CENP-E and dynein, or spindle checkpoint proteins, such as MAD1, MAD2 and BUBR1, localise to the kinetochore at higher levels when the microtubules are not attached (Hoffman *et al.*, 2001). MCPH1(FL) kinetochore localisation is fairly constant from prometaphase

through to anaphase (Figure 4. 4), nor is its localisation significantly affected by kMT attachment status (Figure 4.6B) suggesting that it may comprise part of the structural core of the kinetochore.

Kinetochore proteins are recruited in a temporal, step-wise fashion from G_2 phase through to mitosis (Figure 4.10). A result of this is that the timing of kinetochore localisation and delocalisation can help identify candidate proteins required for MCPH1 recruitment as well as provide information about potential kinetochore function. For example, the Mis12 complex, one of the first kinetochore proteins to be recruited, appears to play a particularly important role in licencing kinetochore assembly (Kline *et al.*, 2006; Obuse *et al.*, 2004). The exact stage of MCPH1 recruitment has not been established, MCPH1(FL) can be observed at kinetochores at early prometaphase but prophase or late G_2 c ells have not been specifically investigated (Figure 4.6). MCPH1 begins to delocalise from the kinetochores during anaphase (Figure 4.6). This suggests that MCPH1 may play a core kinetochore function as it is present during most stages of mitosis. Further refining when MCPH1 is recruited to the kinetochore may also identify candidate proteins required for its kinetochore recruitment. This could then be investigated further by looking at MCPH1 kinetochore localisation following RNAi-mediated depletion of candidate proteins.

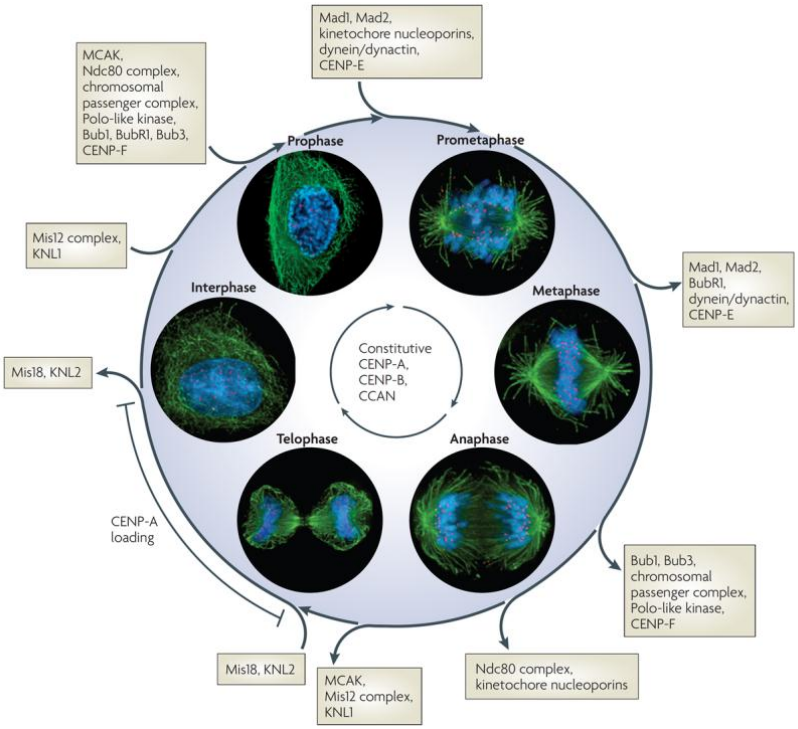

Figure 4.10. Cell-cycle regulated localisation of kinetochore components.
Immunofluorescence pictures of human cells progressing through the cell cycle, DNA (blue), centromeres (red) and microtubules (green). Kinetochore proteins are boxed and the direction of kinetochore localisation and delocalisation are represented by arrows. (Figure reproduced from Cheeseman and Desai, 2008).

Despite MCPH1(FL) being present in the nucleus throughout interphase, it exhibits dynamic, cell cycle regulated localisation to the centromeres during mitosis. It is likely that its localisation is affected by cell cycle regulatory mechanisms involving post-translational modifications, such as phosphorylation. Such modifications could mark sites of kinetochore proteins allowing MCPH1 to be recruited or modify MCPH1 to permit binding to kinetochores. The second possibility, that post-translational modifications of MCPH1 regulate its temporal kinetochore localisation is explored in Chapter 6.

4.8.3. MCPH1 centrosomal localisation

Centrosomal localisation during mitosis has been demonstrated for epitope-tagged *MCPH1* orthologues in *Drosophila* embryos (Brunk *et al.*, 2007) and chicken DT40 cells (Jeffers *et al.*, 2008). In *Drosophila* it is Mcph1(S) but not Mcph1(L) that can localise to the centrosome and only during mitosis (Brunk *et al.*, 2007). Whereas in

chicken DT40 cells, the *MCPH1* orthologue cloned is more similar to MCPH1(Δ8) and it can localise to the centrosome throughout the cell cycle (Jeffers *et al.*, 2008). This led to the prediction that there may be variation in centrosomal localisation between the human MCPH1 isoforms characterised in Chapter 3.

In this chapter, it was demonstrated that GFP-MCPH1(FL) and Δ8 could localise to the centrosome during mitosis (Figure 4.4 & 4.5) and the N-terminus (aa 1-223) was identified as the domain sufficient to direct centrosome localisation (Figure 4.8). It is surprising that GFP-MCPH1(S) does not localise to centrosome, it shares the centrosome targeting region (aa 1-223) and indeed it was the *Drosophila* orthologue of MCPH1(S) that localised to the mitotic centrosome (Brunk *et al.*, 2007). However, GFP-MCPH1(S) also failed to localise to the centrosomes when stably expressed in DT40 cells (Paola Vagnarelli, University of Edinburgh, personal communication) suggesting maybe different developmental contexts could account for the differences between *Drosophila*, chicken and human cell lines. To confirm these observations it would be worthwhile to establish endogenous MCPH1(S) localisation by biochemical purification of the centrosomes.

MCPH1(FL) specifically localises to the centrosome from nuclear envelope breakdown at prometaphase until nuclear envelope reformation during telophase (Figure 4.4B). This is in contrast to MCPH1(Δ8) which localises to the centrosome throughout the cell cycle (Figure 4.2). It is likely that the differences in localisation between the two isoforms are due to their different subcellular localisation; FL is distributed in the nucleus whereas Δ8 is also cytoplasmic allowing it access to the centrosome at interphase (Figure 4.1). It is likely that it is the MCPH1(Δ8) isoform that is detected at the centrosome during interphase by indirect immunofluorescence (Tibelius *et al.*, 2009), particularly as the detecting antibody was raised against epitopes contained within Δ8.

What is the function of MCPH1at the centrosome during interphase? This thesis, established that MCPH1(Δ8) co-localises with γ-tubulin, a marker for the centrioles (Fuller *et al.*, 1995) and pericentriolar material (PCM) (Shu and Joshi, 1995; Stearns *et al.*, 1991) (Figure 4.2). This localisation is consistent with the published role for MCPH1 in PCM recruitment during interphase (Tibelius *et al.*, 2009). The evidence

presented here suggests that MCPH1 function at the centrosome during interphase is attributable to MCPH1(Δ8), although it cannot be ruled out that uncharacterised MCPH1 isoforms could also play a role. In support of this, MCPH1(Δ8) contains the BRCT1 domain that is required for interaction with pericentrin and γ-tubulin (Figure 4.7), two centrosome components that MCPH1 is required to recruit during interphase (Tibelius *et al.*, 2009).

The functional role of MCPH1 at the centrosome during mitosis is not known. It is centrosomal localisation during mitosis that is shared between all of the MCPH1 proteins (Barrera *et al.*, 2010; Hatch *et al.*, 2010; Higgins *et al.*, 2010; Hung *et al.*, 2000; Nicholas *et al.*, 2010) and so defining MCPH1 function at the centrosome during mitosis could help to pinpoint a single shared pathway important during neurogenesis. One possibility, and a natural progression from MCPH1 function during interphase, is that MCPH1 could play a role in centrosome maturation during mitosis. Centrosome maturation describes the increased microtubule nucleation capacity of the mitotic centrosomes (reviewed by Blagden and Glover, 2003). Most of the primary microcephaly proteins can be linked in some way to this process either through roles in centriole duplication (Blachon *et al.*, 2008; Hatch *et al.*, 2010; Kohlmaier *et al.*, 2009; Schmidt *et al.*, 2009; Stevens *et al.*, 2010a; Tang *et al.*, 2009), PCM expansion (Fong *et al.*, 2008) or focusing of microtubules (Higgins *et al.*, 2010; Pfaff *et al.*, 2007). MCPH1 centrosomal localisation is consistent with the possibility that it too could play a role in centrosome maturation. MCPH1 may possibly function in this process through its tandem BRCT domains which can recognise phosphorylated proteins (Manke *et al.*, 2003; Yu *et al.*, 2003). Centrosome maturation also depends upon the activity of mitotic kinases such as polokinase 1 (Lane and Nigg, 1996) and aurora A (Hannak *et al.*, 2001). MCPH1 may act as an assembly platform for these phosphorylated proteins at the mitotic centrosome. The role of MCPH1 in centrosome maturation is investigated further in Chapter 5.

Chapter 5. The characterisation of MCPH1-deficient cells

Chapter 3 and 4 established that MCPH1 is regulated during the cell cycle. MCPH1 protein levels fluctuate with the cell cycle phase and MCPH1 cyclically localises to the centrosome and kinetochores during mitosis. This raises the question what are the functional consequences of this spatio-temporal mitotic regulation.

In this chapter, the function of MCPH1 during mitosis is investigated. Three different tools were utilised to examine the role of MCPH1 in mitosis: RNAi-mediated depletion of MCPH1 in human cell lines, MEFs with *Mcph1* gene-trap and MCPH1 patient-derived lymphoblastoid cells.

5.1. RNAi mediated depletion of MCPH1

5.1.1. Knockdown of MCPH1 isoforms by RNAi

Small interfering RNA (siRNA) oligonucleotides were utilised to efficiently deplete MCPH1 for functional studies. Three siRNA oligonucleotides were designed to target *MCPH1* 3' UTR, the unique sequence of the short isoform and *MCPH1* exon 3 (Figure 5.1A). The first two oligonucleotides were pooled (siMCPH1#1) to ensure all three MCPH1 isoforms were targeted, whereas the oligonucleotide targeting *MCPH1* exon 3 (siMCPH1#2) should deplete all the isoforms.

As shown in Figure 5.1B, the endogenous levels of MCPH1 FL and S were significantly reduced following transfection of HeLa cells with siMCPH1#1 or siMCPH1#2 but not following control transfection with siRNA oligonucleotides against luciferase. This confirms that the oligonucleotides specifically deplete MCPH1 FL and S.

MCPH1(Δ8) is not detectable with current antibody reagents and so evidence of protein depletion by immunoblotting is not possible. However it has been demonstrated that transfection with siMCPH1#2 leads to a similar reduction of Δ8 transcript levels to FL and S isoforms (Figure 3.4B), which are undetectable by

immunoblotting analysis (Figures 3.4B & 5.1B). The reduction of Δ8 transcript levels with siMCPH1#1 is yet to be confirmed but it is likely to be targeted similarly to MCPH1(FL) as they both share the 3' UTR. Thus, siMCPH1#1 and siMCPH1#2 are presumed to efficiently deplete MCPH1 isoforms.

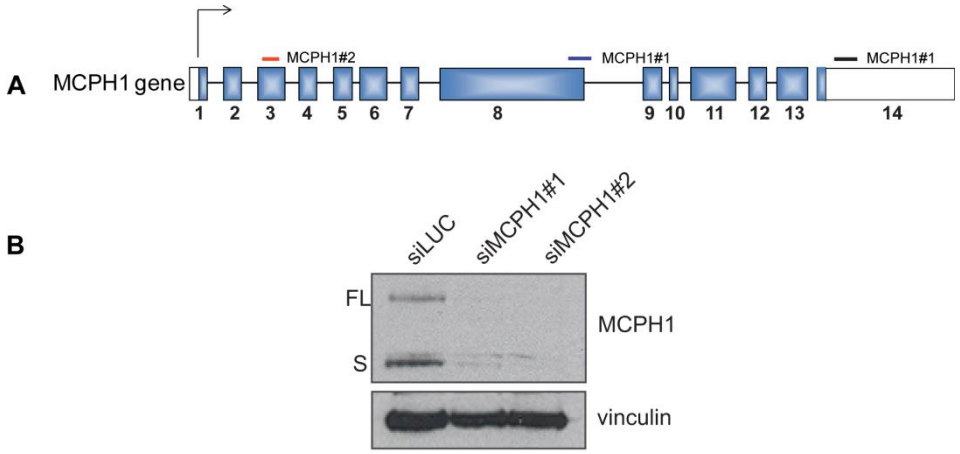

Figure 5.1. MCPH1 isoform depletion by RNAi.
(A) Schematic of *MCPH1* and location of sequences targeted by siRNA. MCPH1#1 is a pool of oligonucleotides designed to target the unique exon junction of S isoform (blue bar) and the 3'UTR (black bar) of MCPH1 FL and Δ8. MCPH1#2 targets all three MCPH1 isoforms (red bar). (B) Depletion of MCPH1 FL and S protein isoforms by siRNA. HeLa cells were transfected with luciferase siRNA (control) or MCPH1 siRNA (described in (A)). After 24 hr, the transfection was repeated and at 72 hr cells were harvested and lysates prepared. The lysates were separated on a 8% Tris-Glycine polyacrylamide gel and Western blotted with MCPH1 and vinculin (loading control) antibodies.

5.1.2. MCPH1 depletion leads to multipolar spindle formation

To examine the effect of MCPH1 depletion on mitosis, HeLa cells were transfected with control or MCPH1 #1 siRNAs. The cells were fixed and mitotic cells assessed by α-tubulin & γ-tubulin immunofluorescence to visualise microtubules & centrosomes, DAPI staining was used to visualise DNA. siRNA mediated depletion of MCPH1 in HeLa cells led to an increase in the number of cells with multipolar spindles (Figure 5.2A). 59 % of mitotic MCPH1 depleted cells had greater than two γ-tubulin foci surrounded by clusters of microtubules whereas only 1.5% of mitotic control cells had this phenotype (Figure 5.2B).

The siMCPH1#1 oligonucleotide pool does not target MCPH1(FL) ORF enabling RNAi rescue experiments to be performed. As shown in Figure 5.2B spindle multipolarity is partially rescued by the transfection of cells with GFP-tagged MCPH1(FL) (42 % in comparison to 59 %). However this difference has not quite reached statistical significance ($p=0.0549$, Fisher's exact test) and so requires further validation (Figure 5.3B). This partial rescue does suggest that spindle multipolarity is a specific defect caused by the depletion of MCPH1 rather than non-specific effects exerted by RNAi oligonucleotides.

Spindle multipolarity was also observed following MCPH1 depletion in U2OS cells (Figure 5.2C) and following transfection with siMCPH1#2 oligonucleotides (Figure 5.2D) confirming that this phenotype is independent of cell type and siRNA oligonucleotide. Thus, MCPH1 appears to be required for spindle bipolarity during mitosis.

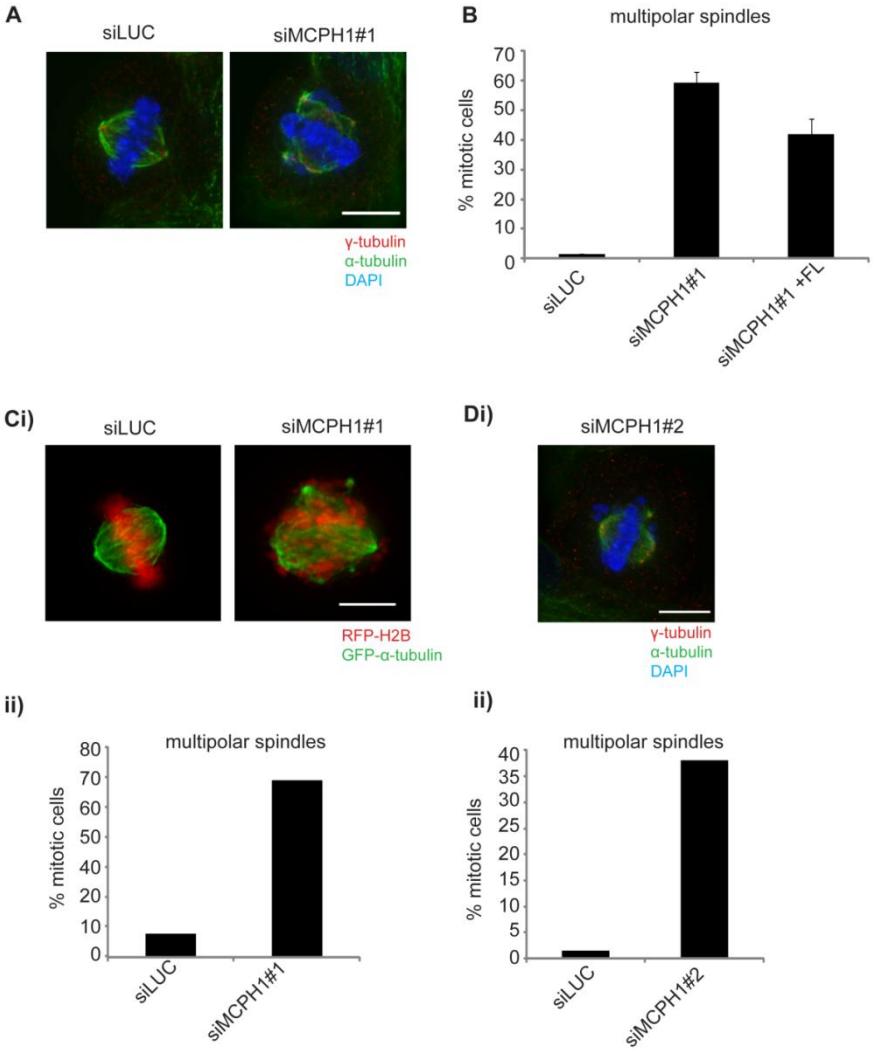

Figure 5.2 MCPH1 depletion by RNAi leads to mitotic spindle multipolarity.
(A) MCPH1 depletion by RNAi leads to mitotic spindle multipolarity. HeLa cells were transfected with luciferase siRNA (siLUC) or MCPH1 siRNA (siMCPH1#1). After 48 hr cells were fixed in methanol and subjected to immunofluorescence staining with ϒ-tubulin (red) and α-tubulin (green) antibodies. DNA was visualized with DAPI (blue). (B) MCPH1(FL) expression partially rescues spindle multipolarity. HeLa cells were transfected with luciferase siRNA (control) or MCPH1 siRNA (siMCPH1#1). After 24 hr, the cells were transfected with luciferase siRNA, MCPH1 siRNA or MCPH1 siRNA and a plasmid expressing GFP-tagged MCPH1(FL). The cells were fixed in methanol 48 hrs after first transfection. Data presented are the percentages of mitotic cells with multipolar spindles (mean +/- s.e.m. of two independent experiments with >50 cells counted per experiment). (C) Spindle multipolarity is independent of cell type. (i) A similar protocol to (A) was followed in U2OS cells stably expressing GFP-α-tubulin and RFP-Histone 2B. (ii) Quantitative analysis of multipolar spindles in cells depleted of MCPH1. The graph represents one experiment of 50 cells. (D) Spindle multipolarity is also present following MCPH1 depletion by MCPH1#2 siRNA. (i) A similar protocol to (A) was followed with siMCPH1#2 oligonucleotides. (ii) Quantitative analysis of multipolar spindles in cells depleted of MCPH1. The graph represents one experiment of 50 cells. Scale bars are 10 μm.

5.1.3. MCPH1 depletion leads to chromosome alignment defects

siRNA-mediated depletion of MCPH1 in HeLa cells also led to an increase in the number of metaphase cells with chromosomes misaligned from the metaphase plate, a partial metaphase plate was formed but many chromosomes were located at the spindle poles (Figure 5.3A). 72 % of MCPH1 depleted cells with a normal bipolar spindle had this phenotype (Figure 5.3A & B) compared to only 1.5% of control metaphase cells (Figure 5.3B).

These defects appear to be partially rescued by the transfection of cells with GFP-tagged MCPH1(FL) (49% in comparison to 72%, $p<0.0005$ (Fisher's exact test)). A similar phenotype was observed following MCPH1 depletion in U2OS cells (Figure 5.3C) and following transfection with siMCPH1#2 oligonucleotides (Figure 5.3D) providing further support that the phenotype observed is specifically due to depletion of MCPH1. Thus, MCPH1 is required for normal chromosome alignment during the metaphase stage of mitosis.

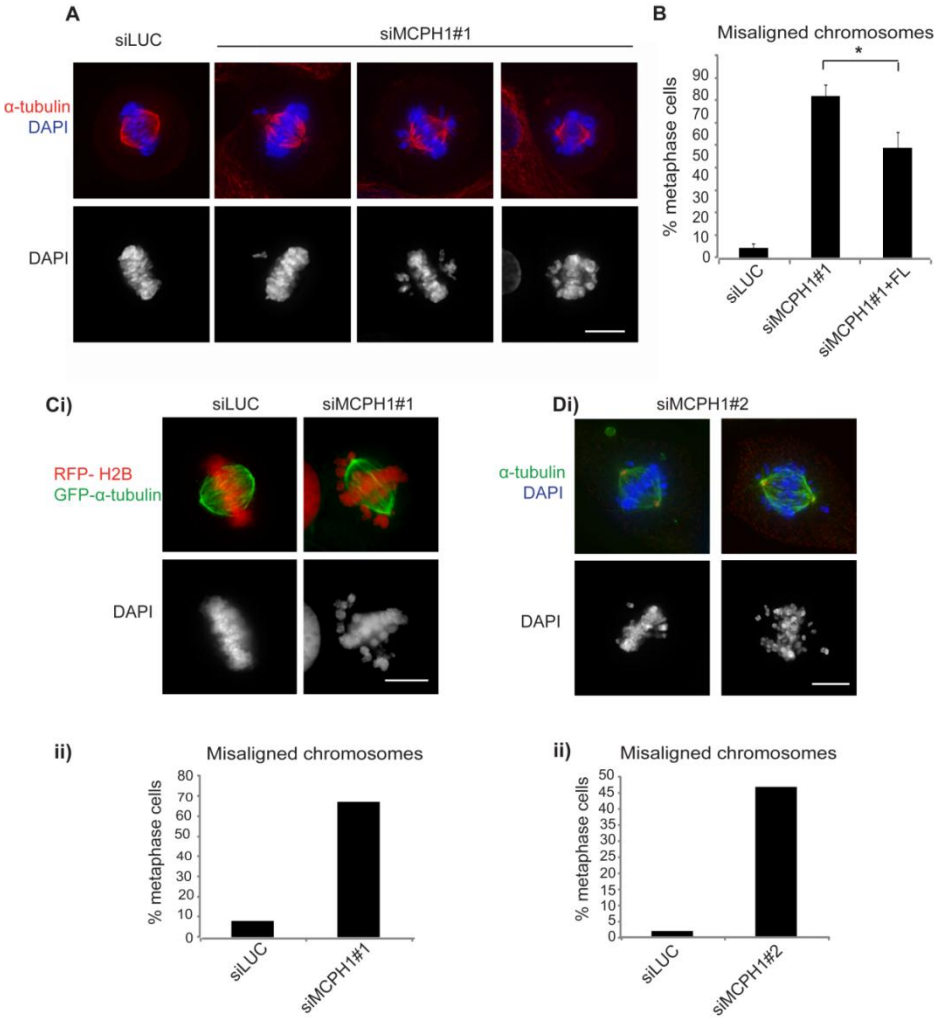

Figure 5.3. MCPH1 depletion by RNAi leads to chromosome alignment defects.
(A) MCPH1 depletion by RNAi leads to chromosome misalignment in metaphase cells with bipolar spindles. HeLa cells were transfected with luciferase siRNA (control) or MCPH1 siRNA (siMCPH1#1). After 48 hr cells were fixed in methanol and stained with α-tubulin antibodies and DAPI. (B) GFP-MCPH1(FL) expression rescues chromosome misalignment defects. HeLa cells were transfected with luciferase siRNA (control) or MCPH1 siRNA (siMCPH1#1). After 24 hr, the transfection was repeated with luciferase siRNA; MCPH1 siRNA; or MCPH1 siRNA and a plasmid expressing GFP-MCPH1(FL). The cells were fixed in methanol 48 hr after first transfection. Data presented are the percentages of metaphase cells with a bipolar spindle which have misaligned chromosomes (mean +/- s.e.m. of two independent experiments with >50 cells counted per experiment). Asterisk denotes a statistically significant difference analysed by a two-tailed Fisher's exact test ($P<0.0005$). (C) Chromosome alignment defects are independent of cell type. (i) A similar protocol to (A) was followed in U2OS cells stably expressing GFP-α-tubulin and RFP-Histone 2B. (ii) Quantitative analysis of misaligned chromosomes in cells depleted of MCPH1. The graph represents one experiment with 50 metaphase cells counted. (D) Similar chromosome alignment defects with MCPH1#2 siRNA. (i) A similar protocol to (A) was followed with siMCPH1#2 oligonucleotides in HeLa cells. (ii) Quantitative analysis of misaligned chromosomes in cells depleted of MCPH1. The graph represents one experiment with 50 metaphase cells counted. Scale bars represent 10 μm.

5.1.4. Live-imaging of MCPH1-deficient cells

siRNA-mediated depletion of MCPH1 resulted in two phenotypes at mitosis i) chromosome misalignment and ii) multipolar spindles. It is unclear if both of these phenotypes are a primary phenomenon or if one precedes the other. Thus, to study the sequence of events, live-cell imaging of U2OS cells stably expressing GFP-tagged α-tubulin and RFP-tagged histone 2B was performed (live-cell imaging was performed in conjunction with Paola Vagnarelli, University of Edinburgh). As shown in Figure 5.4, the control siRNA treated cells underwent normal mitosis (progressing from metaphase to telophase in 20 min) whereas the cells depleted of MCPH1 failed to enter anaphase. These cells spent a prolonged time in metaphase, a normal metaphase plate was formed but subsequently chromosomes were lost from this alignment increasing in number with time. Initially a bipolar spindle is formed but after a prolonged time in metaphase the spindle collapses. Thus, the live-imaging revealed that chromosome misalignment precedes spindle multipolarity but follows normal metaphase plate formation.

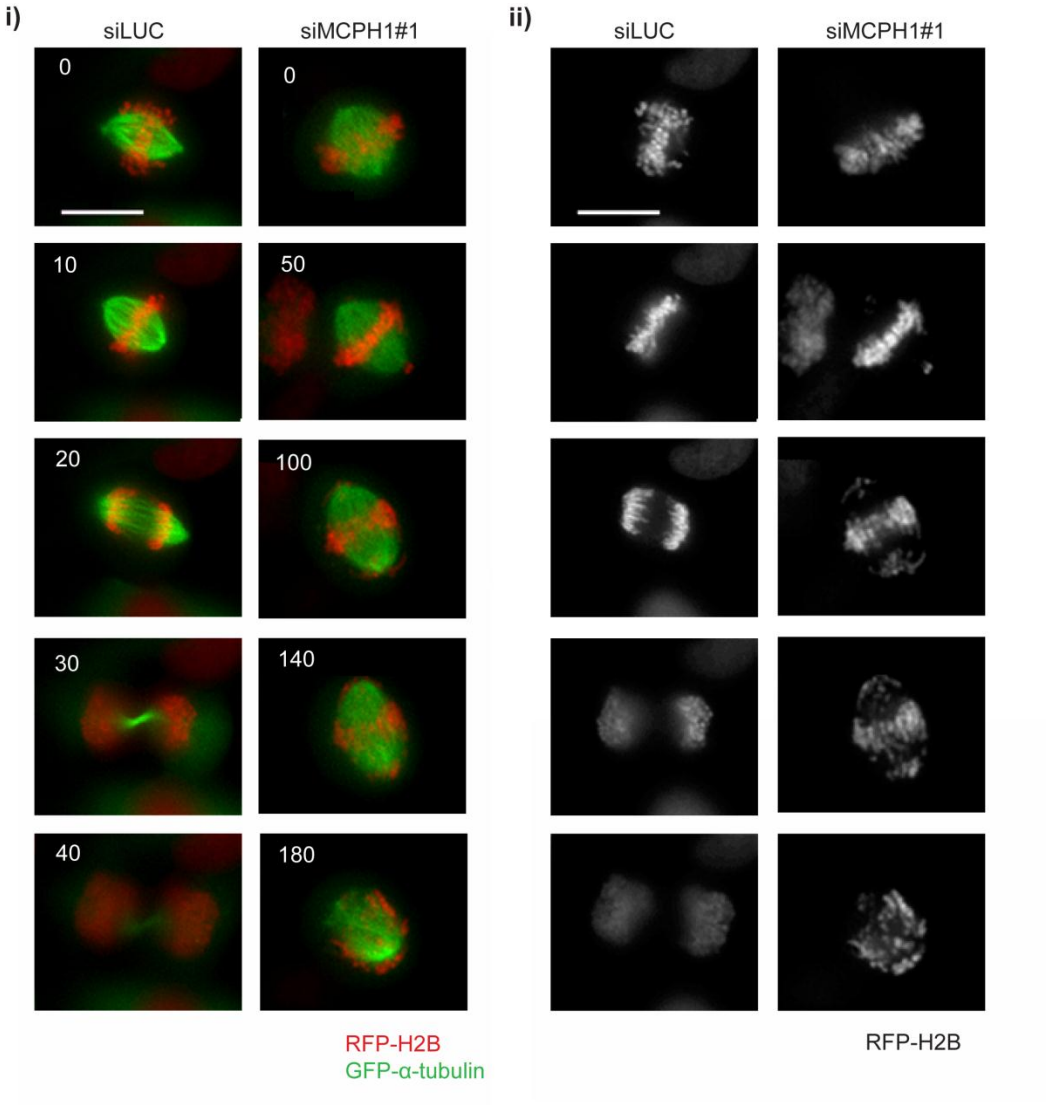

Figure 5.4. Live-imaging of MCPH1 depleted cells.
Stills from time-lapse movies of U2OS cells stably expressing RFP-histone 2B and GFP-α-tubulin in either luciferase (siLUC) or MCPH1 (siMCPH1#1) depleted cells. Numbers in each image represent the relative time in minutes. Time-lapse movies were collected by Paola Vagnarelli (University of Edinburgh). Scale bar is 20 µm.

5.1.5. Spindle checkpoint appears to be active in MCPH1-deficient cells

The prolonged time in metaphase observed after MCPH1 depletion could be due to activation of the spindle checkpoint. Checkpoint activation is achieved by sustained recruitment of checkpoint proteins, such as BUBR1 and MAD2, to the kinetochores which prevents activation of the anaphase promoting complex/cyclosome (APC/C) and targeting of cellular cyclin-B for degradation. Direct confirmation has not yet been possible as detection of BUBR1 localisation to the kinetochores has been difficult to demonstrate due to technical issues with BUBR1 immunofluorescence. However, immunofluorescence of MCPH1 depleted cells with misaligned chromosomes (of various severities) demonstrated a bright stain for cyclin-B1with levels comparable to metaphase siLUC control cells (Figure 5.5). This suggests that cyclin-B1 is not targeted for degradation in metaphase MCPH1-deficient cells, in keeping with spindle checkpoint activation.

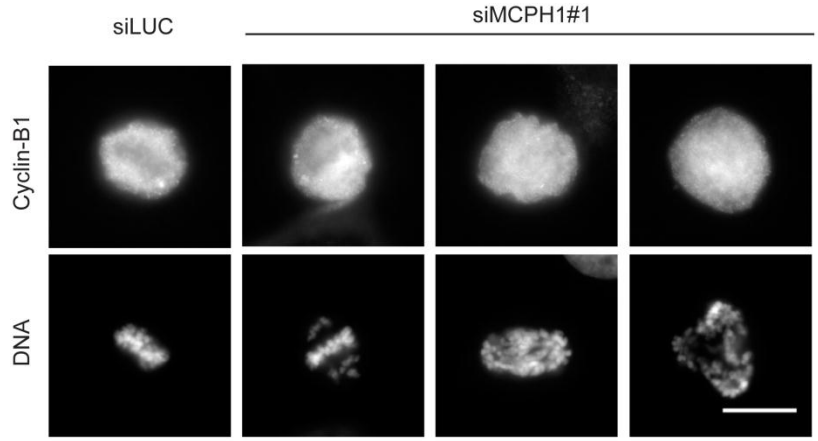

Figure 5.5. High cyclin-B1 levels are present in MCPH1 depleted cells.
HeLa cells were transfected with luciferase or MCPH1 siRNAs and, after 48 hr, fixed in 4 % PFA and subjected to immunofluorescence staining with cyclin-B1 antibodies. DNA was visualized with DAPI (blue). All images were acquired with the same camera exposure. For comparison, a control siRNA transfected cell in metaphase with high cyclin-B1 levels is included. Scale bar represents 10 µm.

5.1.6. Multipolar spindle phenotype is due to fragmentation of PCM

The live-cell imaging established that the formation of multipolar spindles is secondary to chromosome misalignment. Consistent with this, excess γ-tubulin foci in fixed cell preparations was only observed in MCPH1-deficient mitotic cells and not interphase cells, suggesting that multiple centrosomes arise during mitosis (Figure 5.6A). Such multipolar spindles could arise during mitosis through a number of different mechanisms. Firstly, aberrant centriole disengagement could lead to the formation of multipolar spindles (Thein *et al.*, 2007). If this was the case, then each of the spindle poles would contain a single centriole. Centriole staining (using CPAP antibody) of MCPH1 depleted cells revealed that the majority of γ-tubulin foci (68%) did not contain centrioles (Figure 5.6B). In most cells, CPAP localisation overlapped with only two of the γ-tubulin foci. Thus premature centriole separation does not appear to account for the observed spindle multipolarity.

The second possibility is that multipolar spindles are due to fragmentation of the PCM surrounding the centrioles. As shown in Figure 5.6C, PCM proteins, such as aurora A, pericentrin and CDK5RAP2, all localise to each of the spindle poles suggesting that they resemble normal centrosomes regardless of the absence of centrioles. This is consistent with the hypothesis that multipolar spindle phenotype arises due to fragmentation of the PCM during mitosis.

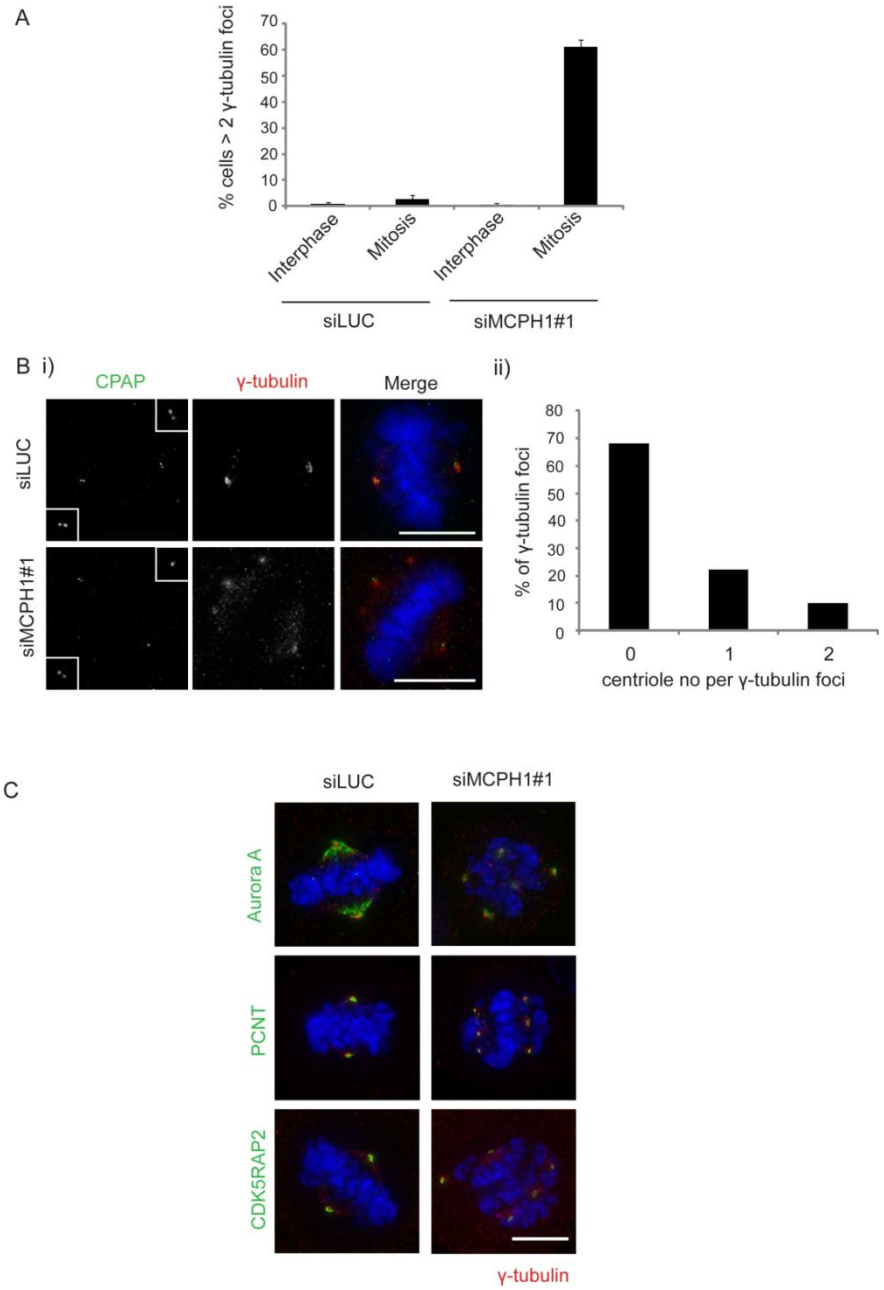

Figure 5.6. Multipolar spindles arise due to fragmentation of PCM.
(A) Proportion of siLUC or siMCPH1 transfected HeLa cells with more than two ϒ-tubulin foci in interphase and mitosis. Quantification of triplicate experiments of at least 50 cells each. (B) (i) Control or MCPH1-depleted cells were stained with antibodies against CPAP (green) and ϒ-tubulin (red). DNA was visualized with DAPI. The insets show 2 x magnified images. (ii) Quantitative analysis of the centriole number at each ϒ-tubulin foci in cells depleted of MCPH1. The number of poles containing zero, one, or two centrioles was plotted as a percentage of the total number of ϒ-tubulin foci. The graph represents one experiment of 50 cells. (C) Control or MCPH1 depleted cells were stained with antibodies against ϒ-tubulin (red), aurora A (green), pericentrin (green) or CDK5RAP2 (green). DNA was visualized with DAPI. Scale bar represents 10 µm.

5.1.7. MCPH1 deficiency compromises chromatid cohesion

Chromosome alignment defects occurring after MCPH1 depletion might result from loss of chromatid cohesion. To investigate this possibility, MCPH1-RNAi cells were stained with the centromeric marker ACA. As shown in Figure 5.7, siMCPH1 transfected cells, with only a few chromosomes misaligned, have centromere doublets escaping from the metaphase plate (Figure 5.7, panel 2). It is only when more DNA is lost from the metaphase plate that single centromeres on separated chromatids are present (Figure 5.7, panel 3 & 4). This suggests that loss of sister chromatid cohesion is unlikely to be the initial cause of chromosome misalignment but a secondary consequence, possibly due to prolonged time in metaphase.

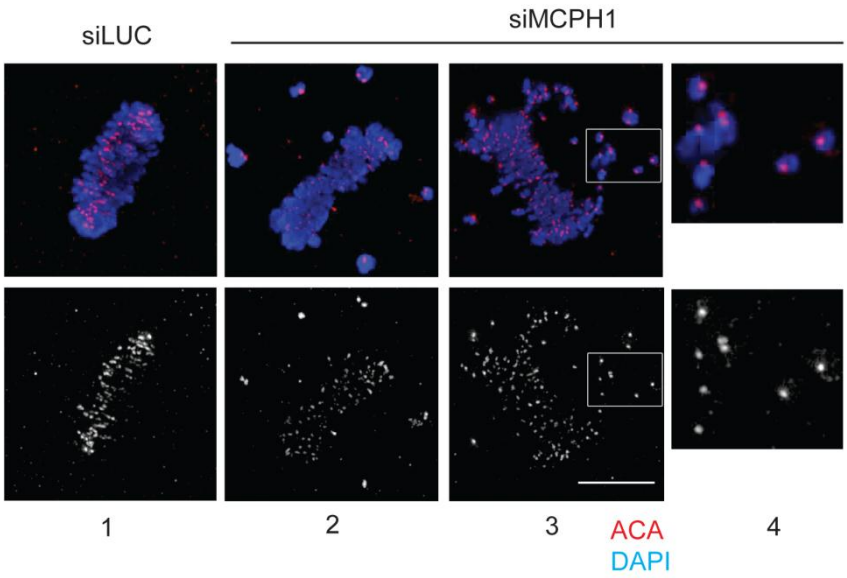

Figure 5.7 Chromatids prematurely separate in MCPH1 deficient cells.
Hela cells were transfected with control or MCPH1 siRNAs, fixed in methanol:acetone and subjected to immunofluorescence staining with centromere autoantibodies (ACA, red). DNA was visualized with DAPI (blue). Immunofluorescence staining and imaging was performed by Paola Vagnarelli. The fourth panel shows 2 x magnified images of panel 3. Scale bar represents 10 µm.

5.2. *Mcph1*$^{-/-}$ MEFs

5.2.1. Generation and characterisation of *Mcph1*$^{-/-}$ MEFs

To validate the MCPH1 RNAi findings, the phenotype of MEFs from *Mcph1* 'knockout first' genetrap mice was investigated. *Mcph1*$^{-/-}$ mice were obtained from the European Conditional Mouse Mutagenesis Program (EUCOMM). In the *Mcph1* gene targeting allele (Figure 5.8A), the cassette was inserted into intron 3 of the *Mcph1* gene and results in the splicing of exon 3 to the splice acceptor in the targeting cassette (En2 SA). This results in the formation of a fusion transcript of *Mcph1* exon 1-3 with β-galactosidase (βgal) and neomycin phosphotransferase (neo), which inactivates the original version of the gene leading to a knockout at the RNA processing level. The functional consequences are likely to be null and therefore the mice are denoted as *Mcph1*$^{-/-}$. In addition, there is a conditional element to the *Mcph1* gene-targeting allele (FRT and LoxP sites) that would enable a conditional genetic knockout of exon 5 but this is not utilised in this study.

To examine the phenotype of primary cells deficient for MCPH1, mice heterozygous for *Mcph1* gene trap were mated and embryos collected. The embryos were genotyped by PCR (Figure 5.8B) with the primers annealing to *Mcph1* sequence indicated in Figure 5.8A. The size of the PCR products enabled the *Mcph1* allele with or without the gene trap to be differentiated. Those with the desired genotype, either *Mcph1*$^{+/+}$ (244 bp PCR product only) or *Mcph1*$^{-/-}$ (366 bp PCR product only), were dissected to generate primary fibroblast cultures.

Phenotypic analysis was used to confirm that the *Mcph1*$^{-/-}$ MEFs were deficient in MCPH1. Cells lacking MCPH1 show abnormal chromosome condensation. This phenotype is distinct, easily characterised and present in all MCPH1-deficient cells analysed, including patient-derived cells (Trimborn *et al.*, 2004), MEFs (Trimborn *et al.*, 2010; Wood *et al.*, 2008) and as a result of RNAi mediated knockdown (Trimborn *et al.*, 2004). Staining of the DNA of *Mcph1*$^{-/-}$ MEFs demonstrated that they too show a significant number of cells with abnormally condensed chromosomes (Figure 5.8Ci). This phenotype is highly penetrant with 35 % of non-mitotic *Mcph1*$^{-/-}$ MEFs displaying prophase-like DNA morphology compared to 3 %

of *Mcph1*$^{+/+}$ MEFs (Figure 5.8Cii). This is in comparison to 30-35 % of *Mcph1*$^{-/-}$ MEFs displaying PCC previously published (Wood *et al.*, 2008). Thus, the *Mcph1* gene-trap does appear to be successfully depleting most, if not all, of the MCPH1 protein and, by inference, is correctly targeted to the endogenous locus.

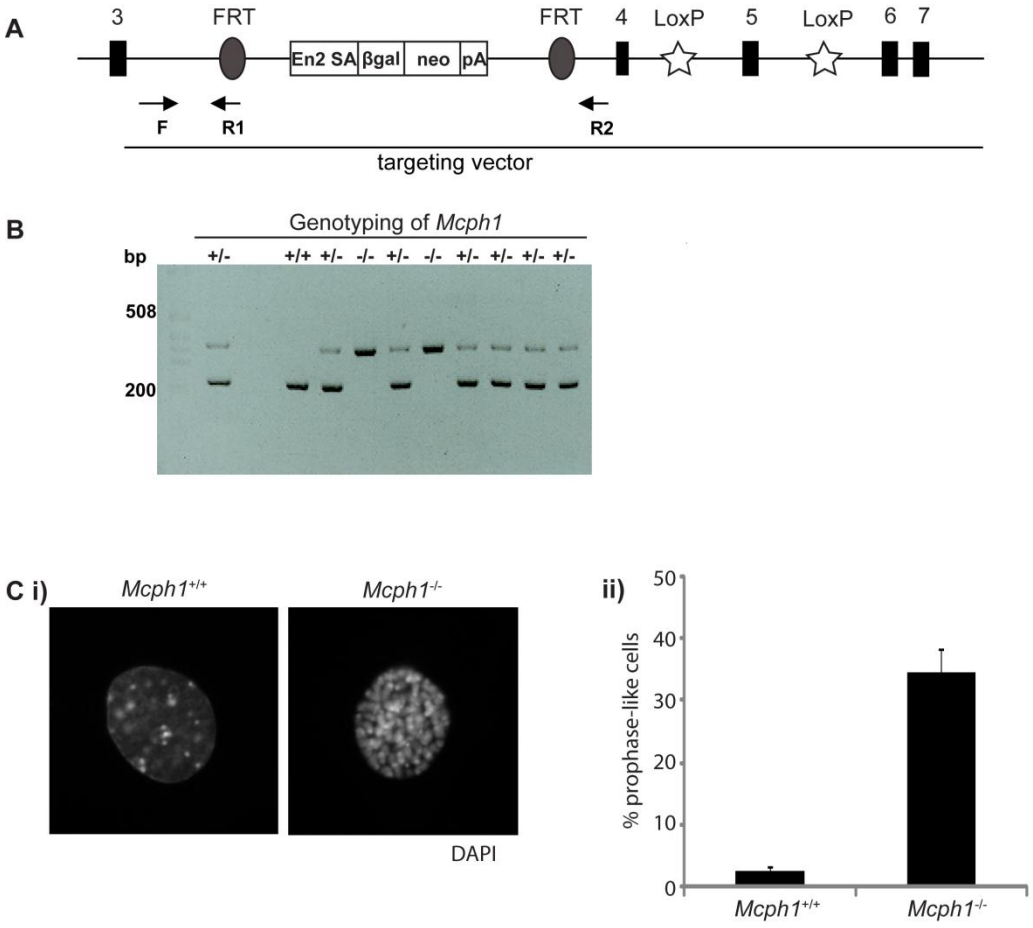

Figure 5.8. Characterisation of the *Mcph1* gene-trap allele.
(A) Schematic of EUCOMM *Mcph1* gene-trap allele. *Mcph1* exons are displayed in black, the FRT sites in grey, the reporter gene and LoxP sites are in white. (B) PCR-based genotype analysis of *Mcph1*$^{+/+}$, *Mcph1*$^{+/-}$ and *Mcph1*$^{-/-}$ mouse embryos. Positions of PCR primers (F, R1 & R2) are indicated in (A). A 244 bp PCR product was detected in the absence of *Mcph1* gene trap and a 366 bp PCR product detected in the presence of *Mcph1* gene trap. (C) Analysis of chromosome condensation in *Mcph1*$^{-/-}$ cells. (i) *Mcph1*$^{+/+}$ or *Mcph1*$^{-/-}$ MEF cell cultures were fixed and stained with DAPI. The right panel shows a prophase-like cell. (ii) Proportion of prophase-like cells in *Mcph1*$^{+/+}$ and *Mcph1*$^{-/-}$ cell cultures. The graph represents triplicate experiments of at least 500 cells.

To determine the role of MCPH1 during mitosis in MEFs, *Mcph1*$^{-/-}$ cells were analysed by immunofluorescence. Initially, chromosome alignment during metaphase was investigated, chromosomes were visualised by DAPI staining and α-tubulin antibody was used to visualise the microtubules. *Mcph1*$^{-/-}$ MEFs showed an increase in cells with misaligned chromosomes compared to *Mcph1*$^{+/+}$ (12.5% in comparison to 3.5%, $p<0.05$ (Fisher's exact test)) (Figure 5.9A). To investigate this further the immunofluorescence was repeated in cells treated with the proteasome inhibitor MG132 for 2 hr. MG132 arrests cells in metaphase by preventing cyclin B and securin degradation (reviewed by Lee and Goldberg, 1998). This treatment increases the number of metaphase cells available to quantify, facilitating analysis of primary cells with a low mitotic index. In addition, MG132 has been reported to enhance the *Cdc20* hypomorphic phenotype in MEFs by increasing the incidence of misaligned chromosomes (Malureanu *et al.*, 2010). Again, the *Mcph1*$^{-/-}$ MEFs showed a statistically significant increase in chromosome alignment defects compared to *Mcph1*$^{+/+}$ MEFs (9.1 % compared to 1.9 %, $p<0.01$ (Fisher's exact test)) following treatment with MG132 (Figure 5.9B). Importantly, the incidence of chromosome misalignment was similar between untreated and MG132-treated *Mcph1*$^{+/+}$ MEFs, so prolonging the time to establish ktMT connections neither improved nor exacerbated this phenotype.

The majority of *Mcph1*$^{-/-}$ MEFs quantified had 2-10 misaligned chromosomes (Figure 5.9B panel 2 & 3). Gross chromosome alignment defects and spindle multipolarity, as with MCPH1 RNAi, were not apparent. An increase in premature chromatid separation was also not evident from chromosome spreads of *Mcph1*$^{-/-}$ MEFs compared to *Mcph1*$^{+/+}$ (Figure 5.9C). Thus, *Mcph1*$^{-/-}$ MEFs show chromosome alignment defects at metaphase but these did not progress in severity to the scale of chromosome misalignment observed due to MCPH1 RNAi.

A

MEF genotype	% cells with misaligned chromosomes
MCPH1$^{+/+}$	3.5 (n=88)
MCPH1$^{-/-}$	12.5 (n=81)

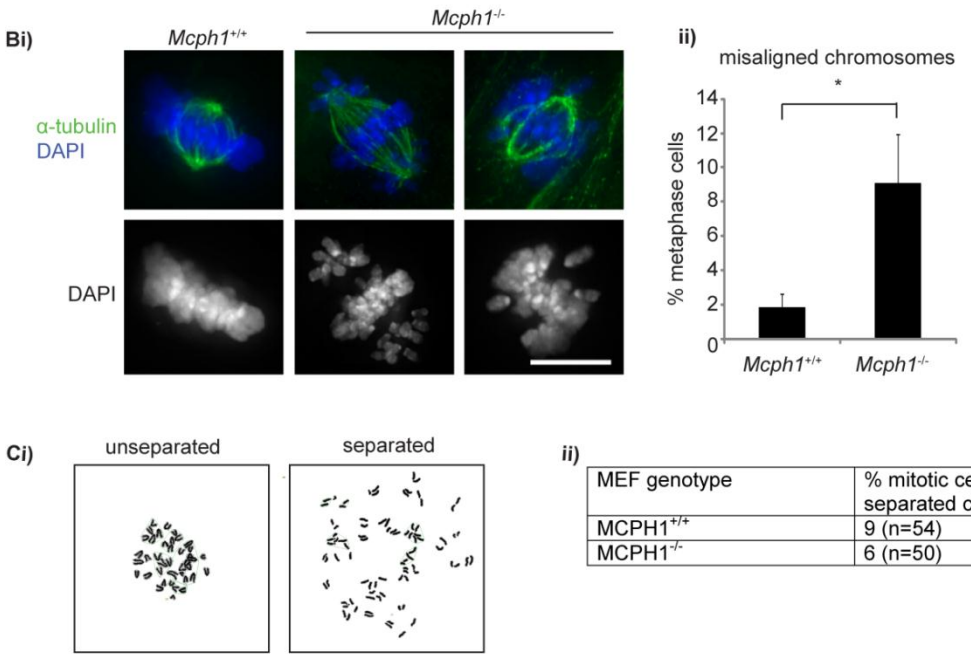

ii)

MEF genotype	% mitotic cells with separated chromatids
MCPH1$^{+/+}$	9 (n=54)
MCPH1$^{-/-}$	6 (n=50)

Figure 5.9. MCPH1-deficient MEFs show chromosome alignment defects.
(A) Analysis of chromosome alignment in *Mcph1*$^{-/-}$ MEFs. Asynchronous *Mcph1*$^{+/+}$ and *Mcph1*$^{-/-}$ MEF cell line cultures were fixed in methanol and stained with α-tubulin antibodies and DAPI. Metaphase cells with a bipolar spindle and misaligned chromosomes were quantified. (B) Increased levels of misaligned chromosomes are also seen in *Mcph1*$^{-/-}$ MEFs following MG132 treatment. Cells were treated with MG132 for 2 hr, fixed in 4 % PFA and stained with α-tubulin antibodies and DAPI. Scale bar represents 10 µm. Data presented are the percentages of metaphase cells with misaligned chromosomes (mean +/- s.e.m. of five independent experiments with 50 cells counted per experiment). An asterisk denotes a statistically significant difference analysed by two-tailed Fisher's exact test ($P<0.01$). (C) Chromosome spreads of *Mcph1*$^{-/-}$ MEFs. Following the addition of colcemid to *Mcph1*$^{-/-}$ and *Mcph1*$^{+/+}$ MEFs for 45 min, cells were collected, treated with KCl and fixed in Methanol:acetic acid (3:1, fixation performed by Margaret Harley). Slides were prepared and images collected by the NHS Cytogenetics Laboratory, Edinburgh.

5.3. MCPH1 patient lymphoblastoid cells

Primary microcephaly proteins could all play a role in the maturation of the centrosome during mitosis. Centrosome maturation is a term used to describe the recruitment of pericentriolar material (PCM), microtubule nucleating and anchoring proteins to confer increased microtubule nucleation capacity to mitotic centrosomes (reviewed by Blagden and Glover, 2003; Palazzo *et al.*, 2000). Various centrosomal proteins such as γ-tubulin (Khodjakov and Rieder, 1999), pericentrin (PCNT) (Zimmerman *et al.*, 2004), CDK5RAP2 (Fong *et al.*, 2008) and polo-like kinase 1 (Lane and Nigg, 1996) are required for this process.

All of the primary microcephaly proteins localise to the centrosome during mitosis and I hypothesise that they may all have a common role in centrosome maturation (Figure 5.10). CPAP, CEP152 and Ana2 (the STIL *Drosophila* orthologue) all play a role in centriole duplication (Cizmecioglu *et al.*, 2010; Hatch *et al.*, 2010; Kohlmaier *et al.*, 2009; Schmidt *et al.*, 2009; Stevens *et al.*, 2010a; Tang *et al.*, 2009) and the centrioles act as a scaffold for the recruitment of PCM (Basto *et al.*, 2006; Bobinnec *et al.*, 1998; Conduit *et al.*, 2010; Kirkham *et al.*, 2003; Salisbury, 2003). Another primary microcephaly protein, CDK5RAP2 is a PCM component, with enhanced levels at mitosis (Haren *et al.*, 2009) and is required for recruitment of γ-tubulin (Fong *et al.*, 2008; Zimmerman *et al.*, 2004), a component of the γTURC complex responsible for microtubule nucleation (reviewed by Wiese and Zheng, 2006). The ASPM orthologue in *Drosophila*, Asp, also plays a role in nucleation and focussing of microtubules (do Carmo Avides and Glover, 1999; do Carmo Avides *et al.*, 2001; Wakefield *et al.*, 2001), and it is possible that ASPM plays a similar role in a vertebrate system (Higgins *et al.*, 2010). Thus, many of the primary microcephaly proteins can already be functionally linked to the process of centrosome maturation.

Analysis of centrosomal maturation had been difficult using the other systems described so far; the MCPH1 RNAi chromosome misalignment phenotype had secondary consequences on centrosome morphology and the relevant antibody reagents were not available for a thorough analysis of *Mcph1*$^{-/-}$ MEFs. Thus, to investigate the role of MCPH1 in centrosome maturation, lymphoblastoid cell lines (LBC) derived from patients with *MCPH1* mutations were utilised.

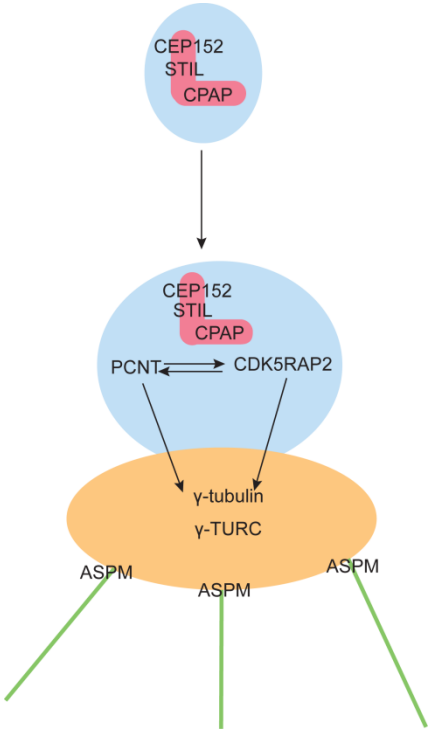

Figure 5.10. Hypothesis: primary microcephaly genes act in a centrosome maturation pathway.
Centriole function, PCM maturation, microtubule nucleation and focussing are all interlinked processes that can affect the mitotic spindle pole. Thus, although the primary microcephaly proteins are implicated in distinct centrosomal functions they may all contribute to mitotic spindle pole formation. (Figure adapted from Haren *et al.*, 2009).

5.3.1. CDK5RAP2, ASPM and γ-tubulin protein abundance is unaffected in MCPH1 LBCs

Given that MCPH1 is reported to regulate BRCA1 and CHK1 levels (Lin et al., 2005; Xu et al., 2004; Yang et al., 2008) the abundance of PCNT, CDK5RAP2, CPAP, ASPM and γ-tubulin was assessed in MCPH1 LBC whole cell extracts. A PCNT LBC was also included in this analysis as it serves as a positive control in subsequent experiments. Immunoblotting of the extracts from two WT LBC lines (WT1 & 2), two MCPH1 patient LBC lines ($MCPH1^{107fs}$ & $MCPH1^{143fs}$) and one PCNT patient LBC line ($PCNT^{E220X}$) confirmed that MCPH1 FL and S protein was absent in $MCPH1^{107fs}$ and $MCPH1^{143fs}$ LBC and PCNT A & B protein isoforms were absent in $PCNT^{E220X}$ LBC (Figure 5.11). The abundance of ASPM,

CDK5RAP2 and γ-tubulin was similar between all the LBC lines (CPAP was not detectable by immunoblotting with the antibody available). Thus, neither MCPH1 nor PCNT regulate total levels of CDK5RAP2, ASPM or GTUB protein in the cell.

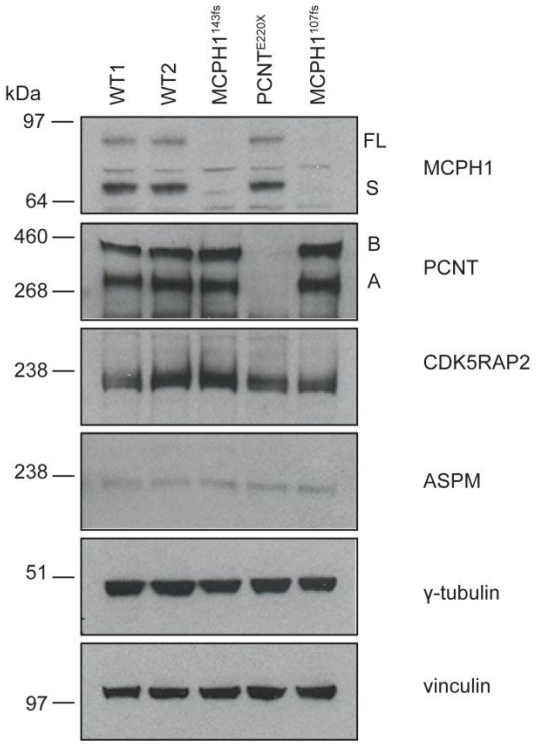

Figure 5.11. Protein levels of PCNT, CDK5RAP2, ASPM and γ-tubulin are unaffected in MCPH1 and PCNT patient LBC.
Cell extracts from LBC of two controls (WT1 & WT2), two MCPH1 patients ($MCPH1^{143fs}$, $MCPH^{107fs}$) and one PCNT patient ($PCNT^{E220X}$) were Western blotted with MCPH1, PCNT, CDK5RAP2, ASPM, γ-tubulin and vinculin antibodies.

5.3.2. CPAP localisation and centriole duplication is unaffected in MCPH1 LBCs

MCPH1 could act in centriole biogenesis, perhaps even by localising the primary microcephaly protein CPAP to the centrioles (Figure 5.12A). To investigate this possibility the role of MCPH1 in centriole duplication was analysed by immunofluorescence with CPAP (Figure 5.12Bi). CPAP levels were similar between $MCPH1^{107fs}$ and control LBC suggesting that MCPH1 is not required for CPAP

recruitment to centrioles. In addition, there were no significant differences in centriole number between MCPH1^{107fs} and control LBC (Figure 5.12Bii). Due to centriole pair orientation relative to the plane of microscope, often only one centriole could be distinguished at the spindle pole by microscopy, however the occurrence of this finding was equal between both LBC lines tested. Thus, MCPH1 does not appear to be required for centriole duplication in LBC.

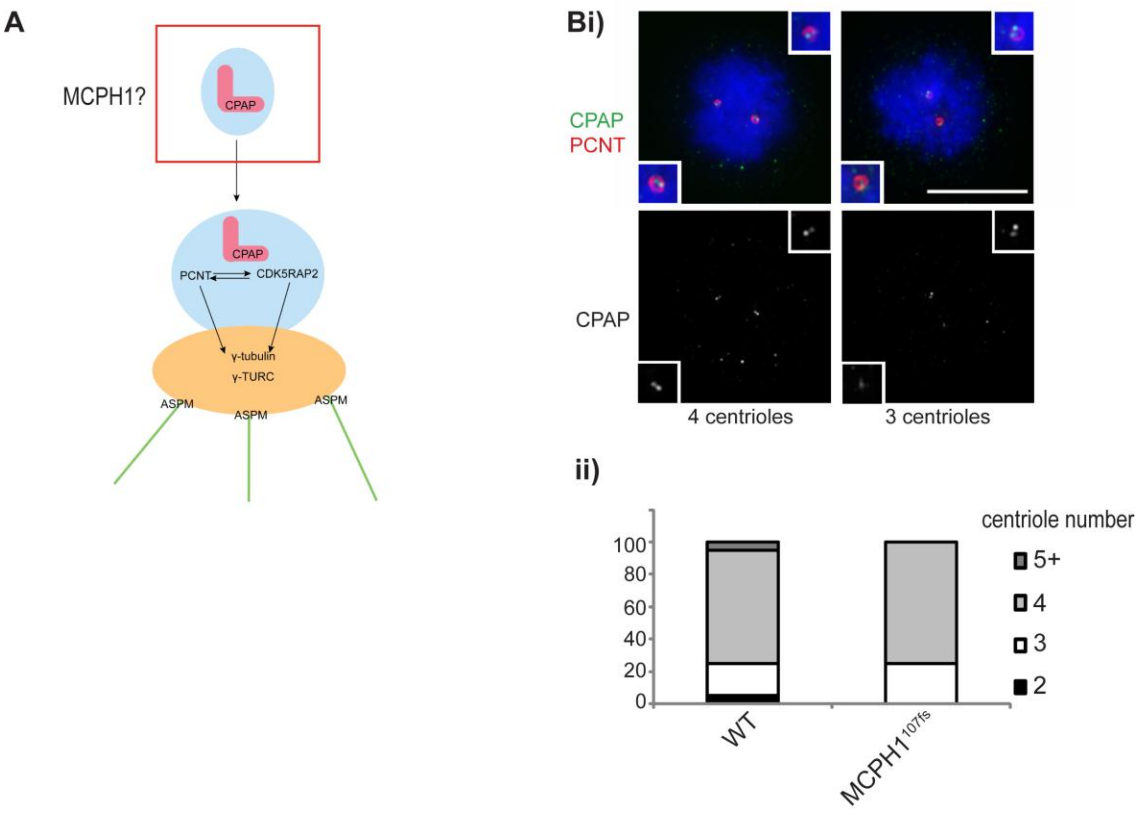

Figure 5.12. CPAP localisation and centriole number is not affected in MCPH1 patient derived LBC.
(A) Hypothesis: MCPH1 could be required for centriole formation and/or structure. (Bi) Control and MCPH1^{107fs} LBC were fixed in methanol and stained with PCNT (red) and CPAP (green) antibodies. DNA was visualised by DAPI staining. The left panel represents a cell with 4 stained centrioles and the right panel represents a cell with 3 centriole signals. Insets show 2 x magnified images. Scale bar is 10 µm. (ii) Quantitation of centriole number in control and MCPH1^{107fs} LBC. The number of cells containing two, three, four or five CPAP stained centrioles plotted as a percentage of the total cell number. The graph represents one experiment of 20 mitotic cells analysed per sample.

5.3.3. Centrosome maturation is unaffected in MCPH1 LBCs

Given that many of the primary microcephaly proteins or their orthologues play a role in PCM expansion (Conduit *et al.*, 2010; Dobbelaere *et al.*, 2008; Haren *et al.*, 2009; Kirkham *et al.*, 2003) and MCPH1 is required for recruitment of some PCM proteins during interphase (Tibelius *et al.*, 2009), the role of MCPH1 in the mitotic recruitment of three PCM markers PCNT, CDK5RAP2 and γ-tubulin was investigated (Figure 5.13A). This was conducted in MCPH1 deficient LBCs ($MCPH^{107fs}$, $MCPH1^{143fs}$). The PCNT patient LBC line ($PCNT^{E220X}$) was also included in this analysis as a positive control as depletion of PCNT is known to have an effect on γ-tubulin and CDK5RAP2 levels at mitosis (Griffith *et al.*, 2008; Haren *et al.*, 2009; Zimmerman *et al.*, 2004).

Immunofluorescence microscopy established that levels of PCNT, CDK5RAP2 and γ-tubulin in MCPH1 LBC are similar to the control LBC (Figure 5.13B i-iii). Pixel intensity of the volume encompassing the centrosome was quantified for each signal in order to confirm the subjective interpretation that there was no substantial difference in levels. As expected, PCNT LBC showed a pronounced reduction of CDK5RAP2 (80%) (Figure 5.13Bi) and γ-tubulin (60%) (Figure 6.3 B iii) compared to WT LBC. Thus, PCNT but not MCPH1 is required for recruitment of PCM proteins during mitosis.

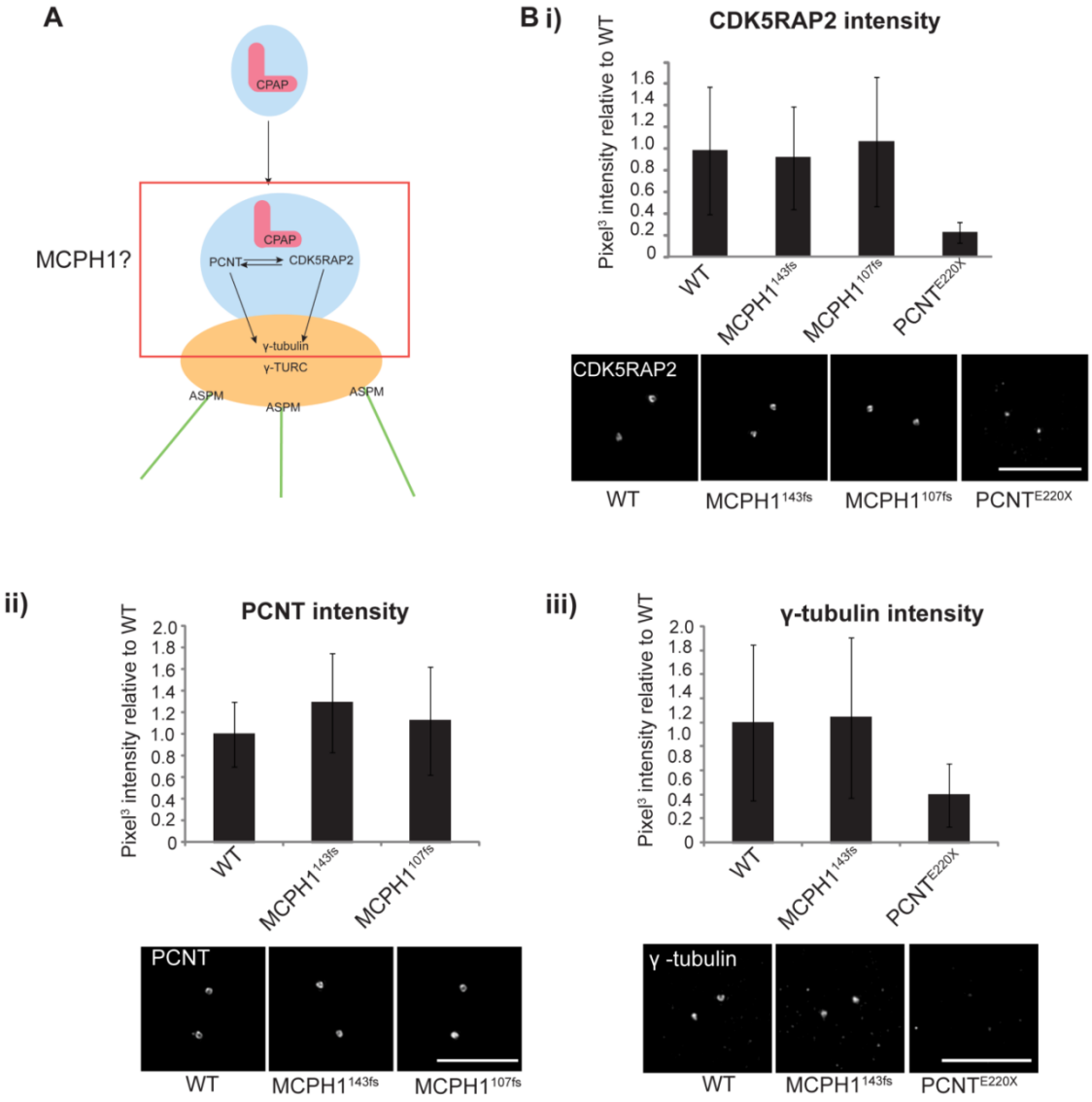

Figure 5.13. Recruitment of CDK5RAP2, PCNT and γ-tubulin are unaffected in MCPH1 patient derived LBCs.

(A) Hypothesis: MCPH1 acts in PCM recruitment during mitosis. (B) LBC were fixed in methanol and stained with (i) CDK5RAP2, (ii) PCNT or (iii) γ-tubulin antibodies. Bar graphs represent quantification of (i) CDK5RAP2, (ii) PCNT or (iii) γ-tubulin signal in prometaphase or metaphase MCPH1^{143fs}, MCPH1^{107fs} and PCNT^{E220X} LBCs, relative to control. Error bars represent s.d. of 20 prometaphase or metaphase cells (for CDK5RAP2 staining two independent experiments of 20 mitotic cells were performed).

5.3.4. Microtubule focussing and ASPM localisation is unperturbed in MCPH1 LBCs

Many of the primary microcephaly proteins or their orthologues play a role in nucleating and organising the microtubules (Choi *et al.*, 2010; do Carmo Avides and Glover, 1999; Fong *et al.*, 2008; Gonzalez *et al.*, 1990). MCPH1 is required for γ-tubulin recruitment to PCM during interphase (Tibelius *et al.*, 2009), which is required to confer microtubule nucleating and organisation capacity to centrosomes (Oakley *et al.*, 1990; Oakley and Oakley, 1989). To assess if MCPH1 is required for spindle morphology during mitosis, MCPH1 LBC were assessed using α-tubulin antibody to visualise microtubules and ASPM to stain the minus-ends of microtubules. Immunofluorescence analysis of ASPM stained cells revealed that levels were similar between MCPH^{107fs} and control LBC and that the minus-end microtubules were appropriately focused around the centrosome (visualised with aurora A antibodies) (Figure 5.14B). Staining of α-tubulin was consistent with ASPM staining showing that microtubule nucleation and focusing at the spindle pole was similar between MCPH^{107fs} and control LBC (Figure 5.14C). Thus, the microtubule nucleation and organisation capacity is not visibly perturbed in MCPH1 LBC.

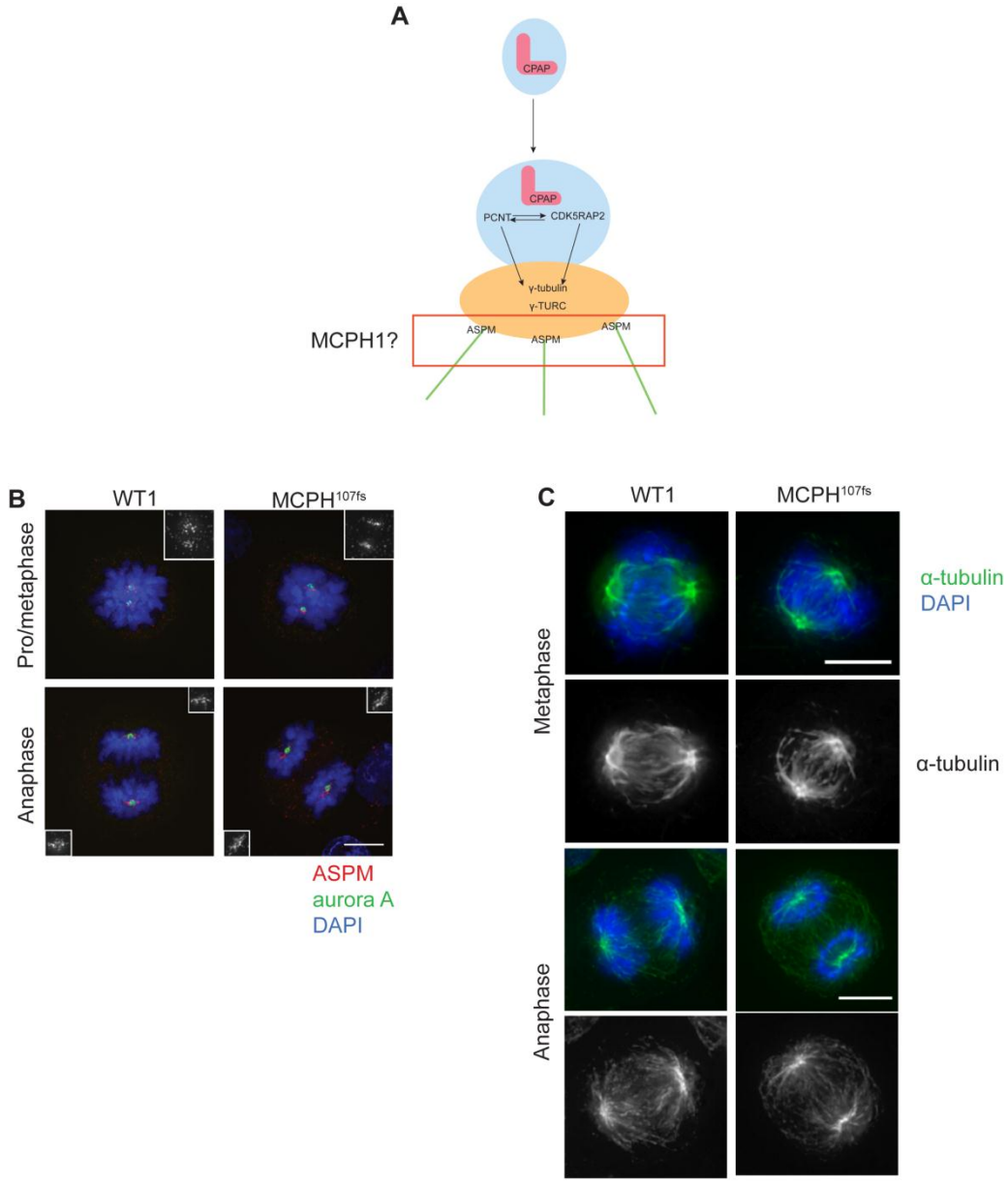

Figure 5.14. Microtubule nucleation and focusing is not affected in MCPH1 patient derived LBC.
(A) Hypothesis: MCPH1 is required for microtubule organisation during mitosis. (B) Control and MCPH1^{107fs} LBC were fixed in 4 % PFA and stained with ASPM (red) and aurora A (green) antibodies. Insets represent ASPM signal alone. (C) Control and MCPH1^{107fs} were fixed in methanol and stained with α-tubulin antibody. DNA was visualised by DAPI staining. Scale bar represents 10 µm.

5.4. Discussion

5.4.1. MCPH1 is required for chromosome alignment

This chapter establishes that MCPH1 is required for chromosome alignment during metaphase. RNAi-mediated depletion of MCPH1, delayed cells at metaphase and during this time chromosomes and chromatids are lost from the metaphase plate (Figure 5.1 & 5.4). Overexpression of GFP-MCPH1(FL) partially rescued this phenotype, consistent with this phenotype arising specifically due to loss of MCPH1 (Figure 5.1B). In addition, genetic ablation of *Mcph1* gene function in MEFs also leads to chromosome alignment defects (Figure 5.9).

The severity and frequency of the phenotype in primary MEF cells is substantially lower than due to RNAi-mediated depletion of transformed HeLa cells (12.5 % compared to 72 %) (Figure 5.2 & 5.9). This is not entirely surprising, *Mcph1*$^{-/-}$ mice are healthy with only subtle phenotypic abnormalities detected to date (www.sanger.ac.uk/mouseportal/search/MGI:2443308) and so the severe mitotic defects observed with MCPH1-RNAi was unlikely. There are a number of possible explanations to account for the differences in phenotype between MEFs and HeLa RNAi cells. First, MEFs are primary cells so they may possess checkpoints and apoptotic responses that have been dampened or lost in transformed cells. As a result the MEFs may be more sensitive to chromosome misalignments which could trigger apoptosis before progression of this phenotype. Second, HeLa cells have a greater chromosome complement than MEFs (approximately 76-80 versus 42) (Bennett, 1965; Macville *et al.*, 1999) and with more chromosomes to align, HeLa cells may have an increased frequency of alignment errors. Third, splice-trap mutations, which was used to knockdown *Mcph1* in MEFs, can often be leaky and hypomorphic (Barrera *et al.*, 2010; Trimborn *et al.*, 2010) and it is possible that there are residual levels of MCPH1 protein that may exert some function. Finally, the severe phenotype observed due to MCPH1 RNAi may reflect the immediate response to MCPH1 depletion, whereas during chronic absence of MCPH1, like in *Mcph1*$^{-/-}$ MEFs, the cells may have been able to adapt to loss of MCPH1 through upregulation of redundant pathways. Consistent with this possibility, phenotype severity differs

between acute and chronic depletion of Aspm in mice (Fish *et al.*, 2006; Pulvers *et al.*, 2010).

5.4.2. Chromatid cohesion is lost in MCPH1-RNAi cells

Chromatid cohesion between sister chromatids during a metaphase arrest is lost in MCPH1 depleted cells (but not *Mcph1*$^{-/-}$ MEFs) (Figure 5.7). Such cohesion is maintained by the cohesin protein complex which tethers sister chromatids at the centromere until anaphase onset (reviewed by Peters *et al.*, 2008). Proteins such as shugoshin 1 (Kitajima *et al.*, 2005; McGuinness *et al.*, 2005; Salic *et al.*, 2004; Tang *et al.*, 2004) and protein phosphatase 2A (PP2A) (Kitajima *et al.*, 2006; Tang *et al.*, 2006) are required to protect centromeric cohesin from cleavage until anaphase. At anaphase, separase mediated cleavage of cohesin releases it from the centromere and allows chromosome segregation to occur (Hauf *et al.*, 2001).

It is unclear if MCPH1 plays a direct role in cohesion protection. Recently it has been demonstrated that spindle pulling forces on kinetochores during a prolonged metaphase can lead to chromatid separation (Daum *et al.*, 2011). Daum *et al*. demonstrated that cohesin is maintained on centromeres of separated chromatids but hypothesised that during metaphase kinetochore-microtubule attachments rupture the molecular linkages of the cohesin complex. There is some evidence to suggest that prolonged time in metaphase could be the cause of chromatid separation due to MCPH1-RNAi. First, fixed-cell preparations of MCPH1-RNAi cells established that separated chromatids were only evident when there was significant loss of DNA from the metaphase plate (Figure 5.7). Live-cell imaging demonstrated the severity of chromosome/chromatid misalignment progressed with prolonged time in metaphase (Figure 5.4) which would suggest that the role of MCPH1 in maintaining chromatid cohesion may be time-dependent. In addition, MCPH1-RNAi cells do form a normal metaphase plate and if MCPH1 was directly required for cohesin protection at the centromeres then chromatid cohesion would likely be lost in prometaphase, after loss of cohesin along the length of sister chromatid arms in prophase (Waizenegger *et al.*, 2000). However, reports do differ on whether chromatid separation due to SGO1 RNAi mediated depletion arises during

prometaphase or metaphase, differences are possibly dependent on efficiency of protein depletion (Daum *et al.*, 2011; Daum *et al.*, 2009; Salic *et al.*, 2004). Thus, although it is more likely that MCPH1 phenotype is related to time spent in metaphase further work to confirm this would be worthwhile. One possibility would be to perform live-cell imaging of a cell line stably expressing GFP-CENP-A following depletion of MCPH1 or SGO1. If the role of MCPH1in chromatid cohesion is dependent on a prolonged metaphase then loss of chromatid cohesion is likely to arise much later during mitosis than due to SGO1 depletion.

5.4.3. MCPH1 is required for spindle bipolarity

RNAi-mediated depletion of MCPH1 leads to spindle multipolarity during mitosis (Figure 5.3A). Overexpression of GFP-tagged MCPH1(FL) can rescue this phenotype, suggesting it arises due to the specific depletion of MCPH1 (Figure 5.3B). However the rescue of spindle multipolarity or chromosome alignment is only partial and further work may be required to get a more significant phenotype rescue. Rescue may be incomplete due to the GFP epitope-tag impairing full biological function and so rescue experiments with untagged MCPH1 may be more penetrant. Alternatively, more than one MCPH1 isoform may need to be expressed for complete rescue of chromosome misalignment or spindle multipolarity. Targeting specific MCPH1 isoforms by RNAi (Figure 3.4) may enable the contribution of each isoform to chromosome segregation and spindle bipolarity to be assigned. Lastly, precise MCPH1 levels may limit rescue efficiency; indeed cells are very sensitive to MCPH1 expression levels (Section 4.3.1). Rescue with MCPH1 under its endogenous promoter element may overcome this limitation. Often rescue experiments are performed with the orthologous gene in murine bacterial artificial chromosomes (Kittler *et al.*, 2005) which is usually resistant to RNAi. However, it is worth noting that a partial phenotype rescue was only achieved in *mcph1 Drosophila* syncytial embryos stably expressing Mcph1 and so it may be that a more penetrant rescue with MCPH1 is not achievable (Brunk *et al.*, 2007).

What is the underlying cause of spindle multipolarity? Multipolar spindles can arise through several distinct pathways: i) failed cell division which can lead to the formation of a tetraploid cell with four centrosomes (Borel *et al.*, 2002; Meraldi *et*

al., 2002); ii) centriole overduplication which can be triggered by prolonged time in S-phase and loss of centriole engagement (Loncarek *et al.*, 2008); iii) compromised centrosome stability (Oshimori *et al.*, 2006). Tetraploidization or centriole amplification would lead to the presence of extra centrioles and centrosomes during interphase which is not the case in MCPH1-RNAi cells. Live and fixed preparations of MCPH1-RNAi cells established that extra PCM foci only appear during mitosis and that most of these foci do not contain centrioles (which also rules out premature centriole disengagement during mitosis as a causative mechanism (Thein *et al.*, 2007)) (Figure 5.6). Thus, it is likely that extra spindles arise due to fragmentation of the PCM from the centrosomes during mitosis (Figure 5.6C).

PCM fragmentation during mitosis could be a primary or secondary phenomenon. Firstly, as MCPH1 does localise to the centrosome it could play a structural role in maintaining centrosome stability during mitosis. It has been demonstrated that microtubule forces on a structurally weakened centrosome can cause the PCM to fragment (Abal *et al.*, 2005; Oshimori *et al.*, 2006). Further characterisation of centrosome morphology before chromosomes misalign may also be helpful in examining the possibility of a primary centrosome phenotype.

Secondly, as spindle multipolarity follows the disintegration of the metaphase plate it could be a secondary consequence of this. Indeed, it has been demonstrated that loss of chromatid cohesion can lead to loss of spindle pole bipolarity during metaphase (Dai *et al.*, 2009). If this was the case for MCPH1-deficient cells, then preventing resolution of DNA catenations by topoisomerase II inhibitor may rescue the phenotype by maintaining association of sister-chromatids (Toyoda and Yanagida, 2006).

5.4.4. What is the primary function of MCPH1 at mitosis?

A range of phenotypes were observed due to RNAi-mediated loss of MCPH1 including metaphase arrest, chromosome misalignment, loss of chromatid cohesion and spindle multipolarity. Fixed and live-cell imaging suggests that loss of chromatid cohesion and spindle multipolarity are secondary defects following metaphase arrest and chromosome misalignment (Figures 5.4, 5.6 & 5.7).

It will be important to determine if the metaphase arrest in the MCPH1-RNAi cells is due to the spindle activation checkpoint (SAC). Activation of the SAC can be inferred by visualisation of kinetochore accumulation of MAD1, MAD2 or BUBR1 during metaphase (Hoffman *et al.*, 2001) or by demonstrating rescue of arrest through inhibition of checkpoint signalling (for example by treatment with the aurora B inhibitor ZM447439 (Ditchfield *et al.*, 2003) or BUBR1/MAD2 RNAi (Meraldi *et al.*, 2004). If the SAC is indeed activated during metaphase then it will be relevant to determine the primary cause of its activation. Two possibilities are kMT attachment defects which sustain SAC activation (reviewed by Musacchio and Salmon, 2007) and/or failure to silence the SAC (reviewed by Vanoosthuyse and Hardwick, 2009b).

As chromosomes become misaligned from the metaphase plate this suggests that MCPH1 may well be required for kMT attachments. However, if kMT attachments are defective, it is surprising that a normal metaphase plate can be formed in MCPH1-deficient cells. One possibility is that defects in kMT attachments increase the time taken for chromosome congression but eventually normal chromosome alignment is achieved, as has been reported for SKAP, ska1 and ska2 (Dunsch *et al.*, 2011; Hanisch *et al.*, 2006; Schmidt *et al.*, 2010). This can be investigated by live-cell imaging of RFP-H2B U2OS cells depleted of MCPH1 to follow chromosome behaviour during progression from prophase through to metaphase. In addition, the stability of kMT attachments could also be directly assessed. When microtubules attach to kinetochores they become much more resistant to depolymerisation induced by cold treatment (Brinkley and Cartwright, 1975). Thus, the role of MCPH1 in kMT attachments could be analysed by measuring kMT fibres in MCPH1-RNAi cells following exposure to cold temperatures (Lampson and Kapoor, 2005).

Another possibility (that is not mutually exclusive to a role in kMT attachment) is that MCPH1 is required to switch off the spindle checkpoint. In this case, the loss of chromosomes may be a consequence of extended time in metaphase arrest. How MCPH1 could potentially function in silencing the checkpoint is undefined. Two mechanisms proposed to account for checkpoint silencing is dynein dependent stripping of spindle checkpoint proteins, such as MAD1 and MAD2, from the kinetochores (Howell *et al.*, 2001) or protein phosphatase 1 (PP1) mediated reversal

of aurora B and other kinase phosphorylation events that occur during SAC activation (Pinsky *et al.*, 2009; Vanoosthuyse and Hardwick, 2009a).

In regards to a how MCPH1 may participate in these processes at the kinetochore, exploring the relationship between MCPH1 and PP1 may be particularly interesting. PP1α has a similar spatio-temporal distribution to MCPH1, localising to the kinetochores at metaphase and then chromatin at late anaphase (Trinkle-Mulcahy *et al.*, 2006). Indeed, a component of the PP1α catalytic domain (PPP1CA) was recently identified as a preliminary MCPH1 interactant in a mass spectrometry screen of proteins associated with GFP-tagged MCPH1 (Margaret Harley, personal communication). Thus, it is possible that MCPH1 may be required for targeting protein phosphatases such as PP1α to the kinetochores to oppose aurora B phosphorylations, stabilising kMT interactions and/or silencing the spindle checkpoint.

There is also a striking similarity between the range of phenotypes identified in MCPH1-deficient cells and that reported for a number of kinetochore proteins such as astrin, the ska1 complex (ska1-3) and SKAP (Fang *et al.*, 2009; Gaitanos *et al.*, 2009; Hanisch *et al.*, 2006; Mack and Compton, 2001). Metaphase arrest and chromosome misalignment have been reported for all these proteins with astrin and ska3 additionally presenting with loss of chromatid cohesion and spindle multipolarity (Daum *et al.*, 2009; Gaitanos *et al.*, 2009; Thein *et al.*, 2007; Theis *et al.*, 2009) (Dunsch *et al.*, 2011; Fang *et al.*, 2009; Hanisch *et al.*, 2006; Schmidt *et al.*, 2010; Welburn *et al.*, 2009). However the interpretation of the primary defect has varied between publications and roles in regulation of separase activity (Fang *et al.*, 2009; Thein *et al.*, 2007), chromosome movement (Welburn *et al.*, 2009), spindle checkpoint silencing (Daum *et al.*, 2009) and kMT attachment have been proposed (Gaitanos *et al.*, 2009; Manning *et al.*, 2010; Raaijmakers *et al.*, 2009; Thein *et al.*, 2007; Theis *et al.*, 2009; Welburn *et al.*, 2009). It would be particularly worthwhile to investigate if MCPH1 functions in the same pathway as any of these proteins since they share the same phenotypes. Further studies could include screening for these proteins as MCPH1 interactants and to determine if MCPH1 is required for the recruitment of these proteins to the kinetochores or vice versa.

5.4.5. MCPH1 does not appear to be required for centrosome maturation

Notably centrosome maturation did not appear to be affected in MCPH1 patient-derived LBC suggesting that this is not a shared pathway contributing to primary microcephaly pathogenesis. MCPH1 LBC, null for MCPH1 FL and S protein (Figure 5.11), had normal centriole numbers (Figure 5.12), efficiently recruited three PCM proteins CDK5RAP2, pericentrin and γ-tubulin during mitosis (Figure 5.13) and formed well-focussed spindle poles (Figure 5.14). Initial observations in *Mcph1*$^{-/-}$ MEFs and MCPH1 RNAi cells are also consistent with these findings in MCPH1 patient-derived LBC. During mitosis, centriole numbers were normal, PCM proteins were recruited (only γ-tubulin antibody reagent was available for MEFs) and spindle pole morphology looked normal (data not shown). However, these preliminary findings require further validation and subtle defects are yet to be excluded.

LBC, HeLa and MEFs are very different to neuronal progenitor cells and so it remains possible that defects in centrosome maturation only manifest in this specific cell type. However, most of the primary microcephaly proteins localise and function at the centrosome in a range of species, cell-types and developmental contexts, for example centrosome phenotypes during mitosis due to CDK5RAP2 depletion are apparent in MEFs, mouse neuronal cells, chicken lymphoblastoid, HeLa, and U2OS (Barr *et al.*, 2010; Barrera *et al.*, 2010; Fong *et al.*, 2008; Lizarraga *et al.*, 2010). Thus, although primary microcephaly mutations result in a brain specific phenotype this may reflect the sensitivity of this tissue to centrosomal dysfunction rather than reflecting a cell-type specific centrosome function.

MCPH1 shares an interphase centrosomal localisation with many of the primary microcephaly proteins and it is possible that an interphase function could contribute to primary microcephaly pathogenesis. It has been demonstrated that MCPH1 is required for the recruitment of pericentrin and γ-tubulin during interphase (Tibelius *et al.*, 2009). This is not inconsistent with the findings in mitotic PCM recruitment as some PCM proteins, such as γ-tubulin, appear to be recruited by different mechanisms during interphase and mitosis (Rapley *et al.*, 2005). In addition to

interphase PCM recruitment, MCPH1 could also share a cilia function with the primary microcephaly proteins. Recently cilia length has been implicated in control of cell-cycle length and linked to neural progenitor cell fate choice (Kim *et al.*, 2011; Li *et al.*, 2011). Indeed, many of primary microcephaly proteins are required for ciliogenesis (CPAP, STIL and CEP152) and so this could be shared function between all the primary microcephaly proteins (Basto *et al.*, 2006; Blachon *et al.*, 2008; Izraeli *et al.*, 1999). Therefore it will be of interest to investigate the cilia in primary microcephaly protein deficient cells and in particular their effect on cell cycle length.

5.4.6. Phenotypic differences between MCPH1 RNAi, *Mcph1*$^{-/-}$ MEFs and MCPH1 LBC

There are some differences in severity of mitotic phenotype between transformed cells depleted of MCPH1 by RNAi, transcriptional ablation of MCPH1 in MEFs and genetic ablation in patient LBCs. There are a number of possibilities which could account for these differences. First it is worth noting that one of the earliest defects, chromosome misalignment, was present due to RNAi depletion of MCPH1 in transformed cells and in *Mcph1*$^{-/-}$ MEFs. This phenotype was not analysed in MCPH1 patient derived LBCs because metaphase plates are much more spread making this phenotype difficult to analyse in this suspension cell line. There are differences in the progression of mitotic phenotype as loss of chromatid cohesion or spindle multipolarity was not apparent in MEFs or LBC due to MCPH1 depletion. This may be accounted for by cell type specific differences. Indeed chromatid scattering due to a prolonged time in metaphase was reported to be of lower penetrance and longer arrest time in karotypically normal cells compared to transformed cells (Stevens *et al.*, 2011). Finally the MCPH1 MEFs or LCLs cells may be able to adapt to loss of MCPH1 following transcriptional or genetic ablation leading to a less severe phenotype whereas chronic MCPH1 depletion may be more severe.

Chapter 6. Post-translational modifications of MCPH1

The temporal localisation and stability of MCPH1 (Chapter 3 and 4) presented the intriguing possibility that MCPH1 may be regulated by post-translational modifications during the cell cycle. The regulation of mitosis relies predominantly on two post-translational mechanisms: protein phosphorylation and proteolysis. As a result, this chapter focuses predominantly on the phosphorylation and proteolysis of MCPH1 during mitosis but does characterise other non-mitotic modifications of this protein.

6.1. GFP-MCPH1 is cleaved by caspases

6.1.1. MCPH1 FL and Δ8 proteins demonstrate cleavage

GFP antibody immunoblotting of GFP-tagged MCPH1 (Chapter 2) often revealed the appearance of a band migrating approximately 25 kDa below GFP-FL and GFP-Δ8 (called FL* and Δ8*) (Figure 6.1A). A band migrating below GFP-S was never observed, making it unlikely that FL* and Δ8* was simply a degradation product or due to non-specific protein detection. Notably FL* was often more apparent when the extracts were from cells treated with nocodazole. The explanation for this is unclear. It is unlikely that generation of FL* is mitosis specific since Δ8* was apparent in asynchronous cells and it is assumed cleavage is by the same mechanism. FL* also appeared in a time-dependent manner upon treatment with cycloheximide, a drug used to inhibit protein translation (Figure 6.1B). This suggested that generation of this band did not require *de novo* protein synthesis and was most likely to result from post-translational modification of FL. Thus, taken together this evidence suggested that both MCPH1 FL and Δ8 are post-translationally cleaved.

The approximate site of cleavage was apparent from the cleavage products produced (Figure 6.1A). The GFP-tag was located at the NH_2-terminus thus the cleaved proteins (detected by GFP antibodies) must contain the NH_2-terminal. MCPH1(S) was not visibly cleaved suggesting that cleavage must occur in a region shared between FL and Δ8 but absent in S. In addition, FL* is approximately the same size

as MCPH1(S) suggesting that the cleavage site must be in the region immediately following the MCPH1(S). Within this region, two putative caspase-3 and caspase-7 cleavage sites were identified (DVLD^{621}↓DSCD^{625}↓) (Talanian *et al.*, 1997; Thornberry *et al.*, 1997) (Figure 6.1C) that may account for this finding.

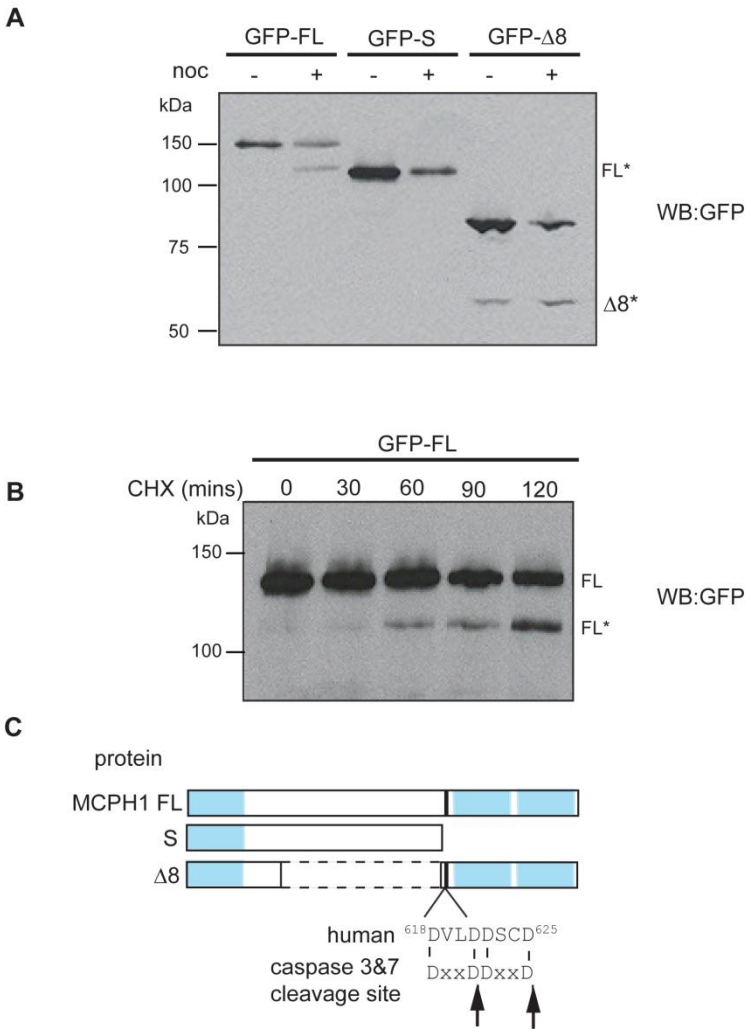

Figure 6.1. GFP-MCPH1 FL and Δ8 are cleaved.
(A) GFP-tagged MCPH1 FL and Δ8 are cleaved. HeLa cells transiently expressing GFP-tagged MCPH1 FL, S or Δ8 were either mock-treated or treated with nocodazole (noc) for 16 hr. Cell lysates were prepared and subjected to immunoblotting with GFP antibodies. (B) Cleavage of MCPH1 FL is not inhibited by cycloheximide (CHX). HeLa cells transiently expressing GFP-tagged MCPH1 FL were treated with 40 µg/ml cycloheximide for up to 2 hr. Cell lysates were prepared at the indicated time points after CHX addition and subjected to immunoblotting with GFP antibodies. (C) Schematic diagram of MCPH1 isoforms and location of putative caspase3 and 7 cleavage sites.

6.1.2. MCPH1 FL and Δ8 are cleaved by a caspase-dependent mechanism

Caspases are the executioners of programmed cell death (apoptosis) and actively cleave substrates when an apoptotic program has been activated. If GFP-MCPH1 is cleaved by a caspase-dependent mechanism then it is likely there is activation of apoptosis. By using cleavage of the caspase substrate PARP1 as an indicator, apoptosis was indeed induced during overexpression of MCPH1(Δ8) or due to nocodazole treatment (Figure 6.2A & B, lane 1). Apoptosis was further confirmed visually by observation of cells with apoptotic morphology. This confirmed caspases were active and I next examined whether they could be involved in MCPH1 FL and Δ8 cleavage. To verify this, cells overexpressing GFP-MCPH1 FL or Δ8 were treated with a pan-caspase inhibitor Z-VAD-FMK. As shown in Figure 6.2A & B, FL* and Δ8* did not appear in the presence of the inhibitor, indicating that caspases contributed to the generation of GFP-MCPH1 FL* and Δ8 * cleavage products. PARP1 cleavage was also suppressed by Z-VAD-FMK confirming inhibition of apoptosis. Thus, GFP-MCPH1 cleavage is mediated by a caspase-dependent mechanism.

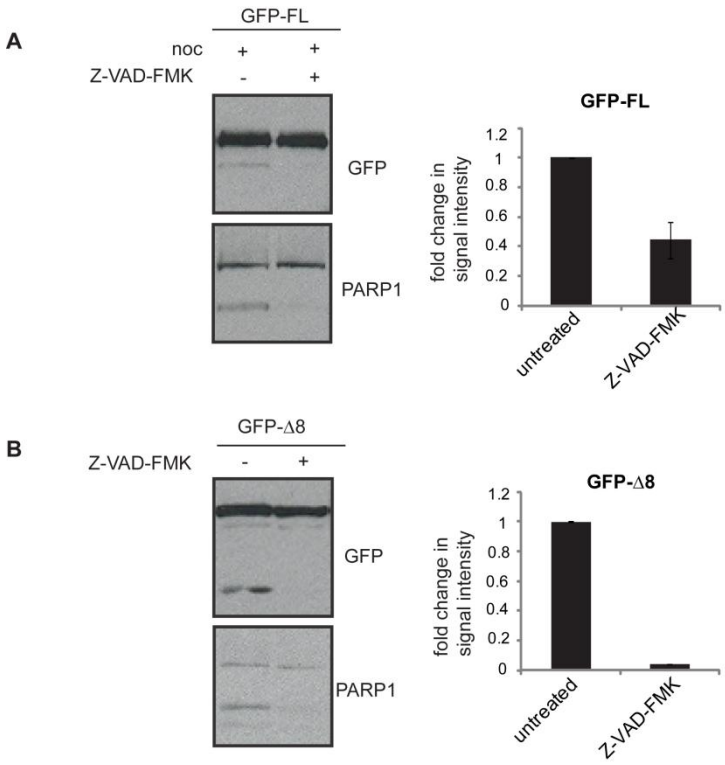

Figure 6.2. GFP-MCPH1 FL and Δ8 are cleaved by a caspase dependent-mechanism. HeLa cells transiently expressing GFP-tagged MCPH1 FL (A) or Δ8 (B) were either untreated (GFP-Δ8) or treated with nocodazole (noc) for 16 hr (GFP-FL). In combination the cells were either mock treated or treated with Z-VAD-FMK for 16 hr. Cell lysates were prepared and subjected to immunoblotting with GFP antibodies. Appropriate inhibition of caspases was confirmed by immunoblotting for cleaved PARP1. The bar graphs represent quantification analysis of the fold change in cleaved protein signal intensity normalised to uncleaved protein levels (mean ± standard deviation of two independent experiments).

6.1.3. MCPH1 FL and Δ8 are cleaved at aspartate 625

Given that cleavage of GFP-FL and GFP-Δ8 required caspases (Figure 6.2); it was tested whether caspases were directly involved in MCPH1 cleavage. In Figure 6.1C, two putative caspase 3 and 7 consensus sites (DVLD^{621}↓DSCD^{625}↓) located within the expected region of cleavage were identified. The classic caspase 3 and 7 recognition consensus is DxxD↓ (Talanian *et al.*, 1997; Thornberry *et al.*, 1997). However, the residue preceding the fourth aspartate (D) (P_1') is also very important and charged or bulky residues are poorly tolerated here (Stennicke *et al.*, 2000). Thus, it is likely that the second caspase consensus site DSCD^{625}↓G presents as a strong candidate for cleavage catalysis whereas DVLD^{621}↓D with a charged aspartate

residue in P_1' position would be poor. To confirm this, each of the caspase cleavage sites was tested for functionality. For each of the candidate caspase consensus sites, the fourth (*i.e.*, distal) aspartate residue was mutated to glutamate and expressed as GFP_MCPH1(Δ8) (Fig. 6.3A) to establish whether the mutagenesis would disrupt cleavage. When these constructs were expressed in HeLa cells, the control GFP-MCPH1(Δ8) protein was still cleaved, but this was abolished in the presence of the D625E substitution (Figure 6.3 B). The D621E substitution may lead to a reduction in cleavage efficiency (Figure 6.3 B) since there was a reduction in Δ8* band intensity relative to uncleaved Δ8 band. Quantification in replicate experiments would be helpful to unequivocally establish this finding. The D625E substitution also abolished cleavage of GFP-FL (Figure 6.3 C) confirming cleavage is by the same mechanism. Thus, MCPH1 is likely cleaved by caspase 3 and/or 7 proteolysis at the primary cleavage site Asp 625 consistent with consensus sequence predictions.

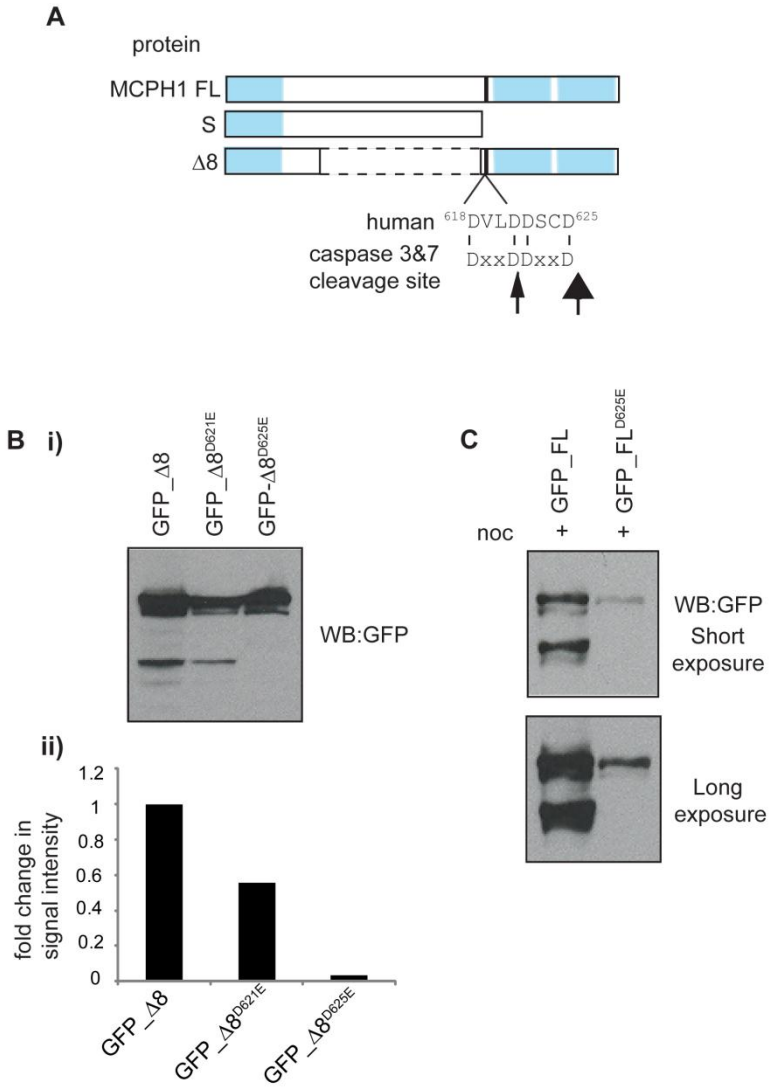

Figure 6.3. GFP-MCPH1 is cleaved after residue aspartate 625.
(A) Schematic diagram of MCPH1 isoforms and location of putative caspase 3 & 7 cleavage sites. Mutation of Asp625 abolishes MCPH1 FL and Δ8 cleavage. HeLa cells were transfected with plasmids expressing GFP-tagged MCPH1 Δ8, Δ8 (D621E), Δ8 (D625E) (B), FL or FL (D625E) (C). HeLa cells transfected with FL constructs were additionally treated to nocodazole (noc) for 16 hr. Lysates were prepared and subjected to immunoblotting with GFP antibodies.

6.2. MCPH1 is degraded in late mitosis and early G_1 phase

Levels of MCPH1 FL and S are cell cycle regulated with a decrease in abundance during mitosis (FL) and G_1 (FL and S) (Chapter 3). In light of the identification of caspase cleavage as a mechanism to regulate MCPH1, cell cycle fluctuation in MCPH1 protein levels was confirmed to be independent of caspase inhibition by Z-VAD-FMK treatment (Appendix 3). Thus, the decrease in protein abundance is not due to an increase in apoptosis at this stage of the cell cycle.

To further investigate the regulation of endogenous MCPH1 protein during the cell cycle, protein levels were followed after release from a prometaphase arrest. MCPH1 FL and S levels rapidly decreased as HeLa cells were released into the cell cycle from a nocodazole-induced arrest (Figure 6.4A). Decrease in MCPH1 FL and S is evident before the completion of mitosis (cells were followed live) and paralleled that of cyclin B1. This is consistent with the findings from the double thymidine block release (Figure 3.7) although the decrease in MCPH1(S) appeared to occur at mitotic exit following release from a prometaphase arrest, rather than G_1 phase as previously concluded. This difference may be accounted for by changes to MCPH1(S) transcript levels following the two synchronisations. Nevertheless, both synchronisations are consistent in showing that MCPH1 FL and S abundance is cell cycle regulated.

The fact that MCPH1 FL and S levels paralleled that of cyclin B1 suggests that MCPH1, like cyclin B1, may be degraded by the anaphase promoting complex or cyclosome (APC/C) (King *et al.*, 1995; Sudakin *et al.*, 1995). The APC/C targets proteins for degradation by the 26S proteasome from prometaphase through to G_1 phase (Pines, 2006). To determine whether MCPH1 FL and S are targeted for degradation by the APC/C, RNAi mediated knockdown of a subunit of the APC/C, APC3, was undertaken, to test consequences on MCPH1 FL and S accumulation. Indeed, this did lead to a considerable increase in the protein abundance of MCPH1 S and FL (Figure 6.4B). This finding is unlikely to be due to an indirect effect on cell cycle progression as although APC3 knockdown does lead to an accumulation of prometaphase cells, the difference in MCPH1 protein levels between asynchronous

and prometaphase cells is not substantial (Figure 6.4B). Thus, MCPH1 is likely to be targeted for degradation by the APC/C.

The APC/C is an E3 ubiquitin ligase that assembles polyubiquitin chains on substrate proteins to target them for destruction by the 26S proteasome (King *et al.*, 1995; Sudakin *et al.*, 1995). To confirm that MCPH1 is a substrate of APC/C it was established that GFP-FL and GFP-S are modified *in vivo* in the presence of $(His)_6$-tagged ubiquitin and MG132, which inhibits the 26S proteasome (Figure 6.4C). As only whole cell extracts were used, further studies are required to establish that the modified form of MCPH1 is due to polyubiquitination (for example, GFP-MCPH1 purification followed by immunoblotting with anti-ubiquitin antibodies). Certainly MCPH1 modification is consistent with polyubiquitination given the substantial mobility shift and dependency on inhibition of the 26S proteasome.

APC/C primarily recognises substrates containing one of two consensus motifs called the D box (Glotzer *et al.*, 1991) and KEN box (Pfleger and Kirschner, 2000). After examining the MCPH1 peptide sequence, only one putative KEN box motif was identified: ^{599}KENxxxG^{605} (Figure 6.4D) which was conserved in mouse and can act as a functional degradation motif in securin (Zur and Brandeis, 2001). This motif was mutated (KEN→AAA) in GFP-MCPH1(FL) and the stability of GFP-MCPH1(FL)$^{KEN\rightarrow AAA}$ compared to GFP-MCPH1(FL) was assayed during mitotic exit and in early G_1 phase. However, overexpressed GFP-MCPH1(FL) was not targeted for degradation at mitotic exit (data not shown). This may be due to GFP-MCPH1(FL) protein abundance, which could prevent cell cycle progression or it may be that the APC/C and 26S proteasome cannot maintain degradation of such large amounts of protein. Thus, it remains unclear whether the MCPH1 KEN box is biologically functional.

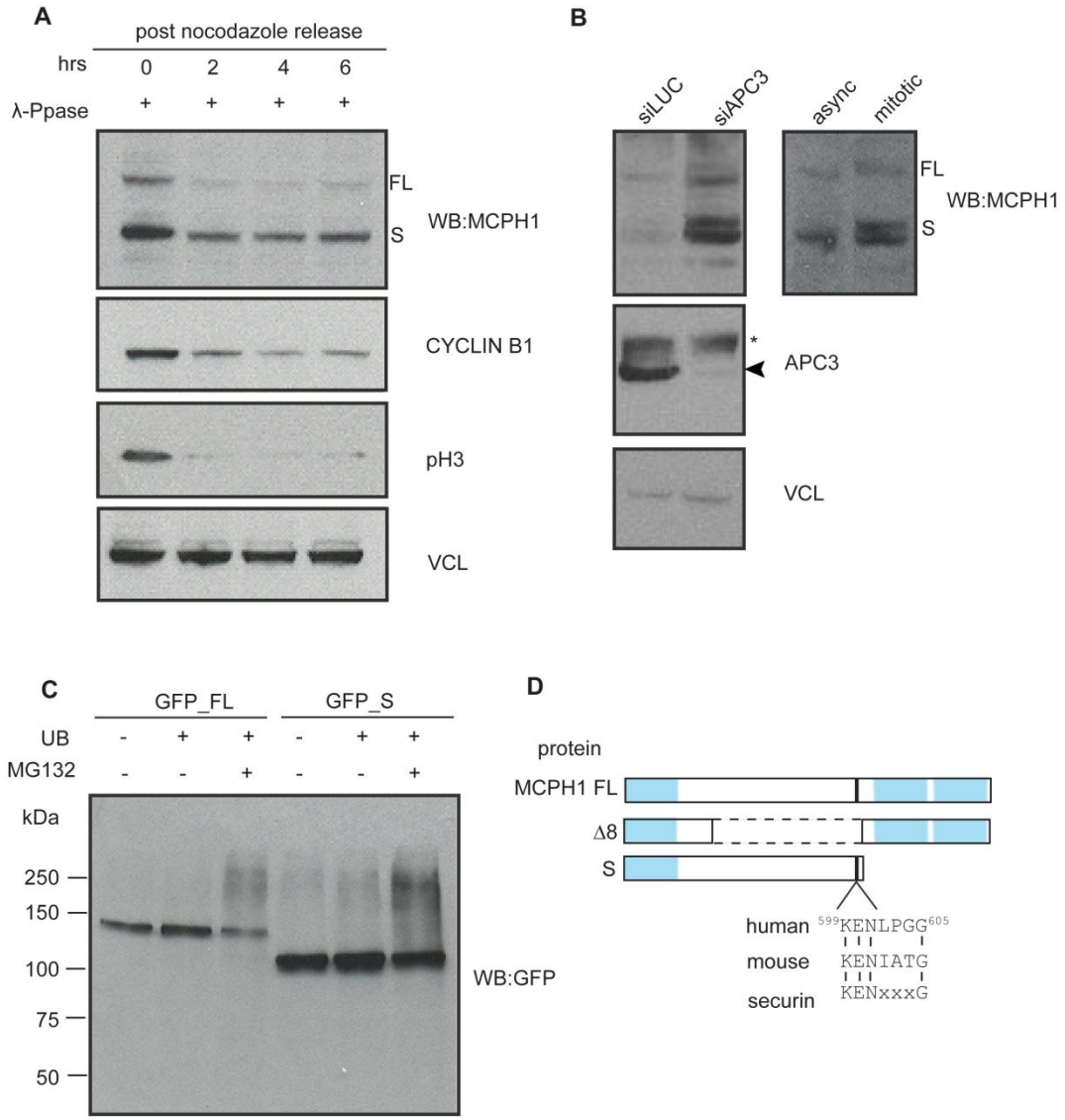

Figure 6.4. MCPH1 is degraded in late mitosis and early G_1 phase.
(A) MCPH1 protein levels decrease following release from a nocodazole block. Extracts prepared from HeLa cells released from a prometaphase arrest by nocodazole treatment and harvested at the indicated timepoints. Extracts were analysed by immunodetection of MCPH1, cyclin B1, phospho histone H3 and vinculin (loading control). Reproducible in two independent experiments. (B) MCPH1 protein levels correlate with APC/C activity. HeLa cells were treated with siRNA oligonucleotides against luciferase (control) or APC3. After 72 hr, the cell lysates were prepared and subjected to immunodetection by MCPH1, APC3 and vinculin antibodies. APC3 inhibition leads to a prometaphase arrest so for a comparison of protein levels a MCPH1 Western blot of extracts from asynchronous and cells arrested at prometaphase by nocodazole was included. (C) MCPH1 is modified by $(His)_6$-ubiquitin during MG132 mediated proteasome inhibition. Extracts prepared from HeLa cells transfected with plasmids expressing GFP-tagged MCPH1 FL or S and $(His)_6$ tagged ubiquitin (UB). Where indicated cells were treated with MG132 for 8 hr before harvesting. GFP-tagged proteins were detected using GFP antibodies. (D) Schematic diagram of MCPH1 isoforms, location and conservation of putative KEN box.

6.3. MCPH1 is phosphorylated during mitosis

Endogenous MCPH1 from prometaphase arrested cells showed a reduced mobility during SDS-PAGE gel electrophoresis compared with MCPH1 from asynchronous cells (Figure 6.4B) suggesting that it may be post-translationally modified during mitosis. To determine whether the shifted form of MCPH1 is phosphorylated, extracts from mitotic cells were treated with λ-phosphatase (Figure 6.5). This treatment removes protein phosphorylation and indeed reversed the mobility shift of extracts from mitotic cells, confirming that endogenous MCPH1 is phosphorylated at mitosis.

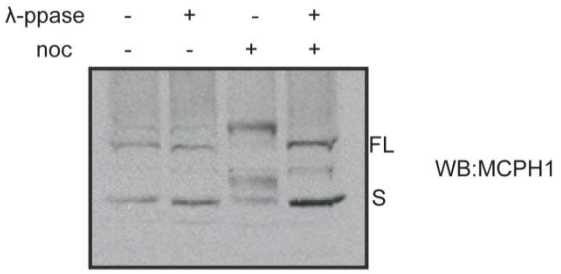

Figure 6.5. MCPH1 is hyperphosphorylated during a prometaphase arrest.
Extracts prepared from asynchronous or nocodazole-arrested HeLa cells were treated with protein phosphatase inhibitors in buffer alone or with λ-phosphatase. All samples were incubated at room temperature for 30 min and subsequently analysed by MCPH1 immunodetection. This result was reproducible in three independent experiments.

6.4. Identification of MCPH1 phosphorylation sites

The substantial band shift between asynchronous and mitotic MCPH1 could suggest that MCPH1 is phosphorylated at multiple sites. This makes it difficult to identify individual phosphorylated residues by a candidate approach. Thus, to identify phosphorylated residues, MCPH1 was analysed by mass-spectrometry and ion-precursor scanning. For maximum tryptic peptide coverage for mass-spectrometry large amounts of purified protein was required. To satisfy this requirement, DT40 cells stably expressing GFP-tagged human MCPH1(S) was used as a source of MCPH1 (DT40 stable cells were created by Paola Vagnarelli, University of

Edinburgh). MCPH1(S) shared the substantial band shift with MCPH1(FL) (Figure 6.5) but is easier to express and purify (Figure 6.6A).

Figure 6.6B summarises the phosphorylated residues identified from mass spectrometry and ion-precursor scanning. A substantial number of phosphorylated residues were identified, although in some cases, the phosphorylation group cannot be confidently localised to an exact residue. Interesting phosphorylation sites include S333, S335 and S548 which have also been identified in large-scale phosphorylation proteomics screens (Chen *et al.*, 2009; Dephoure *et al.*, 2008; Olsen *et al.*, 2010) and phosphorylation sites conserved between humans and mice. S191-S195 and S410-S417 are well conserved regions (Appendix 4).

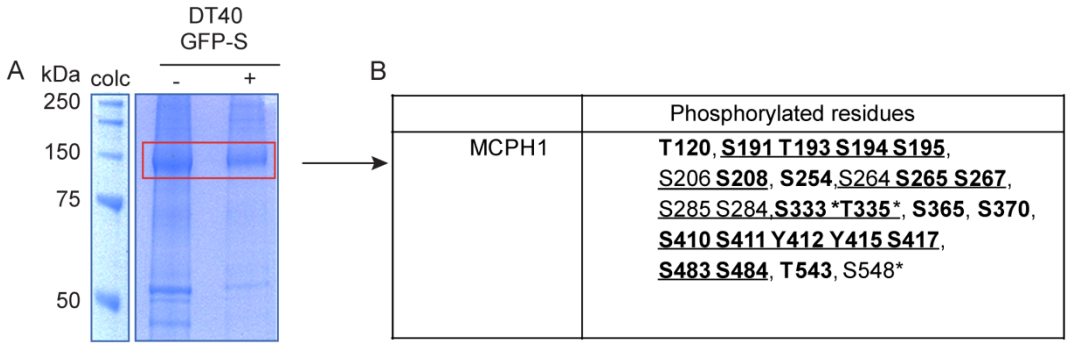

	Phosphorylated residues
MCPH1	**T120**, **S191 T193 S194 S195**, S206 **S208**, **S254**, S264 **S265 S267**, S285 S284, **S333 *T335***, **S365**, **S370**, **S410 S411 Y412 Y415 S417**, **S483 S484**, **T543**, S548*

Figure 6.6. Identification of MCPH1 phosphorylation sites by phosphopeptide mapping. (A) Mapping of phosphorylation sites in MCPH1. DT40 cells stably expressing GFP-MCPH1(S) were either mock-treated or treated with Colcemid (colc) for 16 hr. Cell lysates were prepared and GFP-MCPH1(S) was affinity purified with GFP-TRAP agarose beads, separated on a SDS-PAGE gel and stained with coomassie blue. Bands representing GFP-MCPH1(S) were excised, trypsinised and analysed by nano-LC-MS-MS (Dundee Fingerprints Facility). (B) Summary of phosphorylated residues identified by phosphopeptide mapping. The underlined sites represent ambiguous assignment, the sites in bold represent residues conserved in mouse and the sites denoted by asterisks represent sites also identified in large-scale proteomics screens.

6.5. CDK1 and PLK1 contribute to MCPH1 mitotic phosphorylation

6.5.1. CDK1 mediated phosphorylation of MCPH1

The phosphopeptide mapping led to the identification of a number of phosphorylated residues in CDK1 consensus sites (Figure 6.7A). To determine if CDK1 contributes to MCPH1 phosphorylation during mitosis, CDK kinase activity was inhibited by treatment of nocodazole arrested cells with Roscovitine or Purvalanol A. Roscovitine (Meijer *et al.*, 1997) and Purvalanol A (Gray *et al.*, 1998) inhibit a range of cyclin dependent kinases including CDK1, CDK2 and CDK5. Inhibition of CDK1 can override prometaphase arrest due to microtubule destabilising drugs such as nocodazole (Potapova *et al.*, 2006; Skoufias *et al.*, 2007) and as a result incubation with these drugs was restricted to short time intervals and only rounded mitotic cells were collected by shake off for immunoblotting. Both CDK inhibitors completely reverse the MCPH1 mobility shift, suggesting MCPH1 phosphorylation *in vivo* is mainly driven by CDKs (Figure 6.7B).

To determine whether MCPH1 was directly phosphorylated by CDK1, Strep-tagged MCPH1 fragments were purified (Figure 6.7C) and subjected to an *in vitro* CDK1-cyclin-B1 protein phosphorylation assay. To detect *in vitro* phosphorylation of MCPH1, purified MCPH1 fragments were immunoblotted with MPM-2 antibody which can recognize phospho-epitopes generated by CDK1 (Westendorf *et al.*, 1994; Yaffe *et al.*, 1997). MPM-2 recognized CDK1-phosphorylated MCPH1 NB domain, but not the BRCT1 or BRCT2/3 domains (Figure 6.7D). This was consistent with the findings from phosphopeptide mapping where all the CDK1 consensus phosphorylation sites were located in the NB domain (Figure 6.6) (although it is worth noting that the BRCT2/3 domain was not represented in the phosphopeptide mapping studies). To conclude, CDK1 can contribute to MCPH1 phosphorylation at mitosis.

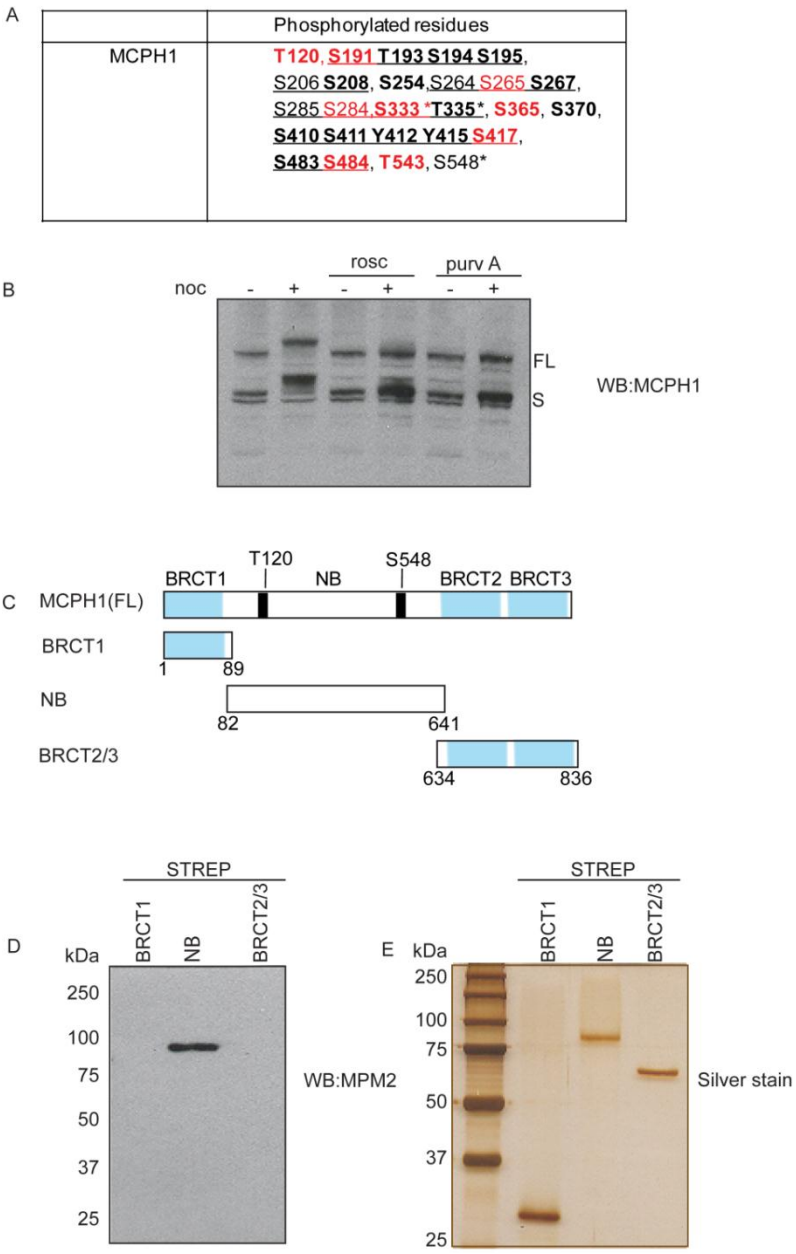

Figure 6.7. MCPH1 is phosphorylated by CDK1 during mitosis.
(A) Summary of MCPH1 CDK1 consensus phosphorylation sites identified by phosphopeptide mapping. CDK1 consensus phosphorylation sites are highlighted in red. (B) MCPH1 hyperphosphorylation is lost following CDK inhibition. Asynchronous or nocodazole-arrested HeLa cells were treated with Roscovitine (rosc) or with Purvalanol A (purv A) for 1 hr. Mitotic cells were collected by shake-off and extracts subjected to immunodetection with MCPH1 antibodies. Blot representative of three independent experiments. (C) Schematic of MCPH1 protein fragments used for *in vitro* pulldowns. The locations of T120 and S548 residues on MCPH1 protein are represented. (D) MCPH1 is phosphorylated *in vitro* by CDK1-cyclin-B1. Recombinant CDK1-cyclin-B1 was incubated with the indicated recombinant strep-tagged MCPH1 fragments in kinase buffer. Phosphorylated protein fragments were detected by immunodetection with MPM2 antibody that recognises CDK1 phospho-epitopes. (E) Equivalent amounts of the GST-tagged proteins were determined by silver staining.

6.5.2. PLK1 mediated phosphorylation of MCPH1

The phosphopeptide mapping also led to the identification of two phosphorylated residues in PLK1 consensus sites (identified by ELM predictions) (Figure 6.8A). To determine if PLK1 contributes to MCPH1 phosphorylation *in vivo*, PLK1 kinase activity was inhibited by the highly specific drug B12536 (Lenart *et al.*, 2007). Mitotic cells arrested in prometaphase were obtained by shake-off after treatment with nocodazole in the presence or absence of B12536. Western blotting of cell extracts revealed that inhibition of PLK1 subtly increased the mobility of MCPH1 during mitosis (Figure 6.8B). This finding was confirmed by RNAi-mediated knockdown of PLK1 that led to a similar shift in MCPH1 migration compared to extracts from siLUC nocodazole arrested cells (Figure 6.8C). Thus, PLK1 contributes to MCPH1 phosphorylation during mitosis.

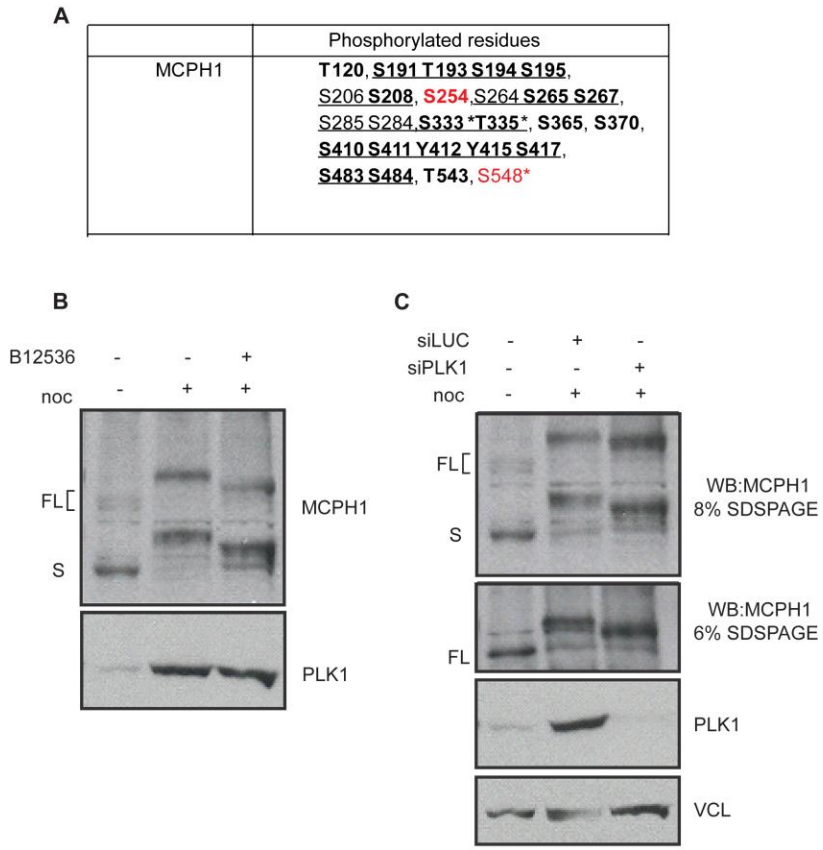

Figure 6.8. MCPH1 is phosphorylated by PLK1 during mitosis.
(A) Summary of MCPH1 PLK1 consensus phosphorylation sites identified by phosphopeptide mapping. PLK1 consensus phosphorylation sites are highlighted in red. (B) PLK1 inhibition leads to increased mobility of mitotic MCPH1 on SDS-PAGE. Asynchronous or nocodazole-arrested HeLa cells were mock-treated or treated with B12536 for 90 min. Mitotic cells were collected by shake-off and extracts subjected to immunodetection with MCPH1 and PLK1 antibodies. This experiment is reproducible in three independent experiments. (C) PLK1 depletion by RNAi leads to increased mobility of mitotic MCPH1 on SDS-PAGE. HeLa cells were treated with siRNA oligonucleotides against luciferase (control) or PLK1. After 32 hr, the cells were either mock-treated or treated with nocodazole for 16 hr. Lysates were prepared and subjected to immunodetection by MCPH1, PLK1 and VCL antibodies.

6.6. PLK1 or CDK1 phosphorylation does not appear to be required for MCPH1 kinetochore localisation

6.6.1. Mutation of PLK1 or CDK1 phosphosites did not affect MCPH1 localisation

Chapter 4 had demonstrated that GFP-MCPH1(FL) localisation to kinetochores was cell cycle regulated. One hypothesis is that phosphorylation modifies MCPH1 to allow it to temporally bind kinetochores.

To determine if phosphorylation plays a role in targeting MCPH1 to the kinetochores, candidate PLK1 and CDK1 phosphorylation sites were mutated in GFP-MCPH1(FL) and the localisation investigated. GFP-tagged MCPH1(FL) was constructed with a series of phosphorylation-dead alanine mutations in either PLK1 consensus phosphorylation motifs (A89, A254, A548, triple mutant) or CDK1 consensus phosphorylation motifs (A120, A191, A333, A365) (Figure 6.9A). All but residue S89 had been identified as potential phosphorylated residues by phosphopeptide mapping (Figure 6.9B, red). The individual mutant proteins were expressed in cells depleted of endogenous MCPH1 by siMCPH1#1 (described in Chapter 5). All the PLK1 and CDK1 alanine mutants localised to the kinetochores during mitosis, suggesting that no individual phosphorylation is sufficient to target MCPH1 to the kinetochores (Figure 6.9Bi & C). The PLK1 triple mutant also localised to the kinetochores (Figure 6.9D) but time constraints did not allow for analysis in MCPH1-depleted background or generation of a CDK1 quadruple mutant.

In addition GFP-tagged MCPH1(FL) with a series of phosphorylation-mimetic aspartate mutations in the PLK1 and CDK1 consensus phosphorylation motifs (D89, D120, D191, D254, D333, D365, D548) were constructed. The PLK1 and CDK1 aspartate mutants localised to the kinetochores normally during mitosis with no aberrant localisation (Figure 6.9Bii).

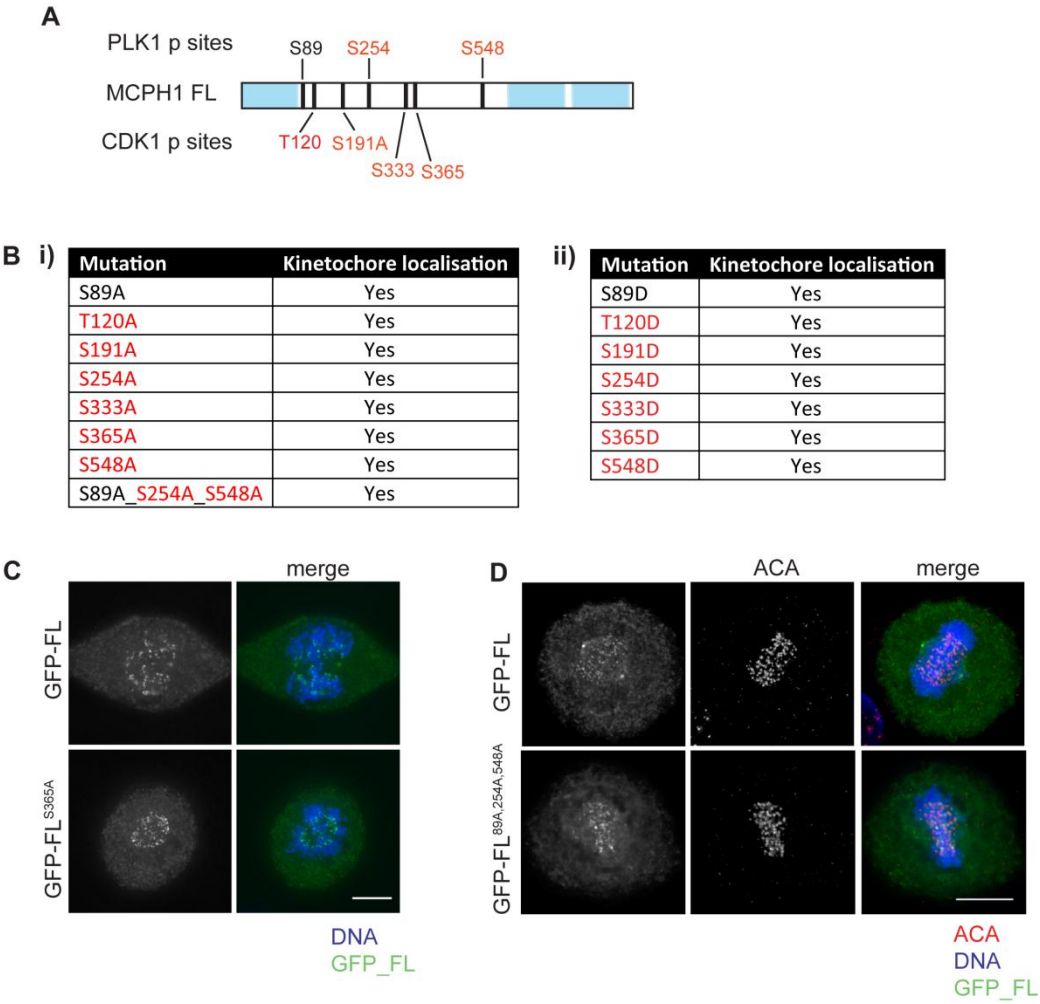

Mutation	Kinetochore localisation
S89A	Yes
T120A	Yes
S191A	Yes
S254A	Yes
S333A	Yes
S365A	Yes
S548A	Yes
S89A_S254A_S548A	Yes

Mutation	Kinetochore localisation
S89D	Yes
T120D	Yes
S191D	Yes
S254D	Yes
S333D	Yes
S365D	Yes
S548D	Yes

Figure 6.9. MCPH1 PLK1 and CDK1 phospho-dead and constitutively active mutants localise to the kinetochores.

(A) Schematic of MCPH1 FL protein and locations of consensus PLK1 and CDK1 phosphorylation sites. Potential phosphorylated residues identified by phosphopeptide mapping were highlighted in red. (B) MCPH1 PLK1 and CDK1 phosphorylation-dead and phosphorylation-mimetic mutants localise to the kinetochores. Table summarising phosphorylation-dead (i) and phosphorylation-mimetic (ii) mutants used. HeLa cells were co-transfected with MCPH1 RNAi oligonucleotides (MCPH1#1) and plasmid expressing GFP-tagged FL with the indicated substitutions. (C) Representative images of findings in table B. HeLa cells expressing GFP-FL or GFP-FL^{S365A}. GFP-FL cell was also included in Figure 4.5. (D) HeLa cells were transfected with plasmids expressing GFP-MCPH1 FL or GFP- FL$^{S89A, S254A, S548A}$ were fixed in methanol and stained with ACA antibodies. For C and D DNA was visualised with DAPI staining. Scale bar represents 10 µm.

6.6.2. MCPH1 localisation appears to be independent of CDK1 phosphorylation of PLK1 binding sites

An alternative hypothesis is that PLK1 recruits MCPH1 to the kinetochores. Both PLK1 and MCPH1 localise to the kinetochores with similar dynamics (Figure 6.10).

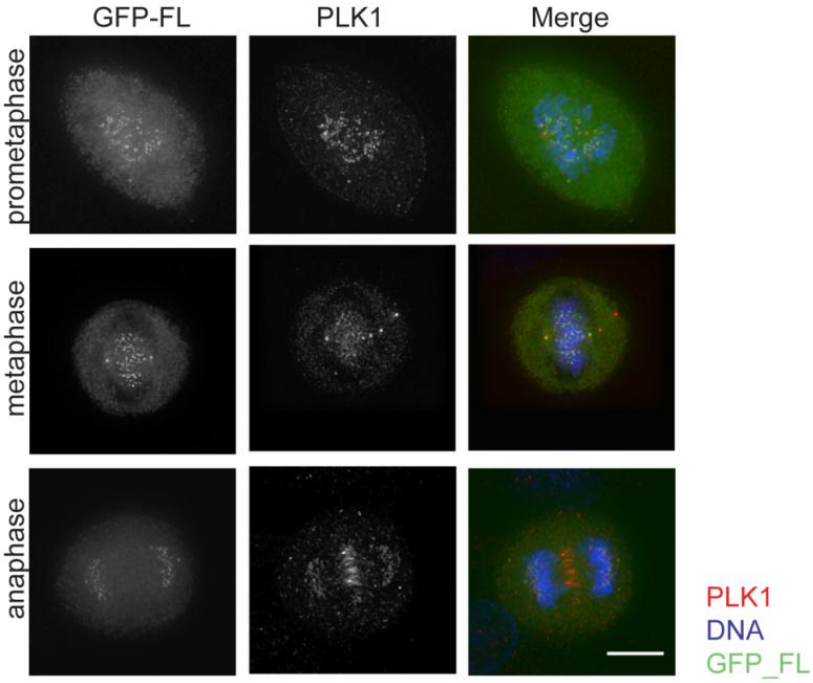

Figure 6.10. MPH1 and PLK1 co-localise at the centrosomes and kinetochores during mitosis.
(A) MPH1 and PLK1 co-localise at the centrosomes and kinetochores during mitosis. HeLa cells transfected with GFP-MCPH1 FL were arrested at G_1/S phase with thymidine, released to progress through the cell cycle and fixed in methanol after 10 hr. Cells were stained with PLK1 (red) antibody and DAPI to visualise DNA. Scale bar represents 10 µm.

PLK1 contains a polo-box domain (PBD) that can interact with a phosphorylated consensus site SpS/T (Elia *et al.*, 2003a; Elia *et al.*, 2003b). This consensus site often overlaps with a CDK1 consensus site, for example, SpS/TP (Elia *et al.*, 2003b), and indeed proteins that bind PLK1 in early and mid-mitosis, such as kinetochore proteins, are often primed by CDK1 (Goto *et al.*, 2006; Qi *et al.*, 2006). MCPH1 contains four PLK1 PBD interaction phosphorylation consensus sequences at CDK1 consensus sites of which two were identified as possible phosphorylated residues by phosphopeptide mapping (Figure 6.11A).

To test whether CDK1 phosphorylation of PLK1 PBD interaction motifs could recruit MCPH1 to kinetochores, GFP-tagged MCPH1(FL) with a series of phosphorylation-dead alanine or phosphorylation-mimetic aspartate mutations in the CDK1 phosphorylation sites (S277A, S287A, S417A, S483A,S769A, quadruple mutant [S277D_S287D_ S417D_ S483D_ S769D]) (Figure 6.11B & C) were constructed. All the CDK1 alanine and aspartate mutants localised to the kinetochores during mitosis with normal dynamics, suggesting that no CDK1 phosphorylation site that could serve as a PLK1 PBD interaction motif was sufficient to target MCPH1 to the kinetochores.

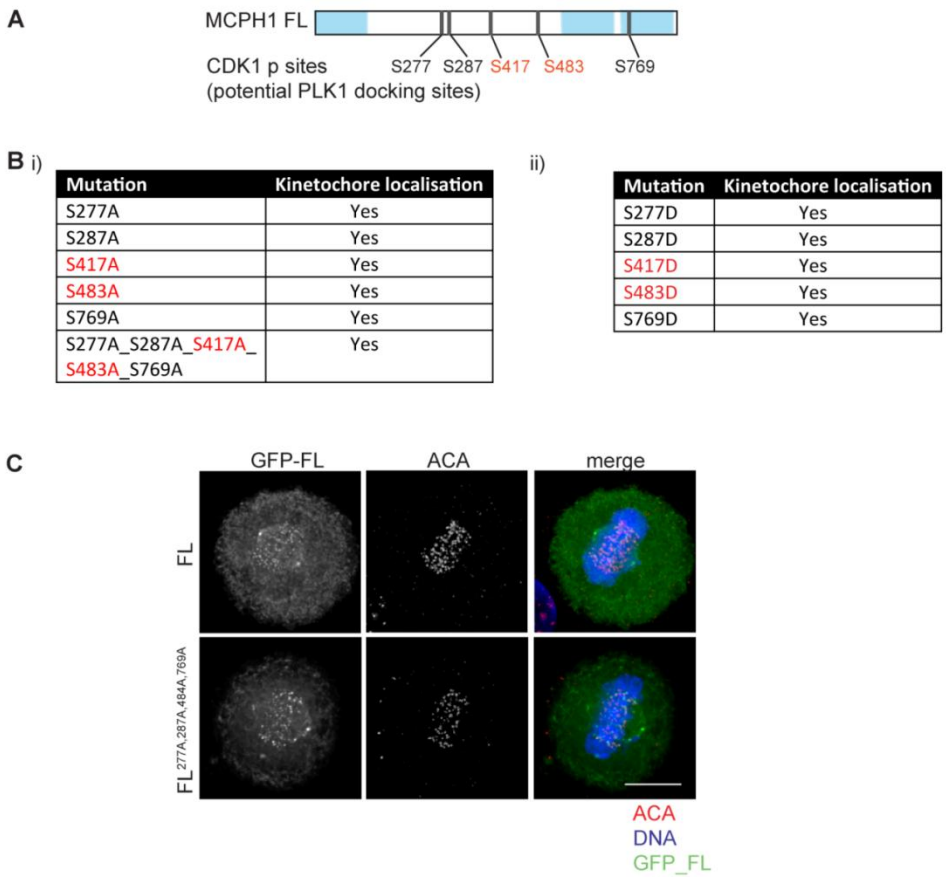

Mutation	Kinetochore localisation
S277A	Yes
S287A	Yes
S417A	Yes
S483A	Yes
S769A	Yes
S277A_S287A_S417A_ S483A_S769A	Yes

Mutation	Kinetochore localisation
S277D	Yes
S287D	Yes
S417D	Yes
S483D	Yes
S769D	Yes

Figure 6.11. MCPH1 kinetochore localisation may be independent of CDK1 phosphorylation.

(A) Schematic of MCPH1 FL protein and locations of consensus CDK1 phosphorylation sites that could act as potential PLK1 docking sites. Sites identified by phosphopeptide mapping were highlighted in red. (B) MCPH1 CDK1 phosphorylation-dead and phosphorylation-mimetic mutants localise to the kinetochores. Table summarising phosphorylation-dead (ii) and phosphorylation mimetic (iii) mutants used. HeLa cells were co-transfected with MCPH1 RNAi oligonucleotides (MCPH1#1) and plasmid expressing GFP-tagged FL with the indicated substitutions. (C) HeLa cells were transfected with plasmids expressing GFP-MCPH1 FL or GFP- FL$^{S277A, S287A, S417A, S483A, S769A}$ were fixed in methanol and stained with ACA antibodies. Image of GFP-FL was also included in Figure 6.9D. DNA was visualised with DAPI staining. Scale bar represents 10 µm.

6.7. Discussion

6.7.1. MCPH1 is proteolytically cleaved by caspases

Protein detection assays shows that a shorter form of MCPH1 FL and Δ8 (FL* and Δ8*) was produced by a post-translational mechanism (Figure 6.1). Several lines of evidence suggested that caspases were responsible for generation of FL* and Δ8*. First, it appeared to be related to activation of apoptosis through either overexpression of MCPH1(Δ8) or by treatment with microtubule destabilising agents (Figure 6.1). Second, cleavage of MCPH1 FL and Δ8 was abolished with a caspase inhibitor (Figure 6.2) and third, mutation of a caspase consensus site (D625) abrogated cleavage (Figure 6.3).

All presented experiments were performed using overexpressed GFP-tagged MCPH1 and it would therefore be worthwhile to establish whether there is physiological caspase-mediated cleavage of endogenous MCPH1. Unfortunately, endogenous NH_2-MCPH1 FL* is indistinguishable from MCPH1(S) with available antibody reagents while endogenous MCPH1(Δ8) is not detectable (Chapter 3). Thus further investigation using the detection of the endogenous COOH-MCPH1 terminal fragment may be the most productive experiment to pursue.

What is the physiological role of caspase-mediated MCPH1 cleavage? In addition to regulation of cell death, caspases have also been implicated in control of the cell cycle (reviewed by Lamkanfi *et al.*, 2007; Los *et al.*, 2001). Many positive and negative regulators of the cell cycle are targeted by non-apoptotic caspase cleavage including Wee1 kinase, $p21^{Waf1}$ and $p27^{Kip1}$ (Alam *et al.*, 1999; Eymin *et al.*, 1999; Frost a *et al.*, 2001; Frost b *et al.*, 2001; Woo *et al.*, 2003) leading to the hypothesis that caspase cleavage could remove proteins that block mitosis and thereby allow cell cycle progression (Levkau *et al.*, 1998; Zhou *et al.*, 1998). MCPH1 is also reported to play a role in cell cycle progression; MCPH1(FL) overexpression leads to G_2/M phase arrest (Andrew Jackson, personal communication) and MCPH1-deficient cells fail to arrest at the G2/M checkpoint following DNA damage (Alderton *et al.*, 2006; Lin *et al.*, 2005). Thus, MCPH1 could be cleaved by caspases in a physiological non-apoptotic, cell cycle-dependent manner. This could account for the concomitant

decreasing levels of endogenous MCPH1(FL) and increasing levels of MCPH1(S) as cells progressed into G_2/M following a double thymidine block (Figure 3.7). Although this hypothesis is still possible, the cell cycle fluctuation of endogenous MCPH1 FL and S protein is independent of caspases suggesting that caspase-mediated cleavage of MCPH1 during the cell cycle is unlikely (Appendix 3).

The alternative possibility is that caspase-mediated cleavage of MCPH1 may function in programmed cell death. Indeed MCPH1 has been implicated in transcriptional regulation of apoptotic factors (Yang *et al.*, 2008). Caspase activation needs to be closely controlled to avoid the inadvertent triggering of programmed cell death. As a result, caspase production, processing, and activity are all tightly regulated (reviewed by Earnshaw *et al.*, 1999). Aberrant transcription of caspases and pro-apoptotic factors can trigger an apoptotic response (Kumar *et al.*, 1997; Tamura *et al.*, 1995; Tamura *et al.*, 1996). The family of transcription factors called E2F, and in particular E2F1, play an important role regulating transcription of pro-apoptotic factors (reviewed by Dimova and Dyson, 2005). Recently, it has been demonstrated that MCPH1 can interact with E2F1 and regulate E2F1 mediated transcription of genes involved in apoptosis such as p73, APAF1, caspase 3 and 7 (Yang *et al.*, 2008).

This suggests that MCPH1 could play an important role in apoptosis but does MCPH1 cleavage have any effect on its function in transcriptional regulation of apoptotic factors? Two protein products would be produced following cleavage, one containing BRCT1 and one containing BRCT2/3. It was demonstrated that the BRCT2/3 domain is required for E2F1 binding and overexpression of this domain showed a dominant negative effect, inhibiting E2F1 mediated apoptosis (Yang *et al.*, 2008). Thus, it is likely that cleavage of MCPH1 would negatively regulate E2F1 mediated transcription of apoptotic factors suggesting that MCPH1 cleavage could be part of a feedback loop to dampen the apoptotic response. Caspase mediated feedback control of the retinoblastoma protein to regulate E2F1 mediated caspase transcription has also been hypothesised (Chau *et al.*, 2002; Guo *et al.*, 2001; Simpson *et al.*, 2001; Tsai *et al.*, 1998).

However it is worth noting that the role of MCPH1 in transcriptional regulation is controversial and in some systems in which MCPH1 is genetically ablated it does not exhibit the same role in transcriptional regulation as reported due to MCPH1 RNAi (Alderton *et al.*, 2006; Gavvovidis *et al.*, 2010; Lin *et al.*, 2005; Trimborn *et al.*, 2010; Xu *et al.*, 2004; Yang *et al.*, 2008). Thus, although this is an interesting hypothesis, establishing the role of MCPH1 in transcriptional regulation of apoptotic factors following genetic ablation would be worthwhile.

6.7.2. Degradation of MCPH1 during mitotic exit

MCPH1 is degraded during mitotic exit and G_1 phase of the cell cycle (Figure 6.4A). The APC/C often targets proteins for degradation at this time of the cell cycle and preliminary evidence is consistent with APC/C playing a role in MCPH1 degradation. The depletion of a subunit of APC/C (APC3) leads to a substantial increase in abundance of MCPH1 FL and S that is not simply explained by changes to cell cycle progression consequent on APC/C inactivation (Figure 6.4B). MCPH1 FL and S proteins may be a substrate of APC/C as both are modified when the proteasome is inhibited *in vivo* and ubiquitin is over-expressed (Figure 6.4C). However, that this modification is ubiquitination needs confirmation to strengthen this conclusion.

APC/C functions with co-activators CDC20 or CDH1, which act at different times of the cell cycle and broaden the range of substrates recognised by the APC/C (Kramer *et al.*, 2000; Visintin *et al.*, 1997). APC/C^{CDC20} recognises substrates containing a destruction (D) box motif (Glotzer *et al.*, 1991; King *et al.*, 1996) whereas APC/C^{CDH1} recognises substrates containing a D box or a KEN box motif (Petersen *et al.*, 2000; Pfleger and Kirschner, 2000). A single KEN box motif is present in MCPH1 protein sequence that may be required for its recognition by APC/C (Figure 6.4D). If the KEN box is functional then CDH1 is likely to function as the APC co-activator. In addition, APC/C^{CDH1} functions later in mitosis than APC/C^{CDC20} usually from anaphase through to G_1 phase mitosis (Pines, 2006) which is consistent with the timings of MCPH1 degradation (Figure 6.4A).

To build on this hypothesis it would be helpful to show that the KEN box is functional and that it is APC/C^{CDH1} that targets MCPH1 for proteolysis. Demonstrating the KEN box is functional has been difficult, probably due to the consequences of MCPH1 overexpression, which inhibits cell cycle progression (Andrew Jackson, personal communication). One way to circumvent this problem may be to look at MCPH1 levels when CDC20 or CDH1 is overexpressed. Overexpression of CDC20 or CDH1 has been reported not to affect cell cycle progression (Donzelli *et al.*, 2002) and MCPH1 levels could then be analysed during interphase.

Ubiquitin ligases such as members of the SKP/cullin/F-box (SCF) family can also have important roles in controlling protein abundance during the cell cycle (reviewed by Ang and Wade Harper, 2005; Cardozo and Pagano, 2004). In contrast to APC/C which functions primarily during mitosis and G_1 phase, SCF complexes function throughout the cell cycle. Thus SCF could additionally contribute to MCPH1 isoform degradation during G_1/S and G_2/M when MCPH1 FL and S protein levels also fluctuated (Figure 3.8). SCF recognizes a phosphorylated domain (phosphodegron) on the substrate and it is the timing of substrate phosphorylation that alters degradation (reviewed by Harper, 2002). All MCPH1 isoforms possess a SCF-FBW7 phosphodegron ^{162} TPxxE^{166} (Elm motif prediction) and although Tyr 162 was not identified as a phosphorylated residue in the phosphopeptide mapping screen it could be cell cycle stage dependent and so may only be apparent by enriching for different cell cycle stages.

What is the purpose of degrading MCPH1 during late mitosis and G_1 phase? Unfortunately the answer to this question remains elusive. There are a very large number of proteins targeted for degradation during different stages of mitosis (Pines, 2006). These include the cyclins, such as cyclin-B1, which must be degraded to inactivate CDK1 and allow the cell to progress from anaphase (Sigrist *et al.*, 1995; Wheatley *et al.*, 1997). Mitotic kinases, such as polo kinase 1 and aurora A, are targeted for degradation (Castro *et al.*, 2002; Lindon and Pines, 2004; Littlepage and Ruderman, 2002; Shirayama *et al.*, 1998).The group also includes structural components of mitosis such as components of mitotic spindle, kinetochores or

chromosome condensation factors, which must be disassembled to allow the cell to return to interphase. MCPH1 degradation at the end of mitosis may ensure efficiency of cell cycle progression for a number of reasons. First, it is a component of the kinetochore, which is disassembled after mitosis. Indeed, MCPH1 kinetochore staining is significantly reduced during late anaphase (Figure 4.6A) which may be important step in disassembling the kinetochore. Second, it is a component of the centrosome which undergoes a number of morphological changes during mitosis and mitotic exit, such as centriole disengagement (Kuriyama and Borisy, 1981; Tsou and Stearns, 2006) and reduction in PCM levels (Khodjakov and Rieder, 1999). Third, MCPH1 plays a role in the regulation of the cell cycle timing (Alderton *et al.*, 2006; Tibelius *et al.*, 2009; Trimborn *et al.*, 2004) and so it is also possible that its degradation may be required to alter cell signalling pathways to facilitate mitotic exit.

6.7.3. Phosphorylation of MCPH1 during mitosis

MCPH1is also phosphorylated during mitosis. MCPH1 from nocodazole arrested cells showed a reduced mobility in SDS-PAGE gels compared to asynchronous cells. This shifted form was lost by treating the extracts from mitotic cells with λ-phosphatase (Figure 6.5). I confirmed two integral mitotic kinases, CDK1 and PLK1, contribute to MCPH1 mitotic phosphorylation *in vivo* (Figure 6.7 & 6.8). This is consistent with phosphopeptide mapping studies of GFP-MCPH1(S) that identified phosphorylated residues in a number of consensus CDK1 and PLK1 consensus sites (Figure 6.6). Although the phosphopeptide mapping studies were of overexpressed human MCPH1(S) in chicken DT40 cells, this system can identify phosphorylations relevant to a mammalian system. Indeed three of the hits (Ser333, Ser335, Ser548) had already been identified as MCPH1 phosphorylation sites in large scale proteomics screens (Chen *et al.*, 2009; Dephoure *et al.*, 2008; Olsen *et al.*, 2010). Thus, although each site could not be confirmed *in vivo*, due to the large number of phosphorylation sites, it is likely that at least some of these phospho sites are relevant to a mammalian system.

What is the functional role of MCPH1 phosphorylation? Protein phosphorylation usually affects the stability, localisation or interactions of a protein. It is very

possible that phosphorylation could affect all of these aspects of MCPH1 function. This thesis has established that MCPH1 is targeted for degradation during the cell cycle (Figures 3.5 & 6.4). MCPH1 stability could be regulated by phosphorylation but because of the biological consequences associated with overexpression of MCPH1 this has not been pursued further (Figure 5.2 D). Currently, no interactions between MCPH1 and mitotic proteins have been established therefore the effect of phosphorylation on MCPH1 interactions has also not been examined. Here, the role of phosphorylation in MCPH1 localisation was characterised; in particular candidate PLK1 and CDK1 phosphorylation sites were under investigation.

GFP-MCPH1(FL) localisation is not affected when candidate CDK1 and PLK1 phosphorylation residues are mutated to either phosphorylation dead or phosphorylation mimetic form (Figures 6.9 & 6.10). All mutated forms of GFP-MCPH1(FL) localised to the kinetochores even when endogenous MCPH1 isoforms were depleted. However this research requires further investigation; MCPH1 is hyperphosphorylated, possibly containing as many as 12 phosphorylation sites, so it is difficult to validate these sites and to establish whether one or a particular combination is required. Thus it is entirely conceivable that phosphorylation does affect localisation since all the phosphorylation sites have not yet been systematically mutated and imaged.

The majority of the CDK1 and PLK1 sites appear to be located in the poorly conserved inter-BRCT space (NB domain) of MCPH1 (Appendix 4). All residues identified by phosphopeptide mapping were located within the NB domain (Figure 6.6) and the NB domain was indeed phosphorylated *in vitro* CDK1 phosphorylation assays (Figure 6.7). The BRCT2/3 domains were not represented in the phosphopeptide mapping but it is unlikely these domains contain many phosphorylation sites as the phosphorylation of BRCT domains have not been widely reported in the literature. Indeed most reported phosphorylation sites in BRCA1, PARP1, XRCC1 and MDC1 (identified using the phosphosite plus database) are not located within BRCT domains .Thus, phosphorylation may be poorly tolerated in the BRCT domains, possibly due to potential disruption to protein interaction surfaces (Glover *et al.*, 2004).

MCPH1(Δ8) lacks most of the NB domain and phosphorylation sites of MCPH1 FL and S which could present a key difference in regulation between the MCPH1 isoforms. Interestingly, there are some differences in the dynamics of MCPH1(FL) and MCPH1(Δ8) localisation that may be accounted for by phosphorylation(s) because although both proteins have the capacity to localise to the kinetochores during mitosis, MCPH1(Δ8) also associates with chromatin during metaphase whereas MCPH1(FL) chromatin localisation is delayed until anaphase (Figure 4.5 & 4.6). It is possible that phosphorylation (s) in the NB domain during metaphase could be required to target MCPH1 to and from the chromatin. However, before the differences between MCPH1(FL) and MCPH1(Δ8) localisation can be fully interpreted, it needs to be confirmed that MCPH1(Δ8) can localise to the kinetochores independently of MCPH1(FL) as it has been established that BRCT2/3 domains can dimerise (Yang *et al.*, 2008). This could be tested by expressing GFP-MCPH1(Δ8) in *MCPH1*$^{-/-}$ cells or by depleting endogenous protein by RNAi. If GFP-MCPH1(Δ8) can indeed localise to the kinetochores independently of endogenous MCPH1 isoforms then this would be very informative in identifying sites relevant to kinetochore localisation as only residues T120, S191,T193,S194 and S195 are present in this isoform.

Instead of phosphorylation of MCPH1 being important for its localisation, an alternative explanation for cell cycle regulated MCPH1(FL) localisation is that MCPH1 recognises phosphorylation marks on kinetochore proteins that allow it to be recruited. This would not be surprising as many tandem BRCT domains are established to be phospho protein binding modules (Manke *et al.*, 2003; Yu *et al.*, 2003). This could be tested by investigating MCPH1 localisation in nocodazole arrested cells following treatment with kinase inhibitors to CDK1, PLK1 and aurora B.

It is likely that at least some of the identified MCPH1 phosphorylation sites have a functional consequence. The mitotic function of MCPH1 was investigated in Chapter 5 and an obvious extension of this work would be to investigate whether phosphorylation could play a role in MCPH1 kinetochore function. It is interesting to note that many of the primary microcephaly proteins are phosphorylated during

mitosis including ASPM, CDK5RAP2 and CPAP, and often on CDK1 and PLK1 consensus sites (Malik *et al.*, 2009; Nousiainen *et al.*, 2006; Santamaria *et al.*, 2011). Indeed in *Drosophila* it has been demonstrated that polo (PLK1 *Drosophila* orthologue) phosphorylation of Cnn (CDK5RAP2 orthologue) or Asp (ASPM orthologue) is required for their roles in centrosome maturation (Dobbelaere *et al.*, 2008) and microtubule nucleation respectively (do Carmo Avides *et al.*, 2001). Thus, phosphorylation is a shared mechanism of regulation between many of the primary microcephaly proteins.

Chapter 7. Discussion

7.1. Summary of the main findings from this thesis

In Chapter 3, I characterise three isoforms of MCPH1generated from the alternative splicing of intron 8 and exon 8 called MCPH1(FL), MCPH1(S) and MCPH1(Δ8). All three isoforms are expressed in human fetal brain and may therefore contribute to MCPH1 function during neurogenesis.

The MCPH1 protein isoforms differ significantly in domain structure. MCPH1(S) lacks tandem BRCT domains which likely act as a phosphopeptide binding module and MCPH1(Δ8) lacks most of the inter-BRCT domain space. Indeed there are significant differences in localisation between the isoforms. MCPH1(Δ8), lacking a strong NLS, localised to the cytoplasm and centrosome during interphase, whereas MCPH1(FL) and MCPH1(S) localised to the nucleus. During mitosis both MCPH1(FL) and MCPH1(Δ8) localise temporally to the centrosome and kinetochores, whereas MCPH1(S) is diffusely localised throughout the cell.

Consistent with MCPH1 kinetochore localisation, MCPH1 is required for normal chromosome alignment. Depletion of MCPH1 by RNAi or MCPH1 deletion in MEFs leads to the formation of a metaphase plate with grossly misaligned chromosomes. Centrosome maturation appeared to occur normally in primary microcephaly patient-derived LBC lacking MCPH1, and although multipolar spindles were observed following RNAi-mediated depletion this appeared to be secondary to chromosome misalignment.

Reinforcing the importance of the mitotic role of MCPH1, the protein is also subject to a number of post-translational modifications during this time. MCPH1 is hyper-phosphorylated during mitosis with two key mitotic kinases, PLK1 and CDK1, contributing to this phosphorylation. It is also degraded as cells exit mitosis, likely targeted by the APC/C. These modifications may play a role in the temporal kinetochore localisation of MCPH1 and/or contribute to MCPH1 functional regulation.

7.1.1. Model of the functional role of MCPH1 at mitosis

At mitosis MCPH1 appears to play a role in chromosome condensation, kinetochore and possibly centrosome function. MCPH1 contains BRCT domains which act as protein and phosphoprotein binding modules and so we hypothesise that MCPH1 can function in these mitotic processes by acting as an assembly platform (Figure 7.1).

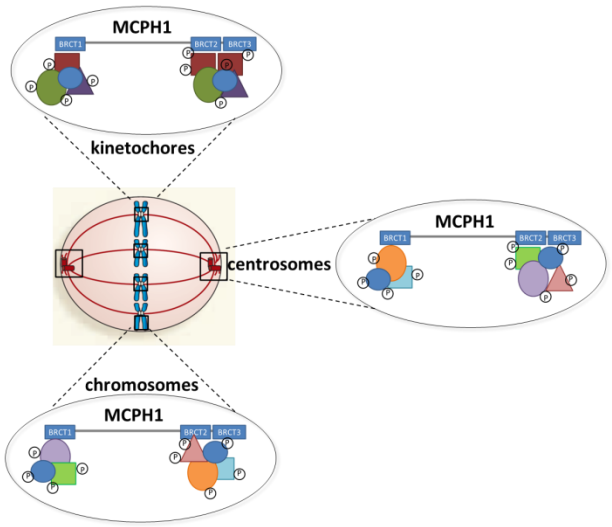

Figure 7.1. Model of MCPH1 function in mitosis
MCPH1 can act as a protein assembly platform to coordinate signal transduction pathways at various locations during mitosis.

7.2. Are the primary microcephaly proteins in a shared pathway?

It has been hypothesised that a single pathway shared by the primary microcephaly proteins can lead to microcephaly (Cox *et al.*, 2006). Given that all of the primary microcephaly proteins localise to the centrosome (Bond *et al.*, 2005; Cizmecioglu *et al.*, 2010; Hatch *et al.*, 2010; Hung *et al.*, 2000; Nicholas *et al.*, 2010; Pfaff *et al.*, 2007; Zhong *et al.*, 2005), such a common pathway may well act at the centrosome. In the introduction of this thesis, potential mechanisms that could affect brain size

during development, all of which could be linked to centrosome function, were discussed. These included cilia formation, spindle orientation and DNA segregation which can influence neuronal progenitor cell fate choice or cell survival.

7.2.1. Cilia function

The primary cilium is a key signal transducer that plays an important role in regulating cell cycle length and neural progenitor cell fate (Kim *et al.*, 2011; Li *et al.*, 2011). The mother centriole acts as a template for the primary cilia (Sorokin, 1962) and therefore centriolar defects can often impact on cilia formation or functioning (Basto *et al.*, 2006; Graser *et al.*, 2007a). Many of the primary microcephaly proteins are required for normal cilia function. For instance, the extra centrioles observed in *Cdk5rap2*$^{-/-}$ MEFs form additional primary cilia per cell (Barrera *et al.*, 2010). The presence of such extra primary cilia has been reported to reduce sonic hedgehog signalling (Megraw *et al.*, 2011) which is a key developmental determinant in neurogenesis (reviewed by Louvi and Grove, 2011). In contrast, *Drosophila dsas4* (CPAP) and *asl* (CEP152) mutants that cannot duplicate their centrioles consequently lack cilia. As adult flies they present with phenotypes characteristic of cilia defects such as uncoordinated movement (due to loss of mechanosensory function in neurons) and immotile sperm (Basto *et al.*, 2006; Blachon *et al.*, 2008). The phenotype of *Stil* mouse knockout is also consistent with cilia dysfunction; embryos present with defects in sonic hedgehog signalling, which cause a failure in left-right specification and neural tube defects (Izraeli *et al.*, 2001; Izraeli *et al.*, 1999). However primary microcephaly patients do not present with phenotypes characteristic of cilia defects (termed ciliopathies) (Cardenas-Rodriguez and Badano, 2009; Fliegauf *et al.*, 2007; Woods *et al.*, 2005) suggesting that there is some distinction in humans.

MCPH1(Δ8) does localise to the centrosome during interphase and so it is possible that through interphase centrosome function, MCPH1 could contribute to cilia formation and function. This possibility could be tested in *Mcph1*$^{-/-}$ MEFs or *MCPH1* patient derived primary fibroblast cells (*MCPH1*$^{\Delta 1\text{-}8}$ cells are available in the lab) in which primary cilliation can be induced by serum starvation (Tucker *et al.*, 1979). *Drosophila mcph1* mutants do not present with ciliopathies (Brunk *et al.*, 2007;

Rickmyre *et al.*, 2007). However, *Mcph1*$^{-/-}$ mice do present with a moderate hearing impairment (http://www.sanger.ac.uk/mouseportal/search?query=MGI:2443308) which can be associated with cilia dysfunction (Fliegauf *et al.*, 2007). However, not all primary microcephaly proteins localise to the interphase centrosome, with ASPM and WDR62 only localising at mitosis, therefore inconsistent with a function in ciliogenesis (Higgins *et al.*, 2010; Nicholas *et al.*, 2010).

7.2.2. Spindle orientation

Centrosomal defects may perturb mitotic spindle orientation in neuronal progenitor cells correlating with changes in cell fate choice (Fish *et al.*, 2006; Lizarraga *et al.*, 2010). Indeed some of the primary microcephaly proteins are required for normal spindle pole orientation in such cells. For instance, *Drosophila asl* (CEP152), *dSas4* (CPAP) and *cnn* (CDK5RAP2) mutants exhibit abnormal spindle pole positioning in asymmetric divisions of larval neuroblast cells (Basto *et al.*, 2006; Blachon *et al.*, 2008; Giansanti *et al.*, 2001; Lucas and Raff, 2007). Furthermore in mice, mutation of *Cdk5rap2* or RNAi-depletion of Aspm leads to abnormal spindle pole orientation in the neuronal progenitor population in embryos, correlating with a decrease in the progenitor population and increase in neuronal population (Fish *et al.*, 2008; Fish *et al.*, 2006; Lizarraga *et al.*, 2010).

MCPH1 isoforms can localise to the centrosome at all stages of the cell cycle (Chapter 4) and centrosome defects were observed during RNAi-mediated MCPH1 depletion, resulting in formation of multipolar spindles (Section 5.1). However, centrosomal phenotypes which could be associated with abnormal spindle orientation (such as defects in PCM recruitment and spindle pole focussing) were absent in MCPH1 patient LBC (Section 5.2). In addition, normal spindle positioning was reported in *mcph1 Drosophila* mutant larval neuroblasts (Brunk *et al.*, 2007). Thus, it is unclear if loss of MCPH1 could impact on spindle pole orientation in patient neuronal progenitor cells and analysis in this system is essential to address this possibility (discussed in Section 7.4).

7.2.3. Chromosome segregation and apoptosis

From the work described in this thesis, the primary function of MCPH1 during mitosis appears to be to ensure chromosome alignment and timely metaphase progression (Sections 5.1 & 5.2) and it is likely that this function is related to MCPH1 kinetochore localisation (Chapter 4). The other primary microcephaly proteins have not been reported to localise to the kinetochore nor are they implicated in kinetochore function. However, a role at the kinetochore remains a possibility. For example, CDK5RAP2 localises to the plus-end of microtubules in interphase cells, mediated through an interaction with EB1 and this localisation could be maintained during mitosis (Fong *et al.*, 2009).

Although the primary mitotic function of MCPH1 appears to be distinct from other primary microcephaly proteins, they could still have the same cellular consequences. The fate of cells following depletion of MCPH1 has not yet been established. MCPH1-RNAi cells in prolonged metaphase may well undergo apoptosis as depletion of astrin leads to a very similar phenotype that terminates with apoptosis (Thein *et al.*, 2007). Genetic ablation of MCPH1 leads to a significantly less severe phenotype than RNAi (Chapter 5) and may result in delayed progression through metaphase and chromosome missegregation rather than apoptosis. Indeed, *Mcph1*$^{-/-}$ mice exhibit increased micronuclei (www.sanger.ac.uk/mouseportal/search/MGI:2443308) which can arise due to chromosome segregation errors during mitosis (Rao *et al.*, 2008). Although this could equally be related to the role of MCPH1 in HR and NHEJ (Liang *et al.*, 2010; Peng *et al.*, 2009; Wood *et al.*, 2008).

Perturbed centrosome function is also linked to chromosome missegregation (Ganem *et al.*, 2009). Thus it is possible that through centrosome dysfunction many of the primary microcephaly proteins could also be associated with errors in chromosome segregation (Figure 7.2). Indeed there are reports of chromosome missegregation due to loss of primary microcephaly proteins. For example, RNAi-mediated depletion of *aspm-1* in *C. elegans* or *asp* mutant *Drosophila* exhibit defects in chromosome segregation during meiosis (Casal *et al.*, 1990; van der Voet *et al.*, 2009). In *Drosophila*, *asl* (CEP152) mutants have evidence of chromosome segregation

defects in spermatocytes during male meiosis (Bonaccorsi *et al.*, 1998) and in neuroblasts (Giansanti *et al.*, 2001). A high level of chromosomal aneuploidy was also reported in primary cultures from cells derived from mice with a truncating *Cdk5rap2* mutation (Eppig and Barker, 1984; Lizarraga *et al.*, 2010). Misaligned chromosomes were also apparent in *Cdk5rap2*$^{-/-}$ MEFs and due to RNAi-mediated CDK5RAP2 and CPAP depletion in cells (Barrera *et al.*, 2010; Cho *et al.*, 2006; Zhang *et al.*, 2009).

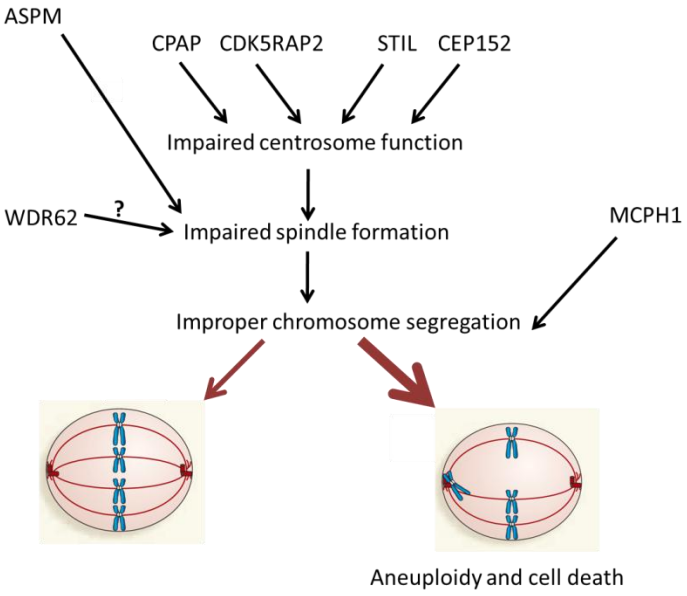

Figure 7.2. Primary microcephaly proteins are required for accurate chromosome segregation.
Schematic showing that the primary microcephaly proteins could potentially share a role in ensuring accurate chromosome segregation during neuronal progenitor cell divisions. CPAP, CDK5RAP2, STIL and CEP152 all play key roles at the centrosome. ASPM is required for spindle microtubule nucleation and focussing during mitosis. MCPH1 is required for chromosome alignment. Disruption of any of these functions could lead to chromosome segregation errors and aneuploidy. (Figure adapted from Pellman, 2007).

In rodents and humans, a surprising number of cerebral cortical neurons are aneuploid arising due to defects in chromosome segregation (Kaushal *et al.*, 2003; McConnell *et al.*, 2004; Rehen *et al.*, 2001; Rehen *et al.*, 2005; Yang *et al.*, 2003).

Absence of any of the primary microcephaly proteins may reduce the fidelity of chromosome segregation causing a higher incidence of chromosome aneuploidy that could decrease cell survival (Torres *et al.*, 2008; Weaver *et al.*, 2007), resulting in a decrease in neuronal cell number and therefore reduction in brain size.

7.3. Summary

In summary, during this thesis I have shown MCPH1 plays an important role in metaphase progression and chromosome alignment. It is likely MCPH1 performs this function at the kinetochore where it localises throughout mitosis. MCPH1 is highly regulated during mitosis, hyper-phosphorylated and targeted for degradation at mitotic exit, reinforcing the importance of this protein during the cell cycle.

7.4. Future work

7.4.1. MCPH1 isoform function

A key unresolved question is what the different functions of MCPH1 isoforms are. Differences in localisation, regulation and post-translational modification of the isoforms clearly suggest there is some separation of function. MCPH1 isoforms may potentially act separately in homologous recombination (Liang *et al.*, 2010; Peng *et al.*, 2009; Wood *et al.*, 2008), interphase centrosome function (Tibelius *et al.*, 2009), chromosome condensation (Trimborn *et al.*, 2010), kinetochore function and timely progression through metaphase (Chapters 4 & 5). The tools are available to knockdown specific MCPH1 isoforms by RNAi (Section 3.4) or knockdown all the isoforms and rescue by expressing individual RNAi-resistant isoforms (Section 5.1). One area of particular interest would be to determine if MCPH1 FL and Δ8 play differing roles in mitosis, particularly at the kinetochore. Currently it is unclear if MCPH1(Δ8) localises to the kinetochores independently of MCPH1(FL). If it does then one of the key differences between these isoforms is the inter-BRCT space which is phosphorylated during mitosis (Sections 6.4 and 6.5). Functional differences between the two isoforms at the kinetochore could therefore be due to differences in the proteins phosphorylation status.

7.4.2. The role of MCPH1 at the kinetochores

Of particular interest is MCPH1 role at the kinetochores, which could well be a major role of MCPH1 during mitosis. The work in this thesis is consistent with a role for MCPH1 in kMT attachment and/or silencing of the SAC. First it is important to establish if the prolonged time spent in metaphase in the MCPH1-RNAi cells is due to activation of SAC. This possibility could be confirmed by immunofluorescence with BUBR1, MAD2 and BUB1 antibodies (Hoffman *et al.*, 2001). If SAC is active in MCPH1-deficient cells then the stability of kMT attachments could be tested by cold temperature assays (Brinkley and Cartwright, 1975).

Once this is established the key issue is how MCPH1 participates in these processes. We hypothesise that MCPH1 can act as an assembly platform in signal transduction pathways (Section 7.1.1). Thus, identification of MCPH1 interactants during mitosis may provide significant insight into the pathways that MCPH1 is acting in. To identify MCPH1 interactants two different strategies could be undertaken. Firstly, a hypothesis independent approach to identify all proteins associated with MCPH1 during mitosis. For example, purification of epitope-tagged MCPH1 during mitosis followed by mass spectrometry to identify MCPH1 associated proteins. This strategy has been very productive in the identification of MCPH1 interactants in chromosome condensation and chromatin remodelling (Leung *et al.*, 2011; Peng *et al.*, 2009; Wood *et al.*, 2008) and could be utilised to specifically investigate mitosis. Alternatively, a hypothesis driven approach could be undertaken. Depletion of astrin, SKA1-3 complex or SKAP proteins have very similar phenotypes to MCPH1-RNAi (Daum *et al.*, 2009; Dunsch *et al.*, 2011; Fang *et al.*, 2009; Gaitanos *et al.*, 2009; Hanisch *et al.*, 2006; Thein *et al.*, 2007; Theis *et al.*, 2009; Welburn *et al.*, 2009) and so using a targeted approach to determine if these proteins interact with MCPH1 may also be worthwhile.

7.4.3. MCPH1 function in neuronal progenitor cells

Lastly it remains to be determined if the function of MCPH1 during mitosis is relevant to primary microcephaly pathogenesis or is it another, possibly non-mitotic role that leads to disease? The former is strongly suggested by other primary microcephaly protein functions. Thus it is important to study the impact of MCPH1 loss in neuronal progenitor cells and the effect it has on metaphase progression, spindle orientation and chromosome segregation, as well as cell fate choice and cell survival. A number of systems are available to study MCPH1 in neural progenitors including *Drosophila*, rodents and humans.

7.4.3.1. Human neuronal progenitor cells as models of primary microcephaly

There are significant differences in the development of the brain in humans, rodents and *Drosophila* (reviewed by Fish *et al.*, 2008) and notably many primary microcephaly models in *Drosophila* and mouse do not demonstrate microcephaly (Barrera *et al.*, 2010; Basto *et al.*, 2006; Dzhindzhev *et al.*, 2010; Lucas and Raff, 2007). Humans have a much larger brain comprising of many more neurons than rodents and *Drosophila*, neuron number is estimated at 10^{11}, 10^{7}, 10^{4}, respectively (Braitenberg, 2001; Scott *et al.*, 2001). Thus more subtle defects in progenitor divisions are likely to only become apparent in humans. In addition, many of the primary microcephaly genes have undergone adaptive evolution (Evans a *et al.*, 2004; Evans b *et al.*, 2004; Evans *et al.*, 2006; Wang and Su, 2004) and so they may have evolved new functions only apparent in primates. For example, EB1 binding is a function that appears to have evolved in CDK5RAP2 with the EB1 binding domain absent in rodents but present in primates (Fong *et al.*, 2009).

Thus, functional studies of the primary microcephaly proteins in human neuronal stem and progenitor cells could provide important insightS. There are a number of *in vitro* systems that could be utilised for this purpose. One possibility would be to create immortalised human neural stem cell lines that stably express MCPH1 shRNA (Carlessi *et al.*, 2009; De Filippis *et al.*, 2007). These cells could then be

differentiated into neural progenitor cells and multiple neuronal lineages enabling the role of MCPH1 in mitosis and cell fate choice to be analysed (Figure 7.3).

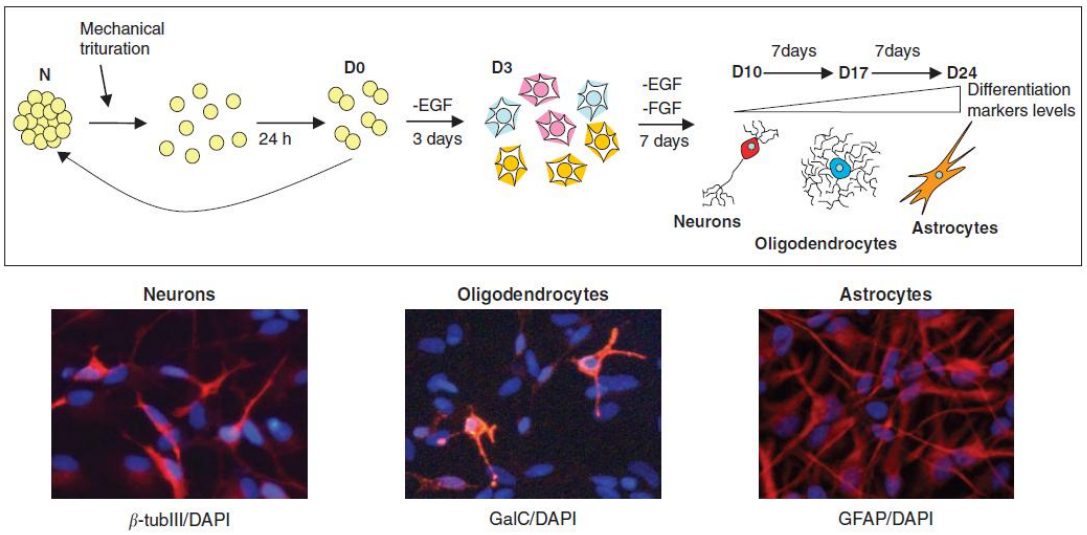

Figure 7.3. Differentiation of immortalised human neural stem cells.
The schematic illustrates the process required to maintain and then differentiate immortalised human neuronal stem cells into neural progenitors and neuronal cell types such as neurons, oligodendrocytes and astrocytes. (Figure reproduced from Carlessi *et al.*, 2009).

Alternatively induced pluripotent stem cells (iPS) could be utilised (reviewed by Yamanaka, 2009). iPS cells are created by transcriptionally reprogramming somatic differentiated cells (Takahashi and Yamanaka, 2006). Recently disease-specific somatic cells isolated from patients have been reprogrammed into iPS cells. These cells can be maintained as neural stem cells and differentiated into multiple neuronal lineages (Dimos *et al.*, 2008; Joannides *et al.*, 2007) enabling disease pathogenesis to be directly studied (Figure 7.4). This technique has been used to develop disease models such as muscular atrophy (Ebert *et al.*, 2009), amyotrophic lateral sclerosis (Dimos *et al.*, 2008) and a variety of genetic diseases such as Huntington, Parkinson disease and schizophrenia (Brennand *et al.*, 2011; Park *et al.*, 2008). Primary microcephaly patient cells with MCPH1 mutations are available and so this technique is possible.

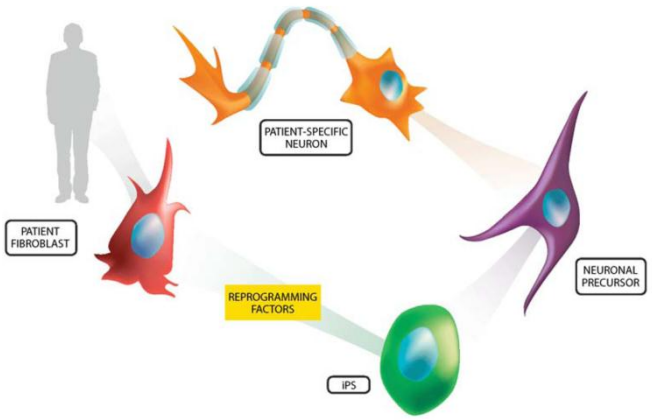

Figure 7.4. Generation and differentiation of iPS cells.
The schematic depicts the process of generating iPS cells from patient fibroblast cells and then differentiating the iPS cells into neuronal precursor cells and neurons which are genetically identical to the patient. (Figure reproduced from Chamberlain *et al.*, 2008).

7.4.3.2. MCPH1 function in neuronal progenitor cells in *Drosophila* and rodents

One limitation of studies in human neuronal progenitor cells is that it is a cellular system and so neuronal progenitor cells would not be studied in a developmental context. In this regard, *Drosophila* and rodents may be useful. Many of the regulatory mechanisms controlling neuronal progenitor divisions and specification of cell fate choice are conserved between humans, *Drosophila* and rodents (reviewed by Brand and Livesey, 2011), suggesting that such systems could provide substantial insight. Indeed the asymmetric divisions of neuroblasts in *Drosophila* larval brain are very well characterised by high resolution live-cell imaging with many of the components influencing these processes being conserved in metazoans (reviewed by Gonczy, 2008; Knoblich, 2010; Lesage *et al.*, 2010). Rodents can also provide a good system to investigate the role of MCPH1 in a developmental context. The neuroepithelium of mouse embryo brain can be analysed by immunofluorescence following genetic ablation or RNAi-mediated knockdown delivered into embryonic brain (Calegari *et al.*, 2002). Both strategies can be successful in investigating spindle orientation, cell fate choice and cell death (Buchman *et al.*, 2010; Fish *et al.*, 2008; Fish *et al.*, 2006; Lizarraga *et al.*, 2010). Thus to fully investigate MCPH1 regulation of brain size, a number of different systems should be utilised to study it in the most relevant cell type but also in a developmental context.

Appendices

Appendix 1. Oligonucleotides

(a) Site-directed mutagenesis

Oligo Name	Sequence	Description
T267G_A269G_F	GGACAGCTGGAGCACACATTGATG AAGCGTTGTTCCCTGCAGCT	Forward primer can be used to introduce T267G and A269G mutation in MCPH1 open reading frame (ORF)
T267G_A269G_R	AGCTGCAGGGAACAACGCTTCATCA ATGTGTGCTCCAGCTGTCC	Reverse primer can be used to introduce T267G and A269G mutation
A360G_F	CGTAAATGTATGCAGCCCAAAGATT TTAA	Forward primer can be used to introduce A360G mutation in MCPH1
A360G_R	CTCTTATCATTTTCTGGTGCTTTAAA ATT	Reverse primer can be used to introduce A360G mutation in MCPH1
A360G _F	TGAAGGAGAAAAGGGAAAATCTTG CCCCCACCTCTT	Forward primer can be used to introduce T573G mutation in MCPH1
T573G_R	AAGAGGTGGGGGCAAGATTTTCCC TTTTCTCCTTCA	Reverse primer can be used to introduce T573G mutation in MCPH1
T762G_F	GAAATCAGGAAAGGAAGTTGGAAG GAGCCATTAATGACATTAAAAG	Forward primer can be used to introduce T762G mutation in MCPH1
T762G_R	CTTTTAATGTCATTAATGGCTCCTTC CAACTTCCTTTCCTGATTTC	Reverse primer can be used to introduce T762G mutation in MCPH1
T831G_F	ATTGAAAGCAAATAATATTCATTCA GCACCATCTTTCACTCACCTCG	Forward primer can be used to introduce T831G mutation in MCPH1
T831_G_R	CGAGGTGAGTGAAAGATGGTGCTG AATGAATATTATTTGCTTTCAAT	Reverse primer can be used to introduce T831G mutation in MCPH1
A861G_G862C_F	ACCATCTTTCACTCACCTCGATAAAT CAGCTCCTCAGAAATTTCTG	Forward primer can be used to introduce A861G and G862C mutation
A861G_G862C_R	CAGAAATTTCTGAGGAGCTGATTTA TCGAGGTGAGTGAAAGATGGT	Reverse primer can be used to introduce A861G and G862C mutation
T999G_F	GAGTATCACATGGCTCCCATGCACC TCCGAAG	Forward primer can be used to introduce T999G mutation in MCPH1
T999G_R	CTTCGGAGGTGCATGGGAGCCATG TGATACTC	Reverse primer can be used to introduce T999G mutation in MCPH1
T1095G_F	GAGTATCACATGGCTCCCATGCACC TCCGAAG	Forward primer can be used to introduce T1095G mutation in MCPH1
T1095G_R	CTTCGGAGGTGCATGGGAGCCATG TGATACTC	Reverse primer can be used to introduce T1095Gmutation in MCPH1
T1251G_F	GTGGGGAGTCTTCATATGATGACTA TTTTGCACCTGATAATCTTAAG	Forward primer can be used to introduce T1251G mutation in MCPH1
T1251G_R	CTTAAGATTATCAGGTGCAAAAT AGTCATCATATGAAGACTCCCCA	Reverse primer can be used to introduce T1251G mutation in

Oligo Name	Sequence	Description
A1752G_G1753C_R	GCTTCTTTCATTTCTTCAAGGGCTCCTTCCAAAGGAGTTAAATCATC	Forward primer used to induce A172G and G1753C mutations in to MCPH1 ORF
A1752G_G1753C_F	GATGATTTAACTCCTTTGGAAGGAGCCCTTGAAGAAATGAAAGAAGC	Reverse primer can be used to introduce A1752G and G1753C mutations in MCPH1 ORF
A2307G_G2308C_F	TCGCCTGCCAGCGCCCCCCCAGTGGC	Forward primer can be used to introduce A2307G and A2308C mutations in MCPH1 ORF
A2307G_G2308C_R	GCCACTGGGGGGGCGCTGGCAGGCGA	Reverse primer can be used to introduce A2307G and G2308C mutation in MCPH1 ORF
T267G_C268A_A269T_F	GGACAGCTGGAGCACACATTGATGAAGATTTGTTCCCTGCAGCT	Forward primer can be used to introduce T267G, C268Aand A269T mutations in MCPH1 ORF
T267G_C268A_A269T_R	AGCTGCAGGGAACAAATCTTCATCAATGTGTGCTCCAGCTGTCC	Reverse primer can be used to introduce T267G, C268A and A269T mutations in MCPH1 ORF
A360G_C361A_A362T_F	GAAATCAGGAAAGGAAGTTGGAAGGAGCCATTAATGACATTAAAAG	Forward primer can be used to introduce A360G, C361Aand A362T mutation in MCPH1 ORF
A360G_C361A_A362T_F	CTTTTAATGTCATTAATGGCTCCTTCCAACTTCCTTTCCTGATTTC	Reverse primer can be used to introduce A360G, C361A and A362T mutations in MCPH1 ORF
T573G_C574A_F	ATTGAAAGCAAATAATATTCATTCAGCACCATCTTTCACTCACCTCG	Forward primer can be used to introduce T573G and C574A mutations in MCPH1 ORF
T573G_C574A_R	CGAGGTGAGTGAAAGATGGTGCTGAATGAATATTATTTGCTTTCAAT	Reverse primer can be used to introduce T573G and C574A mutations in MCPH1 ORF
T762G_C763A_F	ACCATCTTTCACTCACCTCGATAAATCAGCTCCTCAGAAATTTCTG	Forward primer can be used to introduce T762G and C763A mutations in MCPH1 ORF
T762G_C763A_R	CAGAAATTTCTGAGGAGCTGATTTATCGAGGTGAGTGAAAGATGGT	Reverse primer can be used to introduce T762G and C763A mutations in MCPH1 ORF
T831G_C832A_A834T_F	TTCTTCACTTGTATTGAAAGCAAATAATATTCATTCAGATCCATCTTTCACTCACCTCG	Forward primer can be used to introduce T831G, C832A and A834T mutations in MCPH1 ORF
T831G_C832A_A834T_F	CGAGGTGAGTGAAAGATGGATCTGAATGAATATTATTTGCTTTCAATACAAGTGAAGAA	Reverse primer can be used to introduce T831G, C832A and A834T mutations in MCPH1 ORF
A861G_G862A_F	ACGTTTGAAGAGAAGTATCGTTTGGATCCTACCTTATCTTCAACAAAAGG	Forward primer can be used to introduce A861G and G862A mutations in MCPH1 ORF
A861G_G862A_R	CCTTTTGTTGAAGATAAGGTAGGATCCAAACGATACTTCTCTTCAAACGT	Reverse primer can be used to introduce A861G and G862A mutations in MCPH1 ORF

Oligo Name	Sequence	Description
T999G_C1000A_F	GTGGGGAGTCTTCATATGATGACTATTTTGCACCTGATAATCTTAAG	Forward primer can be used to introduce T999G and C1000A mutations in MCPH1 ORF
T999G_C1000A_R	CTTAAGATTATCAGGTGCAAAATAGTCATCATATGAAGACTCCCCAC	Reverse primer can be used to introduce T999G and C1000A mutations in MCPH1 ORF
T1095G_C1096A_A1097T_F	AAAGAGTATCACATGGCTCCCATGATCCTCCGAAGGAAAAATGCAAGT	Forward primer can be used to introduce A1095G, C1096A and A1097T mutations in MCPH1 ORF
T1095G_C1096A_A1097T_R	CTTGCATTTTTCCTTCGGAGGATCATGGGAGCCATGTGATACTCTTT	Reverse primer can be used to introduce A1095G, C1096A and A1097T mutations in MCPH1 ORF
T1251G_C1252A_A1253T_F	CTGTGGGGAGTCTTCATATGATGACTATTTTGATCCTGATAATCTTAAGGAAAGGTA	Forward primer can be used to introduce T1251G, C1252A and A1253T mutations in MCPH1 ORF
T1251G_C1252A_A1253T_R	TACCTTTCCTTAAGATTATCAGGATCAAAATAGTCATCATATGAAGACTCCCCACAG	Reverse primer can be used to introduce T1251G, C1252A and A1253T mutations in MCPH1 ORF
A1449G_G1450A_F	TCACAGCAAAAACCATCTCCGATCCTCGGAAAACTGGAAATG	Forward primer can be used to introduce A1449G and G1450A mutations in MCPH1 ORF
A1449G_G1450A_R	CATTTCCAGTTTTCCGAGGATCGGAGATGGTTTTTGCTGTGA	Reverse primer can be used to introduce A1449G and G1450A mutations in MCPH1 ORF
A1752G_G1753C_F	GCTTCTTTCATTTCTTCAAGGGCTCCTTCCAAAGGAGTTAAATCATC	Forward primer can be used to introduce A1752G and G1753C mutation in MCPH1 ORF
A1752G_G1753C_R	GATGATTTAACTCCTTTGGAAGGAGCCCTTGAAGAAATGAAAGAAGC	Reverse primer can be used to introduce A1752G and G1753C mutation in MCPH1 ORF
A2307G_G2308A_F	CTCGCCTGCCAGCGACCCCCCAGTGGCC	Forward primer can be used to introduce A2307G and G2308A mutations in MCPH1 ORF
A2307G_G2308A_R	GGCCACTGGGGGGTCGCTGGCAGGCGAG	Reverse primer can be used to introduce A2307G and G2308A mutations in MCPH1 ORF
T1865G_F	CAAGGCATGATGTTTTAGAGGACTCATGTGACGGCTTT	Forward primer can be used to introduce T1865G mutation in MCPH1 ORF
T1865G_R	AAAGCCGTCACATGAGTCCTCTAAAACATCATGCCTTG	Reverse primer can be used to introduce T1865G mutation in MCPH1 ORF
C1877G_F	TGATGTTTTAGATGACTCATGTGAGGGCTTTAAGGACCTC	Forward primer can be used to introduce C1877G mutation in MCPH1 ORF
C1877G_R	GAGGTCCTTAAAGCCCTCACATGAGTCATCTAAAACATCA	Reverse primer can be used to introduce C1877G mutation in MCPH1 ORF
A1449G_G1450C_F	CACAGCAAAAACCATCTCCGCTCCTCGGAAAACTGGAAAT	Forward primer can be used to introduce A1449G and G1450C mutation in MCPH1 ORF
A1449G_G1450C_R	ATTTCCAGTTTTCCGAGGAGCGGAGATGGTTTTTGCTGTG	Reverse primer can be used to introduce A1449G and G1450C mutation in MCPH1 ORF

(b) Gateway recombination

To generate PCR products suitable for use as substrates in a gateway BP reaction with a donor vector, *att*B sites were incorporated into the PCR products. To introduce *att*B sites the forward primer contains the following structure:

GGG-ACA-AGT-TTG-TAC-AAA-AAA-GCA-GGC-TCC- template specific sequence

The reverse primer contains the structure:

GGG-AC-CAC-TTT-GTA-CAA-GAA-AGC-TGG-GTC- template specific sequence

Table A1.2 represents the template specific sequence used for *att*B PCR products.

Oligo Name	Sequence	Description
MCPH1_FL_F	ATGGCGGCCCCCATCCTGA	Forward primer at 5' end of MCPH1 full-length (FL) isoform ORF
MCPH1_FL_R	TCCTTGTGACAATAGGTAGTTTTCAG	Reverse primer removing the stop codon at 3' end of MCPH1 FL ORF
MCPH1_FL_RX	TCATTGTGACAATAGGTAGTTTTCAG	Reverse primer at 3' end of MCPH1 FL ORF
MCPH1_S_R	TCTCATACTTCCACTGTATCCTCCGGG	Reverse primer removing the stop codon at 3' end of MCPH1 Short (S)isoform ORF
MCPH1_S_RX	TCACATACTTCCACTGTATCCTCCGGG	Reverse primer at 3' end of MCPH1 S ORF
MCPH1_1-89_RX	TCAAAAAAAACATATGCTACCTTTATAT	Reverse primer introducing a stop codon anneals to nt. 239-267 of MCPH1 FL ORF
MCPH1_1-223_RX	TCATGAACACAAAGTATCACGTGAAATG	Reverse primer introducing a stop codon anneals to nt. 644-669 of MCPH1 FL ORF
MCPH1_NB_F	GGAGCACACATTGATGAATC	Forward primer anneals to nt. 246-266 of MCPH1 FL ORF
MCPH1_NB_R	TCCCCCACTTTTCTTCAATTCCTC	Reverse primer introducing a stop codon anneals to nt. 1902-1923 of MCPH1 FL ORF
MCPH1_B2/3_F	GAGGAATTGAAGAAAAGTGGG	Forward primer anneals to nt. 1902-1923 of MCPH1 FL ORF

(c) Sequencing

Oligo Name	Sequence	Description
MCPH1_F1	GCCCCCATCCTGAAAGAT	MCPH1 nt.7-25
MCPH1_F2	CACATTGATGAATCATTG	MCPH1 nt.252-270
MCPH1_F3	ATTAATAGTAGTCACCAC	MCPH1 nt.501-519
MCPH1_F4	TGGAAGGATCCATTAATG	MCPH1 nt.751-769
MCPH1_F5	CCTTATCTTCAACAAAAG	MCPH1 nt.1003-1021
MCPH1_F6	GATAATCTTAAGGAAAGG	MCPH1 nt.1254-1272
MCPH1_F7	CCCCTGAAGAAGCCCTAA	MCPH1 nt.1503-1521
MCPH1_F8	ATAGTTGACTGTAACATG	MCPH1 nt.1758-1776
MCPH1_F9	TGAAAGGCTTTTCAATTG	MCPH1 nt.2008-2026
MCPH1_F10	AACCCTCTTTGCCGACCA	MCPH1 nt.2316-2334
MCPH1_R10	AATGCAGGACAGCTGGAG	Reverse complement of nt.232-250
M13_F	GTAAAACGACGGCCA	pDONR221 nt. 537-552
M13R_pentry	GTCATAGCTGTTTCCT	pDONR221 nt. 2027-3043
pGEX_F	GGGCTGGCAAGCCACGTTTGGTG	pGEX_4T3 nt. 869-894
pGEX_R	CCGGGAGCTGCATGTGTCAGAGG	pGEX_4T3 nt. 1018-1039

(d) PCR and qPCR

Oligo Name	Sequence	Description
PBGD_F	AGCTATGAAGGATGGGCAAC	Forward primer anneals to nt. 964-983 in porphobilinogen deanimase (PBGD) ORF
PBGD_R	TTGTATGCTATCTGAGCCGTCTA	Reverse complement of PDGB nt.1011-1033
qFL/S_F	AAGGCGAAGCCCAGAGTG	Forward primer anneals to nt. 1723-1741 in MCPH1 FL ORF
qFL_R	CTATTTTTAACACTTCCACTGTATCC	Reverse complement of MCPH1 FL nt.1812-1838
qS_R	CGAAGGTGACTTGGAAAAGG	Reverse primer anneals to nt. 12-32 in MCPH1 intron 8
qΔ8_F	CAGCGCAATGGAGAAGAGAT	Forward primer anneals to nt.518-538 MCPH1 FL ORF
qΔ8_R	CTATTTTTAACACCTGAACACAAAG	Reverse primer anneals to nt. 658-670 & 1825-1838 in MCPH1 FL ORF
qS_int8_F	AGAGCTTTGGGACCTTCAGTC	Forward primer anneals to MCPH1 intron 8
qS_int8_R	TTTGCAGTTGTATGCTTGTAGAC	Reverse primer anneals to MCPH1 intron 8
mMcph1_F	GTGGAGTTTGGAGGGTGCTTC	Forward primer anneals to MCPH1 intron 3
mMcph1_R1	ATTCCCCACACCCCTACATT	Reverse primer anneals to *Flippase* Recognition Target (FRT) site
mMcph1_R2	CAACGGGTTCTTCTGTTAGTC	Reverse primer anneals to MCPH1 intron 3

(e) siRNA

All RNA oligonucleotides were synthesised with dTdT at the 3'end of the sense strand to facilitate RNA-induced silencing complex (RISC) loading (Dharmacon).

Oligo Name	Sequence (sense strand)	Description
LUC	CUUACGCUGAGUACUUCGAdTdT	Control that targets luciferase
MCPH1_1	GCACAGUACUGCCAAAUAAUUdTdT	Targets MCPH1 FL 3' UTR
MCPH1_2	GCGCAAUGGAGAAGAGAUUdTdT	Targets nt. 520-539 of MCPH1 FL ORF
MCPH1_3	GGAGCACACAUUGAUGAAUdTdT	Targets nt. 246-265 of MCPH1 FL ORF
MCPH1_FL	GGAUACAGUGGAAGUGUUAAA	Targets nt. 1812-1834 of MCPH1FL ORF
MCPH1_S	GGAUACAGUGGAAGUAUGUdTdT	Targets nt. 1812-1831 of MCPH1 S ORF
PLK1	AATTCTCCGAACGTGTCACGTdTdT	(Oshimori *et al.*, 2006)
APC3_1	GGAAAUAGCCGAGAGGUAAUUdTdT	(Nilsson *et al.*, 2008)
APC3_2	CAAAAGAGCCUUAGUUUAAUUdTdT	(Nilsson *et al.*, 2008)
MCPH1_4	AGGAAGUUGGAAGGAUCCA	Targets MCPH1 FL and S

Appendix 2. Antisera

(a) Primary antibodies

Antibody	Species	Dilution for WB or IF	Reference
Actin (C-11)	Goat	1:1000 (WB)	Santa Cruz Biotechnology (sc-1615)
ASPM (IHC)	Rabbit	1:1000(WB) 1:500(IF)	Bethyl Laboratories (IHC-00058)
Aurora-A Kinase/IAK1	Mouse	1:500(WB) 1:1000(IF)	BD Transduction Laboratories (610939)
CDK5RAP2	Rabbit	1:1000(WB) 1;2000(IF)	Bethyl Laboratories (A300-554A)
CPAP	Mouse	1:500(IF)	Santa Cruz Biotechnology (sc-81432)
cyclin A (H-432)	Rabbit	1:500(WB)	Santa Cruz Biotechnology (sc-751)
cyclin B (V152)	Mouse	1:500(WB)	Cell Signaling Technology (4135)
GFP (JL8)	Mouse	1:1000(WB)	BD Transduction Laboratories (8371-1)
MCPH1	Rabbit	1:1000(WB)	Generous gift from P.Lin (Lin *et al.*, 2005)
Pericentrin	Rabbit	1:1000(WB)	Abcam (ab4448)
Plk1	Rabbit	1:2000(WB)	Cell Signalling
Plk1	Mouse	1:200(IF) 1:1000(WB)	Santa Cruz Biotechnology (sc-17783)
α- Tubulin (B512)	Mouse	1:10,000(WB) 1:1000(IF)	Sigma-Aldrich (T6074)
γ-Tubulin	Rabbit	1:500(IF)	Sigma-Aldrich (T5192)
γ-Tubulin (GTU-88)	Mouse	1:3000(WB) 1:500(IF)	Sigma-Aldrich (T5326)
Tubulin (glutamylated) (GT335)	Mouse	1:500(IF)	Generous gift from C.Janke (Wolff *et al.*, 1992)
Vinculin	Mouse	1:1000(WB)	Sigma-Aldrich (V9264)

(b) Secondary antibodies

Antibody	Species	Dilution for WB or IF	Reference
Anti-rabbit IgG, HRP linked	Goat	1:5000(WB)	Cell signalling (7074)
Anti-mouse IgG, HRP linked	Rabbit	1:5000(WB)	Dako (P0260)
Anti-rabbit IgG Alexa Fluor 488 linked	Goat	1:500(IF)	Invitrogen (A11034)
Anti-rabbit IgG Alexa Fluor 568 linked	Goat	1:500(IF)	Invitrogen (A11036)
Anti-human IgG Alexa Fluor 568 linked	Goat	1:500(IF)	Invitrogen (A21090)
Anti-mouse IgG Alexa Fluor 568 linked	Goat	1:500(IF)	Invitrogen (A11031)
Anti-mouse IgG Alexa Fuor 488 linked	Goat	1:500(IF)	Invitrogen (A11029)

Appendix 3. Cell cycle regulation of MCPH1 is independent of caspases

HeLa cells were synchronised by a double thymidine block, treated with Z-VAD-FMK and released to progress through the cell cycle. Extracts were prepared at various time points, separated on a polyacrylamide gel and immunoblotted with MCPH1 antibodies.

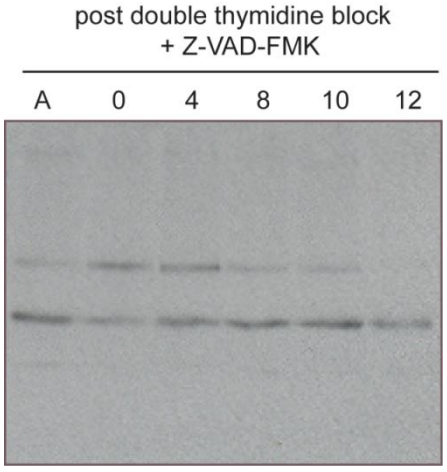

Appendix 4. Conservation of microcephalin phosphorylation sites between human and mouse

Amino acid sequence alignment of human (H.s.) and mouse (M.m.) MCPH1. Black shading in H.s. sequence represents phosphorylated residues identified by phospho-peptide mapping studies (Figure 6.6) and black shading in M.m. sequence represents conserved residues.

```
H. s.   1    MAAPILKDVVAYVEVWSSNGTENYSKTFTTQLVDMGAKVSKTFNKQVTHVIFKDGYQSTW  60
             +    LKDVVAYVEVWSS GTENYS+TF  QL DMGA VSKT NKQVTHVIFKDGYQSTW
M. m.   7    VGGAFLKDVVAYVEVWSSKGTENYSRTFAKQLEDMGATVSKTLNKQVTHVIFKDGYQSTW  66

H. s.  61    DKAQKRGVKLVSVLWVEKCRTAGAHIDESLFPAANMNEHLSSLIKKKRKCMQPKDFNFKT 120
             DKAQK G KLVSVLWVEKCR AGA +DESLFPA N +EHL +L +KK KCMQPKDF  KT
M. m.  67    DKAQKTGAKLVSVLWVEKCRMAGALVDESLFPAVNTDEHLPNLSRKKHKCMQPKDFILKT 126

H. s. 121    PENDKRFQKKFEKMAKELQRQKTNLDDDVPILLFESNGSLIYTPTIEINSRHHSAMEKRL 180
             PENDKR QKKFEKMA+ELQRQK  LDDDVP+LLFES  SL+Y+  + +       M++RL
M. m.  127   PENDKRLQKKFEKMAEELQRQKAALDDDVPVLLFESPRSLVYSSPVNV-------MKRRL 179

H. s. 181    QEMKEKRENLSPTSSQMIQQSHDNPSNSLCEAPLNISRDTLCSDEYFAGGLHSSFDDLCG 240
             Q+MKEKRENLSPTSSQM++QS  NP  S  E  LNIS   L SDE FA G HSSF D
M. m.  180   QDMKEKRENLSPTSSQMLEQSQQNPCVSLFETSLNISHQPLSSDESFASGSHSSFGD--- 236

H. s. 241    NSGCGNQERKLEGSINDIKSDVCISSLVLKANNIHSSPSFTHLDKSSPQKFLSNLSKEEI 300
                CG+QERKL  S N++ +  C SS VL+A++ + S S  HL +  PQK   + SKE I
M. m.  237   --SCGDQERKLGRSANEMTTVTCPSSPVLRASSFYGSASPNHLRQPRPQKAPDSPSKESI 294

H. s. 301    NLQRNIAGKVVTPDQKQAAGMSQETFEEKYRLSPTLSSTKGHLLIHSRPRSSSVKRKRVS 360
             N Q++  G V   ++KQAAG+SQ   +EK  LSPT+S  + H  +   P++SS KRKR +
M. m.  295   NCQKDATGAVADSERKQAAGVSQGVPDEKLCLSPTMSIIEEHQ-VRLGPKNSSAKRKRAA 353

H. s. 361    HGSHSPPKEKCKRKRSTRRSIMPRLQLCRSEDR----LQHVAG-PALEALSCGESSYDDY 415
                 SP   K K K+  +R     +QL +S+      ++ + G P +EA     SSY  DY
M. m.  354   DLGSSP---KGKLKKRYKRKSALAIQLFKSDQSPPSTIRLIPGTPDVEA-----SSYEDY 405

H. s. 416    FSPDNLKERYSENLPPESQLPSSPAQLSCRSLSKKERTSIFEMSDFSCVGKKTRTVDITN 475
             FSPDNLKER SE LPPE+Q  +SP+   CR LSK ER ++ EM DF+C+G+K R++   +
M. m.  406   FSPDNLKERNSERLPPEAQQLASPSLFHCRGLSKWERRNMLEMCDFTCIGEKHRSISSIS 465

H. s. 476    FTAKT-ISSPRKTGNGEGRATSSC---VTSAPEEALRCCRQAG---KEDACPEGNGFSYT 528
                    SS   K    E    S+C   V ++  ++   C Q G   ++D  PEG+    T
M. m.  466   DLISKSASSLEKPVKEEVNTASTCLLLVETSANDSPGLCSQPGPQLRDDTGPEGSSHPDT 525

H. s. 529    IEDPALPKGHDDDLTPLEGSLEEMKEAVGLKSTQNKGTTSKISNSSEGEAQSEHEPCFIV 588
             +   A        +TPL+G+  E ++    K +  +G+T   S S E E       C +
M. m.  526   LSSSA------HHITPLKGNSTETRDPGDGKGSPKEGSTPPASASPEDEVHI----CNLS 575

H. s. 589    ---DCNMETSTEEKENLPGGYSGSVKNRPTRHDVLDDSCDGFKDLIKPHEELKKSGRGKK 645
                DCN+E S EEKEN+  GYS SVKN P R D  D SC G   L++P ++ KKS + +K
M. m.  576   LGEDCNVEKSVEEKENIATGYSESVKNGPGRPDPSDSSCTG---LVRPQQKPKKSEKEEK 632

H. s. 646    PTRTLVMTSMPSEKQNVVIQVVDKLKGFSIAPDVCETTTHVLSGKPLRTLNVLLGIARGC 705
             PTRTLVMTSMPSEKQ ++IQVV  LKGFS AP+VCETTTHVL GK  RTLNVL+GIARGC
M. m.  633   PTRTLVMTSMPSEKQTLIIQVVSTLKGFSFAPEVCETTTHVLVGKSARTLNVLMGIARGC 692

H. s. 706    WVLSYDWVLWSLELGHWISEEPFELSHHFPAAPLCRSECHLSAGPYRGTLFADQPAMFVS 765
             W+LSY+WVL SLELGHWISEEPFELS  FPAAP+CR E HLS   Y+GTLFA+QP MF++
M. m.  693   WILSYEWVLLSLELGHWISEEPFELSETFPAAPICRLERHLSTQQYQGTLFANQPKMFIA 752

H. s. 766    PASSPPVAKLCELVHLCGGRVSQVPRQASIVIGPYSGKKKATVKYLSEKWVLDSITQHKV 825
             PASSPP AKLCELV LCGG+VS  P+ AS++IGPY GKKKA ++YLSEKWVLDSITQHK+
M. m.  753   PASSPPRAKLCELVLLCGGQVSPAPQLASLIIGPYKGKKKARIQYLSEKWVLDSITQHKI 812

H. s. 826    CAPENYLLSQ  835
             C   NY L Q
M. m.  813   CDFNNYQLLQ  822
```

Bibliography

Abal M., Keryer G. and Bornens M. (2005) Centrioles resist forces applied on centrosomes during G2/M transition. *Biol Cell* **97**, 425-34.

Abe S., Nagasaka K., Hirayama Y., Kozuka-Hata H., Oyama M., Aoyagi Y., Obuse C. and Hirota T. (2011) The initial phase of chromosome condensation requires Cdk1-mediated phosphorylation of the CAP-D3 subunit of condensin II. *Genes Dev* **25**, 863-74.

Al-Dosari M. S., Shaheen R., Colak D. and Alkuraya F. S. (2010) Novel CENPJ mutation causes Seckel syndrome. *J Med Genet* **47**, 411-4.

Alam A., Cohen L. Y., Aouad S. and Sekaly R. P. (1999) Early activation of caspases during T lymphocyte stimulation results in selective substrate cleavage in nonapoptotic cells. *J Exp Med* **190**, 1879-90.

Alderton G. K., Galbiati L., Griffith E., Surinya K. H., Neitzel H., Jackson A. P., Jeggo P. A. and O'Driscoll M. (2006) Regulation of mitotic entry by microcephalin and its overlap with ATR signalling. *Nat Cell Biol* **8**, 725-33.

Alderton G. K., Joenje H., Varon R., Borglum A. D., Jeggo P. A. and O'Driscoll M. (2004) Seckel syndrome exhibits cellular features demonstrating defects in the ATR-signalling pathway. *Hum Mol Genet* **13**, 3127-38.

Amor D. J., Kalitsis P., Sumer H. and Choo K. H. (2004) Building the centromere: from foundation proteins to 3D organization. *Trends Cell Biol* **14**, 359-68.

Anderson C. T. and Stearns T. (2009) Centriole age underlies asynchronous primary cilium growth in mammalian cells. *Curr Biol* **19**, 1498-502.

Anderson R. G. and Brenner R. M. (1971) The formation of basal bodies (centrioles) in the Rhesus monkey oviduct. *J Cell Biol* **50**, 10-34.

Ang X. L. and Wade Harper J. (2005) SCF-mediated protein degradation and cell cycle control. *Oncogene* **24**, 2860-70.

Angevine J. B., Jr. and Sidman R. L. (1961) Autoradiographic study of cell migration during histogenesis of cerebral cortex in the mouse. *Nature* **192**, 766-8.

Attardo A., Calegari F., Haubensak W., Wilsch-Brauninger M. and Huttner W. B. (2008) Live imaging at the onset of cortical neurogenesis reveals differential appearance of the neuronal phenotype in apical versus basal progenitor progeny. *PLoS One* **3**, e2388.

Azimzadeh J. and Bornens M. (2007) Structure and duplication of the centrosome. *J Cell Sci* **120**, 2139-42.

Azimzadeh J. and Marshall W. F. (2010) Building the centriole. *Curr Biol* **20**, R816-25.

Baek S. H., Kioussi C., Briata P., Wang D., Nguyen H. D., Ohgi K. A., Glass C. K., Wynshaw-Boris A., Rose D. W. and Rosenfeld M. G. (2003) Regulated subset of G1 growth-control genes in response to derepression by the Wnt pathway. *Proc Natl Acad Sci U S A* **100**, 3245-50.

Bahe S., Stierhof Y. D., Wilkinson C. J., Leiss F. and Nigg E. A. (2005) Rootletin forms centriole-associated filaments and functions in centrosome cohesion. *J Cell Biol* **171**, 27-33.

Barr A. R., Kilmartin J. V. and Gergely F. (2010) CDK5RAP2 functions in centrosome to spindle pole attachment and DNA damage response. *J Cell Biol* **189**, 23-39.

Barrera J. A., Kao L. R., Hammer R. E., Seemann J., Fuchs J. L. and Megraw T. L. (2010) CDK5RAP2 regulates centriole engagement and cohesion in mice. *Dev Cell* **18**, 913-26.

Basto R., Brunk K., Vinadogrova T., Peel N., Franz A., Khodjakov A. and Raff J. W. (2008) Centrosome amplification can initiate tumorigenesis in flies. *Cell* **133**, 1032-42.

Basto R., Lau J., Vinogradova T., Gardiol A., Woods C. G., Khodjakov A. and Raff J. W. (2006) Flies without centrioles. *Cell* **125**, 1375-86.

Bennett D. (1965) The Karyotype of the Mouse, with Identification of a Translocation. *Proc Natl Acad Sci U S A* **53**, 730-7.

Bhat V., Girimaji S., Mohan G., Arvinda H., Singhmar P., Duvvari M. and Kumar A. (2011) Mutations in WDR62, encoding a centrosomal and nuclear protein, in Indian primary microcephaly families with cortical malformations. *Clin Genet, Advanced online publication*, DOI: 10.1111.

Bilguvar K., Ozturk A. K., Louvi A., Kwan K. Y., Choi M., Tatli B., Yalnizoglu D., Tuysuz B., Caglayan A. O., Gokben S., Kaymakcalan H., Barak T., Bakircioglu M., Yasuno K., Ho W., Sanders S., Zhu Y., Yilmaz S., Dincer A., Johnson M. H., Bronen R. A., Kocer N., Per H., Mane S., Pamir M. N., Yalcinkaya C., Kumandas S., Topcu M., Ozmen M., Sestan N., Lifton R. P., State M. W. and Gunel M. (2010) Whole-exome sequencing identifies recessive WDR62 mutations in severe brain malformations. *Nature* **467**, 207-10.

Blachon S., Gopalakrishnan J., Omori Y., Polyanovsky A., Church A., Nicastro D., Malicki J. and Avidor-Reiss T. (2008) Drosophila asterless and vertebrate Cep152 Are orthologs essential for centriole duplication. *Genetics* **180**, 2081-94.

Blagden S. P. and Glover D. M. (2003) Polar expeditions--provisioning the centrosome for mitosis. *Nat Cell Biol* **5**, 505-11.

Bobinnec Y., Khodjakov A., Mir L. M., Rieder C. L., Edde B. and Bornens M. (1998) Centriole disassembly in vivo and its effect on centrosome structure and function in vertebrate cells. *J Cell Biol* **143**, 1575-89.

Bobrow M. N., Litt G. J., Shaughnessy K. J., Mayer P. C. and Conlon J. (1992) The use of catalyzed reporter deposition as a means of signal amplification in a variety of formats. *J Immunol Methods* **150**, 145-9.

Bonaccorsi S., Giansanti M. G. and Gatti M. (1998) Spindle self-organization and cytokinesis during male meiosis in asterless mutants of Drosophila melanogaster. *J Cell Biol* **142**, 751-61.

Bond J., Roberts E., Mochida G. H., Hampshire D. J., Scott S., Askham J. M., Springell K., Mahadevan M., Crow Y. J., Markham A. F., Walsh C. A. and Woods C. G. (2002) ASPM is a major determinant of cerebral cortical size. *Nat Genet* **32**, 316-20.

Bond J., Roberts E., Springell K., Lizarraga S. B., Scott S., Higgins J., Hampshire D. J., Morrison E. E., Leal G. F., Silva E. O., Costa S. M., Baralle D., Raponi M., Karbani G., Rashid Y., Jafri H., Bennett C., Corry P., Walsh C. A. and

Woods C. G. (2005) A centrosomal mechanism involving CDK5RAP2 and CENPJ controls brain size. *Nat Genet* **37**, 353-5.
Bond J., Scott S., Hampshire D. J., Springell K., Corry P., Abramowicz M. J., Mochida G. H., Hennekam R. C., Maher E. R., Fryns J. P., Alswaid A., Jafri H., Rashid Y., Mubaidin A., Walsh C. A., Roberts E. and Woods C. G. (2003) Protein-truncating mutations in ASPM cause variable reduction in brain size. *Am J Hum Genet* **73**, 1170-7.
Bond J. and Woods C. G. (2006) Cytoskeletal genes regulating brain size. *Curr Opin Cell Biol* **18**, 95-101.
Borel F., Lohez O. D., Lacroix F. B. and Margolis R. L. (2002) Multiple centrosomes arise from tetraploidy checkpoint failure and mitotic centrosome clusters in p53 and RB pocket protein-compromised cells. *Proc Natl Acad Sci U S A* **99**, 9819-24.
Boutros R., Dozier C. and Ducommun B. (2006) The when and wheres of CDC25 phosphatases. *Curr Opin Cell Biol* **18**, 185-91.
Braitenberg V. (2001) Brain size and number of neurons: an exercise in synthetic neuroanatomy. *J Comput Neurosci* **10**, 71-7.
Brand A. H. and Livesey F. J. (2011) Neural stem cell biology in vertebrates and invertebrates: more alike than different? *Neuron* **70**, 719-29.
Brennand K. J., Simone A., Jou J., Gelboin-Burkhart C., Tran N., Sangar S., Li Y., Mu Y., Chen G., Yu D., McCarthy S., Sebat J. and Gage F. H. (2011) Modelling schizophrenia using human induced pluripotent stem cells. *Nature* **473**, 221-5.
Brinkley B. R. and Cartwright J., Jr. (1975) Cold-labile and cold-stable microtubules in the mitotic spindle of mammalian cells. *Ann N Y Acad Sci* **253**, 428-39.
Brown J. A., Bourke E., Liptrot C., Dockery P. and Morrison C. G. (2010) MCPH1/BRIT1 limits ionizing radiation-induced centrosome amplification. *Oncogene* **29**, 5537-44.
Brunk K., Vernay B., Griffith E., Reynolds N. L., Strutt D., Ingham P. W. and Jackson A. P. (2007) Microcephalin coordinates mitosis in the syncytial Drosophila embryo. *J Cell Sci* **120**, 3578-88.
Buchman J. J. and Tsai L. H. (2007) Spindle regulation in neural precursors of flies and mammals. *Nat Rev Neurosci* **8**, 89-100.
Buchman J. J., Tseng H. C., Zhou Y., Frank C. L., Xie Z. and Tsai L. H. (2010) Cdk5rap2 interacts with pericentrin to maintain the neural progenitor pool in the developing neocortex. *Neuron* **66**, 386-402.
Bultje R. S., Castaneda-Castellanos D. R., Jan L. Y., Jan Y. N., Kriegstein A. R. and Shi S. H. (2009) Mammalian Par3 regulates progenitor cell asymmetric division via notch signaling in the developing neocortex. *Neuron* **63**, 189-202.
Bundey S. (1992) Microcephaly. In *In: Genetics and neurology*, p. pp. 20-24. Churchill Livingstone, Edinburgh.
Busino L., Donzelli M., Chiesa M., Guardavaccaro D., Ganoth D., Dorrello N. V., Hershko A., Pagano M. and Draetta G. F. (2003) Degradation of Cdc25A by beta-TrCP during S phase and in response to DNA damage. *Nature* **426**, 87-91.
Bystron I., Blakemore C. and Rakic P. (2008) Development of the human cerebral cortex: Boulder Committee revisited. *Nat Rev Neurosci* **9**, 110-22.

Bystron I., Rakic P., Molnar Z. and Blakemore C. (2006) The first neurons of the human cerebral cortex. *Nat Neurosci* **9**, 880-6.
Cai L., Hayes N. L. and Nowakowski R. S. (1997) Local homogeneity of cell cycle length in developing mouse cortex. *J Neurosci* **17**, 2079-87.
Calegari F., Haubensak W., Haffner C. and Huttner W. B. (2005) Selective lengthening of the cell cycle in the neurogenic subpopulation of neural progenitor cells during mouse brain development. *J Neurosci* **25**, 6533-8.
Calegari F., Haubensak W., Yang D., Huttner W. B. and Buchholz F. (2002) Tissue-specific RNA interference in postimplantation mouse embryos with endoribonuclease-prepared short interfering RNA. *Proc Natl Acad Sci U S A* **99**, 14236-40.
Calegari F. and Huttner W. B. (2003) An inhibition of cyclin-dependent kinases that lengthens, but does not arrest, neuroepithelial cell cycle induces premature neurogenesis. *J Cell Sci* **116**, 4947-55.
Canman C. E., Lim D. S., Cimprich K. A., Taya Y., Tamai K., Sakaguchi K., Appella E., Kastan M. B. and Siliciano J. D. (1998) Activation of the ATM kinase by ionizing radiation and phosphorylation of p53. *Science* **281**, 1677-9.
Cardenas-Rodriguez M. and Badano J. L. (2009) Ciliary biology: understanding the cellular and genetic basis of human ciliopathies. *Am J Med Genet C Semin Med Genet* **151C**, 263-80.
Cardozo T. and Pagano M. (2004) The SCF ubiquitin ligase: insights into a molecular machine. *Nat Rev Mol Cell Biol* **5**, 739-51.
Carlessi L., De Filippis L., Lecis D., Vescovi A. and Delia D. (2009) DNA-damage response, survival and differentiation in vitro of a human neural stem cell line in relation to ATM expression. *Cell Death Differ* **16**, 795-806.
Casal J., Gonzalez C., Wandosell F., Avila J. and Ripoll P. (1990) Abnormal meiotic spindles cause a cascade of defects during spermatogenesis in asp males of Drosophila. *Development* **108**, 251-60.
Castiel A., Danieli M. M., David A., Moshkovitz S., Aplan P. D., Kirsch I. R., Brandeis M., Kramer A. and Izraeli S. (2010) The Stil protein regulates centrosome integrity and mitosis through suppression of Chfr. *J Cell Sci* **124**, 532-9.
Castro A., Vigneron S., Bernis C., Labbe J. C., Prigent C. and Lorca T. (2002) The D-Box-activating domain (DAD) is a new proteolysis signal that stimulates the silent D-Box sequence of Aurora-A. *EMBO Rep* **3**, 1209-14.
Cavalier-Smith T. (1974) Basal body and flagellar development during the vegetative cell cycle and the sexual cycle of Chlamydomonas reinhardii. *J Cell Sci* **16**, 529-56.
Caviness V. S., Jr., Takahashi T. and Nowakowski R. S. (1995) Numbers, time and neocortical neuronogenesis: a general developmental and evolutionary model. *Trends Neurosci* **18**, 379-83.
Chamberlain S. J., Li X. J. and Lalande M. (2008) Induced pluripotent stem (iPS) cells as in vitro models of human neurogenetic disorders. *Neurogenetics* **9**, 227-35.
Chau B. N., Borges H. L., Chen T. T., Masselli A., Hunton I. C. and Wang J. Y. (2002) Signal-dependent protection from apoptosis in mice expressing caspase-resistant Rb. *Nat Cell Biol* **4**, 757-65.

Cheeseman I. M. and Desai A. (2008) Molecular architecture of the kinetochore-microtubule interface. *Nat Rev Mol Cell Biol* **9**, 33-46.
Chen R. Q., Yang Q. K., Lu B. W., Yi W., Cantin G., Chen Y. L., Fearns C., Yates J. R., 3rd and Lee J. D. (2009) CDC25B mediates rapamycin-induced oncogenic responses in cancer cells. *Cancer Res* **69**, 2663-8.
Chenn A. and McConnell S. K. (1995) Cleavage orientation and the asymmetric inheritance of Notch1 immunoreactivity in mammalian neurogenesis. *Cell* **82**, 631-41.
Chenn A. and Walsh C. A. (2002) Regulation of cerebral cortical size by control of cell cycle exit in neural precursors. *Science* **297**, 365-9.
Cho J. H., Chang C. J., Chen C. Y. and Tang T. K. (2006) Depletion of CPAP by RNAi disrupts centrosome integrity and induces multipolar spindles. *Biochem Biophys Res Commun* **339**, 742-7.
Choi Y. K., Liu P., Sze S. K., Dai C. and Qi R. Z. (2010) CDK5RAP2 stimulates microtubule nucleation by the gamma-tubulin ring complex. *J Cell Biol* **191**, 1089-95.
Chretien D., Buendia B., Fuller S. D. and Karsenti E. (1997) Reconstruction of the centrosome cycle from cryoelectron micrographs. *J Struct Biol* **120**, 117-33.
Cimprich K. A. and Cortez D. (2008) ATR: an essential regulator of genome integrity. *Nat Rev Mol Cell Biol* **9**, 616-27.
Cizmecioglu O., Arnold M., Bahtz R., Settele F., Ehret L., Haselmann-Weiss U., Antony C. and Hoffmann I. (2010) Cep152 acts as a scaffold for recruitment of Plk4 and CPAP to the centrosome. *J Cell Biol* **191**, 731-9.
Conduit P. T., Brunk K., Dobbelaere J., Dix C. I., Lucas E. P. and Raff J. W. (2010) Centrioles regulate centrosome size by controlling the rate of Cnn incorporation into the PCM. *Curr Biol* **20**, 2178-86.
Conduit P. T. and Raff J. W. (2010) Cnn dynamics drive centrosome size asymmetry to ensure daughter centriole retention in drosophila neuroblasts. *Curr Biol* **20**, 2187-92.
Costa M. R., Wen G., Lepier A., Schroeder T. and Gotz M. (2008) Par-complex proteins promote proliferative progenitor divisions in the developing mouse cerebral cortex. *Development* **135**, 11-22.
Cowie V. (1960) The genetics and sub-classification of microcephaly. *J Ment Defic Res* **4**, 42-7.
Cox J., Jackson A. P., Bond J. and Woods C. G. (2006) What primary microcephaly can tell us about brain growth. *Trends Mol Med* **12**, 358-66.
Cunha-Ferreira I., Rodrigues-Martins A., Bento I., Riparbelli M., Zhang W., Laue E., Callaini G., Glover D. M. and Bettencourt-Dias M. (2009) The SCF/Slimb ubiquitin ligase limits centrosome amplification through degradation of SAK/PLK4. *Curr Biol* **19**, 43-9.
Currat M., Excoffier L., Maddison W., Otto S. P., Ray N., Whitlock M. C. and Yeaman S. (2006) Comment on "Ongoing adaptive evolution of ASPM, a brain size determinant in Homo sapiens" and "Microcephalin, a gene regulating brain size, continues to evolve adaptively in humans". *Science* **313**, 172; author reply 172.
Dai J., Kateneva A. V. and Higgins J. M. (2009) Studies of haspin-depleted cells reveal that spindle-pole integrity in mitosis requires chromosome cohesion. *J Cell Sci* **122**, 4168-76.

Darvish H., Esmaeeli-Nieh S., Monajemi G. B., Mohseni M., Ghasemi-Firouzabadi S., Abedini S. S., Bahman I., Jamali P., Azimi S., Mojahedi F., Dehghan A., Shafeghati Y., Jankhah A., Falah M., Soltani Banavandi M. J., Ghani-Kakhi M., Garshasbi M., Rakhshani F., Naghavi A., Tzschach A., Neitzel H., Ropers H. H., Kuss A. W., Behjati F., Kahrizi K. and Najmabadi H. (2010) A clinical and molecular genetic study of 112 Iranian families with primary microcephaly. *J Med Genet* **47**, 823-8.

Daum J. R., Potapova T. A., Sivakumar S., Daniel J. J., Flynn J. N., Rankin S. and Gorbsky G. J. (2011) Cohesion Fatigue Induces Chromatid Separation in Cells Delayed at Metaphase. *Curr Biol*.

Daum J. R., Wren J. D., Daniel J. J., Sivakumar S., McAvoy J. N., Potapova T. A. and Gorbsky G. J. (2009) Ska3 is required for spindle checkpoint silencing and the maintenance of chromosome cohesion in mitosis. *Curr Biol* **19**, 1467-72.

De Filippis L., Lamorte G., Snyder E. Y., Malgaroli A. and Vescovi A. L. (2007) A novel, immortal, and multipotent human neural stem cell line generating functional neurons and oligodendrocytes. *Stem Cells* **25**, 2312-21.

Delattre M., Leidel S., Wani K., Baumer K., Bamat J., Schnabel H., Feichtinger R., Schnabel R. and Gonczy P. (2004) Centriolar SAS-5 is required for centrosome duplication in C. elegans. *Nat Cell Biol* **6**, 656-64.

Depaepe V., Suarez-Gonzalez N., Dufour A., Passante L., Gorski J. A., Jones K. R., Ledent C. and Vanderhaeghen P. (2005) Ephrin signalling controls brain size by regulating apoptosis of neural progenitors. *Nature* **435**, 1244-50.

Dephoure N., Zhou C., Villen J., Beausoleil S. A., Bakalarski C. E., Elledge S. J. and Gygi S. P. (2008) A quantitative atlas of mitotic phosphorylation. *Proc Natl Acad Sci U S A* **105**, 10762-7.

Derheimer F. A. and Kastan M. B. (2010) Multiple roles of ATM in monitoring and maintaining DNA integrity. *FEBS Lett* **584**, 3675-81.

Dimos J. T., Rodolfa K. T., Niakan K. K., Weisenthal L. M., Mitsumoto H., Chung W., Croft G. F., Saphier G., Leibel R., Goland R., Wichterle H., Henderson C. E. and Eggan K. (2008) Induced pluripotent stem cells generated from patients with ALS can be differentiated into motor neurons. *Science* **321**, 1218-21.

Dimova D. K. and Dyson N. J. (2005) The E2F transcriptional network: old acquaintances with new faces. *Oncogene* **24**, 2810-26.

Ditchfield C., Johnson V. L., Tighe A., Ellston R., Haworth C., Johnson T., Mortlock A., Keen N. and Taylor S. S. (2003) Aurora B couples chromosome alignment with anaphase by targeting BubR1, Mad2, and Cenp-E to kinetochores. *J Cell Biol* **161**, 267-80.

Dix C. I. and Raff J. W. (2007) Drosophila Spd-2 recruits PCM to the sperm centriole, but is dispensable for centriole duplication. *Curr Biol* **17**, 1759-64.

do Carmo Avides M. and Glover D. M. (1999) Abnormal spindle protein, Asp, and the integrity of mitotic centrosomal microtubule organizing centers. *Science* **283**, 1733-5.

do Carmo Avides M., Tavares A. and Glover D. M. (2001) Polo kinase and Asp are needed to promote the mitotic organizing activity of centrosomes. *Nat Cell Biol* **3**, 421-4.

Dobbelaere J., Josue F., Suijkerbuijk S., Baum B., Tapon N. and Raff J. (2008) A genome-wide RNAi screen to dissect centriole duplication and centrosome maturation in Drosophila. *PLoS Biol* **6**, e224.

Dobson-Stone C., Gatt J. M., Kuan S. A., Grieve S. M., Gordon E., Williams L. M. and Schofield P. R. (2007) Investigation of MCPH1 G37995C and ASPM A44871G polymorphisms and brain size in a healthy cohort. *Neuroimage* **37**, 394-400.

Donzelli M., Squatrito M., Ganoth D., Hershko A., Pagano M. and Draetta G. F. (2002) Dual mode of degradation of Cdc25 A phosphatase. *EMBO J* **21**, 4875-84.

Dunsch A. K., Linnane E., Barr F. A. and Gruneberg U. (2011) The astrin-kinastrin/SKAP complex localizes to microtubule plus ends and facilitates chromosome alignment. *J Cell Biol* **192**, 959-68.

Dzhindzhev N. S., Yu Q. D., Weiskopf K., Tzolovsky G., Cunha-Ferreira I., Riparbelli M., Rodrigues-Martins A., Bettencourt-Dias M., Callaini G. and Glover D. M. (2010) Asterless is a scaffold for the onset of centriole assembly. *Nature* **467**, 714-8.

Earnshaw W. C., Martins L. M. and Kaufmann S. H. (1999) Mammalian caspases: structure, activation, substrates, and functions during apoptosis. *Annu Rev Biochem* **68**, 383-424.

Earnshaw W. C. and Rothfield N. (1985) Identification of a family of human centromere proteins using autoimmune sera from patients with scleroderma. *Chromosoma* **91**, 313-21.

Ebert A. D., Yu J., Rose F. F., Jr., Mattis V. B., Lorson C. L., Thomson J. A. and Svendsen C. N. (2009) Induced pluripotent stem cells from a spinal muscular atrophy patient. *Nature* **457**, 277-80.

Elia A. E., Cantley L. C. and Yaffe M. B. (2003a) Proteomic screen finds pSer/pThr-binding domain localizing Plk1 to mitotic substrates. *Science* **299**, 1228-31.

Elia A. E., Rellos P., Haire L. F., Chao J. W., Ivins F. J., Hoepker K., Mohammad D., Cantley L. C., Smerdon S. J. and Yaffe M. B. (2003b) The molecular basis for phosphodependent substrate targeting and regulation of Plks by the Polo-box domain. *Cell* **115**, 83-95.

Ellison V. and Stillman B. (2003) Biochemical characterization of DNA damage checkpoint complexes: clamp loader and clamp complexes with specificity for 5' recessed DNA. *PLoS Biol* **1**, E33.

Enomoto M., Goto H., Tomono Y., Kasahara K., Tsujimura K., Kiyono T. and Inagaki M. (2009) Novel positive feedback loop between Cdk1 and Chk1 in the nucleus during G2/M transition. *J Biol Chem* **284**, 34223-30.

Eppig J. T. and Barker J. E. (1984) Chromosome abnormalities in mice with Hertwig's anemia. *Blood* **64**, 727-32.

Erez A., Perelman M., Hewitt S. M., Cojacaru G., Goldberg I., Shahar I., Yaron P., Muler I., Campaner S., Amariglio N., Rechavi G., Kirsch I. R., Krupsky M., Kaminski N. and Izraeli S. (2004) Sil overexpression in lung cancer characterizes tumors with increased mitotic activity. *Oncogene* **23**, 5371-7.

Estivill-Torrus G., Pearson H., van Heyningen V., Price D. J. and Rashbass P. (2002) Pax6 is required to regulate the cell cycle and the rate of progression from symmetrical to asymmetrical division in mammalian cortical progenitors. *Development* **129**, 455-66.

Evans a P. D., Anderson J. R., Vallender E. J., Gilbert S. L., Malcom C. M., Dorus S. and Lahn B. T. (2004) Adaptive evolution of ASPM, a major determinant of cerebral cortical size in humans. *Hum Mol Genet* **13**, 489-94.

Evans b P. D., Anderson J. R., Vallender E. J., Choi S. S. and Lahn B. T. (2004) Reconstructing the evolutionary history of microcephalin, a gene controlling human brain size. *Hum Mol Genet* **13**, 1139-45.

Evans P. D., Gilbert S. L., Mekel-Bobrov N., Vallender E. J., Anderson J. R., Vaez-Azizi L. M., Tishkoff S. A., Hudson R. R. and Lahn B. T. (2005) Microcephalin, a gene regulating brain size, continues to evolve adaptively in humans. *Science* **309**, 1717-20.

Evans P. D., Vallender E. J. and Lahn B. T. (2006) Molecular evolution of the brain size regulator genes CDK5RAP2 and CENPJ. *Gene* **375**, 75-9.

Eymin B., Sordet O., Droin N., Munsch B., Haugg M., Van de Craen M., Vandenabeele P. and Solary E. (1999) Caspase-induced proteolysis of the cyclin-dependent kinase inhibitor p27Kip1 mediates its anti-apoptotic activity. *Oncogene* **18**, 4839-47.

Fang L., Seki A. and Fang G. (2009) SKAP associates with kinetochores and promotes the metaphase-to-anaphase transition. *Cell Cycle* **8**, 2819-27.

Feng Y. and Walsh C. A. (2004) Mitotic spindle regulation by Nde1 controls cerebral cortical size. *Neuron* **44**, 279-93.

Fietz S. A. and Huttner W. B. (2010) Cortical progenitor expansion, self-renewal and neurogenesis-a polarized perspective. *Curr Opin Neurobiol* **21**, 23-35.

Finlay B. L. and Darlington R. B. (1995) Linked regularities in the development and evolution of mammalian brains. *Science* **268**, 1578-84.

Fish J. L., Dehay C., Kennedy H. and Huttner W. B. (2008) Making bigger brains-the evolution of neural-progenitor-cell division. *J Cell Sci* **121**, 2783-93.

Fish J. L., Kosodo Y., Enard W., Paabo S. and Huttner W. B. (2006) Aspm specifically maintains symmetric proliferative divisions of neuroepithelial cells. *Proc Natl Acad Sci U S A* **103**, 10438-43.

Fliegauf M., Benzing T. and Omran H. (2007) When cilia go bad: cilia defects and ciliopathies. *Nat Rev Mol Cell Biol* **8**, 880-93.

Flory M. R. and Davis T. N. (2003) The centrosomal proteins pericentrin and kendrin are encoded by alternatively spliced products of one gene. *Genomics* **82**, 401-5.

Flynn R. L. and Zou L. (2011) ATR: a master conductor of cellular responses to DNA replication stress. *Trends Biochem Sci* **36**, 133-40.

Fong K. W., Choi Y. K., Rattner J. B. and Qi R. Z. (2008) CDK5RAP2 is a pericentriolar protein that functions in centrosomal attachment of the gamma-tubulin ring complex. *Mol Biol Cell* **19**, 115-25.

Fong K. W., Hau S. Y., Kho Y. S., Jia Y., He L. and Qi R. Z. (2009) Interaction of CDK5RAP2 with EB1 to track growing microtubule tips and to regulate microtubule dynamics. *Mol Biol Cell* **20**, 3660-70.

Frost a V., Al-Mehairi S. and Sinclair A. J. (2001) Exploitation of a non-apoptotic caspase to regulate the abundance of the cdkI p27(KIP1) in transformed lymphoid cells. *Oncogene* **20**, 2737-48.

Frost b V., Delikat S., Al-Mehairi S. and Sinclair A. J. (2001) Regulation of p27KIP1 in Epstein-Barr virus-immortalized lymphoblastoid cell lines involves non-apoptotic caspase cleavage. *J Gen Virol* **82**, 3057-66.

Fuentealba L. C., Eivers E., Geissert D., Taelman V. and De Robertis E. M. (2008) Asymmetric mitosis: Unequal segregation of proteins destined for degradation. *Proc Natl Acad Sci U S A* **105**, 7732-7.

Fuller S. D., Gowen B. E., Reinsch S., Sawyer A., Buendia B., Wepf R. and Karsenti E. (1995) The core of the mammalian centriole contains gamma-tubulin. *Curr Biol* **5**, 1384-93.

Gaitanos T. N., Santamaria A., Jeyaprakash A. A., Wang B., Conti E. and Nigg E. A. (2009) Stable kinetochore-microtubule interactions depend on the Ska complex and its new component Ska3/C13Orf3. *EMBO J* **28**, 1442-52.

Gal J. S., Morozov Y. M., Ayoub A. E., Chatterjee M., Rakic P. and Haydar T. F. (2006) Molecular and morphological heterogeneity of neural precursors in the mouse neocortical proliferative zones. *J Neurosci* **26**, 1045-56.

Ganem N. J., Godinho S. A. and Pellman D. (2009) A mechanism linking extra centrosomes to chromosomal instability. *Nature* **460**, 278-82.

Garcia-Moreno F., Lopez-Mascaraque L. and De Carlos J. A. (2007) Origins and migratory routes of murine Cajal-Retzius cells. *J Comp Neurol* **500**, 419-32.

Gavvovidis I., Pohlmann C., Marchal J. A., Stumm M., Yamashita D., Hirano T., Schindler D., Neitzel H. and Trimborn M. (2010) MCPH1 patient cells exhibit delayed release from DNA damage-induced G 2/M checkpoint arrest. *Cell Cycle* **9**, 4893-9.

Giansanti M. G., Bucciarelli E., Bonaccorsi S. and Gatti M. (2008) Drosophila SPD-2 is an essential centriole component required for PCM recruitment and astral-microtubule nucleation. *Curr Biol* **18**, 303-9.

Giansanti M. G., Gatti M. and Bonaccorsi S. (2001) The role of centrosomes and astral microtubules during asymmetric division of Drosophila neuroblasts. *Development* **128**, 1137-45.

Gillingham A. K. and Munro S. (2000) The PACT domain, a conserved centrosomal targeting motif in the coiled-coil proteins AKAP450 and pericentrin. *EMBO Rep* **1**, 524-9.

Glickstein S. B., Monaghan J. A., Koeller H. B., Jones T. K. and Ross M. E. (2009) Cyclin D2 is critical for intermediate progenitor cell proliferation in the embryonic cortex. *J Neurosci* **29**, 9614-24.

Glotzer M., Murray A. W. and Kirschner M. W. (1991) Cyclin is degraded by the ubiquitin pathway. *Nature* **349**, 132-8.

Glover J. N., Williams R. S. and Lee M. S. (2004) Interactions between BRCT repeats and phosphoproteins: tangled up in two. *Trends Biochem Sci* **29**, 579-85.

Goetz S. C. and Anderson K. V. (2010) The primary cilium: a signalling centre during vertebrate development. *Nat Rev Genet* **11**, 331-44.

Gomez-Ferreria M. A., Rath U., Buster D. W., Chanda S. K., Caldwell J. S., Rines D. R. and Sharp D. J. (2007) Human Cep192 is required for mitotic centrosome and spindle assembly. *Curr Biol* **17**, 1960-6.

Gonczy P. (2008) Mechanisms of asymmetric cell division: flies and worms pave the way. *Nat Rev Mol Cell Biol* **9**, 355-66.

Gonzalez C., Saunders R. D., Casal J., Molina I., Carmena M., Ripoll P. and Glover D. M. (1990) Mutations at the asp locus of Drosophila lead to multiple free centrosomes in syncytial embryos, but restrict centrosome duplication in larval neuroblasts. *J Cell Sci* **96 (Pt 4)**, 605-16.

Goshima G., Wollman R., Goodwin S. S., Zhang N., Scholey J. M., Vale R. D. and Stuurman N. (2007) Genes required for mitotic spindle assembly in Drosophila S2 cells. *Science* **316**, 417-21.

Goto H., Kiyono T., Tomono Y., Kawajiri A., Urano T., Furukawa K., Nigg E. A. and Inagaki M. (2006) Complex formation of Plk1 and INCENP required for metaphase-anaphase transition. *Nat Cell Biol* **8**, 180-7.

Gotz M. and Huttner W. B. (2005) The cell biology of neurogenesis. *Nat Rev Mol Cell Biol* **6**, 777-88.

Graser S., Stierhof Y. D., Lavoie S. B., Gassner O. S., Lamla S., Le Clech M. and Nigg E. A. (2007a) Cep164, a novel centriole appendage protein required for primary cilium formation. *J Cell Biol* **179**, 321-30.

Graser S., Stierhof Y. D. and Nigg E. A. (2007b) Cep68 and Cep215 (Cdk5rap2) are required for centrosome cohesion. *J Cell Sci* **120**, 4321-31.

Gray N. S., Wodicka L., Thunnissen A. M., Norman T. C., Kwon S., Espinoza F. H., Morgan D. O., Barnes G., LeClerc S., Meijer L., Kim S. H., Lockhart D. J. and Schultz P. G. (1998) Exploiting chemical libraries, structure, and genomics in the search for kinase inhibitors. *Science* **281**, 533-8.

Griffith E., Walker S., Martin C. A., Vagnarelli P., Stiff T., Vernay B., Al Sanna N., Saggar A., Hamel B., Earnshaw W. C., Jeggo P. A., Jackson A. P. and O'Driscoll M. (2008) Mutations in pericentrin cause Seckel syndrome with defective ATR-dependent DNA damage signaling. *Nat Genet* **40**, 232-6.

Guernsey D. L., Jiang H., Hussin J., Arnold M., Bouyakdan K., Perry S., Babineau-Sturk T., Beis J., Dumas N., Evans S. C., Ferguson M., Matsuoka M., Macgillivray C., Nightingale M., Patry L., Rideout A. L., Thomas A., Orr A., Hoffmann I., Michaud J. L., Awadalla P., Meek D. C., Ludman M. and Samuels M. E. (2010) Mutations in centrosomal protein CEP152 in primary microcephaly families linked to MCPH4. *Am J Hum Genet* **87**, 40-51.

Guichard P., Chretien D., Marco S. and Tassin A. M. (2010) Procentriole assembly revealed by cryo-electron tomography. *EMBO J* **29**, 1565-72.

Gul A., Hassan M. J., Mahmood S., Chen W., Rahmani S., Naseer M. I., Dellefave L., Muhammad N., Rafiq M. A., Ansar M., Chishti M. S., Ali G., Siddique T. and Ahmad W. (2006) Genetic studies of autosomal recessive primary microcephaly in 33 Pakistani families: Novel sequence variants in ASPM gene. *Neurogenetics* **7**, 105-10.

Guo Z., Yikang S., Yoshida H., Mak T. W. and Zacksenhaus E. (2001) Inactivation of the retinoblastoma tumor suppressor induces apoptosis protease-activating factor-1 dependent and independent apoptotic pathways during embryogenesis. *Cancer Res* **61**, 8395-400.

Hagemann C., Anacker J., Gerngras S., Kuhnel S., Said H. M., Patel R., Kammerer U., Vordermark D., Roosen K. and Vince G. H. (2008) Expression analysis of the autosomal recessive primary microcephaly genes MCPH1 (microcephalin) and MCPH5 (ASPM, abnormal spindle-like, microcephaly associated) in human malignant gliomas. *Oncol Rep* **20**, 301-8.

Hall J. G., Flora C., Scott C. I., Jr., Pauli R. M. and Tanaka K. I. (2004) Majewski osteodysplastic primordial dwarfism type II (MOPD II): natural history and clinical findings. *Am J Med Genet A* **130A**, 55-72.

Han Y. G. and Alvarez-Buylla A. (2010) Role of primary cilia in brain development and cancer. *Curr Opin Neurobiol* **20**, 58-67.

Hanisch A., Sillje H. H. and Nigg E. A. (2006) Timely anaphase onset requires a novel spindle and kinetochore complex comprising Ska1 and Ska2. *EMBO J* **25**, 5504-15.

Hannak E., Kirkham M., Hyman A. A. and Oegema K. (2001) Aurora-A kinase is required for centrosome maturation in Caenorhabditis elegans. *J Cell Biol* **155**, 1109-16.

Haren L., Stearns T. and Luders J. (2009) Plk1-dependent recruitment of gamma-tubulin complexes to mitotic centrosomes involves multiple PCM components. *PLoS One* **4**, e5976.

Harper J. W. (2002) A phosphorylation-driven ubiquitination switch for cell-cycle control. *Trends Cell Biol* **12**, 104-7.

Hartfuss E., Forster E., Bock H. H., Hack M. A., Leprince P., Luque J. M., Herz J., Frotscher M. and Gotz M. (2003) Reelin signaling directly affects radial glia morphology and biochemical maturation. *Development* **130**, 4597-609.

Hatch E. M., Kulukian A., Holland A. J., Cleveland D. W. and Stearns T. (2010) Cep152 interacts with Plk4 and is required for centriole duplication. *J Cell Biol* **191**, 721-9.

Hauf S., Waizenegger I. C. and Peters J. M. (2001) Cohesin cleavage by separase required for anaphase and cytokinesis in human cells. *Science* **293**, 1320-3.

Haydar T. F., Ang E., Jr. and Rakic P. (2003) Mitotic spindle rotation and mode of cell division in the developing telencephalon. *Proc Natl Acad Sci U S A* **100**, 2890-5.

Haydar T. F., Kuan C. Y., Flavell R. A. and Rakic P. (1999) The role of cell death in regulating the size and shape of the mammalian forebrain. *Cereb Cortex* **9**, 621-6.

Higgins J., Midgley C., Bergh A. M., Bell S. M., Askham J. M., Roberts E., Binns R. K., Sharif S. M., Bennett C., Glover D. M., Woods C. G., Morrison E. E. and Bond J. (2010) Human ASPM participates in spindle organisation, spindle orientation and cytokinesis. *BMC Cell Biol* **11**, 85.

Hoffman D. B., Pearson C. G., Yen T. J., Howell B. J. and Salmon E. D. (2001) Microtubule-dependent changes in assembly of microtubule motor proteins and mitotic spindle checkpoint proteins at PtK1 kinetochores. *Mol Biol Cell* **12**, 1995-2009.

Howell B. J., McEwen B. F., Canman J. C., Hoffman D. B., Farrar E. M., Rieder C. L. and Salmon E. D. (2001) Cytoplasmic dynein/dynactin drives kinetochore protein transport to the spindle poles and has a role in mitotic spindle checkpoint inactivation. *J Cell Biol* **155**, 1159-72.

Hung L. Y., Chen H. L., Chang C. W., Li B. R. and Tang T. K. (2004) Identification of a novel microtubule-destabilizing motif in CPAP that binds to tubulin heterodimers and inhibits microtubule assembly. *Mol Biol Cell* **15**, 2697-706.

Hung L. Y., Tang C. J. and Tang T. K. (2000) Protein 4.1 R-135 interacts with a novel centrosomal protein (CPAP) which is associated with the gamma-tubulin complex. *Mol Cell Biol* **20**, 7813-25.

Hutchins J. R., Toyoda Y., Hegemann B., Poser I., Heriche J. K., Sykora M. M., Augsburg M., Hudecz O., Buschhorn B. A., Bulkescher J., Conrad C., Comartin D., Schleiffer A., Sarov M., Pozniakovsky A., Slabicki M. M., Schloissnig S., Steinmacher I., Leuschner M., Ssykor A., Lawo S., Pelletier L., Stark H., Nasmyth K., Ellenberg J., Durbin R., Buchholz F., Mechtler K.,

Hyman A. A. and Peters J. M. (2010) Systematic analysis of human protein complexes identifies chromosome segregation proteins. *Science* **328**, 593-9.
Huttner W. B. and Kosodo Y. (2005) Symmetric versus asymmetric cell division during neurogenesis in the developing vertebrate central nervous system. *Curr Opin Cell Biol* **17**, 648-57.
Huyton T., Bates P. A., Zhang X., Sternberg M. J. and Freemont P. S. (2000) The BRCA1 C-terminal domain: structure and function. *Mutat Res* **460**, 319-32.
Iacopetti P., Michelini M., Stuckmann I., Oback B., Aaku-Saraste E. and Huttner W. B. (1999) Expression of the antiproliferative gene TIS21 at the onset of neurogenesis identifies single neuroepithelial cells that switch from proliferative to neuron-generating division. *Proc Natl Acad Sci U S A* **96**, 4639-44.
Izraeli S., Lowe L. A., Bertness V. L., Campaner S., Hahn H., Kirsch I. R. and Kuehn M. R. (2001) Genetic evidence that Sil is required for the Sonic Hedgehog response pathway. *Genesis* **31**, 72-7.
Izraeli S., Lowe L. A., Bertness V. L., Good D. J., Dorward D. W., Kirsch I. R. and Kuehn M. R. (1999) The SIL gene is required for mouse embryonic axial development and left-right specification. *Nature* **399**, 691-4.
Jackson A. P., Eastwood H., Bell S. M., Adu J., Toomes C., Carr I. M., Roberts E., Hampshire D. J., Crow Y. J., Mighell A. J., Karbani G., Jafri H., Rashid Y., Mueller R. F., Markham A. F. and Woods C. G. (2002) Identification of microcephalin, a protein implicated in determining the size of the human brain. *Am J Hum Genet* **71**, 136-42.
Jackson A. P., McHale D. P., Campbell D. A., Jafri H., Rashid Y., Mannan J., Karbani G., Corry P., Levene M. I., Mueller R. F., Markham A. F., Lench N. J. and Woods C. G. (1998) Primary autosomal recessive microcephaly (MCPH1) maps to chromosome 8p22-pter. *Am J Hum Genet* **63**, 541-6.
Jakobsen L., Vanselow K., Skogs M., Toyoda Y., Lundberg E., Poser I., Falkenby L. G., Bennetzen M., Westendorf J., Nigg E. A., Uhlen M., Hyman A. A. and Andersen J. S. (2011) Novel asymmetrically localizing components of human centrosomes identified by complementary proteomics methods. *EMBO J* **30**, 1520-35.
Januschke J., Llamazares S., Reina J. and Gonzalez C. (2011) Drosophila neuroblasts retain the daughter centrosome. *Nat Commun* **2**, 243.
Jeffers L. J., Coull B. J., Stack S. J. and Morrison C. G. (2008) Distinct BRCT domains in Mcph1/Brit1 mediate ionizing radiation-induced focus formation and centrosomal localization. *Oncogene* **27**, 139-44.
Jerison H. J. (1973) *Evolution of the brain and intelligence*. Academic Press, New York.
Jin J., Shirogane T., Xu L., Nalepa G., Qin J., Elledge S. J. and Harper J. W. (2003) SCFbeta-TRCP links Chk1 signaling to degradation of the Cdc25A protein phosphatase. *Genes Dev* **17**, 3062-74.
Joannides A. J., Fiore-Heriche C., Battersby A. A., Athauda-Arachchi P., Bouhon I. A., Williams L., Westmore K., Kemp P. J., Compston A., Allen N. D. and Chandran S. (2007) A scaleable and defined system for generating neural stem cells from human embryonic stem cells. *Stem Cells* **25**, 731-7.

Kaindl A. M., Passemard S., Kumar P., Kraemer N., Issa L., Zwirner A., Gerard B., Verloes A., Mani S. and Gressens P. (2010) Many roads lead to primary autosomal recessive microcephaly. *Prog Neurobiol* **90**, 363-83.

Kalay E., Yigit G., Aslan Y., Brown K. E., Pohl E., Bicknell L. S., Kayserili H., Li Y., Tuysuz B., Nurnberg G., Kiess W., Koegl M., Baessmann I., Buruk K., Toraman B., Kayipmaz S., Kul S., Ikbal M., Turner D. J., Taylor M. S., Aerts J., Scott C., Milstein K., Dollfus H., Wieczorek D., Brunner H. G., Hurles M., Jackson A. P., Rauch A., Nurnberg P., Karaguzel A. and Wollnik B. (2010) CEP152 is a genome maintenance protein disrupted in Seckel syndrome. *Nat Genet* **43**, 23-6.

Kaltschmidt J. A., Davidson C. M., Brown N. H. and Brand A. H. (2000) Rotation and asymmetry of the mitotic spindle direct asymmetric cell division in the developing central nervous system. *Nat Cell Biol* **2**, 7-12.

Kaushal D., Contos J. J., Treuner K., Yang A. H., Kingsbury M. A., Rehen S. K., McConnell M. J., Okabe M., Barlow C. and Chun J. (2003) Alteration of gene expression by chromosome loss in the postnatal mouse brain. *J Neurosci* **23**, 5599-606.

Kemp C. A., Kopish K. R., Zipperlen P., Ahringer J. and O'Connell K. F. (2004) Centrosome maturation and duplication in C. elegans require the coiled-coil protein SPD-2. *Dev Cell* **6**, 511-23.

Khodjakov A. and Rieder C. L. (1999) The sudden recruitment of gamma-tubulin to the centrosome at the onset of mitosis and its dynamic exchange throughout the cell cycle, do not require microtubules. *J Cell Biol* **146**, 585-96.

Kim H., Lee O. H., Xin H., Chen L. Y., Qin J., Chae H. K., Lin S. Y., Safari A., Liu D. and Songyang Z. (2009) TRF2 functions as a protein hub and regulates telomere maintenance by recognizing specific peptide motifs. *Nat Struct Mol Biol* **16**, 372-9.

Kim H. S., Takahashi M., Matsuo K. and Ono Y. (2007) Recruitment of CG-NAP to the Golgi apparatus through interaction with dynein-dynactin complex. *Genes Cells* **12**, 421-34.

Kim S., Zaghloul N. A., Bubenshchikova E., Oh E. C., Rankin S., Katsanis N., Obara T. and Tsiokas L. (2011) Nde1-mediated inhibition of ciliogenesis affects cell cycle re-entry. *Nat Cell Biol* **13**, 351-60.

King R. W., Glotzer M. and Kirschner M. W. (1996) Mutagenic analysis of the destruction signal of mitotic cyclins and structural characterization of ubiquitinated intermediates. *Mol Biol Cell* **7**, 1343-57.

King R. W., Peters J. M., Tugendreich S., Rolfe M., Hieter P. and Kirschner M. W. (1995) A 20S complex containing CDC27 and CDC16 catalyzes the mitosis-specific conjugation of ubiquitin to cyclin B. *Cell* **81**, 279-88.

Kirkham M., Muller-Reichert T., Oegema K., Grill S. and Hyman A. A. (2003) SAS-4 is a C. elegans centriolar protein that controls centrosome size. *Cell* **112**, 575-87.

Kitajima T. S., Hauf S., Ohsugi M., Yamamoto T. and Watanabe Y. (2005) Human Bub1 defines the persistent cohesion site along the mitotic chromosome by affecting Shugoshin localization. *Curr Biol* **15**, 353-9.

Kitajima T. S., Sakuno T., Ishiguro K., Iemura S., Natsume T., Kawashima S. A. and Watanabe Y. (2006) Shugoshin collaborates with protein phosphatase 2A to protect cohesin. *Nature* **441**, 46-52.

Kittler R., Pelletier L., Ma C., Poser I., Fischer S., Hyman A. A. and Buchholz F. (2005) RNA interference rescue by bacterial artificial chromosome transgenesis in mammalian tissue culture cells. *Proc Natl Acad Sci U S A* **102**, 2396-401.

Kleylein-Sohn J., Westendorf J., Le Clech M., Habedanck R., Stierhof Y. D. and Nigg E. A. (2007) Plk4-induced centriole biogenesis in human cells. *Dev Cell* **13**, 190-202.

Kline S. L., Cheeseman I. M., Hori T., Fukagawa T. and Desai A. (2006) The human Mis12 complex is required for kinetochore assembly and proper chromosome segregation. *J Cell Biol* **173**, 9-17.

Knoblich J. A. (2010) Asymmetric cell division: recent developments and their implications for tumour biology. *Nat Rev Mol Cell Biol* **11**, 849-60.

Kohlmaier G., Loncarek J., Meng X., McEwen B. F., Mogensen M. M., Spektor A., Dynlacht B. D., Khodjakov A. and Gonczy P. (2009) Overly long centrioles and defective cell division upon excess of the SAS-4-related protein CPAP. *Curr Biol* **19**, 1012-8.

Komai T., Kishimoto K. and Ozaki Y. (1955) Genetic study of microcephaly based on Japanese material. *Am J Hum Genet* **7**, 51-65.

Konno D., Shioi G., Shitamukai A., Mori A., Kiyonari H., Miyata T. and Matsuzaki F. (2008) Neuroepithelial progenitors undergo LGN-dependent planar divisions to maintain self-renewability during mammalian neurogenesis. *Nat Cell Biol* **10**, 93-101.

Kosodo Y., Roper K., Haubensak W., Marzesco A. M., Corbeil D. and Huttner W. B. (2004) Asymmetric distribution of the apical plasma membrane during neurogenic divisions of mammalian neuroepithelial cells. *EMBO J* **23**, 2314-24.

Kouprina N., Pavlicek A., Mochida G. H., Solomon G., Gersch W., Yoon Y. H., Collura R., Ruvolo M., Barrett J. C., Woods C. G., Walsh C. A., Jurka J. and Larionov V. (2004) Accelerated evolution of the ASPM gene controlling brain size begins prior to human brain expansion. *PLoS Biol* **2**, E126.

Kramer A., Mailand N., Lukas C., Syljuasen R. G., Wilkinson C. J., Nigg E. A., Bartek J. and Lukas J. (2004) Centrosome-associated Chk1 prevents premature activation of cyclin-B-Cdk1 kinase. *Nat Cell Biol* **6**, 884-91.

Kramer E. R., Scheuringer N., Podtelejnikov A. V., Mann M. and Peters J. M. (2000) Mitotic regulation of the APC activator proteins CDC20 and CDH1. *Mol Biol Cell* **11**, 1555-69.

Kuida K., Haydar T. F., Kuan C. Y., Gu Y., Taya C., Karasuyama H., Su M. S., Rakic P. and Flavell R. A. (1998) Reduced apoptosis and cytochrome c-mediated caspase activation in mice lacking caspase 9. *Cell* **94**, 325-37.

Kuida K., Zheng T. S., Na S., Kuan C., Yang D., Karasuyama H., Rakic P. and Flavell R. A. (1996) Decreased apoptosis in the brain and premature lethality in CPP32-deficient mice. *Nature* **384**, 368-72.

Kumar A., Blanton S. H., Babu M., Markandaya M. and Girimaji S. C. (2004) Genetic analysis of primary microcephaly in Indian families: novel ASPM mutations. *Clin Genet* **66**, 341-8.

Kumar A., Commane M., Flickinger T. W., Horvath C. M. and Stark G. R. (1997) Defective TNF-alpha-induced apoptosis in STAT1-null cells due to low constitutive levels of caspases. *Science* **278**, 1630-2.

Kumar A., Girimaji S. C., Duvvari M. R. and Blanton S. H. (2009) Mutations in STIL, encoding a pericentriolar and centrosomal protein, cause primary microcephaly. *Am J Hum Genet* **84**, 286-90.
Kuriyama R. and Borisy G. G. (1981) Centriole cycle in Chinese hamster ovary cells as determined by whole-mount electron microscopy. *J Cell Biol* **91**, 814-21.
Lamkanfi M., Festjens N., Declercq W., Vanden Berghe T. and Vandenabeele P. (2007) Caspases in cell survival, proliferation and differentiation. *Cell Death Differ* **14**, 44-55.
Lampson M. A. and Kapoor T. M. (2005) The human mitotic checkpoint protein BubR1 regulates chromosome-spindle attachments. *Nat Cell Biol* **7**, 93-8.
Landrieu P. and Goffinet A. (1979) Mitotic spindle fiber orientation in relation to cell migration in the neo-cortex of normal and reeler mouse. *Neurosci Lett* **13**, 69-72.
Lane H. A. and Nigg E. A. (1996) Antibody microinjection reveals an essential role for human polo-like kinase 1 (Plk1) in the functional maturation of mitotic centrosomes. *J Cell Biol* **135**, 1701-13.
Lange C., Huttner W. B. and Calegari F. (2009) Cdk4/cyclinD1 overexpression in neural stem cells shortens G1, delays neurogenesis, and promotes the generation and expansion of basal progenitors. *Cell Stem Cell* **5**, 320-31.
Lavin M. F. (2007) ATM and the Mre11 complex combine to recognize and signal DNA double-strand breaks. *Oncogene* **26**, 7749-58.
Lee D. H. and Goldberg A. L. (1998) Proteasome inhibitors: valuable new tools for cell biologists. *Trends Cell Biol* **8**, 397-403.
Lee J. E. and Gleeson J. G. (2011) Cilia in the nervous system: linking cilia function and neurodevelopmental disorders. *Curr Opin Neurol* **24**, 98-105.
Leidel S., Delattre M., Cerutti L., Baumer K. and Gonczy P. (2005) SAS-6 defines a protein family required for centrosome duplication in C. elegans and in human cells. *Nat Cell Biol* **7**, 115-25.
Leidel S. and Gonczy P. (2003) SAS-4 is essential for centrosome duplication in C elegans and is recruited to daughter centrioles once per cell cycle. *Dev Cell* **4**, 431-9.
Lenart P., Petronczki M., Steegmaier M., Di Fiore B., Lipp J. J., Hoffmann M., Rettig W. J., Kraut N. and Peters J. M. (2007) The small-molecule inhibitor BI 2536 reveals novel insights into mitotic roles of polo-like kinase 1. *Curr Biol* **17**, 304-15.
Lesage B., Gutierrez I., Marti E. and Gonzalez C. (2010) Neural stem cells: the need for a proper orientation. *Curr Opin Genet Dev* **20**, 438-42.
Leung J. W., Leitch A., Wood J. L., Shaw-Smith C., Metcalfe K., Bicknell L. S., Jackson A. P. and Chen J. (2011) Set protein associates with microcephalin/MCPH1 and regulates chromosome condensation. *J Biol Chem*.
Levkau B., Koyama H., Raines E. W., Clurman B. E., Herren B., Orth K., Roberts J. M. and Ross R. (1998) Cleavage of p21Cip1/Waf1 and p27Kip1 mediates apoptosis in endothelial cells through activation of Cdk2: role of a caspase cascade. *Mol Cell* **1**, 553-63.
Li A., Saito M., Chuang J. Z., Tseng Y. Y., Dedesma C., Tomizawa K., Kaitsuka T. and Sung C. H. (2011) Ciliary transition zone activation of phosphorylated

Tctex-1 controls ciliary resorption, S-phase entry and fate of neural progenitors. *Nat Cell Biol* **13**, 402-11.
Li L. and Zou L. (2005) Sensing, signaling, and responding to DNA damage: organization of the checkpoint pathways in mammalian cells. *J Cell Biochem* **94**, 298-306.
Li Q., Hansen D., Killilea A., Joshi H. C., Palazzo R. E. and Balczon R. (2001) Kendrin/pericentrin-B, a centrosome protein with homology to pericentrin that complexes with PCM-1. *J Cell Sci* **114**, 797-809.
Liang Y., Gao H., Lin S. Y., Peng G., Huang X., Zhang P., Goss J. A., Brunicardi F. C., Multani A. S., Chang S. and Li K. (2010) BRIT1/MCPH1 is essential for mitotic and meiotic recombination DNA repair and maintaining genomic stability in mice. *PLoS Genet* **6**, e1000826.
Lin S. Y., Rai R., Li K., Xu Z. X. and Elledge S. J. (2005) BRIT1/MCPH1 is a DNA damage responsive protein that regulates the Brca1-Chk1 pathway, implicating checkpoint dysfunction in microcephaly. *Proc Natl Acad Sci U S A* **102**, 15105-9.
Lindon C. and Pines J. (2004) Ordered proteolysis in anaphase inactivates Plk1 to contribute to proper mitotic exit in human cells. *J Cell Biol* **164**, 233-41.
Littlepage L. E. and Ruderman J. V. (2002) Identification of a new APC/C recognition domain, the A box, which is required for the Cdh1-dependent destruction of the kinase Aurora-A during mitotic exit. *Genes Dev* **16**, 2274-85.
Liu Q., Guntuku S., Cui X. S., Matsuoka S., Cortez D., Tamai K., Luo G., Carattini-Rivera S., DeMayo F., Bradley A., Donehower L. A. and Elledge S. J. (2000) Chk1 is an essential kinase that is regulated by Atr and required for the G(2)/M DNA damage checkpoint. *Genes Dev* **14**, 1448-59.
Livak K. J. and Schmittgen T. D. (2001) Analysis of relative gene expression data using real-time quantitative PCR and the 2(-Delta Delta C(T)) Method. *Methods* **25**, 402-8.
Lizarraga S. B., Margossian S. P., Harris M. H., Campagna D. R., Han A. P., Blevins S., Mudbhary R., Barker J. E., Walsh C. A. and Fleming M. D. (2010) Cdk5rap2 regulates centrosome function and chromosome segregation in neuronal progenitors. *Development* **137**, 1907-17.
Loncarek J., Hergert P., Magidson V. and Khodjakov A. (2008) Control of daughter centriole formation by the pericentriolar material. *Nat Cell Biol* **10**, 322-8.
Loncarek J. and Khodjakov A. (2009) Ab ovo or de novo? Mechanisms of centriole duplication. *Mol Cells* **27**, 135-42.
Los M., Stroh C., Janicke R. U., Engels I. H. and Schulze-Osthoff K. (2001) Caspases: more than just killers? *Trends Immunol* **22**, 31-4.
Louvi A. and Grove E. A. (2011) Cilia in the CNS: the quiet organelle claims center stage. *Neuron* **69**, 1046-60.
Lucas E. P. and Raff J. W. (2007) Maintaining the proper connection between the centrioles and the pericentriolar matrix requires Drosophila centrosomin. *J Cell Biol* **178**, 725-32.
Luders J. and Stearns T. (2007) Microtubule-organizing centres: a re-evaluation. *Nat Rev Mol Cell Biol* **8**, 161-7.

Lukaszewicz A., Savatier P., Cortay V., Kennedy H. and Dehay C. (2002) Contrasting effects of basic fibroblast growth factor and neurotrophin 3 on cell cycle kinetics of mouse cortical stem cells. *J Neurosci* **22**, 6610-22.
Mack G. J. and Compton D. A. (2001) Analysis of mitotic microtubule-associated proteins using mass spectrometry identifies astrin, a spindle-associated protein. *Proc Natl Acad Sci U S A* **98**, 14434-9.
MacPhail E. M. (1982) *Brain and intelligence in vertebrates*. Clarendon Press
Oxford University Press, Oxford
New York.
Macville M., Schrock E., Padilla-Nash H., Keck C., Ghadimi B. M., Zimonjic D., Popescu N. and Ried T. (1999) Comprehensive and definitive molecular cytogenetic characterization of HeLa cells by spectral karyotyping. *Cancer Res* **59**, 141-50.
Maiato H., DeLuca J., Salmon E. D. and Earnshaw W. C. (2004) The dynamic kinetochore-microtubule interface. *J Cell Sci* **117**, 5461-77.
Majewski F. and Goecke T. (1982) Studies of microcephalic primordial dwarfism I: approach to a delineation of the Seckel syndrome. *Am J Med Genet* **12**, 7-21.
Majka J., Binz S. K., Wold M. S. and Burgers P. M. (2006) Replication protein A directs loading of the DNA damage checkpoint clamp to 5'-DNA junctions. *J Biol Chem* **281**, 27855-61.
Malik R., Lenobel R., Santamaria A., Ries A., Nigg E. A. and Korner R. (2009) Quantitative analysis of the human spindle phosphoproteome at distinct mitotic stages. *J Proteome Res* **8**, 4553-63.
Malureanu L., Jeganathan K. B., Jin F., Baker D. J., van Ree J. H., Gullon O., Chen Z., Henley J. R. and van Deursen J. M. (2010) Cdc20 hypomorphic mice fail to counteract de novo synthesis of cyclin B1 in mitosis. *J Cell Biol* **191**, 313-29.
Manke I. A., Lowery D. M., Nguyen A. and Yaffe M. B. (2003) BRCT repeats as phosphopeptide-binding modules involved in protein targeting. *Science* **302**, 636-9.
Manning A. L., Bakhoum S. F., Maffini S., Correia-Melo C., Maiato H. and Compton D. A. (2010) CLASP1, astrin and Kif2b form a molecular switch that regulates kinetochore-microtubule dynamics to promote mitotic progression and fidelity. *EMBO J* **29**, 3531-43.
Marshall W. F. (2009) Centriole evolution. *Curr Opin Cell Biol* **21**, 14-9.
Marthiens V. and ffrench-Constant C. (2009) Adherens junction domains are split by asymmetric division of embryonic neural stem cells. *EMBO Rep* **10**, 515-20.
Martinez-Campos M., Basto R., Baker J., Kernan M. and Raff J. W. (2004) The Drosophila pericentrin-like protein is essential for cilia/flagella function, but appears to be dispensable for mitosis. *J Cell Biol* **165**, 673-83.
Matsusaka T. and Pines J. (2004) Chfr acts with the p38 stress kinases to block entry to mitosis in mammalian cells. *J Cell Biol* **166**, 507-16.
Matsuyama M., Goto H., Kasahara K., Kawakami Y., Nakanishi M., Kiyono T., Goshima N. and Inagaki M. (2011) Nuclear Chk1 prevents premature mitotic entry. *J Cell Sci* **124**, 2113-9.
McConnell M. J., Kaushal D., Yang A. H., Kingsbury M. A., Rehen S. K., Treuner K., Helton R., Annas E. G., Chun J. and Barlow C. (2004) Failed clearance of aneuploid embryonic neural progenitor cells leads to excess aneuploidy in the

Atm-deficient but not the Trp53-deficient adult cerebral cortex. *J Neurosci* **24**, 8090-6.
McCreary B. D., Rossiter J. P. and Robertson D. M. (1996) Recessive (true) microcephaly: a case report with neuropathological observations. *J Intellect Disabil Res* **40 (Pt 1)**, 66-70.
McGuinness B. E., Hirota T., Kudo N. R., Peters J. M. and Nasmyth K. (2005) Shugoshin prevents dissociation of cohesin from centromeres during mitosis in vertebrate cells. *PLoS Biol* **3**, e86.
Megraw T. L., Li K., Kao L. R. and Kaufman T. C. (1999) The centrosomin protein is required for centrosome assembly and function during cleavage in Drosophila. *Development* **126**, 2829-39.
Megraw T. L., Sharkey J. T. and Nowakowski R. S. (2011) Cdk5rap2 exposes the centrosomal root of microcephaly syndromes. *Trends Cell Biol*.
Meijer L., Borgne A., Mulner O., Chong J. P., Blow J. J., Inagaki N., Inagaki M., Delcros J. G. and Moulinoux J. P. (1997) Biochemical and cellular effects of roscovitine, a potent and selective inhibitor of the cyclin-dependent kinases cdc2, cdk2 and cdk5. *Eur J Biochem* **243**, 527-36.
Mekel-Bobrov N., Gilbert S. L., Evans P. D., Vallender E. J., Anderson J. R., Hudson R. R., Tishkoff S. A. and Lahn B. T. (2005) Ongoing adaptive evolution of ASPM, a brain size determinant in Homo sapiens. *Science* **309**, 1720-2.
Mekel-Bobrov N., Posthuma D., Gilbert S. L., Lind P., Gosso M. F., Luciano M., Harris S. E., Bates T. C., Polderman T. J., Whalley L. J., Fox H., Starr J. M., Evans P. D., Montgomery G. W., Fernandes C., Heutink P., Martin N. G., Boomsma D. I., Deary I. J., Wright M. J., de Geus E. J. and Lahn B. T. (2007) The ongoing adaptive evolution of ASPM and Microcephalin is not explained by increased intelligence. *Hum Mol Genet* **16**, 600-8.
Meraldi P., Draviam V. M. and Sorger P. K. (2004) Timing and checkpoints in the regulation of mitotic progression. *Dev Cell* **7**, 45-60.
Meraldi P., Honda R. and Nigg E. A. (2002) Aurora-A overexpression reveals tetraploidization as a major route to centrosome amplification in p53-/- cells. *EMBO J* **21**, 483-92.
Merdes A., Ramyar K., Vechio J. D. and Cleveland D. W. (1996) A complex of NuMA and cytoplasmic dynein is essential for mitotic spindle assembly. *Cell* **87**, 447-58.
Miyoshi K., Asanuma M., Miyazaki I., Matsuzaki S., Tohyama M. and Ogawa N. (2006) Characterization of pericentrin isoforms in vivo. *Biochem Biophys Res Commun* **351**, 745-9.
Morales-Mulia S. and Scholey J. M. (2005) Spindle pole organization in Drosophila S2 cells by dynein, abnormal spindle protein (Asp), and KLP10A. *Mol Biol Cell* **16**, 3176-86.
Morin X., Jaouen F. and Durbec P. (2007) Control of planar divisions by the G-protein regulator LGN maintains progenitors in the chick neuroepithelium. *Nat Neurosci* **10**, 1440-8.
Morrison A. J., Highland J., Krogan N. J., Arbel-Eden A., Greenblatt J. F., Haber J. E. and Shen X. (2004) INO80 and gamma-H2AX interaction links ATP-dependent chromatin remodeling to DNA damage repair. *Cell* **119**, 767-75.

Mueller P. R., Coleman T. R., Kumagai A. and Dunphy W. G. (1995) Myt1: a membrane-associated inhibitory kinase that phosphorylates Cdc2 on both threonine-14 and tyrosine-15. *Science* **270**, 86-90.

Muhammad F., Mahmood Baig S., Hansen L., Sajid Hussain M., Anjum Inayat I., Aslam M., Anver Qureshi J., Toilat M., Kirst E., Wajid M., Nurnberg P., Eiberg H., Tommerup N. and Kjaer K. W. (2009) Compound heterozygous ASPM mutations in Pakistani MCPH families. *Am J Med Genet A* **149A**, 926-30.

Musacchio A. and Salmon E. D. (2007) The spindle-assembly checkpoint in space and time. *Nat Rev Mol Cell Biol* **8**, 379-93.

Nash H. A. (1981) Integration and excision of bacteriophage lambda: the mechanism of conservation site specific recombination. *Annu Rev Genet* **15**, 143-67.

Nasmyth K. and Haering C. H. (2005) The structure and function of SMC and kleisin complexes. *Annu Rev Biochem* **74**, 595-648.

Neitzel H., Neumann L. M., Schindler D., Wirges A., Tonnies H., Trimborn M., Krebsova A., Richter R. and Sperling K. (2002) Premature chromosome condensation in humans associated with microcephaly and mental retardation: a novel autosomal recessive condition. *Am J Hum Genet* **70**, 1015-22.

Nicholas A. K., Khurshid M., Desir J., Carvalho O. P., Cox J. J., Thornton G., Kausar R., Ansar M., Ahmad W., Verloes A., Passemard S., Misson J. P., Lindsay S., Gergely F., Dobyns W. B., Roberts E., Abramowicz M. and Woods C. G. (2010) WDR62 is associated with the spindle pole and is mutated in human microcephaly. *Nat Genet* **42**, 1010-4.

Nicholas A. K., Swanson E. A., Cox J. J., Karbani G., Malik S., Springell K., Hampshire D., Ahmed M., Bond J., Di Benedetto D., Fichera M., Romano C., Dobyns W. B. and Woods C. G. (2009) The molecular landscape of ASPM mutations in primary microcephaly. *J Med Genet* **46**, 249-53.

Nicholson P. and Muhlemann O. (2010) Cutting the nonsense: the degradation of PTC-containing mRNAs. *Biochem Soc Trans* **38**, 1615-20.

Nilsson J., Yekezare M., Minshull J. and Pines J. (2008) The APC/C maintains the spindle assembly checkpoint by targeting Cdc20 for destruction. *Nat Cell Biol* **10**, 1411-20.

Noctor S. C., Flint A. C., Weissman T. A., Wong W. S., Clinton B. K. and Kriegstein A. R. (2002) Dividing precursor cells of the embryonic cortical ventricular zone have morphological and molecular characteristics of radial glia. *J Neurosci* **22**, 3161-73.

Northcutt R. G. and Kaas J. H. (1995) The emergence and evolution of mammalian neocortex. *Trends Neurosci* **18**, 373-9.

Nousiainen M., Sillje H. H., Sauer G., Nigg E. A. and Korner R. (2006) Phosphoproteome analysis of the human mitotic spindle. *Proc Natl Acad Sci U S A* **103**, 5391-6.

Nowakovski R. S. and Hayes N. L. (2005) Cell Proliferation in the Developing Mammalian Brain. In *In: Developmental neurobiology* (Edited by Rao M. S. and Jacobson M.). Kluwer Academic/Plenum, New York

O'Connell K. F., Caron C., Kopish K. R., Hurd D. D., Kemphues K. J., Li Y. and White J. G. (2001) The C. elegans zyg-1 gene encodes a regulator of

centrosome duplication with distinct maternal and paternal roles in the embryo. *Cell* **105**, 547-58.
O'Driscoll M., Ruiz-Perez V. L., Woods C. G., Jeggo P. A. and Goodship J. A. (2003) A splicing mutation affecting expression of ataxia-telangiectasia and Rad3-related protein (ATR) results in Seckel syndrome. *Nat Genet* **33**, 497-501.
Oakley B. R., Oakley C. E., Yoon Y. and Jung M. K. (1990) Gamma-tubulin is a component of the spindle pole body that is essential for microtubule function in Aspergillus nidulans. *Cell* **61**, 1289-301.
Oakley C. E. and Oakley B. R. (1989) Identification of gamma-tubulin, a new member of the tubulin superfamily encoded by mipA gene of Aspergillus nidulans. *Nature* **338**, 662-4.
Obuse C., Iwasaki O., Kiyomitsu T., Goshima G., Toyoda Y. and Yanagida M. (2004) A conserved Mis12 centromere complex is linked to heterochromatic HP1 and outer kinetochore protein Zwint-1. *Nat Cell Biol* **6**, 1135-41.
Olsen J. V., Vermeulen M., Santamaria A., Kumar C., Miller M. L., Jensen L. J., Gnad F., Cox J., Jensen T. S., Nigg E. A., Brunak S. and Mann M. (2010) Quantitative phosphoproteomics reveals widespread full phosphorylation site occupancy during mitosis. *Sci Signal* **3**, ra3.
Oshimori N., Ohsugi M. and Yamamoto T. (2006) The Plk1 target Kizuna stabilizes mitotic centrosomes to ensure spindle bipolarity. *Nat Cell Biol* **8**, 1095-101.
Palazzo R. E., Vogel J. M., Schnackenberg B. J., Hull D. R. and Wu X. (2000) Centrosome maturation. *Curr Top Dev Biol* **49**, 449-70.
Pan J. and Snell W. (2007) The primary cilium: keeper of the key to cell division. *Cell* **129**, 1255-7.
Pardo B., Gomez-Gonzalez B. and Aguilera A. (2009) DNA repair in mammalian cells: DNA double-strand break repair: how to fix a broken relationship. *Cell Mol Life Sci* **66**, 1039-56.
Park I. H., Arora N., Huo H., Maherali N., Ahfeldt T., Shimamura A., Lensch M. W., Cowan C., Hochedlinger K. and Daley G. Q. (2008) Disease-specific induced pluripotent stem cells. *Cell* **134**, 877-86.
Parker L. L. and Piwnica-Worms H. (1992) Inactivation of the p34cdc2-cyclin B complex by the human WEE1 tyrosine kinase. *Science* **257**, 1955-7.
Passemard S., Titomanlio L., Elmaleh M., Afenjar A., Alessandri J. L., Andria G., de Villemeur T. B., Boespflug-Tanguy O., Burglen L., Del Giudice E., Guimiot F., Hyon C., Isidor B., Megarbane A., Moog U., Odent S., Hernandez K., Pouvreau N., Scala I., Schaer M., Gressens P., Gerard B. and Verloes A. (2009) Expanding the clinical and neuroradiologic phenotype of primary microcephaly due to ASPM mutations. *Neurology* **73**, 962-9.
Pelletier L., O'Toole E., Schwager A., Hyman A. A. and Muller-Reichert T. (2006) Centriole assembly in Caenorhabditis elegans. *Nature* **444**, 619-23.
Pelletier L., Ozlu N., Hannak E., Cowan C., Habermann B., Ruer M., Muller-Reichert T. and Hyman A. A. (2004) The Caenorhabditis elegans centrosomal protein SPD-2 is required for both pericentriolar material recruitment and centriole duplication. *Curr Biol* **14**, 863-73.
Pellman D. (2007) Cell biology: aneuploidy and cancer. *Nature* **446**, 38-9.

Peng G., Yim E. K., Dai H., Jackson A. P., Burgt I., Pan M. R., Hu R., Li K. and Lin S. Y. (2009) BRIT1/MCPH1 links chromatin remodelling to DNA damage response. *Nat Cell Biol* **11**, 865-72.

Peters J. M., Tedeschi A. and Schmitz J. (2008) The cohesin complex and its roles in chromosome biology. *Genes Dev* **22**, 3089-114.

Petersen B. O., Wagener C., Marinoni F., Kramer E. R., Melixetian M., Lazzerini Denchi E., Gieffers C., Matteucci C., Peters J. M. and Helin K. (2000) Cell cycle- and cell growth-regulated proteolysis of mammalian CDC6 is dependent on APC-CDH1. *Genes Dev* **14**, 2330-43.

Pfaff K. L., Straub C. T., Chiang K., Bear D. M., Zhou Y. and Zon L. I. (2007) The zebra fish cassiopeia mutant reveals that SIL is required for mitotic spindle organization. *Mol Cell Biol* **27**, 5887-97.

Pfleger C. M. and Kirschner M. W. (2000) The KEN box: an APC recognition signal distinct from the D box targeted by Cdh1. *Genes Dev* **14**, 655-65.

Pilaz L. J., Patti D., Marcy G., Ollier E., Pfister S., Douglas R. J., Betizeau M., Gautier E., Cortay V., Doerflinger N., Kennedy H. and Dehay C. (2009) Forced G1-phase reduction alters mode of division, neuron number, and laminar phenotype in the cerebral cortex. *Proc Natl Acad Sci U S A* **106**, 21924-9.

Pines J. (2006) Mitosis: a matter of getting rid of the right protein at the right time. *Trends Cell Biol* **16**, 55-63.

Pinsky B. A., Nelson C. R. and Biggins S. (2009) Protein phosphatase 1 regulates exit from the spindle checkpoint in budding yeast. *Curr Biol* **19**, 1182-7.

Potapova T. A., Daum J. R., Pittman B. D., Hudson J. R., Jones T. N., Satinover D. L., Stukenberg P. T. and Gorbsky G. J. (2006) The reversibility of mitotic exit in vertebrate cells. *Nature* **440**, 954-8.

Przewloka M. R. and Glover D. M. (2009) The kinetochore and the centromere: a working long distance relationship. *Annu Rev Genet* **43**, 439-65.

Pulvers J. N., Bryk J., Fish J. L., Wilsch-Brauninger M., Arai Y., Schreier D., Naumann R., Helppi J., Habermann B., Vogt J., Nitsch R., Toth A., Enard W., Paabo S. and Huttner W. B. (2010) Mutations in mouse Aspm (abnormal spindle-like microcephaly associated) cause not only microcephaly but also major defects in the germline. *Proc Natl Acad Sci U S A* **107**, 16595-600.

Qazi Q. H. and Reed T. E. (1973) A problem in diagnosis of primary versus secondary microcephaly. *Clin Genet* **4**, 46-52.

Qi W., Tang Z. and Yu H. (2006) Phosphorylation- and polo-box-dependent binding of Plk1 to Bub1 is required for the kinetochore localization of Plk1. *Mol Biol Cell* **17**, 3705-16.

Raaijmakers J. A., Tanenbaum M. E., Maia A. F. and Medema R. H. (2009) RAMA1 is a novel kinetochore protein involved in kinetochore-microtubule attachment. *J Cell Sci* **122**, 2436-45.

Radakovits R., Barros C. S., Belvindrah R., Patton B. and Muller U. (2009) Regulation of radial glial survival by signals from the meninges. *J Neurosci* **29**, 7694-705.

Rai R., Dai H., Multani A. S., Li K., Chin K., Gray J., Lahad J. P., Liang J., Mills G. B., Meric-Bernstam F. and Lin S. Y. (2006) BRIT1 regulates early DNA damage response, chromosomal integrity, and cancer. *Cancer Cell* **10**, 145-57.

Rai R., Phadnis A., Haralkar S., Badwe R. A., Dai H., Li K. and Lin S. Y. (2008) Differential regulation of centrosome integrity by DNA damage response proteins. *Cell Cycle* **7**, 2225-33.
Rakic P. (1974) Neurons in rhesus monkey visual cortex: systematic relation between time of origin and eventual disposition. *Science* **183**, 425-7.
Rakic P. (1988) Specification of cerebral cortical areas. *Science* **241**, 170-6.
Rakic P. (1995) A small step for the cell, a giant leap for mankind: a hypothesis of neocortical expansion during evolution. *Trends Neurosci* **18**, 383-8.
Rakic P. (2009) Evolution of the neocortex: a perspective from developmental biology. *Nat Rev Neurosci* **10**, 724-35.
Ramaswamy S., Ross K. N., Lander E. S. and Golub T. R. (2003) A molecular signature of metastasis in primary solid tumors. *Nat Genet* **33**, 49-54.
Rao X., Zhang Y., Yi Q., Hou H., Xu B., Chu L., Huang Y., Zhang W., Fenech M. and Shi Q. (2008) Multiple origins of spontaneously arising micronuclei in HeLa cells: direct evidence from long-term live cell imaging. *Mutat Res* **646**, 41-9.
Rapley J., Baxter J. E., Blot J., Wattam S. L., Casenghi M., Meraldi P., Nigg E. A. and Fry A. M. (2005) Coordinate regulation of the mother centriole component nlp by nek2 and plk1 protein kinases. *Mol Cell Biol* **25**, 1309-24.
Rappaport R. (1996) *Cytokinesis in animal cells*. Cambridge University Press, Cambridge.
Rebollo E., Sampaio P., Januschke J., Llamazares S., Varmark H. and Gonzalez C. (2007) Functionally unequal centrosomes drive spindle orientation in asymmetrically dividing Drosophila neural stem cells. *Dev Cell* **12**, 467-74.
Rehen S. K., McConnell M. J., Kaushal D., Kingsbury M. A., Yang A. H. and Chun J. (2001) Chromosomal variation in neurons of the developing and adult mammalian nervous system. *Proc Natl Acad Sci U S A* **98**, 13361-6.
Rehen S. K., Yung Y. C., McCreight M. P., Kaushal D., Yang A. H., Almeida B. S., Kingsbury M. A., Cabral K. M., McConnell M. J., Anliker B., Fontanoz M. and Chun J. (2005) Constitutional aneuploidy in the normal human brain. *J Neurosci* **25**, 2176-80.
Richards M. W., Leung J. W., Roe S. M., Li K., Chen J. and Bayliss R. (2010) A pocket on the surface of the N-terminal BRCT domain of Mcph1 is required to prevent abnormal chromosome condensation. *J Mol Biol* **395**, 908-15.
Rickmyre J. L., Dasgupta S., Ooi D. L., Keel J., Lee E., Kirschner M. W., Waddell S. and Lee L. A. (2007) The Drosophila homolog of MCPH1, a human microcephaly gene, is required for genomic stability in the early embryo. *J Cell Sci* **120**, 3565-77.
Rimol L. M., Agartz I., Djurovic S., Brown A. A., Roddey J. C., Kahler A. K., Mattingsdal M., Athanasiu L., Joyner A. H., Schork N. J., Halgren E., Sundet K., Melle I., Dale A. M. and Andreassen O. A. (2010) Sex-dependent association of common variants of microcephaly genes with brain structure. *Proc Natl Acad Sci U S A* **107**, 384-8.
Roberts E., Hampshire D. J., Pattison L., Springell K., Jafri H., Corry P., Mannon J., Rashid Y., Crow Y., Bond J. and Woods C. G. (2002) Autosomal recessive primary microcephaly: an analysis of locus heterogeneity and phenotypic variation. *J Med Genet* **39**, 718-21.
Ross J. J. a. F. (1977) Microcephaly. In *In: Congenital malformations*

of the brain and skull Part 1, Vol 30, p. pp. 507-524. North Holland Publ. Co., Amsterdam.
Rusan N. M. and Peifer M. (2007) A role for a novel centrosome cycle in asymmetric cell division. *J Cell Biol* **177**, 13-20.
Rushton J. P., Vernon P. A. and Bons T. A. (2007) No evidence that polymorphisms of brain regulator genes Microcephalin and ASPM are associated with general mental ability, head circumference or altruism. *Biol Lett* **3**, 157-60.
Saadi A., Borck G., Boddaert N., Chekkour M. C., Imessaoudene B., Munnich A., Colleaux L. and Chaouch M. (2009) Compound heterozygous ASPM mutations associated with microcephaly and simplified cortical gyration in a consanguineous Algerian family. *Eur J Med Genet* **52**, 180-4.
Salic A., Waters J. C. and Mitchison T. J. (2004) Vertebrate shugoshin links sister centromere cohesion and kinetochore microtubule stability in mitosis. *Cell* **118**, 567-78.
Salisbury J. L. (2003) Centrosome size is controlled by centriolar SAS-4. *Trends Cell Biol* **13**, 340-3.
SantaLucia J., Jr. (1998) A unified view of polymer, dumbbell, and oligonucleotide DNA nearest-neighbor thermodynamics. *Proc Natl Acad Sci U S A* **95**, 1460-5.
Santamaria A., Wang B., Elowe S., Malik R., Zhang F., Bauer M., Schmidt A., Sillje H. H., Korner R. and Nigg E. A. (2011) The Plk1-dependent phosphoproteome of the early mitotic spindle. *Mol Cell Proteomics* **10**, M110 004457.
Savitsky K., Bar-Shira A., Gilad S., Rotman G., Ziv Y., Vanagaite L., Tagle D. A., Smith S., Uziel T., Sfez S., Ashkenazi M., Pecker I., Frydman M., Harnik R., Patanjali S. R., Simmons A., Clines G. A., Sartiel A., Gatti R. A., Chessa L., Sanal O., Lavin M. F., Jaspers N. G., Taylor A. M., Arlett C. F., Miki T., Weissman S. M., Lovett M., Collins F. S. and Shiloh Y. (1995) A single ataxia telangiectasia gene with a product similar to PI-3 kinase. *Science* **268**, 1749-53.
Sawin K. E., Lourenco P. C. and Snaith H. A. (2004) Microtubule nucleation at non-spindle pole body microtubule-organizing centers requires fission yeast centrosomin-related protein mod20p. *Curr Biol* **14**, 763-75.
Schmidt J. C., Kiyomitsu T., Hori T., Backer C. B., Fukagawa T. and Cheeseman I. M. (2010) Aurora B kinase controls the targeting of the Astrin-SKAP complex to bioriented kinetochores. *J Cell Biol* **191**, 269-80.
Schmidt T. I., Kleylein-Sohn J., Westendorf J., Le Clech M., Lavoie S. B., Stierhof Y. D. and Nigg E. A. (2009) Control of centriole length by CPAP and CP110. *Curr Biol* **19**, 1005-11.
Scott K., Brady R., Jr., Cravchik A., Morozov P., Rzhetsky A., Zuker C. and Axel R. (2001) A chemosensory gene family encoding candidate gustatory and olfactory receptors in Drosophila. *Cell* **104**, 661-73.
Shen J., Eyaid W., Mochida G. H., Al-Moayyad F., Bodell A., Woods C. G. and Walsh C. A. (2005) ASPM mutations identified in patients with primary microcephaly and seizures. *J Med Genet* **42**, 725-9.
Shiloh Y. (1997) Ataxia-telangiectasia and the Nijmegen breakage syndrome: related disorders but genes apart. *Annu Rev Genet* **31**, 635-62.

Shimada H., Kuboshima M., Shiratori T., Nabeya Y., Takeuchi A., Takagi H., Nomura F., Takiguchi M., Ochiai T. and Hiwasa T. (2007) Serum anti-myomegalin antibodies in patients with esophageal squamous cell carcinoma. *Int J Oncol* **30**, 97-103.

Shirayama M., Zachariae W., Ciosk R. and Nasmyth K. (1998) The Polo-like kinase Cdc5p and the WD-repeat protein Cdc20p/fizzy are regulators and substrates of the anaphase promoting complex in Saccharomyces cerevisiae. *EMBO J* **17**, 1336-49.

Shu H. B. and Joshi H. C. (1995) Gamma-tubulin can both nucleate microtubule assembly and self-assemble into novel tubular structures in mammalian cells. *J Cell Biol* **130**, 1137-47.

Sigrist S., Jacobs H., Stratmann R. and Lehner C. F. (1995) Exit from mitosis is regulated by Drosophila fizzy and the sequential destruction of cyclins A, B and B3. *EMBO J* **14**, 4827-38.

Silk A. D., Holland A. J. and Cleveland D. W. (2009) Requirements for NuMA in maintenance and establishment of mammalian spindle poles. *J Cell Biol* **184**, 677-90.

Siller K. H. and Doe C. Q. (2008) Lis1/dynactin regulates metaphase spindle orientation in Drosophila neuroblasts. *Dev Biol* **319**, 1-9.

Silva A. O., Ercole C. E. and McLoon S. C. (2002) Plane of cell cleavage and numb distribution during cell division relative to cell differentiation in the developing retina. *J Neurosci* **22**, 7518-25.

Simpson M. T., MacLaurin J. G., Xu D., Ferguson K. L., Vanderluit J. L., Davoli M. A., Roy S., Nicholson D. W., Robertson G. S., Park D. S. and Slack R. S. (2001) Caspase 3 deficiency rescues peripheral nervous system defect in retinoblastoma nullizygous mice. *J Neurosci* **21**, 7089-98.

Skoufias D. A., Indorato R. L., Lacroix F., Panopoulos A. and Margolis R. L. (2007) Mitosis persists in the absence of Cdk1 activity when proteolysis or protein phosphatase activity is suppressed. *J Cell Biol* **179**, 671-85.

Smart I. H. (1973) Proliferative characteristics of the ependymal layer during the early development of the mouse neocortex: a pilot study based on recording the number, location and plane of cleavage of mitotic figures. *J Anat* **116**, 67-91.

Sorensen C. S., Syljuasen R. G., Falck J., Schroeder T., Ronnstrand L., Khanna K. K., Zhou B. B., Bartek J. and Lukas J. (2003) Chk1 regulates the S phase checkpoint by coupling the physiological turnover and ionizing radiation-induced accelerated proteolysis of Cdc25A. *Cancer Cell* **3**, 247-58.

Sorokin S. (1962) Centrioles and the formation of rudimentary cilia by fibroblasts and smooth muscle cells. *J Cell Biol* **15**, 363-77.

Stearns T. (2009) Stem cells: A fateful age gap. *Nature* **461**, 891-2.

Stearns T., Evans L. and Kirschner M. (1991) Gamma-tubulin is a highly conserved component of the centrosome. *Cell* **65**, 825-36.

Stennicke H. R., Renatus M., Meldal M. and Salvesen G. S. (2000) Internally quenched fluorescent peptide substrates disclose the subsite preferences of human caspases 1, 3, 6, 7 and 8. *Biochem J* **350 Pt 2**, 563-8.

Stevens D., Gassmann R., Oegema K. and Desai A. (2011) Uncoordinated loss of chromatid cohesion is a common outcome of extended metaphase arrest. *PLoS One* **6**, e22969.

Stevens N. R., Dobbelaere J., Brunk K., Franz A. and Raff J. W. (2010a) Drosophila Ana2 is a conserved centriole duplication factor. *J Cell Biol* **188**, 313-23.
Stevens N. R., Roque H. and Raff J. W. (2010b) DSas-6 and Ana2 coassemble into tubules to promote centriole duplication and engagement. *Dev Cell* **19**, 913-9.
Sudakin V., Ganoth D., Dahan A., Heller H., Hershko J., Luca F. C., Ruderman J. V. and Hershko A. (1995) The cyclosome, a large complex containing cyclin-selective ubiquitin ligase activity, targets cyclins for destruction at the end of mitosis. *Mol Biol Cell* **6**, 185-97.
Takahashi K. and Yamanaka S. (2006) Induction of pluripotent stem cells from mouse embryonic and adult fibroblast cultures by defined factors. *Cell* **126**, 663-76.
Takahashi T., Nowakowski R. S. and Caviness V. S., Jr. (1995a) The cell cycle of the pseudostratified ventricular epithelium of the embryonic murine cerebral wall. *J Neurosci* **15**, 6046-57.
Takahashi T., Nowakowski R. S. and Caviness V. S., Jr. (1995b) Early ontogeny of the secondary proliferative population of the embryonic murine cerebral wall. *J Neurosci* **15**, 6058-68.
Takahashi T., Nowakowski R. S. and Caviness V. S., Jr. (1996) The leaving or Q fraction of the murine cerebral proliferative epithelium: a general model of neocortical neuronogenesis. *J Neurosci* **16**, 6183-96.
Talanian R. V., Quinlan C., Trautz S., Hackett M. C., Mankovich J. A., Banach D., Ghayur T., Brady K. D. and Wong W. W. (1997) Substrate specificities of caspase family proteases. *J Biol Chem* **272**, 9677-82.
Tamura T., Ishihara M., Lamphier M. S., Tanaka N., Oishi I., Aizawa S., Matsuyama T., Mak T. W., Taki S. and Taniguchi T. (1995) An IRF-1-dependent pathway of DNA damage-induced apoptosis in mitogen-activated T lymphocytes. *Nature* **376**, 596-9.
Tamura T., Ueda S., Yoshida M., Matsuzaki M., Mohri H. and Okubo T. (1996) Interferon-gamma induces Ice gene expression and enhances cellular susceptibility to apoptosis in the U937 leukemia cell line. *Biochem Biophys Res Commun* **229**, 21-6.
Tang C. J., Fu R. H., Wu K. S., Hsu W. B. and Tang T. K. (2009) CPAP is a cell-cycle regulated protein that controls centriole length. *Nat Cell Biol* **11**, 825-31.
Tang Z., Shu H., Qi W., Mahmood N. A., Mumby M. C. and Yu H. (2006) PP2A is required for centromeric localization of Sgo1 and proper chromosome segregation. *Dev Cell* **10**, 575-85.
Tang Z., Sun Y., Harley S. E., Zou H. and Yu H. (2004) Human Bub1 protects centromeric sister-chromatid cohesion through Shugoshin during mitosis. *Proc Natl Acad Sci U S A* **101**, 18012-7.
The_Bloulder_Committee. (1970) Embryonic vertebrate central nervous system: revised terminology. The Boulder Committee. *Anat Rec* **166**, 257-61.
Thein K. H., Kleylein-Sohn J., Nigg E. A. and Gruneberg U. (2007) Astrin is required for the maintenance of sister chromatid cohesion and centrosome integrity. *J Cell Biol* **178**, 345-54.
Theis M., Slabicki M., Junqueira M., Paszkowski-Rogacz M., Sontheimer J., Kittler R., Heninger A. K., Glatter T., Kruusmaa K., Poser I., Hyman A. A., Pisabarro M. T., Gstaiger M., Aebersold R., Shevchenko A. and Buchholz F.

(2009) Comparative profiling identifies C13orf3 as a component of the Ska complex required for mammalian cell division. *EMBO J* **28**, 1453-65.
Thomaidou D., Mione M. C., Cavanagh J. F. and Parnavelas J. G. (1997) Apoptosis and its relation to the cell cycle in the developing cerebral cortex. *J Neurosci* **17**, 1075-85.
Thompson S. L. and Compton D. A. (2008) Examining the link between chromosomal instability and aneuploidy in human cells. *J Cell Biol* **180**, 665-72.
Thornberry N. A., Rano T. A., Peterson E. P., Rasper D. M., Timkey T., Garcia-Calvo M., Houtzager V. M., Nordstrom P. A., Roy S., Vaillancourt J. P., Chapman K. T. and Nicholson D. W. (1997) A combinatorial approach defines specificities of members of the caspase family and granzyme B. Functional relationships established for key mediators of apoptosis. *J Biol Chem* **272**, 17907-11.
Tibelius A., Marhold J., Zentgraf H., Heilig C. E., Neitzel H., Ducommun B., Rauch A., Ho A. D., Bartek J. and Kramer A. (2009) Microcephalin and pericentrin regulate mitotic entry via centrosome-associated Chk1. *J Cell Biol* **185**, 1149-57.
Timpson N., Heron J., Smith G. D. and Enard W. (2007) Comment on papers by Evans et al. and Mekel-Bobrov et al. on Evidence for Positive Selection of MCPH1 and ASPM. *Science* **317**, 1036; author reply 1036.
Tirnauer J. S., Canman J. C., Salmon E. D. and Mitchison T. J. (2002) EB1 targets to kinetochores with attached, polymerizing microtubules. *Mol Biol Cell* **13**, 4308-16.
Torres E. M., Williams B. R. and Amon A. (2008) Aneuploidy: cells losing their balance. *Genetics* **179**, 737-46.
Toyoda Y. and Yanagida M. (2006) Coordinated requirements of human topo II and cohesin for metaphase centromere alignment under Mad2-dependent spindle checkpoint surveillance. *Mol Biol Cell* **17**, 2287-302.
Trimborn M., Bell S. M., Felix C., Rashid Y., Jafri H., Griffiths P. D., Neumann L. M., Krebs A., Reis A., Sperling K., Neitzel H. and Jackson A. P. (2004) Mutations in microcephalin cause aberrant regulation of chromosome condensation. *Am J Hum Genet* **75**, 261-6.
Trimborn M., Ghani M., Walther D. J., Dopatka M., Dutrannoy V., Busche A., Meyer F., Nowak S., Nowak J., Zabel C., Klose J., Esquitino V., Garshasbi M., Kuss A. W., Ropers H. H., Mueller S., Poehlmann C., Gavvovidis I., Schindler D., Sperling K. and Neitzel H. (2010) Establishment of a mouse model with misregulated chromosome condensation due to defective Mcph1 function. *PLoS One* **5**, e9242.
Trimborn M., Richter R., Sternberg N., Gavvovidis I., Schindler D., Jackson A. P., Prott E. C., Sperling K., Gillessen-Kaesbach G. and Neitzel H. (2005) The first missense alteration in the MCPH1 gene causes autosomal recessive microcephaly with an extremely mild cellular and clinical phenotype. *Hum Mutat* **26**, 496.
Trimborn M., Schindler D., Neitzel H. and Hirano T. (2006) Misregulated chromosome condensation in MCPH1 primary microcephaly is mediated by condensin II. *Cell Cycle* **5**, 322-6.

Trinkle-Mulcahy L., Andersen J., Lam Y. W., Moorhead G., Mann M. and Lamond A. I. (2006) Repo-Man recruits PP1 gamma to chromatin and is essential for cell viability. *J Cell Biol* **172**, 679-92.
Tsai K. Y., Hu Y., Macleod K. F., Crowley D., Yamasaki L. and Jacks T. (1998) Mutation of E2f-1 suppresses apoptosis and inappropriate S phase entry and extends survival of Rb-deficient mouse embryos. *Mol Cell* **2**, 293-304.
Tsou M. F. and Stearns T. (2006) Mechanism limiting centrosome duplication to once per cell cycle. *Nature* **442**, 947-51.
Tsou M. F., Wang W. J., George K. A., Uryu K., Stearns T. and Jallepalli P. V. (2009) Polo kinase and separase regulate the mitotic licensing of centriole duplication in human cells. *Dev Cell* **17**, 344-54.
Tsukuda T., Fleming A. B., Nickoloff J. A. and Osley M. A. (2005) Chromatin remodelling at a DNA double-strand break site in Saccharomyces cerevisiae. *Nature* **438**, 379-83.
Tucker R. W., Pardee A. B. and Fujiwara K. (1979) Centriole ciliation is related to quiescence and DNA synthesis in 3T3 cells. *Cell* **17**, 527-35.
Vaizel-Ohayon D. and Schejter E. D. (1999) Mutations in centrosomin reveal requirements for centrosomal function during early Drosophila embryogenesis. *Curr Biol* **9**, 889-98.
van Attikum H., Fritsch O., Hohn B. and Gasser S. M. (2004) Recruitment of the INO80 complex by H2A phosphorylation links ATP-dependent chromatin remodeling with DNA double-strand break repair. *Cell* **119**, 777-88.
Van Den Bosch J. (1959) Microcephaly in the Netherlands: a clinical and genetical study. *Ann Hum Genet* **23**, 91-116.
van der Voet M., Berends C. W., Perreault A., Nguyen-Ngoc T., Gonczy P., Vidal M., Boxem M. and van den Heuvel S. (2009) NuMA-related LIN-5, ASPM-1, calmodulin and dynein promote meiotic spindle rotation independently of cortical LIN-5/GPR/Galpha. *Nat Cell Biol* **11**, 269-77.
van Gijlswijk R. P., Zijlmans H. J., Wiegant J., Bobrow M. N., Erickson T. J., Adler K. E., Tanke H. J. and Raap A. K. (1997) Fluorochrome-labeled tyramides: use in immunocytochemistry and fluorescence in situ hybridization. *J Histochem Cytochem* **45**, 375-82.
Vanoosthuyse V. and Hardwick K. G. (2009a) A novel protein phosphatase 1-dependent spindle checkpoint silencing mechanism. *Curr Biol* **19**, 1176-81.
Vanoosthuyse V. and Hardwick K. G. (2009b) Overcoming inhibition in the spindle checkpoint. *Genes Dev* **23**, 2799-805.
Varon R., Vissinga C., Platzer M., Cerosaletti K. M., Chrzanowska K. H., Saar K., Beckmann G., Seemanova E., Cooper P. R., Nowak N. J., Stumm M., Weemaes C. M., Gatti R. A., Wilson R. K., Digweed M., Rosenthal A., Sperling K., Concannon P. and Reis A. (1998) Nibrin, a novel DNA double-strand break repair protein, is mutated in Nijmegen breakage syndrome. *Cell* **93**, 467-76.
Venkatram S., Tasto J. J., Feoktistova A., Jennings J. L., Link A. J. and Gould K. L. (2004) Identification and characterization of two novel proteins affecting fission yeast gamma-tubulin complex function. *Mol Biol Cell* **15**, 2287-301.
Verde I., Pahlke G., Salanova M., Zhang G., Wang S., Coletti D., Onuffer J., Jin S. L. and Conti M. (2001) Myomegalin is a novel protein of the

golgi/centrosome that interacts with a cyclic nucleotide phosphodiesterase. *J Biol Chem* **276**, 11189-98.
Visintin R., Prinz S. and Amon A. (1997) CDC20 and CDH1: a family of substrate-specific activators of APC-dependent proteolysis. *Science* **278**, 460-3.
Vorobjev I. A. and Chentsov Yu S. (1982) Centrioles in the cell cycle. I. Epithelial cells. *J Cell Biol* **93**, 938-49.
Waizenegger I. C., Hauf S., Meinke A. and Peters J. M. (2000) Two distinct pathways remove mammalian cohesin from chromosome arms in prophase and from centromeres in anaphase. *Cell* **103**, 399-410.
Wakefield J. G., Bonaccorsi S. and Gatti M. (2001) The drosophila protein asp is involved in microtubule organization during spindle formation and cytokinesis. *J Cell Biol* **153**, 637-48.
Wang J. K., Li Y. and Su B. (2008) A common SNP of MCPH1 is associated with cranial volume variation in Chinese population. *Hum Mol Genet* **17**, 1329-35.
Wang X., Tsai J. W., Imai J. H., Lian W. N., Vallee R. B. and Shi S. H. (2009) Asymmetric centrosome inheritance maintains neural progenitors in the neocortex. *Nature* **461**, 947-55.
Wang Y. Q. and Su B. (2004) Molecular evolution of microcephalin, a gene determining human brain size. *Hum Mol Genet* **13**, 1131-7.
Weaver B. A., Silk A. D., Montagna C., Verdier-Pinard P. and Cleveland D. W. (2007) Aneuploidy acts both oncogenically and as a tumor suppressor. *Cancer Cell* **11**, 25-36.
Welburn J. P., Grishchuk E. L., Backer C. B., Wilson-Kubalek E. M., Yates J. R., 3rd and Cheeseman I. M. (2009) The human kinetochore Ska1 complex facilitates microtubule depolymerization-coupled motility. *Dev Cell* **16**, 374-85.
Westendorf J. M., Rao P. N. and Gerace L. (1994) Cloning of cDNAs for M-phase phosphoproteins recognized by the MPM2 monoclonal antibody and determination of the phosphorylated epitope. *Proc Natl Acad Sci U S A* **91**, 714-8.
Wheatley S. P., Hinchcliffe E. H., Glotzer M., Hyman A. A., Sluder G. and Wang Y. (1997) CDK1 inactivation regulates anaphase spindle dynamics and cytokinesis in vivo. *J Cell Biol* **138**, 385-93.
Wiese C. and Zheng Y. (2006) Microtubule nucleation: gamma-tubulin and beyond. *J Cell Sci* **119**, 4143-53.
Wolff A., de Nechaud B., Chillet D., Mazarguil H., Desbruyeres E., Audebert S., Edde B., Gros F. and Denoulet P. (1992) Distribution of glutamylated alpha and beta-tubulin in mouse tissues using a specific monoclonal antibody, GT335. *Eur J Cell Biol* **59**, 425-32.
Woo M., Hakem R., Furlonger C., Hakem A., Duncan G. S., Sasaki T., Bouchard D., Lu L., Wu G. E., Paige C. J. and Mak T. W. (2003) Caspase-3 regulates cell cycle in B cells: a consequence of substrate specificity. *Nat Immunol* **4**, 1016-22.
Wood B. and Collard M. (1999) The human genus. *Science* **284**, 65-71.
Wood J. L., Liang Y., Li K. and Chen J. (2008) Microcephalin/MCPH1 associates with the Condensin II complex to function in homologous recombination repair. *J Biol Chem* **283**, 29586-92.

Wood J. L., Singh N., Mer G. and Chen J. (2007) MCPH1 functions in an H2AX-dependent but MDC1-independent pathway in response to DNA damage. *J Biol Chem* **282**, 35416-23.

Woods C. G., Bond J. and Enard W. (2005) Autosomal recessive primary microcephaly (MCPH): a review of clinical, molecular, and evolutionary findings. *Am J Hum Genet* **76**, 717-28.

Woods R. P., Freimer N. B., De Young J. A., Fears S. C., Sicotte N. L., Service S. K., Valentino D. J., Toga A. W. and Mazziotta J. C. (2006) Normal variants of Microcephalin and ASPM do not account for brain size variability. *Hum Mol Genet* **15**, 2025-9.

Wu X., Mondal G., Wang X., Wu J., Yang L., Pankratz V. S., Rowley M. and Couch F. J. (2009) Microcephalin regulates BRCA2 and Rad51-associated DNA double-strand break repair. *Cancer Res* **69**, 5531-6.

Xiao Z., Chen Z., Gunasekera A. H., Sowin T. J., Rosenberg S. H., Fesik S. and Zhang H. (2003) Chk1 mediates S and G2 arrests through Cdc25A degradation in response to DNA-damaging agents. *J Biol Chem* **278**, 21767-73.

Xu B., Kim S. and Kastan M. B. (2001) Involvement of Brca1 in S-phase and G(2)-phase checkpoints after ionizing irradiation. *Mol Cell Biol* **21**, 3445-50.

Xu X., Lee J. and Stern D. F. (2004) Microcephalin is a DNA damage response protein involved in regulation of CHK1 and BRCA1. *J Biol Chem* **279**, 34091-4.

Yaffe M. B., Schutkowski M., Shen M., Zhou X. Z., Stukenberg P. T., Rahfeld J. U., Xu J., Kuang J., Kirschner M. W., Fischer G., Cantley L. C. and Lu K. P. (1997) Sequence-specific and phosphorylation-dependent proline isomerization: a potential mitotic regulatory mechanism. *Science* **278**, 1957-60.

Yamanaka S. (2009) A fresh look at iPS cells. *Cell* **137**, 13-7.

Yamashita Y. M., Mahowald A. P., Perlin J. R. and Fuller M. T. (2007) Asymmetric inheritance of mother versus daughter centrosome in stem cell division. *Science* **315**, 518-21.

Yang A. H., Kaushal D., Rehen S. K., Kriedt K., Kingsbury M. A., McConnell M. J. and Chun J. (2003) Chromosome segregation defects contribute to aneuploidy in normal neural progenitor cells. *J Neurosci* **23**, 10454-62.

Yang J., Adamian M. and Li T. (2006) Rootletin interacts with C-Nap1 and may function as a physical linker between the pair of centrioles/basal bodies in cells. *Mol Biol Cell* **17**, 1033-40.

Yang S. Z., Lin F. T. and Lin W. C. (2008) MCPH1/BRIT1 cooperates with E2F1 in the activation of checkpoint, DNA repair and apoptosis. *EMBO Rep* **9**, 907-15.

Yang X., Klein R., Tian X., Cheng H. T., Kopan R. and Shen J. (2004) Notch activation induces apoptosis in neural progenitor cells through a p53-dependent pathway. *Dev Biol* **269**, 81-94.

Yu F., Hill R. S., Schaffner S. F., Sabeti P. C., Wang E. T., Mignault A. A., Ferland R. J., Moyzis R. K., Walsh C. A. and Reich D. (2007) Comment on "Ongoing adaptive evolution of ASPM, a brain size determinant in Homo sapiens". *Science* **316**, 370.

Yu T. W., Mochida G. H., Tischfield D. J., Sgaier S. K., Flores-Sarnat L., Sergi C. M., Topcu M., McDonald M. T., Barry B. J., Felie J. M., Sunu C., Dobyns W. B., Folkerth R. D., Barkovich A. J. and Walsh C. A. (2010) Mutations in WDR62, encoding a centrosome-associated protein, cause microcephaly with simplified gyri and abnormal cortical architecture. *Nat Genet* **42**, 1015-20.

Yu X., Chini C. C., He M., Mer G. and Chen J. (2003) The BRCT domain is a phospho-protein binding domain. *Science* **302**, 639-42.

Yuan B., Latek R., Hossbach M., Tuschl T. and Lewitter F. (2004) siRNA Selection Server: an automated siRNA oligonucleotide prediction server. *Nucleic Acids Res* **32**, W130-4.

Zhang J. and Megraw T. L. (2007) Proper recruitment of gamma-tubulin and D-TACC/Msps to embryonic Drosophila centrosomes requires Centrosomin Motif 1. *Mol Biol Cell* **18**, 4037-49.

Zhang X., Liu D., Lv S., Wang H., Zhong X., Liu B., Wang B., Liao J., Li J., Pfeifer G. P. and Xu X. (2009) CDK5RAP2 is required for spindle checkpoint function. *Cell Cycle* **8**, 1206-16.

Zhong X., Liu L., Zhao A., Pfeifer G. P. and Xu X. (2005) The abnormal spindle-like, microcephaly-associated (ASPM) gene encodes a centrosomal protein. *Cell Cycle* **4**, 1227-9.

Zhong X., Pfeifer G. P. and Xu X. (2006) Microcephalin encodes a centrosomal protein. *Cell Cycle* **5**, 457-8.

Zhou B. B., Li H., Yuan J. and Kirschner M. W. (1998) Caspase-dependent activation of cyclin-dependent kinases during Fas-induced apoptosis in Jurkat cells. *Proc Natl Acad Sci U S A* **95**, 6785-90.

Zhu F., Lawo S., Bird A., Pinchev D., Ralph A., Richter C., Muller-Reichert T., Kittler R., Hyman A. A. and Pelletier L. (2008) The mammalian SPD-2 ortholog Cep192 regulates centrosome biogenesis. *Curr Biol* **18**, 136-41.

Zimmerman W. C., Sillibourne J., Rosa J. and Doxsey S. J. (2004) Mitosis-specific anchoring of gamma tubulin complexes by pericentrin controls spindle organization and mitotic entry. *Mol Biol Cell* **15**, 3642-57.

Zou L. and Elledge S. J. (2003) Sensing DNA damage through ATRIP recognition of RPA-ssDNA complexes. *Science* **300**, 1542-8.

Zou L., Liu D. and Elledge S. J. (2003) Replication protein A-mediated recruitment and activation of Rad17 complexes. *Proc Natl Acad Sci U S A* **100**, 13827-32.

Zur A. and Brandeis M. (2001) Securin degradation is mediated by fzy and fzr, and is required for complete chromatid separation but not for cytokinesis. *EMBO J* **20**, 792-801.